University Library



A gateway to Melbourne's research publications

Minerva Access is the Institutional Repository of The University of Melbourne

Author/s:
Sanaei, Mohammad Reza

Title:
Protease-activated receptor-2 in bone morphogenesis and pathology: Is par2 essential in osteoblastic bone homeostasis?

Date:
2017

Persistent Link:
https://hdl.handle.net/11343/197897

Terms and Conditions:
Terms and Conditions: Copyright in works deposited in Minerva Access is retained by the copyright owner. The work may not be altered without permission from the copyright owner. Readers may only download, print and save electronic copies of whole works for their own personal non-commercial use. Any use that exceeds these limits requires permission from the copyright owner. Attribution is essential when quoting or paraphrasing from these works.

PROTEASE-ACTIVATED RECEPTOR-2 IN BONE MORPHOGENESIS AND PATHOLOGY: IS PAR_2 ESSENTIAL IN OSTEOBLASTIC BONE HOMEOSTASIS?

Mohammad Reza Sanaei

ORCID: 0000-0002-2692-0935

Submitted in total fulfillment of the requirements for the degree of

Doctor of Philosophy

September 2017

Faculty of Veterinary and Agricultural Sciences

The University of Melbourne

ABSTRACT

Protease activated receptor-2 (PAR_2) is a member of the small family of protease-activated G protein-coupled receptors. PAR_2 is widely expressed in most tissues including bone and has been shown to regulate cell proliferation and survival, cytokine production and release as well as nociception. Recent unpublished data suggest that PAR_2 plays a role in bone homeostasis by regulating the osteogenic and adipogenic differentiation of mesenchymal stem cells (MSCs). Due to the potential impact of such regulation on age-related bone loss and osteoporosis, the current study undertook to investigate the hypothesis that PAR_2 activation regulates the determination of mesenchymal cell fate such that osteoblastogenesis is preferred over adipogenesis both *in vivo* and *in vitro* and that such regulation impacts the potential outcome of ageing in bone. Moreover, as PAR_2 is a pro-inflammatory receptor, it was also hypothesised that PAR_2 is a mediator of inflammation induced osteopoenia and as such its deletion will improve the resulting bone phenotype.

Comparison of the bone phenotype in ageing global PAR_2 null mice with the wildtype controls showed that the global lack of PAR_2 *in vivo* was associated with a low bone mass profile and bone tissue mineral density which was compounded by a relatively rapid structural deterioration. These observations were more pronounced in the male knockout mice. *In vitro* gene silencing experiments with bipotential Kusa 4b10 mesenchymal cells suggested a pro-osteogenic and anti-adipogenic role for the receptor in the differentiation of MSCs. Gene expression studies revealed a number of novel genes downstream of PAR_2 that were not previously associated with these processes. These included *Cnr1*, *Il6*, *Ramp3* and *Enpep* which were more highly expressed following PAR_2 knockdown and *C1qtnf3, Snorc* and *Gpr35,* which were suppressed. Investigation of IL-6 concentrations in the medium by ELISA as well as use of anti-IL-6 neutralising antibody suggested that PAR_2 promoted osteogenesis and inhibited adipogenesis partly by suppressing expression of IL-6.

To further examine the role of the receptor in osteoblasts *in vivo,* osteoblast-specific deletion of PAR_2 was achieved through the expression of Cre-recombinase that was

driven by the Osterix (*Osx*) promoter. Surprisingly, osteoblast-specific ablation of PAR_2 in growing mice not only resulted in an increased bone formation rate in 7 week old females, but also culminated in a higher bone mass profile at 13 weeks whilst males remained unaffected. The paradoxical finding may be explained by the presence of PAR_2 during the critical earlier stages of MSC differentiation and its ablation only after cells have become committed *Osx*-expressing osteoprogenitor cells. These results suggest that PAR_2 plays a role in the determination of osteoblasts prior to the stage at which gene deletion occurs in the osteoblast-specific PAR_2 null mice.

To investigate the role of the receptor in the pathogenesis of inflammation-induced osteopoenia, the bone phenotype of PAR_2 null and wildtype dystrophin deficient mice (mdx mice) was compared. Results revealed that PAR_2 deficiency protected the mdx mice from the impact of muscular dystrophy on bone structural and material properties.

This study provides evidence that PAR_2 slows ageing-related bone loss, possibly by promotion of osteoblast differentiation and suppression of adipogenesis in MSCs. In contrast, evidence is provided that PAR_2 contributes to inflammation-induced bone loss.

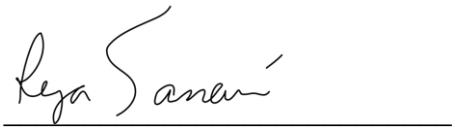
DECLARATION

This is to certify that

i. This thesis comprises only my original work towards the PhD except where indicated in the preface.

ii. Due acknowledgement has been made in the text to all other materials used.

iii. This thesis is fewer than 100,000 words in length, exclusive of tables, maps, bibliographies and appendices.



Mohammad Reza Sanaei
September 2017

PREFACE

I certify that except where due acknowledgement has been made, the work is that of the author alone. The work has not been submitted previously, in whole or in part, to qualify for any other academic award. The content of the thesis is the result of work which has been carried out since the official commencement date of the approved research program. No editorial work has been carried out by a third party on this thesis and all ethics procedures and guidelines have been followed. Unless otherwise indicated, all figures included in this thesis were created by M. Reza Sanaei© The University of Melbourne 2017. This research has been made possible by the Endeavour International Postgraduate Research Scholarship (IPRS) and Australian Postgraduate Award (APA).

ACKNOWLEDGEMENTS

A work like such requires passion and patience, but more, support and guidance. I am grateful to many people for their assistance, encouragement and advice in completing this research. First and foremost, I would like to express my deep appreciation to my supervisors, Professor Eleanor Mackie and Dr. Charles Pagel. It has been a rewarding experience working in your laboratory as a PhD student being assured that there is always support and guidance when I need it. I would also like to thank you for the patience and care you have always shown towards me and finally for providing me the opportunity to delve into the science world and start a new career path.

Many thanks to Professor James Gilkerson for chairing my advisory committee, for always being open and helpful throughout these years. I would also like to sincerely thank Associate Professor Natalie Sims as well as Ms. Ingrid Poulton for their contributions of time and technical knowledge when I first started doing bone histomorphometry at the Bone Cell Biology and Disease Unit, St Vincent Institute of Medical Research. Thanks also for kindly providing the Kusa 4b10 cells and the Osx-Cre line and sharing of your experience with me. It is highly appreciated.

Especial thanks have to go to, my then fellow PhD student, now Dr. Neda Taghavi for generating the PAR_2 null mdx mice and conducting a part of their micro CT evaluations. Thanks also for the insights and support you provided since day 1 of my candidature. I would also like to extend my thanks to our animal house manager, Mr. Bob Geyer, our sterilisation facility manager, Ms. Cynthia Brown and our asset manager Mr. Victor Iwanov for their service and technical contributions. I am truly thankful to all fellow PhD students and researchers of the Laboratory for Bone and Muscle Cell Biology and the Centre for Animal Biotechnology for their friendship, cheerful insights and assistance.

My gratitude also goes to Dr. Christina Murray and Associate Professor Helen Davies, for providing me with the opportunity to participate in the teaching of anatomy practicals to DVM students. This has been a wonderful and positive experience; something I most definintely needed to get by. Thanks for all the encouragement, tips and feedback. I feel

fulfilled just thinking about all the things I learnt during this time. Thanks also have to go to Mr. Brendan Kehoe for making the experience even more rewarding by his timely provisions and excellent laboratory based support.

I am deeply grateful to my parents for constantly instilling the importance of education and knowledge throughout my life. I am indebted forever to you for your unhesitant support and love without which I could never be a person that I am now. My love for eternity is all that I have in return.

My deepest gratitude goes to my lovely wife, Fereshte, who despite far distances, patiently and graciously waited, and despite all my uncertainties, never stopped believing in me. No words can even begin to describe my gratefulness angel. I could not have done this without your devoted love and emotional support.

TABLE OF CONTENTS

Abstract i

Declaration iii

Preface iv

Acknowledgements v

List of Figures xii

List of tables xv

List of abbreviations xviii

Chapter 1: Introduction and Literature Review 1

1.1 Bone 1

1.1.1 Architecture and Function 1

1.1.2 Osteoblasts 2

1.1.3 Osteocytes 4

1.1.4 Bone Lining Cells 5

1.1.5 Osteoclasts 5

1.1.6 Bone Extracellular Matrix 6

1.1.7 Bone Development, Growth and Ageing 7

1.1.8 Inflammation-Induced Bone Loss 9

1.2 Adipose Tissue 12

1.2.1 Morphology and Function 12

1.2.2 Adipocytes 13

1.2.3 Adipose Tissue Development and Differentiation 14

1.3 The Reciprocal Relationship Between Bone and Fat 15

1.3.1 Osteoblast/Adipocyte Plasticity in Ageing and Osteoporosis 16

1.3.2 Coordination of Osteoblastogenesis and Adipogenesis 20

1.3.2.1 Transcriptional Regulation of Osteoblastogenesis 20

1.3.2.2 Transcriptional Regulation of Adipogenesis 25

1.3.2.3 Extracellular Signalling in Osteoblastogenesis/Adipogenesis 28

1.4 Protease-activated Receptor 2 (PAR_2) 36

1.4.1 Protease-activated Receptors as a family **36**
1.4.2 PAR_2 Signalling, Agonism and Antagonism **41**
1.4.3 PAR_2 Expression and Pathophysiological Functions **43**
1.4.4 PAR_2 and Bone **47**
1.5 Aims of the study **49**
Chapter 2: Materials and Methods **51**
2.1 Materials **51**
2.1.1 Animals **51**
2.1.1.1 Global PAR_2 Null Mouse 51
2.1.1.2 Dystrophin Deficient PAR_2 Null Mouse 51
2.1.1.3 Osteoblast specific PAR_2 null Mouse 52
2.1.2 Media and Reagents **52**
2.1.3 Equipment **53**
2.2 Genotyping and Polymerase Chain Reaction **54**
2.2.1 Genomic DNA Isolation **54**
2.2.2 DNA Extraction from Agarose Gels **54**
2.2.3 Total RNA Isolation **54**
2.2.4 Primer Design and Validation **55**
2.2.5 Polymerase Chain Reaction **55**
2.2.6 Complementary DNA Synthesis **59**
2.2.7 Quantitative Polymerase Chain Reaction **59**
2.2.8 DNA Sequencing **61**
2.2.9 Genotyping of Mice **61**
2.2.9.1 Global PAR_2 Null Mice 61
2.2.9.2 Osteoblast Specific PAR_2 Null Mice 62
2.2.9.3 Dystrophin Deficient (mdx) Mice 63
2.3 Cell Culture **64**
2.3.1 Kusa 4b10 Cell Line **64**
2.3.2 Primary Osteoblast Cultures **64**
2.3.3 Mycoplasma Screening **65**
2.3.4 Intracellular Calcium Mobilisation Assay **66**
2.4 Evaluation of the Role of PAR_2 in the Murine Bone Phenotype **67**
2.4.1 Confirmation of Osteoblast Specific Deletion of PAR_2 ..... **67**
2.4.2 Micro Computed Tomography **67**

2.4.3 Bone Histomorphometry **69**
2.4.3.1 Fluorochrome Labelling 70
2.4.3.2 Preparation of Plastic Sections and Histomorphometry 70
2.5 Evaluation of the Role of PAR_2 in Cultures of Kusa 4b10 Cells **70**
2.5.1 Trypsin-like Amydolytic Activity **70**
2.5.2 Kallikrein-like Activity **71**
2.5.3 PAR_2 Knockdown **72**
2.5.3.1 Lentiviral Transduction Particles 72
2.5.3.2 Puromycin Titration (Kill Curve) 72
2.5.3.3 Transduction and Selection 73
2.5.4 Alizarin Red-S Mineralisation Assay **74**
2.5.5 Oil-Red O Staining and Cell Morphometry **74**
2.5.6 Measurement of IL-6 Concentration in Cultures of Kusa 4b10 Cells **75**
2.5.7 Neutralising IL-6 in Cultures of Kusa 4b10 Cells **75**
2.6 Statistical Analysis **76**
Chapter 3: Effect of Global PAR_2 Gene Ablation on Murine Bone Phenotype in Context of Age **78**
3.1 Introduction and Aims **78**
3.2 Results **79**
3.2.1 Body Weight and Bone Length **79**
3.2.2 Tibial Trabecular Bone **80**
3.2.3 Vertebral Trabecular Bone **86**
3.2.4 Tibial Cortical Bone **91**
3.3 Discussion **96**
Chapter 4: Effect of Global PAR_2 Gene Ablation on Bone Loss in Dystrophin - defficient Mice **103**
4.1 Introduction and Aims **103**
4.2 Results **104**
4.2.1 PAR_2 null mdx mice **104**
4.2.1.1 Weight and Bone Length **104**
4.2.1.2 Tibial Trabecular Bone **104**

4.2.1.3 Tibial Cortical Bone **106**

4.3 Discussion **116**

Chapter 5: Role of PAR_2 in the Reciprocal Relationship Between Osteoblastogenesis and Adipogenesis **121**

5.1 Introduction and Aims **121**

5.2 Results **123**

5.2.1 Expression of PAR_2 by Kusa 4b10 Cells **123**

5.2.2 Expression of PAR_2 Activators and Spontaneous Protease Activity in Cultures of Kusa 4b10 Cells **123**

5.2.2.1 Expression of PAR_2 activators 123

5.2.2.2 Endogenous Protease Activity 124

5.2.3 Effects of PAR_2 Deficiency on Osteoblastogenesis and Adipogenesis **127**

5.2.3.1 PAR_2 knockdown 127

5.2.3.1 Adipogenesis in Cultures Under Osteogenic Conditions 127

5.2.3.2 Mineralisation of Cultures Under Osteogenic Conditions 128

5.2.3.3 Effects of PAR_2 Deficiency on Expression of Differentiation-Associated Genes 132

5.2.4 Identification of Molecular Mediators of PAR_2 Action in Kusa 4b10 Cells **134**

5.2.4.1 RT-qPCR Analysis of GOI Expression Under Osteogenic Conditions 134

5.2.4.2 Interleukin-6 ELISA 139

5.2.4.3 Interleukin-6 Neutralisation 139

5.3 Discussion **141**

Chapter 6: Effect of Osteoblast-specific Ablation of PAR_2 Gene on Murine Bone Phenotype **148**

6.1 Introduction and Aims **148**

6.2 Results **149**

6.2.1 Phenotype of *F2rl1*$^{wt/wt}$ and *F2rl1*$^{fl/fl}$ **149**

6.2.1.1 Body Weight and Bone Length 149

6.2.1.2 Tibial Metaphyseal Trabecular Bone 150

6.2.1.3 Tibial Metaphyseal Cortical Bone 156

6.2.1.4 Tibial Diaphyseal Cortical Bone 157

6.2.1.5 Bone Marrow Adiposity 159

6.2.2 Phenotype of *Osx-Cre.F2rl1*$^{wt/wt}$ and *Osx-Cre.F2rl1*$^{\Delta/\Delta}$ mice **161**

6.2.2.1 Confirmation of Osteoblast Specific PAR_2 deletion 161
6.2.2.2 Body Weight and Bone Length 163
6.2.2.3 Tibial Metaphyseal Trabecular Bone 165
6.2.2.4 Tibial Metaphyseal Cortical Bone 172
6.2.1.5 Tibial Diaphyseal Cortical Bone 176
6.2.2.5 Bone Marrow Adiposity 181
6.2.3 The Effect of *Osx-Cre* Transgene on the Phenotype of C57BL/6J Mice 183
6.3 Discussion 186
Chapter 7: Conclusions and Future Directions 192
7.1 Main Findings and Implications of the Research 192
7.2 Limitations of the Research and Future Work 197
References 200
Appendix A: Complementary Data - Micro CT of Global PAR_2 Null and Wildtype Mice 253
Appendix B: Complementary Data - Micro CT of Mdx-PAR_2 Null and 259
Mdx-wildtype Mice 259
Appendix C: List of Genes of Interest Examined *in vitro* 263
Appendix D: Complementary Data - Micro CT and Adipocyte Histomorphometry of *F2rl1*$^{wt/wt}$ and *F2rl1*$^{fl/fl}$ mice 267
Appendix E: Complementary Data - Micro CT of *Osx-Cre* Mice 279
Appendix F: List of Publications and Presentations Arising from This Thesis ... 283

LIST OF FIGURES

Figure 1.1 Age induced changes in the balance of osteoblastogenesis and adipogenesis. 18
Figure 1.2 Extracellular signals and transcriptional regulation of the bone-fat switch. 22
Figure 1.3 PAR activation and signal transduction. 37
Figure 1.4 Extracellular regulating signals of osteo/adipogenesis. 50
Figure 2.1 PCR based genotyping of osteoblast specific PAR_2 null mice. 63
Figure 2.2 micro CT Evaluation of Tibiae. 69
Figure 3.1 Body weight and tibial lengths in male and female mice. 80
Figure 3. 2 3D models of the metaphyseal trabecular bone in KO and WT mice. 82
Figure 3.3 Percent difference in metaphyseal trabecular indices - males. 83
Figure 3.4 Percent difference in metaphyseal trabecular indices - females. 84
Figure 3.5 Representative micro CT slices from the L5 vertebrae of KO and WT mice. 87
Figure 3.6 Percent difference in vertebral trabecular indices - males. 88
Figure 3.7 Percent difference in vertebral trabecular indices - females. 89
Figure 3.8 Percent difference in diaphyseal cortical indices - males. 92
Figure 3.9 Percent difference in diaphyseal cortical indices - females. 93
Figure 3.10 Main mass indices of the metaphyseal, vertebral and midshaft regions. 94
Figure 4.1 Body weight and tibial lengths in PAR_2 knockout and wildtype mdx mice. 106
Figure 4.2 3D models of the metaphyseal trabecular bone in KO and WT mdx mice. 108
Figure 4.3 Percent difference in metaphyseal trabecular indices - males. 109
Figure 4.4 Percent difference in metaphyseal trabecular indices - females. 110
Figure 4.5 Percent difference in diaphyseal cortical indices - males. 112
Figure 4.6 Percent difference in diaphyseal cortical indices - females. 113
Figure 4.7 Main mass indices of the metaphyseal and midshaft regions in mdx mice. 114

Figure 5.1 Expression of PAR_2 mRNA and some of its activators by Kusa 4b10 cells. 125
Figure 5.2 Trypsin-like and kallikrein-like activity in cultures of Kusa 4b10 cells. 126
Figure 5.3 Confirmation of PAR_2 knockdown following shRNA lentiviral transduction. 127
Figure 5.4 The extent of adipogenesis and mineralisation following PAR_2 knockdown. 129
Figure 5.5 Effect of PAR_2 deficiency on differentiation of Kusa 4b10 cells - time course. 130
Figure 5.6 Effect of PAR_2 deficiency on differentiation of Kusa 4b10 cells at day 7. 131
Figure 5.7 Effects of PAR2 deficiency on the expression of differentiation-associated genes. 133
Figure 5.8 RT-qPCR analysis of the category 1 GOIs. 136
Figure 5.9 RT-qPCR analysis of the category 2 GOIs. 137
Figure 5.10 RT-qPCR analysis of the category 3 GOIs. 138
Figure 5.11 ELISA investigation of IL-6 in vector control and *F2rl1* KD cultures. 139
Figure 5.12 Effect of Anti IL-6 antibody on the differentiation of Kusa 4b10 cells. 140
Figure 6.1 Body weight and tibial length in $F2rl1^{wt/wt}$ and $F2rl1^{fl/fl}$ mice. 150
Figure 6.2 3D models of the metaphyseal trabecular bone in $F2rl1^{wt/wt}$ and $F2rl1^{fl/fl}$ mice. 152
Figure 6.3 Main mass indices of metaphyseal and diaphyseal regions - $F2rl1^{wt/wt}$ and $F2rl1^{fl/fl}$ mice. 158
Figure 6.4 Marrow density of the metaphyseal and diaphyseal ROIs - $F2rl1^{wt/wt}$ and $F2rl1^{fl/fl}$ mice. 160
Figure 6. 5 Knockdown (KD) of PAR_2 DNA and mRNA. 162
Figure 6.6 Body weight and tibial lengths in *Osx-Cre*.$F2rl1^{wt/wt}$ and *Osx-Cre*.$F2rl1^{\Delta/\Delta}$ mice. 164
Figure 6.7 Corrected body weight and bone length in 13 week old male *Osx-Cre* mice. 165

Figure 6.8 3D models of the metaphyseal trabecular bone in *Osx-Cre* mice. 167
Figure 6.9 Percent difference in metaphyseal trabecular indices - male *Osx-Cre* mice. 168
Figure 6.10 Percent difference in metaphyseal trabecular indices - female *Osx-Cre* mice. 169
Figure 6.11 Percent difference in metaphyseal cortical indices - male *Osx-Cre* mice. 173
Figure 6.12 Percent difference in metaphyseal cortical indices - female *Osx-Cre* mice. 174
Figure 6.13 Percent difference in diaphyseal cortical indices - male *Osx-Cre* mice. 177
Figure 6.14 Percent difference in diaphyseal cortical indices - female *Osx-Cre* mice. 178
Figure 6.15 Main mass indices of the metaphyseal and midshaft regions in *Osx-Cre* mice. 180
Figure 6.16 Marrow density of the metaphyseal and diaphyseal ROIs - *Osx-Cre* mice. 182
Figure 6.17 Comparison of tibial lengths between *Osx-Cre* positive and negative mice. 184
Figure 6.18 Comparison of body weight between *Osx-Cre* positive and negative mice. 185
Figure 7.1 The dual role of PAR_2 in differentiation and function. 196
Figure D.1 Histomorphometric evaluation of marrow adiposity - *F2rl1*$^{wt/wt}$ and *F2rl1*$^{fl/fl}$ mice. 277
Figure D.2 Histomorphometric evaluation of marrow adiposity - *Osx-Cre* mice. 278

LIST OF TABLES

Table 1.1 Endogenous activators of PAR_2. 44
Table 2.1 PCR primers. 56
Table 2.2 PCR primers used for mycoplasma screening. 66
Table 2.3 Small hairpin RNA constructs used for PAR_2 knockdown. 73
Table 3.1 Time related change in the tibial metaphyseal trabecular bone. 85
Table 3.2 Time related change in the L5 trabecular bone. 90
Table 3.3 Time related change in the tibial midshaft cortical bone. 95
Table 4.1 Time related change in the tibial metaphyseal trabecular bone. 111
Table 4.2 Time related change in the tibial midshaft cortical bone. 115
Table 5.1 Expression of PAR_2 activating proteases by Kusa 4b10 cells. 126
Table 6.1 Metaphyseal trabecular indices determined by micro CT - *F2rl1*$^{wt/wt}$ and *F2rl1*$^{fl/fl}$ mice. 153
Table 6.2 Time related change in the metaphyseal trabecular bone assessed by micro CT - *F2rl1*$^{wt/wt}$ and *F2rl1*$^{fl/fl}$ mice. 154
Table 6.3 Trabecular histomorphometric indices - *F2rl1*$^{wt/wt}$ and *F2rl1*$^{fl/fl}$ mice. 155
Table 6.4 Analysis of trabecular indices affected by the presence of the floxed allele. 170
Table 6.5 Time related change in metaphyseal trabecular bone - *Osx-Cre* mice. 170
Table 6.6 Trabecular histomorphometric indices - *Osx-Cre* mice. 171
Table 6.7 Time related change in metaphyseal cortical bone assessed by micro CT - *Osx-Cre* mice. 175
Table 6.8 Time related change in diaphyseal cortical bone assessed by micro CT - *Osx-Cre* mice. 179
Table A.1 Micro CT of proximal tibiae in PAR_2 null & WT mice - Males. 254
Table A.2 Micro CT of proximal tibiae in PAR_2 null & WT mice - Females. 254
Table A.3 Micro CT of L5 vertebrae in PAR_2 null & WT mice - Males. 255
Table A.4 Micro CT of L5 vertebrae in PAR_2 null & WT mice - Females. 255
Table A.5 Micro CT of midshaft tibial cortex in PAR_2 null & WT mice - Males. 257
Table A.6 Micro CT of midshaft tibial cortex in PAR_2 null & WT mice - Females. 258

Table B.1 Micro CT indices of proximal tibiae in mdx-PAR_2 null & WT mice - Males. 260
Table B.2 Micro CT indices of proximal tibiae in mdx-PAR_2 null & WT mice -Females. 260
Table B.3 Micro CT of midshaft tibial cortex in mdx-PAR_2 null & WT mice - Males. 261
Table B.4 Micro CT of midshaft tibial cortex in mdx-PAR_2 null & WT mice - Females. 262
Table C.1 Selected genes of interest. 264
Table D.1 Metaphyseal cortical indices determined by micro CT - *F2rl1*$^{wt/wt}$ and *F2rl1*$^{fl/fl}$ mice. 268
Table D.2 Time related change in metaphyseal cortical bone assessed by micro CT - *F2rl1*$^{wt/wt}$ and *F2rl1*$^{fl/fl}$ mice. 269
Table D.3 Diaphyseal cortical indices determined by micro CT - *F2rl1*$^{wt/wt}$ and *F2rl1*$^{fl/fl}$ mice. 270
Table D.4 Time related change in diaphyseal cortical bone assessed by micro CT - *F2rl1*$^{wt/wt}$ and *F2rl1*$^{fl/fl}$ mice. 271
Table D.5 Micro CT of tibial metaphysis in *F2rl1*$^{wt/wt}$ and *F2rl1*$^{fl/fl}$ mice - Males. 272
Table D.6 Micro CT of tibial metaphysis in *F2rl1*$^{wt/wt}$ and *F2rl1*$^{fl/fl}$ mice - Females. 272
Table D.7 Micro CT of metaphyseal cortex in *F2rl1*$^{wt/wt}$ and *F2rl1*$^{fl/fl}$ mice - Males. 273
Table D.8 Micro CT of metaphyseal cortex in *F2rl1*$^{wt/wt}$ and *F2rl1*$^{fl/fl}$ mice - Females. 274
Table D.9 Micro CT of midshaft cortex in *F2rl1*$^{wt/wt}$ and *F2rl1*$^{fl/fl}$ mice - Males. 275
Table D.10 Micro CT of midshaft cortex in *F2rl1*$^{wt/wt}$ and *F2rl1*$^{fl/fl}$ mice - Females. . 276
Table E.1 Micro CT of tibial metaphysis in *Osx-Cre* mice - Males. 280
Table E.2 Micro CT of tibial metaphysis in *Osx-Cre* mice - Females. 280
Table E.3 Micro CT of metaphyseal cortex in *Osx-Cre* mice - Males. 281
Table E.4 Micro CT of metaphyseal cortex in *Osx-Cre* mice - Females. 281

Table E.5 Micro CT of midshaft cortex in *Osx-Cre* mice - Males. 282
Table E.6 Micro CT of midshaft cortex in *Osx-Cre* mice - Females. 282

LIST OF ABBREVIATIONS

Ad.Ar	Adipocyte Area
Ad.N	Adipocyte Number
ALP	Alkaline Phosphatase
ANCOVA	Analysis of Covariance
ANOVA	Analysis of Variance
AP-1	Activator protein 1
Avg.Po.V	Average Pore Volume
B.Ar	Bone Area
B.Pm	Bone Perimeter
B.S	Bone Surface
BAPNA	Benzyl-dl-arginine para-nitroanilide
BFR	Bone Formation Rate
bHLH	Basic Helix-Loop-Helix
BLAST	Basic Local Alignment Tool
BMP	Bone Morphogenetic Protein
BMPR	Bone Morphogenetic Protein Receptor
BSA	Bovine Serum Albumin
BV	Bone Volume
BV/TV	Bone Volume Fraction
cAMP	Cyclic Adenosine Monophosphate
CBF	Core Binding Factor
CEBP	CCAAT/Enhancer-Binding Proteins
Col1a1	Collagen Type 1α1
Conn.D	Connectivity density
COX-1/2	Cyclooxygenase 1/2
Cre	Cre recombinase
Ct.Ar	Cortical Area
Ct.Ar/Tt.Ar	Cortical Area Fraction
Ct.Po	Cortical Porosity
Ct.Th	Cortical Thickness
DA	Degree of Anisotropy

df	Degree of freedom
DKK	Dickkopf
Dlx	Distal-less-related
DMD	Duchenne Muscular Dystrophy
DMSO	Dimethyl Sulfoxide
dNTP	Deoxynucleotide Triphosphates
DSH	Disheveled
ERα/β	Oestrogen Receptor α/β
ERK1/2	Extracellular Signal-Regulated Kinase-1/2
Fl	First Filial Generation
F2rl1	Coagulation Factor II (Thrombin) receptor-like 1
FCS	Foetal Calf Serum
FGF	Fibroblast Growth Factor
FGFR	Fibroblast Growth Factor Receptor
FZD	Frizzled Receptor
GLI	Glioma-Associated Oncogene Homolog 1
GOIs	Genes of interest
GPCR	G protein Coupled Receptor
GTP	Guanosine Triphosphate
HH	Hedgehog
hMSC	human Mesenchymal Stem Cell
IGF	Insulin-Like Growth Factor
IHH	Indian Hedgehog
IKKα/β	Inhibitory κB Kinase α/β
IL-6	Interleukin-6
J	Polar Moment of Inertia
JNK	c-Jun N-terminal Kinase
KLK	Kallikrein
KO	Knockout
kVp	Peak Kilovoltage
LEF/TCF	Lymphoid Enhancer-binding Factor/T Cell Factor
LPL	Lipoprotein Lipase
LRP	Low-density lipoprotein Receptor-related Protein

M-CSF	Macrophage Colony Stimulating Factor
Ma.Ar	Marrow Area
Ma.Dm	Marrow Diameter
Ma.Dn	Marrow Density
MAPK	Mitogen-Activated Protein Kinase
MAR	Mineral Apposition Rate
Micro CT	Microcomputed Tomography
MiRs	Micro RNAs
MMP	Matrix Metalloproteinase
MSCs	Mesenchymal Stem Cells
MS/BS	Mineralising Surface
N.Ad	Number of Adipocytes
N.Ob	Number of Osteoblasts
N.Oc	Number of Osteoclasts
O.Ar	Osteoid Area
O.Pm	Osteoid Perimeter
O.Th	Osteoid Thickness
Ob.Pm	Osteoblast Perimeter
Oc.Pm	Osteoclast Perimeter
Ocn	Osteocalcin
OMD	Osteomodulin
OPG	Osteoprotegerin
Osx	Osterix
OVX	Ovariectomised
PAR	Protease-Activated Receptor
PBS	Phosphate Buffered Saline
PCR	Polymerase Chain Reaction
PDGF	Platelet-Derived Growth Factor
PFA	Paraformaldehyde
PGE2	Prostaglandin E2
PI 3-K	Phosphatidylinositol 3-Kinase
PKB	Protein Kinase B
PKC	Protein Kinase C

Po.Dn	Pore Density
Po.N	Pore Number
Po.V	Pore Volume
Pparg	Peroxisome proliferator-activated receptor γ
Prx1	Paired related homeobox 1
PTC1/2	patched receptors 1/2
PTH	Parathyroid Hormone
PTHR	Parathyroid Hormone Receptor
PTHrP	Parathyroid Hormone-related Protein
qPCR	Quantitative Polymerase Chain Reaction
RANK	Receptor Activator of Nuclear Factor-κB
RANKL	Receptor Activator of Nuclear Factor-κB Ligand
RT-PCR	Reverse Transcription Polymerase Chain Reaction
Runx2	Runt-related transcription factor 2
SE_{diff}	Standard Error of difference
SFRPs	Secreted Frizzled-Related Proteins
SHH	Sonic Hedgehog
SLIGKV	Ser-Leu-Ile-Gly-Lys-Val, human PAR_2 activating peptide
SLIGRL	Ser-Leu-Ile-Gly-Arg-Leu, murine PAR2 activating peptide
SMI	Structural Model Index
Smo	Smoothened Receptor
Sost	Sclerostin
T.Ar	Tissue Area
Tb.N	Trabecular Number
Tb.Sp	Trabecular Separation
Tb.Th	Trabecular Thickness
TGF-β	Transforming Growth Factor-β
TMD	Tissue Mineral Density
TNF-α	Tumour Necrosis Factor-α
Tt.Ar	Total Cross-sectional Area
Tt.N	Total Number of Cells
TV	Total Volume
TZD	Thiazolidinediones

UV	Ultraviolet
wk	Week(s)
Wnt	Wingless Type Protein
WT	Wild Type
/max	Maximum Moment Of Inertia
/min	Minimum Moment Of Inertia

CHAPTER 1: INTRODUCTION AND LITERATURE REVIEW

1.1 Bone

1.1.1 Architecture and Function

Bone, the major constituent of the skeleton, is a type of dense connective tissue. Despite the general tendency to consider bone as a purely mechanical entity, bone is in fact a dynamic vital tissue that is highly vascularised, metabolically active and tightly regulated. As a part of the skeleton, the function of bones is to provide soft tissue support, leverage for locomotion, protection for vital organs, a repository for minerals, fat storage and haematopoiesis (Harada and Rodan 2003).

Based on microscopic organisation of bone matrix and its composition, there are two types of bone commonly recognised. In primary bone tissue also known as woven bone, collagen fibres are randomly organised and the lattice of intermingling fine and coarse collagen fibres gives it a woven appearance. It is predominantly found in the foetal skeleton and within the primary spongiosa, nonetheless, it is also formed in adults as a result of fractures or exposure to a variety of pathologic conditions such as parathyroidism and Paget's disease as well as early in the course of systemic treatment with fluoride. Secondary bone tissue also known as lamellar bone in contrast has highly organised layers of collagen that are oriented at slightly alternating angles. This gives the lamellar bone its unique mechanical rigidity. Lamellar bone makes up almost all the bone in the adult skeleton (Jowsey 1977; Clarke 2008; Reznikov et al. 2014).

Based on grossly visible structure, bone can be classified as two distinct types. Cortical or compact bone, which comprises up to 80% of the adult skeleton is a solid and mechanically durable type of bone with a low rate of remodelling that as the name implies, covers virtually all bones of the skeleton (Reznikov et al. 2014). Cortical bone is made up of concentric cylindrical lamellae surrounding vascular structures each collectively comprising an osteon or Haversian system. Depending on the species, cortical bone

typically contains less than 5% pores. Pores are sites of resorption and new bone deposition, which occur during the process of bone remodelling. As a result of such remodelling, cortical bone in adults generally becomes thinner over time (Clarke 2008). Trabecular or cancellous bone, on the other hand, is less dense and more porous than cortical bone, comprising up to 20% of bone mass and 80% of bone surface in the adult skeleton. It has a higher rate of remodelling as compared to cortical bone (Hadjidakis and Androulakis 2006; Evans and de Lahunta 2013). The structural unit in trabecular bone is the trabecula. Trabeculae are rods and plates of lamellar bone that form a honeycomb meshwork of bony structures harbouring the marrow and vascular sinusoids (Jowsey 1977; Clarke 2008). Trabecular bone is generally found inside metaphyses and epiphyses of long bones, bodies of vertebrae, or sandwiched between the cortical tables of flat bones (diploë; Hoyte 1971). Due to a high turnover rate, trabecular bone comprises the most metabolically active compartment of the skeleton with a crucial role in mineral homeostasis (Kini and Nandeesh 2012).

Despite such structural and metabolic differences, cortical and trabecular bones share the very basic features of their ultrastructure and cellularity. No matter what shape or structure, bone is always composed of cells and extracellular matrix. The cellular component includes osteoblasts, osteocytes, bone-lining cells, osteoclasts, fibroblasts and supporting endothelial cells. The matrix itself is made up of a hydrated organic phase also called osteoid and a mineral phase which is mostly hydroxyapatite (Reznikov et al. 2014).

1.1.2 Osteoblasts

Osteoblasts are the cells responsible for forming bone that are derived from mesenchymal stem cells (MSCs). Osteoblasts are normally found in clusters of basophilic cuboidal cells overlying the active fronts of ossification associated with both primary and secondary bone formation foci. Research has shown that such close proximity of osteoblasts is essential for their communication and function (Civitelli et al. 1993). It is also thought that such organisation is crucial in the deposition of large masses of parallel fibres of collagen that is necessary for efficient bone formation (An and Martin 2003; Hadjidakis and Androulakis 2006). The cytoplasm in osteoblasts contains abundant cytoskeletal macromolecules including actin and myosin, and their cytoplasmic membranes possess numerous extensions through which they connect with other osteoblasts and embedded osteocytes as

well as the lining cells (An and Martin 2003). Cadherins are a group of proteins that function to connect actin fibres of neighbouring cells. Different populations of osteoblasts express different ratios of these macromolecules, and the ratio may change during various stages of differentiation (Shin et al. 2000).

Osteoblasts are responsible for synthesis, deposition and mineralisation of new bone matrix. Osteoblasts produce a large number of biomolecules that include several structural proteins e.g. collagen type I, small amounts of collagen type V and sialoproteins; growth factors, e.g. transforming growth factor-β (TGF-β), bone morphogenetic proteins (BMPs), insulin-like growth factor (IGF), fibroblast growth factor-2 (FGF-2), platelet-derived growth factor (PDGF), receptor activator of nuclear factor-κB ligand (RANKL) and osteoprotegerin (OPG); and enzymes, e.g. latent proteases, alkaline phosphatase (ALP) and pyrophosphatase (Florencio-Silva et al. 2015).

As osteoblasts express cellular receptors of the growth factors they secrete, it is thought that they are partly regulated by autocrine and paracrine mechanisms (Tonna and Sims 2014). Osteoblasts also respond to systemic hormones through a range of receptors for such factors as parathyroid hormone (Rizzoli et al. 1986), insulin (Levy et al. 2009), the active form of vitamin D3 (Zanello and Norman 2004), progesterone (Wei et al. 1993), oestrogen (Arts et al. 2011), androgens (Colvard et al. 1989), thyroid hormone and other steroids (Bland 2000). Additionally, osteoblasts influence osteoclastogenesis through expression of RANKL, OPG and macrophage colony stimulating factor (M-CSF; Kodama et al. 1991; Takami et al. 1999; Katagiri and Takahashi 2002).

Osteoblastogenesis involves a series of complex gene expression patterns that leads to differentiation of osteoblasts from MSCs. The process entails four stages of lineage commitment, proliferation, extracellular matrix maturation and matrix mineralisation (Taipaleenmäki et al. 2012). During stage 1, MSCs are triggered, mainly by bone morphogenetic proteins (BMPs), to become committed osteoprogenitor cells. Osteoprogenitor cells of stage 2 are characterised by a high rate of proliferation and high levels of expression of osteoblast specific transcription factors, in particular Runt-related transcription factor 2 (Runx2) and Osterix as well as collagen type I. During stage 3, osteoprogenitor cells become preosteoblasts and start to express alkaline phosphatase

(ALP), collagen type I and bone sialoprotein II under the effect of parathyroid hormone (PTH) and hence the production of bone matrix is initiated. In stage 4, preosteoblasts differentiate into mature osteoblasts and exhibit a slightly different gene expression pattern now including osteocalcin, collagenases, osteopontin and bone sialoprotein II under the influence of IGF1 and prostaglandin E2 (PGE2; Titorencu et al. 2014). Some of the important features of osteoblastogenesis are reviewed under section 1.3.

1.1.3 Osteocytes

Near the completion of a matrix-secreting cycle, some mature osteoblasts become entrapped in newly formed bone and further differentiate into osteocytes. Osteoblasts that are just entrapped in the not yet fully mineralised matrix (osteoid) represent a transitional stage between osteoblasts and osteocytes with distinctive morphological characteristics (Franz Odendaal et al. 2006). These are sometimes referred to as osteocytic-osteoblasts or osteoid-osteocytes. There is evidence that these cells are involved in the mineralisation of matrix (Palumbo 1986).

The space within which an osteocyte resides is called a lacuna. Lacunae are connected to one another through a network of thin canaliculi through which osteocytes are connected (Jowsey 1977; Menton et al. 1984). Between the walls of the lacunae or canaliculi and cells or their processes, an extracellular fluid exists in which osteocytes are bathed. This fluid is believed to facilitate nutrient and gas exchange and may be important in transmitting the mechanical forces to osteocytes (Wang et al. 2004).

Osteocytes are strain-sensitive cells able to transduce mechanical forces into signals necessary for regulation of remodelling and modelling activities aimed at mechanical and functional adaptation of bone (Robling et al. 2006). The lacunocanalicular network is believed to be essential for this mechanism (Burger and Klein-Nulend 1999). It has been shown that osteocytes rely heavily on Wnt-β-catenin signalling to execute their functions (Robling 2017).

Osteocytes contribute to maintenance of old bone by recruiting osteoclasts and osteoblasts in response to microdamage (Kennedy et al. 2012). Recruitment of osteoclasts occurs when osteocytes die as a result of apoptosis or necrosis (Bonewald 2011). Apoptotic cells are

known to generate apoptotic bodies that express RANKL and induce localised bone resorption (Bonewald 2011).

1.1.4 Bone Lining Cells

Bone-lining cells are flat, elongated cells that are found virtually on any bony surface that is not being modified by osteoblasts or osteoclasts. Classically, these cells are regarded as quiescent osteoblasts that are not embedded in matrix at the end of their bone forming cycle (Menton et al. 1984; Nijweide et al. 1986; Iñiguez-Ariza and Clarke 2015). They have been found in the endosteal lining of the marrow cavity as well as periosteum and also in association with walls of Haversian canals and are thought to form a barrier participating in ion transport and mineral homeostasis (Menton et al. 1984; Miller et al. 1989; Iñiguez-Ariza and Clarke 2015), bone remodelling (Everts et al. 2002), mechanoreception (Chow et al. 1998) and haematopoiesis (Deldar et al. 1985).

1.1.5 Osteoclasts

Osteoclasts, are multinucleated cells of myeloid lineage that are formed by fusion of their mononuclear haematopoietic precursors. They are the largest cells in bone (>40 μm) and are responsible for bone resorption (Hadjidakis and Androulakis 2006; Boyce 2013a). It has been shown that osteoclast differentiation is dependent on osteoblastic interactions with their progenitor cells and subsequent activation (Takami et al. 1999). Likewise, it has also been shown that osteoclasts can recruit osteoblasts at the end of each resorption cycle. This could in part explain the coupling of bone formation and resorption as a means of stabilising the total bone mass (Matsuo and Irie 2008; Sims and Martin 2014).

Regulation of osteoclasts occurs at two levels: (1) differentiation and (2) mature osteoclast activity (Boyce 2013b). Osteoclastogenesis and osteoclastic function depend largely on the initiation of various intracellular mechanisms in the haematopoietic precursor cells upon activation of cell surface receptor activator of nuclear factor-κB (RANK) by its specific RANK ligand (RANKL; Wada et al. 2006). Osteoblasts actively participate in the coordination of osteoclast differentiation and function by expressing membrane bound RANKL although other cell types such as T cells may contribute by shedding RANKL in the soluble form. OPG, a decoy receptor also produced by osteoblasts, is a known regulator

and functional inhibitor of the RANKL/RANK system (Singh et al. 2012). Osteoblasts also produce M-CSF, which promotes osteoclastogenesis (Kimble et al. 1996).

1.1.6 Bone Extracellular Matrix

Bone matrix is the extracellular substance of bone. It is comprised of a mineral phase that constitutes 50 to 70% of the weight of bone and an organic matrix also called osteoid. The mineral phase is mostly composed of calcium hydroxyapatite $[Ca_3(PO_4)_2]_3.Ca(OH)_2$ crystals and small amounts of carbonate, magnesium and acid phosphate (Clarke 2008). Compared to geologic hydroxyapatite, these crystals are much smaller and more soluble, which facilitates participation in mineral metabolism (Clarke 2008).

The organic matrix is made of collagen (30% of bone weight) and non-collagenous proteins. Collagen type I (two $\alpha 1$ and one $\alpha 2$ chains) makes up to 90% of the organic matrix. The noncollagenous components of the bone matrix comprise various structural proteins and growth factors that have been produced by the osteoblasts (Hadjidakis and Androulakis 2006; Titorencu et al. 2014). Following the release by osteoblasts of collagen monomers into the extracellular space and their subsequent assembly into triple helical procollagen molecules, the mineral phase begins to form in both intra- and interfibrillar spaces (Young 2003).

Several matrix proteins facilitate this transition from osteoid to fully mineralised bone matrix. The most abundant noncollagenous matrix protein, osteonectin is one such protein that also influences cell cycle and acts as a positive bone formation regulator (Boskey and PG 2013). Osteopontin, bone sialoprotein and osteocalcin are other regulators of matrix mineralisation (Boskey and PG 2013).

Alkaline phosphatase (ALP), is also believed to play a role in matrix mineralisation by increasing local phosphate concentrations. It is delivered into the newly forming osteoid by the osteoblasts via 50 to 200 nm matrix vesicles. ALP acts to cleave various biomolecules in order to release their phosphate ions. Hydroxyapatite crystallisation is normally initiated at these foci and the crystals are then transported into the matrix by unknown mechanisms (Orimo 2010). Pyrophosphatase is another product of osteoblasts that breaks down

pyrophosphates that accumulate in the extracellular fluid and inhibit hydroxyapatite formation and matrix mineralisation (Murshed 2005).

1.1.7 Bone Development, Growth and Ageing

Within the foetal bone anlagen, mesenchymal cells start condensing by expressing specific adhesion molecules (Hall and Miyake 2000). Notably in the flat bones, the cells of these condensations directly differentiate into osteoblasts and form bone through the process of intramembranous ossification (Kronenberg 2003). In all other areas however, these rudimentary condensations turn into cartilage before being replaced by bone. This phenomenon is called endochondral ossification and is responsible for the majority of skeletal development (Kronenberg 2007).

Early in the process, condensed mesenchymal cells start differentiating into chondrocytes (Kronenberg 2007). As chondrocytes proliferate, they also secrete the cartilage matrix (Akiyama et al. 2002). In the centre of the cartilage model, some cells stop proliferating and start to undergo hypertrophy. An array of factors expressed and secreted by hypertrophic chondrocytes is believed to be a major orchestrator of the subsequent phenomena resulting in mineralisation and degradation of the cartilage matrix and initiation of osteogenesis (Carlevaro et al. 2000; Thompson et al. 2015).

Having undergone hypertrophy, chondrocytes undergo a unique type of programmed cell death which coincides with formation of a bone collar around the model. This will eventually form the cortex of the mature bone (Mackie et al. 2008a; Thompson et al. 2015). Osteoblast precursors gradually migrate from this collar into the paths cleared by chondroclasts and blood vessels and deposit osteoid using the scaffold provided by the cartilage matrix. This is now called the primary centre of ossification (Olsen et al. 2003). The growth of the bone model at this stage largely depends on the proliferation capacity of the chondrocytes surrounding the primary ossification front (Kronenberg 2003). As bone grows, haematopoietic cells that have also arrived with the blood vessels contribute to the primitive bone marrow (Olsen et al. 2003).

Eventually, within both proximal and distal extremities, what will later be the epiphyses, the same series of differentiating chondrocytes, hypertrophic chondrocytes and bone

deposition ensues, giving rise to the formation of secondary centres of ossification. The chondrocytes left between the primary and secondary centres of ossification will form the growth plate and continue to proliferate until adolescence providing the longitudinal physeal growth of long bones (Hunziker 1994; Kronenberg 2003).

With age, as the number of chondrocytes and their rate of proliferation in the growth plates decline, the rate at which ossification takes place exceeds that of the growth plate expansion leading to a complete loss of growth plate and cessation of longitudinal growth in adults. There is a well-established correlation between fusion of the growth plate and surging oestrogen levels during puberty (Weise et al. 2001).

Once bone is formed, it will be constantly remodelled throughout life. Remodelling comprises back to back cycles of old-bone removal and its replacement with new tissue as a result of coupling of osteoclastic-osteoblastic activities. Each remodelling cycle consists of three phases. During the first phase, osteoclasts differentiate, become functional and start to resorb bone (Boyce et al. 2012). During the second phase, also called reversal, the surface of the resorbed cavity is covered by lining cells that function to retouch the surface and regulate the differentiation and function of osteoblasts (Everts et al. 2002). Once formed, these osteoblasts fill the resorbed cavity with newly formed bone, which concludes a remodelling cycle (Boyce et al. 2012).

It is currently thought that osteocytes and perhaps bone lining cells are the initiators of the remodelling of bone (Chow et al. 1998; Robling et al. 2006; Kennedy et al. 2012) although T-lymphocytes have been suggested to be also important (Boyce et al. 2012). Osteocytes and bone lining cells sense the mechanical loading of bone as well as presence of microdamage and guide the next wave of remodelling to critical locations. The result is a constant adaptation of bone form and architecture to daily mechanical needs as well as removal of structural flaws that could accumulate and lead to mechanical failure (Robling et al. 2006). Remodelling is also regulated, both directly and indirectly, by hormonal mechanisms and is important in homeostasis of calcium and ions (Siddiqui and Partridge 2016).

Even under normal circumstances, remodelling is never fully effective in restoring all the bone that is being resorbed. As a result, after the initial maximal bone mass accumulation usually around puberty, bone mass tends to drop over the years. Loss of bone mass, therefore, is an unavoidable consequence of ageing. Another consequence of a discrepancy between the rates of bone resorption and formation is appositional bone growth or surface accretion. As a result of a higher rate of osteoblastic activity on the periosteal surfaces and a greater rate of resorption at the endosteal surfaces, over time, the overall diameter of the long bone and its marrow cavity increase whilst the cortical thickness also gradually declines (Dequeker 1971; Parfitt 1984). Appositional growth continues over an individual's life time although its rate decreases substantially with ageing (Epker and Frost 1965; Epker and Frost 1966).

1.1.8 Inflammation-Induced Bone Loss

Chronic inflammation of almost any aetiology is often associated with bone loss. This occurs through either the limiting effect of inflammation on bone formation, promotion of bone resorption or a combination of both. Evidence for a direct involvement of inflammatory mediators in osteoblastic differentiation and bone formation exists. One such mediator is tumour necrosis factor-α (TNF-α) which can inhibit the differentiation of calvarial osteoblasts *in vitro* (Gilbert et al. 2000). There is evidence that TNF-α does so by stimulating the secretion of dickkopf-1 (DKK1), which in turn could inhibit local bone formation through a suppressive effect on osteoblastogenesis (Diarra et al. 2007)see section 1.3.2.3). Similar studies also indicate that the proinflammatory cytokine, interleukin-6 (IL-6), can either stimulate (Fukuyo et al. 2014; Bastidas-Coral and Bakker 2016) or inhibit osteoblastogenesis (Kaneshiro et al. 2014).

Osteoclastic differentiation and function, on the other hand, are well known to be stimulated by various proinflammatory cytokines, e.g. IL-6, IL-11, prostaglandin E2 (PGE2), TNF-α, etc. (Redlich and Smolen 2012). The RANKL-RANK system is the key instructive signal in the process of osteoclastogenesis (Nagy and Penninger 2015). Research so far indicates that upregulation of RANKL by cells of the osteoblastic lineage (Yasuda et al. 1998; Jimi et al. 2004; Baum and Gravallese 2013) and perhaps B cells and activated T lymphocytes (Kong et al. 1999; Kawai et al. 2006) is the major mechanism through which these cytokines exert their pro-osteoclastogenic effects (Hardy and Cooper 2009). Evidence also

suggests that osteocytes can be induced to undergo apoptosis by some of these factors, which results in the generation of apoptotic bodies that express RANKL and thus induction of localised bone resorption (O'Brien et al. 2013; Algate et al. 2015).

Duchenne muscular dystrophy (DMD) is a clinical example of a situation in which bone resorption and remodelling indices are heightened due to inflammatory muscle disease (Rufo et al. 2011). Patients with DMD lack a protein (dystrophin) that links the contractile apparatus directly to the extracellular matrix (Kunkel 1986; Hoffman et al. 1987; Yiu and Kornberg 2015). Without dystrophin, eccentric contraction of muscle fibres causes microdamage at the level of cell membranes and cytoskeleton culminating in disruption of calcium homeostasis and cell necrosis. This is compensated by regeneration during the earlier phase of the disorder which ceases later due to ageing and exhaustion of myoblasts followed by extensive fibrosis (Deconinck and Dan 2007).

Studies have found that patients with muscular dystrophy suffer reduced bone mineral density, structural integrity and biomechanical strength with severe clinical and life expectancy implications (Larson and Henderson 2000; Novotny et al. 2011). These observations have been often explained in the context of glucocorticoid therapy (Morgenroth et al. 2012), reduced mechanical load due to altered muscle mechanics (Novotny et al. 2011) and lack of dystrophin (Nakagaki et al. 2011). More recently however, studies have suggested that chronic muscle inflammation (and proinflammatory cytokines) play important roles in the process (Rufo et al. 2011; Rufo et al. 2013; Abou Khalil et al. 2014). Muscles of DMD patients show various chronic inflammatory changes including elevated cytokines, complement system activation and infiltration by inflammatory cells (Haslett et al. 2002; Kharraz et al. 2014). These patients also have elevated serum IL-6 levels which is suggested to be one of the main reasons behind bone loss observed in DMD (Rufo et al. 2011).

The mdx mouse is a model of DMD, which naturally lacks dystrophin due to a mutation in exon 23 of the dystrophin gene resulting in the absence of the protein (Sicinski et al. 1989). As a result, these mice develop an analogous phenotype to that of the human version of DMD (Coulton et al. 1988). The mdx phenotype is characterised by muscle fibre degeneration, increased circulating creatine kinase levels, fibre size variability and centrally

nucleated fibres (Rodrigues et al. 2016). Due to the extent of regeneration and upregulation of utrophin, however, the phenotype is considered milder than the human DMD because there is less accumulation of fibrofatty tissue (Grady et al. 1997; Rodrigues et al. 2016). As a result, the lifespan of mdx mice is only diminished by 25% as opposed to the 75% decrease in human patients. The disease in mdx mice has been classically defined to occur in a few stages: at 1 to 2 weeks, muscles appear normal; from 3 to 6 weeks, muscles undergo extensive necrosis which is followed by the third stage of substantial regeneration such that muscles appear hypertrophic and swollen; this continues until mice are approximately 15 months of age after which more severe symptoms such as cardiomyopathy ensue (Bostick et al. 2009; McGreevy et al. 2015).

Work on bone strength and quality in mdx mice overall indicates their close resemblence to human disease. Four and 18 week old mdx mice show lower ultimate load, smaller cross sectional area and thinner cortices than the wildtypes in their tibiae (Anderson et al. 1993). Although in one occasion, authors report stronger, wider and denser femurs in 16 week old mdx mice compared to wildtypes, the results have been explained by relative weight to bone ratios which remain similar to normal mice (Montgomery et al. 2005). Other more recent observations indicate significantly lower tibial metaphyseal BV/TV, Tb.N and a higher Tb.Sp in 7 week old and in 6- and 24 month old mdx mice than observed in their wildtype counterparts. These mice also have lower Tt.Ar and Ct.Ar in their tibial midshafts with a consequent reduced moment of inertia and mechanical strength (Novotny et al. 2011; Rufo et al. 2011). Previous works have shown that like human DMD patients, mdx mice exhibit an increased inflammatory profile (i.e. increased IL-6 levels) which is accompanied by increased osteoclastic parameters and bone resorption (Novotny et al. 2011; Rufo et al. 2011).

Rheumatoid arthritis (RA) and periodontitis are two other examples of inflammatory diseases that are associated with bone loss. RA is an autoimmune disease that manifests as local erosive lesions of cartilage and bone within joints and is often accompanied by a gradual generalised osteoporosis (McInnes and Schett 2017). The disease is marked by high rates of osteoclastogenesis and osteoclastic activity (Gravallese et al. 1998) which is caused by the pro-inflammatory cytokines such as TNF-α, IL-1, IL-6 and IL-17 (McInnes et al. 2015).

Periodontal desease is the inflammation of tooth supporting structures as a result of microbial overgrowth and is characterised by formation of periodontal pockets and alveolar bone loss (Joshi et al. 2014). The bacteria produce a range of toxins and enzymes that trigger host inflammatory mechanisms. Here too, inflammatory cytokines are responsible for the induction of osteoclastic bone resorption, which results in alveolar bone loss (Pers et al. 2008; Algate et al. 2016). Recent studies suggest an association between periodontitis and the systemic bone loss of osteoporosis (Wang and McCauley 2016; Anbinder et al. 2016).

1.2 Adipose Tissue

1.2.1 Morphology and Function

Adipose tissue (or fat) is a loose connective tissue mostly made of adipose cells or adipocytes. Preadipocytes, endothelial cells, macrophages and perhaps fibroblasts, collectively referred to as the stromal-vascular fraction, are the other constituents of the adipose tissue (Geloen et al. 1989b; Bourin et al. 2013). Multipotent stem cells are also found in this compartment and have recently been exploited for a variety of clinical and research purposes (Zuk et al. 2002; Rodriguez et al. 2005). Classically, adipose tissue is thought of as the body's main energy storage system in the form of various lipids that could be redistributed to other organs in times of need (Zimmermann et al. 2004; Pellegrinelli et al. 2016). It has also been noted as an excellent heat insulator that also provides protection for the underlying/engulfed tissues and internal organs (LeBlanc 1954; Rabkin 2007; Pellegrinelli et al. 2016). Nevertheless, only recently have various endocrine/paracrine functions been attributed to this tissue and now adipose tissue is widely accepted as a distinct endocrine organ (Scherer 2006; Wozniak et al. 2009).

Beside roles in steroidogenesis (Mohamed-Ali et al. 1998), adipose tissue has been found to actively participate in synthesis and secretion of hormones, i.e. leptin (Zhang et al. 1994), adiponectin (Maeda et al. 1997) and resistin (Steppan et al. 2001) as well as a variety of other adipokines (Trayhurn and Beattie 2001; McGown et al. 2014). Adipose tissue is also highly involved in the homeostasis of glucose as has been shown by the multitude of abnormalities present in lipodystrophic mice (Moitra et al. 1998; Shimomura et al. 1998). Additionally, the proliferating preadipocytes express markers of the monocyte-macrophage

lineage and exhibit phagocytosis implying a direct role for the adipose tissue in inflammation (Cousin et al. 1999). Adipose tissue is distributed across the body in particular anatomic locations, referred to as fat depots. Almost 80% of body fat is stored in the subcutaneous depot. The rest is distributed in a sex-dependent manner throughout the viscera, bone marrow and the intermuscular tissue (Arner 1997; Pellegrinelli et al. 2016). Research has shown that fat of various locations may possess various biochemical profiles which might be of interest when pathologies such as diabetes and inflammatory conditions are studied (Ibrahim 2010). Whilst some depots are more associated with pathology, i.e. visceral fat, it is suggested that some may possess metabolic and physical protection characteristics (Rabkin 2007; Porter et al. 2009).

Two types of adipose tissue identified, white and brown fat (Cannon and Nedergaard 2008). Brown adipose tissue is generally more abundant in neonates and is responsible for non-shivering thermogenesis necessary to sustain the new-born (Aherne and Hull 1966). It has been shown that uncoupling protein 1 (UCP1) expressed in mitochondria of brown adipose cells allows the energy pathways of the cell to release the energy in the form of heat rather than being captured in ATP molecules (Fedorenko et al. 2012). For the purpose of this manuscript, any mention of the adipose tissue or adipocytes will only refer to the white fat, unless otherwise specified.

1.2.2 Adipocytes

Adipocytes are the main cellular constituents of the adipose tissue (Geloen et al. 1989b). These are mature terminally differentiated cells that are unable to proliferate, however they may be able to hypertrophy during states of positive energy balance and hormonal disturbances (Geloen et al. 1989a; Rebuffe Scrive et al. 2009). Despite such hypertrophy, a fraction of the gain in adipose tissue mass under such conditions also occurs due to an increase in cell number. This increase is evidently the result of proliferation of preadipocytes and perhaps adipoblasts that are present in the stromal vascular fraction, a capability that would normally continue into adulthood and is well documented in various species (Faust and Miller 1983; Geloen et al. 1989a; Ochi et al. 1991). In fact, it may well be because of this capability of preadipocytes to differentiate postnatally in response to sex specific hormones that gender specific differences in the ratios of fat depots exist (Anderson

et al. 2011). Adipocytes synthesise and secrete a variety of regulatory biomolecules including leptin and adiponectin (McGown et al. 2014).

1.2.3 Adipose Tissue Development and Differentiation

Adipocytes, like osteoblasts, originate from the mesenchyme (Gesta et al. 2007; Tang and Lane 2012) and the prenatal process of adipogenesis has been described to be initiated by condensation of the mesenchymal cells around vascular glomeruli. Glomeruli are extended networks of capillary bed that originate from the earlier small blood vessels. The mesenchymal cells then become putative adipoblasts and later differentiate into preadipocytes (Poissonnet et al. 1983; Gesta et al. 2007). The mesenchymal cells that surround these future fat lobules later condense into the interlobular septa (Poissonnet et al. 1983).

Observations in both porcine and human embryos indicate that the preceding angiogenesis is absolutely essential for adipocyte differentiation (Poissonnet et al. 1983; Hausman and Thomas 1986). Work by Fukumura supports these observations documenting the paracrine interactions amongst endothelial cells to be crucial in mediating the differentiation of preadipocytes (Fukumura et al. 2003; Berendsen and Olsen 2013). Interestingly, adipocytes themselves express a range of angiogenic growth factors that seem to promote the developing adipose capillary network (Li et al. 2002; Panigrahy et al. 2002; Fukumura et al. 2003). Monobutyrin is one such factor and is considered an adipose specific angiogenic factor (Wilkison et al. 1991; Salajegheh 2016). Preadipocytes retain their capacity to proliferate until they complete the final stages of differentiation (Pilgrim 1971). Immature adipocytes may still undergo one or a few cycles of post-confluence mitosis and thereafter permanently lose their ability to divide (Pairault and Green 1979; Sugihara et al. 1988; Rosen and MacDougald 2006). By this time, most cells have well-developed intracytosolic stores of lipids and are round and readily identifiable as mature adipocytes. It has been suggested that downregulation of actin and tubulin towards the end of the differentiation may be partly responsible for these morphological changes (Spiegelman and Farmer 1982; Tang and Lane 2012). At this stage, cells express a variety of early adipogenic markers but importantly lipoprotein lipase (LPL), the transcription factors CCAAT/enhancer-binding proteins (C/EBPs), peroxisome proliferator-activated receptors (PPARs) and sterol regulatory element binding protein-1c (SREBP-1c) also known as

adipocyte determination and differentiation factor 1 (ADD1; Gregoire et al. 1998; Moreno-Navarrete and Fernández-Real 2017). Later during the terminal phase, expression of enzymes involved in triglyceride metabolism will surge as adipocytes become functional. These may include fatty acid synthase, glycerol-3- phosphate dehydrogenase (GPDH), acyl-CoA synthetase and stearoyl-CoA desaturase-1 (Rayalam and Baile 2016). Adipocytes express the receptors for insulin, triiodothyronine, and β-adrenergic receptors during the final stages of differentiation. These hormones are essential regulators of adipocyte differentiation and lipid metabolism (Ailhaud 1982; Rayalam and Baile 2016). Glucocorticoids and growth hormone are other important positive regulators of adipocyte differentiation and function (Lundholm et al. 1985; Catalioto et al. 2009).

1.3 The Reciprocal Relationship Between Bone and Fat

MSCs are pleuripotential stromal cells that are present in the bone marrow and other tissues and are capable of self renewal and differentiation into various lineages such as osteoblasts, adipocytes, chondrocytes, myoblasts, fibroblasts, tenocytes, etc. (Guadix et al. 2017). The exact location of MSCs within tissues has not yet been fully elucidated, but nevertheless, the perception that they reside within the perivascular space has become popular in the past few years (Corselli et al. 2012; James et al. 2012; Corselli et al. 2013). In the bone marrow milieu, MSCs give rise to both osteoblasts and adipocytes (Owen 1988). It is currently accepted that an inverse relationship between osteoblastogenesis and adipogenesis exists, such that one can predominate only at the expense of the other (Bethel et al. 2013). The notion that osteoblastogenesis and adipogenesis are the two ends of the spectrum perhaps arises from the early *in vitro* observations of clonal mesenchymal cells where differentiation into either lineage is accompanied by suppression of the other counterpart (Beresford et al. 1992; Dorheim et al. 1993). It is now believed that this reciprocal relationship might be responsible for the pathology of various clinical conditions affecting bone (Berendsen and Olsen 2014). For instance, the increase in the adiposity of bone marrow and osteoporosis that is observed with ageing can be explained by a decrease in osteogenesis in favour of adipogenesis (Figure 1.1) although other explanations such as lipotoxic and radiotoxic induction of bone resorption are also proposed (Kawai et al. 2009). Notably, ageing has been shown to alter the intrinsic potential of marrow MSCs for differentiation in addition to their biochemical profile, creating an antiosteogenic/proadipogenic microenvironment

(Moerman et al. 2004). A similar feature has been described following disuse or conditions of unloading of the limbs such as during a space flight and microgravity (Minaire et al. 1974; Wronski et al. 1981; Ahdjoudj et al. 2002).

The fate of MSCs is determined by a delicate balance of various hormones, growth factors and nutrients as well as mechanical influences. These physiological forces will then activate lineage specific transcription factors, e.g. Runx2 and PPARγ that result in the respective lineage specific phenotype (Prockop 1997). Accordingly, the osteoblast-adipocyte switch may be best stated to occur just before the determination phase of each lineage i.e. expression of lineage specific transcription factors. Nevertheless, it has been noted that some degree of plasticity still exists following the initial stages of differentiation. For instance, osteoblasts derived from collagenase digestion of human trabecular bone fragments transdifferentiate into adipocytes in the presence of adequate hormonal stimuli (Nöth et al. 2002). Likewise, rabbit marrow-derived adipocytes can revert to a proliferative state and then differentiate into osteoblasts (Bennett et al. 1991).

Finally, the relationship between osteoblasts and adipocytes is further complicated by the endocrine nature of the adipose tissue. The close proximity of bone to marrow fat makes it more likely to be influenced by adipocyte mediated paracrine mechanisms. Such regulation can be both protective, i.e. aromatase conversion of testosterone to oestradiol by adipocytes, and destructive, e.g. production of IL-6 (Gimble et al. 1996; Wang et al. 2016a). Such observations, as well as identification of a number of cellular pathways involved in the osteoblast-adipocyte switch, have caused some to go even further and speculate that osteoporosis may be a form of bone obesity (Rosen and Bouxsein 2006).

1.3.1 Osteoblast/Adipocyte Plasticity in Ageing and Osteoporosis

Some diseases are thought to result from an aberrant coordination of osteoblastogenesis and adipocyte differentiation. Of these, age related osteoporosis has received considerable attention. Osteoporosis is defined as “a skeletal disease characterized by low bone mass and microarchitectural deterioration of bone tissue with a consequent increase in bone fragility and susceptibility to fracture” (Harvey et al. 2013). This could be due in part to a decrease in quantity and quality of bone formation by osteoblasts, and in part to an increased osteoclastic bone resorption or a combination of both (Raisz 2005).

For the purpose of patient evaluation and diagnosis and to facilitate grading of such patients clinically, osteoporosis has classically been viewed as two major categories, namely osteopoenia and established osteoporosis. Osteopoenia is loosely defined as bone mineral density (BMD) values that are at least two standard deviations below the mean of the normal 30 year old population of the same ethnicity and gender. In contrast, established osteoporosis is said to be present when pathological fractures related to decreased bone mass exist (Melton et al. 2005).

It is estimated that one in every three women and one in every twelve men over the age of 50 will ultimately experience at least one osteoporosis related fracture in their life time (Melton et al. 2005). In men only, the incidence of osteoporosis related hip fracture is expected to increase by 310% worldwide by 2050 (Sidlauskas et al. 2014). In terms of premature morbidity and mortality, osteoporosis causes an amount equal to 25,000 healthy years of life lost to Australians per annum costing an estimated value of $7 billion each year (Sambrook et al. 2002).

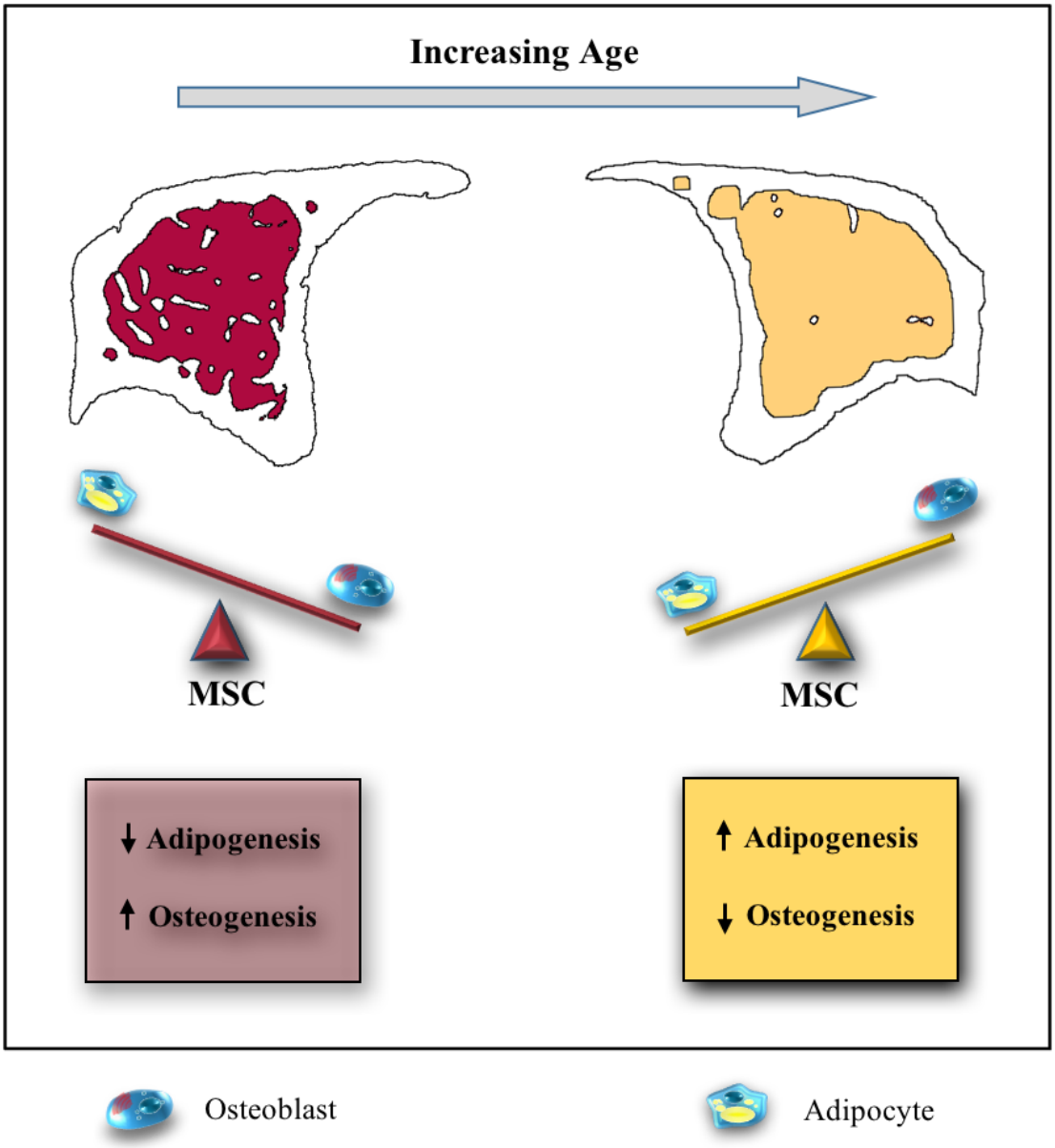


Figure 1.1 Age induced changes in the balance of osteoblastogenesis and adipogenesis.

The age related gradual loss of bone particularly in the trabecular areas is coincident with an increased marrow adiposity. This bone loss could be explained by a decline in bone formation in the face of ongoing/heightened bone resorption. This may be the result of increased adipogenic differentiation of MSCs at the expense of other lineages especially osteoblasts.

Understanding the pathogenesis of osteoporosis has not been straightforward. Multiple factors are believed to interact and confusion often exists as to which is more crucial. Genetic and environmental factors are both to blame. During growth, before the onset of puberty, both male and female bones keep on growing. Upon adolescence, accumulation of

bone mass slows substantially, nonetheless, BMD values continue to rise for some time after puberty. This results in more bone accumulation in males largely due to a later onset of puberty (Sidlauskas et al. 2014). As ageing progresses, bone mass starts to decline in both genders which puts females at a greater risk of osteoporosis due to their earlier cessation of bone accumulation and lower bone mass (Recker and Heaney 1993). Oestrogen insufficiency also contributes to this gender skewed prevalence of osteoporosis mediated by an increased presentation of RANKL on the surface of bone marrow cells leading to higher rates of osteoclastogenesis and bone loss (Eghbali-Fatourechi et al. 2003).

Age dependent bone loss is usually associated with an increased adiposity of the bone marrow (Rozman et al. 1989; Charbord et al. 1996; Kirkland et al. 2002). This has grown into the hypothesis that age dependent osteopoenia, may be a clinical manifestation of a change in cellular niche of MSCs (Moerman et al. 2004; Zhang et al. 2008). Even in premenopausal women with idiopathic osteoporosis, marrow adipocytes are more numerous and voluminous (Duque et al. 2011). Moreover, the amount of marrow fat negatively correlates with trabecular BMD in women and positively correlates with risk of vertebral fractures in men (Schwartz et al. 2013).

Further evidence that supports this view comes from several clinical trials on type 2 diabetic patients where use of thiazolidinediones (TZDs) was found to be associated with loss of bone mass and a predisposition to fractures (Yaturu et al. 2007; Berberoglu et al. 2007; Kahn et al. 2008; Zinman et al. 2010; Aubert et al. 2010). The TZDs are a group of potent oral hypoglycaemic agents that are used either alone or as an adjunct to other drugs in the treatment of type 2 diabetes mellitus. The drug improves insulin sensitivity of muscle and particularly adipose tissue while inhibiting hepatic gluconeogenesis. TZD agents work by directly targeting the transcription factor, peroxisome proliferator-activated receptor γ (PPARγ) and the resulting upregulation of genes in various tissues, particularly fat (Stumvoll and Häring 2002). Nevertheless, *in vitro* application of these agents in mesenchymal cell cultures has been associated with an increased rate of adipogenesis (Kletzien et al. 1992; Sandouk et al. 1993; Lehmann et al. 1995). Notably, use of these agents in various animal models enhances bone loss and marrow adiposity, somehow

mimicking the effects of ageing (Sottile et al. 2004; Lazarenko et al. 2007; Ali et al. 2011; Rzonca et al. 2011).

Given the mutually exclusive nature of adipocyte and osteoblast differentiation of MSCs (Bethel et al. 2013), and data indicating the tendency of aged marrow MSCs to undergo adipogenesis (Moerman et al. 2004), it seems likely that this phenomenon is at least partly responsible for the pathogenesis of osteoporosis.

1.3.2 Coordination of Osteoblastogenesis and Adipogenesis

A great body of research in the past decade has been dedicated to identifying the multitude of biomolecules that govern the fate of MSCs with respect to the bone-fat switch. The cell signalling machinery that drives the differentiation of adipocytes and osteoblasts is extensive with some signalling pathways indispensable for both cell lineages (Figure 1.2). All these signalling pathways culminate in the activation of lineage specific transcription factors, i.e. Runx2 and Osterix in the case of osteoblastogenesis, and C/EBPs and PPAR-γ in the case of adipogenesis. These will be reviewed here.

1.3.2.1 Transcriptional Regulation of Osteoblastogenesis

Runt-related Transcription Factors

Runt-related transcription factors (Runx) also known as core-binding factors (CBFs) are a family of 3 heterodimeric proteins each consisting of two unrelated subunits first isolated and identified in 1994 (Levanon 1994). One of these, Runx2, also known as Cbfa1, is an instructive transcription factor for osteoblastogenesis (Ducy and Karsenty 1995; Merriman et al. 1995; Ducy et al. 1997). At least three different Runx2 isoforms have been reported and data suggests that they slightly differ in terms of function and tissue specificity (Li and Xiao 2007). For example, isoform I is associated with intramembranous ossification whereas isoform II mediates endochondral ossification (Xiao et al. 2004). Isoform III has only been observed in mice (Ducy et al. 1997). The pivotal role of Runx2 in osteoblastic differentiation has been clearly shown in a few loss of function studies (Ducy et al. 1997; Komori et al. 1997; Otto et al. 1997).

During early embryogenesis, Runx2 expression precedes osteoblast formation by a few days and has proven critical in the commitment of mesenchymal cells to the osteoblastic lineage (Otto et al. 1997; Komori 2017). Ectopic expression of Runx2 under the cartilage-specific collagen type II promoter also results in hypertrophy and endochondral ossification (Takeda et al. 2001; Ueta et al. 2001). Postnatally, Runx2 is linked to mechanoreception and adaptation of bone to physical stimuli (Ziros et al. 2002; Kanno et al. 2007). Moreover, evidence supports a Runx2 dependent regulation of bone resorption and a lack of osteoclasts in Runx2 knockout mice (Komori et al. 1997; Geoffroy et al. 2002; Komori 2017). These results emphasise not only the role of Runx2 in embryonic development of osseous tissue, but also underline its significance in the maintenance and function of bone during the postnatal phase.

Runx2 function depends on its ability to bind DNA and upregulate the expression of various osteoblast related genes. Transient transfection of MC3T3-E1 calvarial cells, C3H10T1/2 cells and even mouse skin fibroblasts with *Cbfa1* vector causes upregulation of *Col1a1* (collagen 1α1), *Bsp* (bone sialoprotein), *Spp1* (osteopontin) and *Bglap* (osteocalcin). More recently, Runx2 overexpression studies in several cell lines found that genes involved in ossification, cellular motility, adhesion, chromosome organisation and the mitochondrial milieu are amongst the most commonly regulated (Kuhlwilm et al. 2013; Stephens and Morrison 2014). Runx2 activation in MSCs is considered synonymous with osteoblast specific gene expression and phenotype. Interestingly, Runx2 null mesenchymal cells preferentially differentiate into adipocytes (Kobayashi et al. 2000). Therefore, although not directly involved in adipogenesis, Runx2 activation in MSCs can adequately discount the possibility of adipocyte differentiation from these progenitors (James 2013).

There is considerable evidence that Runx2 plays its regulatory effect in synergy with the downstream transcription factor Osterix, which will be discussed separately (Nakashima et al. 2002; James 2013). Due to the importance of Runx2 in osteoblastogenesis, it is tightly regulated in bone. Such regulation occurs at both transcriptional and posttranscriptional levels. Runx2 is in fact a major target of various cell signalling pathways as will be discussed under section 1.3.2.3.

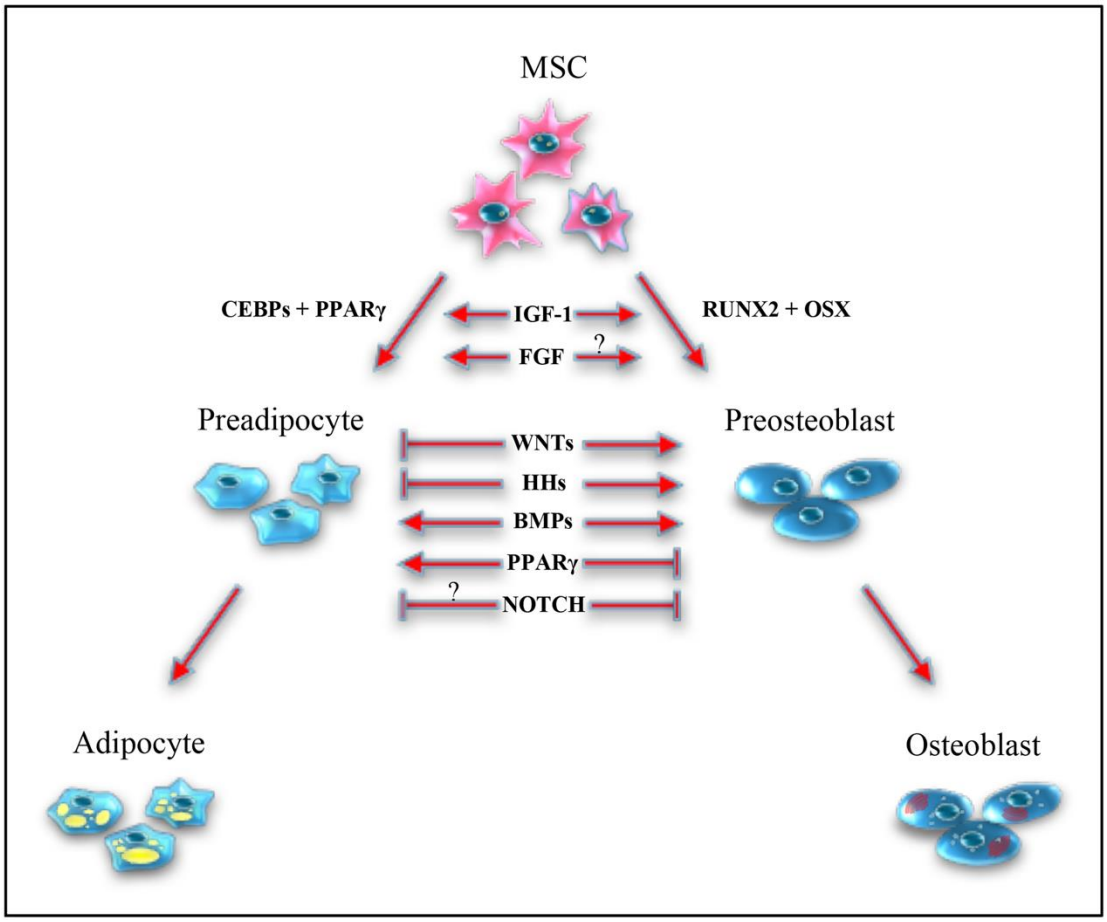


Figure 1.2 Extracellular signals and transcriptional regulation of the bone-fat switch.

The bone-fat switch is said to occur at either the determination phase of MSC differentiation or just before their committing to a given lineage. Multiple transcription factors are at play which seem to interact with multiple signalling pathways. The net balance of these regulating signals drives the MSCs towards a given lineage during the early phase of differentiation. However, preosteoblasts and preadipocytes can later dedifferentiate and re-differentiate into the other lineage in response to changing hormonal factors (adapted form Takada et al., 2009).

Osterix

Osterix (*Osx*) is a vertebrate specific zinc finger transcription factor from the specificity protein (SP) family of transcription factors based on common structural traits (Hojo et al. 2016). As a result of alternate splicing, Osterix possesses two transcriptionally different isoforms which are also differentially regulated: Osterix-1 and Osterix-2. Of these, Osterix-1 is more abundantly expressed (Ortuño et al. 2013; Sinha and Zhou 2013).

Mice lacking Osterix (*Osx*$^{-/-}$) do not develop any osteoblasts whilst the skeletal cartilage patterning remains undisturbed (Nakashima et al. 2002). Osterix plays a pivotal role in differentiation of osteoblasts, function of osteocytes and even resorption of calcified cartilaginous matrix during endochondral ossification (Zhou et al. 2010). Although Osterix promoter contains a Runx2 responsive element and it is suggested that Osterix requires Runx2 for its expression (Nakashima et al. 2002; Nishio et al. 2006), Osterix can still be induced by BMP-2 administration in the complete absence of Runx2 which itself is Dlx5 dependent (Lee et al. 2003). The upstream position of Dlx5 has been further confirmed by similar results (Ulsamer et al. 2008; Hojo et al. 2016).

Osterix, regulates the expressions of osteocalcin, osteonectin, osteopontin and bone sialoprotein II and collagen type I (Nakashima et al. 2002; Ortuño et al. 2013). When overexpressed in association with BMP-6, Osterix also inhibits proliferation of MSCs and induces expression of a novel set of proteoglycans, i.e. osteomodulin (OMD), osteoglycin, and asporin culminating in an increased rate of matrix mineralisation. As expected, knockdown of Osterix, reversed all these responses suggesting a role for Osterix in the terminal phase of differentiation (Zhu et al. 2012). There is evidence that phosphorylation of Osterix is critical for some of its actions (Han et al. 2016).

Osterix additionally regulates the expression of *Col5a3* and *Col5a1* in osteoblasts (Yun-Feng et al. 2010; Wu et al. 2010), and directly binds the promoter region and upregulates VEGF in osteoblasts as well (Tang et al. 2012). The protein is also involved in the expression of all 19 Wnt genes and Wnt target gene *Axin2* in osteoprogenitor cells allowing them to regulate their own proliferation and differentiation (Tan et al. 2014). Physical and functional association of Osterix with Runx2 is essential during the later stages of endochondral ossification by induction of MMP-13 expression in chondrocytes (Nishimura et al. 2012). So far, it has been determined that two mico RNAs (MiRs), MiR-204/211and MiR-113a, both regulators of *Runx2* (and potentially *Sost* and *Alp*) and MiR141/200a, the regulator of *Dlx5*, are targeted by Osterix (Chen et al. 2013).

Miscellaneous Transcription Factors

A large number of transcription and co-transcription factors are involved in the complex regulation of osteoblastogenesis (Fakhry et al. 2013). A number of important transcription factors in this regard are briefly reviewed here.

Activator protein 1 (AP-1) is a dimeric transcription factor that regulates the expression of ALP, collagen type I, collagenase and osteocalcin (Owen et al. 1990). AP-1 is formed by binding of Fos (c-Fos, FosB, Fra-1, Fra-2) and Jun proteins (c-Jun, JunB and JunD; Angel and Karin 1991). Variation in the subset of the factors that form the dimer can confer variability on promoter binding characteristics of AP-1. These subsets seem to be expressed differentially at various stages of osteoblastogenesis, e.g. nuclear fraction levels of all seven subsets are maximal early in the course of differentiation whereas Fra-2 and JunD predominate in the mature osteoblast (McCabe et al. 1996).

Attempts at elucidating the underlying mechanisms behind skeletal abnormalities seen in the X-linked mental retardation syndrome, Coffin-Lowry (CLS), has revealed the critical role of activating transcription factor 4 (ATF4) in the early and late events of osteoblastogenesis. ATF4 is required for timely regulation of bone development during embryogenesis and its deficiency is linked to low bone mass postnatally. Further, ATF4 was found to mediate osteoblast-specific genes particularly collagen type I and osteocalcin in concert with Runx2 (Yang et al. 2004; Xiao et al. 2005).

Distal-less-related DNA-binding homeobox (Dlx) genes comprise six genes organised in three bi-gene clusters: Dlx1/2, Dlx3/4 and Dlx5/6. Dlx genes are important in the development of craniofacial bones and appendage outgrowth during embryogenesis (Robledo et al. 2002; Gordeladze et al. 2010). Targeted disruption in mice of Dlx1 and Dlx2 or both in combination results in various craniofacial defects and presence of ectopic skull features resembling lower vertebrates (Qiu et al. 1997). Dlx5 and Dlx6 null mice similarly show craniofacial and vestibular anomalies as well as abnormal osteogenesis (Acampora et al. 1999; Robledo et al. 2002). Dlx5 is a target of the BMP signalling pathway and a contributor to osteocalcin upregulation by antagonising the inhibition of another homeobox factor Msx2 (Miyama et al. 1999; Shirakabe et al. 2001; Chen et al. 2012).

The Drosophila *msh* gene family is a group of homeodomain-containing proteins that consists of Msx1, -2 and -3. Msx1 and -2 have been shown as important factors in skeletal morphogenesis (Dodig et al. 1999; Gordeladze et al. 2010). Overexpression of Msx2 causes an increased rate of cranial osteoblast differentiation and bone growth (Liu et al. 1999; Dodig et al. 1999). Msx2 deficient mice show abnormal craniofacial bone formation patterns and persistent parietal foramina as a result of defective osteoprogenitor cell proliferation and differentiation. Msx2 inhibits the *Col1a1* promoter and depending on the cell type either stimulates or inhibits that of the osteocalcin gene (Towler et al. 1994; Dodig et al. 1996).

Basic helix-loop-helix (bHLH)-containing transcription factors, Twist 1 and -2 are expressed during the early stages of skeletogenesis (Cakouros et al. 2010). These proteins transiently silence the osteoblastic phenotype by direct interaction with the DNA binding domain of Runx2. The decrease in their expression shortly afterwards, removes the suppressive effect and unleashes osteoblast-specific gene coordination that coincides with the start of skeletogenesis (Ishii et al. 2003; Bialek et al. 2004).

1.3.2.2 Transcriptional Regulation of Adipogenesis

Peroxisome Proliferator-activated Receptor-γ

Peroxisome proliferator-activated receptors (PPARs) are members of the nuclear hormone receptor superfamily of ligand-activated transcription factors. Three related isotypes of the family of PPARs include PPARα, PPARβ and PPARγ (Dreyer et al. 1992; Zhu et al. 1993; Tontonoz et al. 1994a; Kliewer et al. 1994). Like other nuclear receptors, PPAR dependent regulation of transcription requires binding of receptor specific ligands, i.e. fatty acids and eicosanoids (Kliewer et al. 1995; Devchand et al. 1996; Kliewer et al. 1997), although other mechanisms are suggested as well (Gearing et al. 1993; Keller et al. 1993; Shalev et al. 1996; Poirier et al. 1997).

The most studied isotype is PPARγ due to its role in adipogenesis. Use of several thiazolidinedione (TZD) analogues, known to specifically bind and activate PPARγ, invariably induces differentiaton of both pleuripotential or even nonadipogenic fibroblastic cells into adipocytes (Kletzien et al. 1992; Sandouk et al. 1993; Tontonoz et al. 1994b;

Lehmann et al. 1995). Missense mutations of the *PPARγ* gene in humans is associated with lipodystrophy and wildtype-*Pparγ* null chimeric mice do not develop any *Pparγ* null adipocytes (Rosen et al. 1999; Barroso et al. 1999; Agarwal and Garg 2009). PPARγ regulates the expression and activity of several adipose markers such as LPL, adipocyte P2, phosphoenolpyruvate carboxykinase, fatty acid synthase, Glut4, acetyl CoA carboxylase, adipocyte-selective fatty acid binding protein and the insulin receptor (Tontonoz et al. 1994a; Schoonjans et al. 1996; Muruganandan et al. 2008).

Beside the major role PPARγ plays in adipogenesis, considerable data exists indicating that this master transcription factor suppresses osteoblastogenesis by repressing the transcription of *Runx2*, *Osx* and *Dlx5* (Ali et al. 2011; Rzonca et al. 2011). *In vitro* experiments with natural and synthetic ligands show that based on the ligand used, various combinations of pro-adipogenic and anti-osteogenic effects are possible (Venter et al. 2001; Lecka-Czernik et al. 2002). Additionally, *Pparγ* null embryonic cells spontaneously differentiate into osteoblasts but are unable to differentiate into adipocytes, which could be rescued by reintroduction of the *Pparγ* gene (Akune et al. 2004).

In vivo, TZD treated mice show significant reduction in BMD, bone formation rate (BFR), trabecular parameters and osteogenic markers as well as increased marrow adiposity (Ali et al. 2011; Rzonca et al. 2011). Similarly, use of TZD agents in diabetic patients increases the risk of osteoporosis and pathologic fractures due to aberrant bone formation and resorption (Grey 2008). Interestingly, hypomorphic mutation or haplodeficiency of the *Pparγ* gene in mice is associated with increased bone mass and obliterated marrow spaces and cellularity (Akune et al. 2004; Cock et al. 2004). PPARγ, therefore, is one of the key biomolecules involved in the regulation of the adipocyte-osteoblast switch (Berendsen and Olsen 2014).

CCAAT/Enhancer-binding Proteins

C/EBPs include isoforms from the basic-leucine zipper class of transcription factors that bind a CCAAT motif in the promoter/enhancer regions of certain viruses as well as the albumin gene (MacDougald and Lane 1995). The six recognised members include C/EBPα, C/EBPβ, C/EBPδ, C/EBPγ, C/EBPε and CHOP (C/EBP homologous protein;

Tanaka et al. 1997). Of these, C/EBPα, C/EBPβ and C/EBPδ are proadipogenic whilst CHOP seems to block adipocyte differentiation by forming non-DNA-binding dimers with C/EBPβ (Adelmant et al. 1998).

During the differentiation of adipocytes, C/EBPβ/δ/α and CHOP work in a time sensitive cascade of events intercalated by PPARγ to culminate in expression of various adipose specific genes conducive to adipocytic phenotype (Cao et al. 1991; Ron and Habener 1992; Wu et al. 1995). Early after hormonal induction of clonal preadipocytes in culture, a rapid brief period of increased C/EBPβ and C/EBPδ expression is observed. Differentiating cells then continue to divide for two additional cycles and this is followed by an increase in the expression levels of C/EBPα and PPARγ which is coincident with the cessation of mitosis and appearance of conspicuous adipocyte morphology (Yeh et al. 1995; Darlington et al. 1998; Guo et al. 2015). Presence of at least one of the two early C/EBPs, i.e. C/EBPβ or C/EBPδ appears to be indispensable for normal adipogenesis, however, C/EBPβ is more potent than its counterpart (Guo et al. 2015).

Once PPARγ and C/EBPα are induced, they seem to be able to sustain their own expression despite the apparent lack of C/EBPβ/δ later through differentiation. After PPARγ expression is initiated, it likely enters a positive feedback loop with C/EBPα where both counterparts promote one another and function to initiate the expression of adipocyte specific genes (Wu et al. 1999; Tang and Lane 2012).

The relevance of C/EBPs in the coordination of the bone-fat switch lies in their strategic position together with PPARγ within the transcriptional cascade of adipogenesis. The proadipogenic effect of BMPs is partly exerted by the cooperative effects of Schnurri-2 (Shn-2), Smad1/4 and C/EBPα on the promoter of *PPARγ2* (Jin et al. 2006). Inhibition of adipogenesis by Wnt signalling also seems to be mediated via suppression of C/EBPα (Tao and Umek 1999; Ross et al. 2000; Fu et al. 2005). Evidence also indicates that hedgehog signalling mediates its antiadipogenic effects through C/EBPα (Fontaine et al. 2008). Further details of these interactions will be examined under the corresponding signalling pathways.

1.3.2.3 Extracellular Signalling in Osteoblastogenesis/Adipogenesis

Wingless Type (Wnt) Signalling Pathways

Wnts are secreted cysteine-rich glycosylated proteins that were first identified in 1982 (Nusse and Varmus 1982; Nusse and Varmus 1992). Cellular sensing of Wnts is mediated by 10 Frizzled receptors (FZD; Koike et al. 1999; Wang et al. 2016b) and three low-density lipoprotein receptor-related proteins (LRPs): LRP4, LRP5 and LRP6 (Tamai et al. 2000; Leupin et al. 2011). Secreted frizzled-related proteins (SFRPs) and Wnt inhibitory factor 1 (WIF1) inhibit Wnt pathways by binding and blocking the Wnts directly (Kawano and Kypta 2003; Malinauskas et al. 2011). Dickkopfs (DKK) are another group of secreted factors that bind and internalise LRP5/6 (Ai et al. 2005; Aslan et al. 2006; Chan et al. 2011). Sclerostin (SCL), the product of *SOST* gene, likewise targets LRP5/6, but acts to directly dissociate it from FZD and Wnts (Li et al. 2005). A similar factor, sclerostin domain containing 1 (*Sost-dc1*) targets LRP4 and LRP6 and inhibits the subsequent signalling (Lintern et al. 2009; Ohazama et al. 2010).

Depending on cell type and stage of development, Wnt signalling occurs through canonical Wnt-β-catenin pathway and/or the non-canonical pathways. The non-canonical Wnt pathways include the planar cell polarity (Wnt-PCP) pathway, trimeric G-protein coupled receptor pathways including calcium ion (Wnt-Ca^{2+}) signaling, Rho family GTPase pathways, and the JNK pathways (Monroe et al. 2012). In bone and fat, the canonical Wnt-β-catenin pathway is the most important.

The canonical signals revolve around a cytoplasmic protein called β-catenin. Under normal physiologic conditions, β-catenin is quickly degraded by a destruction protein complex comprising of axin1/2, adenomatosis polyposis coli protein (APC), casein kinase 1 (CK1) and glycogen synthase kinase 3β (GSK3β; Westendorf et al. 2004). In this mode of signal transduction, Wnt molecules induce dimerization of a FZD and LRP5/6 which recruits GSK3β and CK1 to the membrane and in turn activates the disheveled protein (DSH). These events release the β-catenin from the destruction complex, thus increase its cytoplasmic concentrations. Consequently, salvaged β-catenin becomes available for translocation into the nucleus where it displaces the corepressors of nuclear transcription factors i.e. lymphoid enhancer-binding factor/T cell factor (LEF/TCF) resulting in Wnt induced gene transcription (Zeng et al. 2005; Bilić et al. 2007; MacDonald et al. 2009).

The inverse relationship between osteogenesis and adipogenesis is perhaps best demonstrated by the pro-osteogenic and anti-adipogenic properties of Wnt signals. Wnt signalling is fundamental to bone development and acquisition of peak bone mass (Kobayashi and Kronenberg 2004). During osteoblastogenesis, Wnt2, Wnt2b, Wnt4, Wnt5a, Wnt10b, Wnt11, *Fzd6*, *Sfrp2*, and *Sfrp3* are upregulated whereas *Wnt9a* and *Fzd*7 are downregulated (Boland et al. 2004; Mak et al. 2009). Loss and/or gain of function studies with Wnt10b, *Fzd9, Lrp5* and *Lrp6* indicate their positive role in osteogenesis and accumulation of bone mass phenotype (Francke 1999; Fujino et al. 2003; Akhter et al. 2004; Holmen et al. 2004; Bennett et al. 2007; Albers et al. 2011).

Wnt1 and Wnt3a inhibit adipogenesis and block the induction of PPARγ by C/EBPβ/δ (Moldes et al. 2003; Kawai et al. 2007). Forced expression of *Wnt1* and *Wnt10b* in bipotential ST2 mesenchymal cells increases osteoblastogenesis and the associated upregulation of *Runx2*, *Dlx5* and *Osx,* whereas adipogenesis is inhibited and *Cebpα* and *Pparγ* are downregulated (Bennett et al. 2005). Consistently, expression of *Sfrp* in clonal preadipocytes or deficiency of *Lrp6* induces spontaneous adipocyte conversion (Bennett et al. 2002; Kawai et al. 2007). In further support of such observations, *in vivo* transgenic expression of *Wnt10b* under the *FABP4* promoter in mice causes a decrease in the accumulation of fat and prevents diet-induced obesity. These mice also have high bone mass that is resistant to age related and oestrogen deficiency bone loss (Bennett et al. 2005).

Pharmacological inhibition of GSK3 inhibits adipogenesis and promotes osteoblastogenesis by stabilising cytosolic β-catenin in a C/EBPα and PPARγ dependent way (Bennett et al. 2002; Bennett et al. 2005). In contrast to these findings, troglitazone dependent adipogenic conversion of PPARγ expressing fibroblasts is not inhibited by expression of GSK3-phosphorylation resistant β-catenin although a subset of adipocyte specific genes was blocked in a C/EBPα dependent manner (Liu and Farmer 2004). Taken together, these reports suggest that a GSK3/β-catenin mechanism is involved in the differentiation of adipocytes and that PPARγ mediates its effects by targeting this mechanism (Moldes et al. 2003; Liu and Farmer 2004). β-catenin mediated suppression of adipogenesis itself also involves suppression of C/EBPα and PPARγ by two downstream

critical cell cycle control proteins, c-myc and cyclin D1 respectively (Freytag and Geddes 1992; Tao and Umek 1999; Wang et al. 2003; Fu et al. 2005).

With the non-canonical Wnt5a, while some report no anti-adipogenic effects (Bennett et al. 2005), others report inhibition of adipogenesis and a proosteogenic response due to repression of PPARγ (Takada et al. 2007). The link between the non-canonical pathways and osteoblast differentiation and function has only started to be appreciated (Baron and Kneissel 2013).

Hedgehog (HH) Signalling

Hedgehog (HH) signalling encompasses the activation of cell receptor complexes which includes patched receptors 1 and 2 (PTC1, -2) and smoothened (SMO) by hedgehog proteins (HH). The result is either activation or suppression of the GLI family of transcription factors (Rohatgi et al. 2007; Ruat et al. 2014). There are three HH proteins currently identified in human and murine genomes: sonic hedgehog (*SHH*), indian hedgehog (*IHH*) and desert hedgehog (*DSH*; Varjosalo and Taipale 2008).

Many clonal osteoblast-like cells as well as calvarial cells express various components of HH signalling including IHH, PTC and SMO. The expression of SHH in particular is increased during osteoblast differentiation. SHH treatment of mesenchymal cells induces ALP expression and extracellular matrix mineralisation as well as PTHrP expression and secretion (Jemtland et al. 2003). Activation of HH signalling by SHH in C3H10T1/2, ST2 and calvarial cells improves the osteogenic response to BMP-2 by improving Smad1 dependent gene transcriptional activity (Spinella-Jaegle et al. 2001). During endochondral ossification (section 1.1.7), IHH is required for the proliferation of chondrocytes in the prehypertrophic zone of the growth plate (Kronenberg 2003). IHH also participates in the osteoblastic induction of perichondrial cells, nevertheless, observations suggest *Ihh* may be dispensable for intramembranous ossification (St-Jacques et al. 1999).

HH signals also possess a very well preserved anti-adipogenic function across all vertebrates (Suh et al. 2006). Various components of HH signalling including HH receptors SMO, PTC1 and PTC2 as well as the GLI family are expressed in developing and adult murine adipose tissue (Suh et al. 2006). Global lack of HH co-receptor, BOC, causes excess

body fat associated with adipocyte hypertrophy *in vivo* and improved adipogenic differentiation of embryonic fibroblasts associated with lower expression of HH components *in vitro* (Lee et al. 2015).

Exposure to SHH inhibits the adipogenic conversion of various clonal mesenchymal cells and calvarial primary cultures in association with suppression of C/EBP, PPARγ and a combination of other adipocyte differentiaton markers such as AP2 (Spinella-Jaegle et al. 2001; Suh et al. 2006; Fleury et al. 2016). Whilst some studies suggest that HH-induced adipogenic blockade occurs rather early during adipogenic differentiation (Suh et al. 2006), others have reported substantial retardation of the later stages of adipogenesis such as impairment of triacylglycerol accumulation and insulin resistance (Fontaine et al. 2008). Consistently, SHH activation of HH signalling increases the expression of various osteogenic markers including Runx2 and Osterix which underpins the pro-osteogenic and anti-adipogenic potential of this signalling mechanism (Spinella-Jaegle et al. 2001; Suh et al. 2006).

BMP Signalling Pathway

Bone morphogenetic proteins are a group comprised of 21 members from the superfamily of TGF-β growth factors (Alarmo and Kallioniemi 2010). BMPs 2, 4, 6 and 7 are significant regulators of bone and adipose homeostasis (Carreira et al. 2014). BMP initiated signal transduction occurs through either canonical or non-canonical pathways (Chen et al. 2012).

In the canonical Smad dependent mechanism, BMPs come to interact with cellular receptors. There are two types of BMP receptors (BMPRs): the serine/threonine kinase BMP receptors I and II (BMPR-I/II). Upon activation by the ligand, two pairs of BMPRI and II assemble together to form a heterotetrameric-activated receptor complex. In the complex, BMPRII, which has constitutive kinase activity, phosphorylates BMPRI. Activated BMPR-I then phosphorylates an R-Smad (Moustakas 2002). Depending on the ligand, this can be any of the structurally similar Smads1, -5 or -8. The phosphorylated Smad1/5/8 then forms a complex with Smad4, also known as the co-Smad, which then translocates into the nucleus (Miyazono et al. 2010). In the nucleus, these complexes either bind directly to DNA or interact with a variety of other transcription factors including

Runx2, Osterix in order to induce expression of their target genes (Derynck et al. 1998; Keiji et al. 2002; Nakashima et al. 2002; Sánchez-Duffhues et al. 2015).

There is also evidence that BMP signalling could recruit pathways independent of Smads (non-canonical pathways) which involves extracellular signal-regulated kinase 1/2 (ERK1/2) and p38 mitogen-activated protein-kinase (p38-MAPK) signalling (KS et al. 2002; Lai and Cheng 2002; Sánchez-Duffhues et al. 2015). Both pathways have been shown to converge on Runx2 and Osterix mediated transcription of osteoblast specific genes (Wang et al. 2007; Chen et al. 2012). Both ERK and p38-MAPK also cause an increased AP-1 activity in osteoblasts (Lai and Cheng 2002). Negative regulation of BMP signalling can take place at various levels. Extracellular factors such as noggins, chordin, and Gremlin antagonise BMP ligands by binding to them (Kameda et al. 1999; Pereira et al. 2000). Sclerostin is structurally homologous to these antagonists and is particularly abundant in osteoblasts and osteocytes (Winkler et al. 2003).

Some BMPs, particularly BMP-2, induce *de novo* endochondral bone formation even in ectopic sites (Urist 1965; Wozney and Rosen 1998). *In vitro,* use of BMP-2 induces C2C12 cells to undergo osteoblastogenesis (Katagiri et al. 1994). Bmp7 knockout mice die shortly after birth due to defective kidney formation but also show a mild bone deficient phenotype (Dudley et al. 1995; Luo et al. 1995). Moreover, it has been shown through various conditional deletions that Smad1/5 is essential for endochondral bone formation (Retting et al. 2009). Based on these studies and others, it is accepted that BMPs are indispensable in the process of osteoblastogenesis (Sánchez-Duffhues et al. 2015).

BMPs also participate in adipogenesis. Transfection of C3H10T1 fibroblasts with BMP-2 expressing vector produces a mix of adipocytes and osteoblasts and their treatment with exogenous BMP-2 is either adipogenic or osteo/chondrogenic depending on the concentration used (Wang et al. 2009). Likewise, treatment of C3H10T1/2 cells with BMP-4 facilitates adipogenic conversion. Even growth arrested cells that cannot be hormonally induced, undergo adipogenesis in the presence of exogenous BMP-4 (Tang et al. 2004; Bowers et al. 2006; Bowers and Lane 2007). Subcloning of these cells after exposure to the methylation inhibitor 5-azacytidine, has been reported to produce cells of committed adipogenic lineage which no longer require exogenous BMP-4 for their differentiation.

These cells spontaneously express BMP-4 that could be antagonised by noggin suggesting a role for BMP-4 during the early commitment phase (Bowers et al. 2006; Bowers and Lane 2007). Similar observations have also been reported by other studies (Ahrens et al. 1993; Gustafson et al. 2015). Interestingly, expression of the BMP-4/7 inhibitor Gremlin-1, by human subcutaneous preadipocytes maintains their undifferentiated state and prevents their spontaneous adipogenesis. Addition of BMP-4 or Gremlin-1 silencing results in PPARγ induction and adipogenic differentiation accordingly (Gustafson et al. 2015).

The major determinant of lineage-specific response to BMP activation appears to be the type of BMPR-I involved in the associated signalling pathway. Under cell culture conditions, activation of BMPR-IA drives the fate of MSCs towards the adipocyte lineage whereas BMP-IB activation is rather pro-osteogenic (Chen 1998; James 2013). Consistently, *BMPR1A*-enriched human adipose derived MSCs, have greater adipogenic potential than controls both in culture and when implanted in immune deficient mice (Zielins et al. 2016). Nevertheless, osteoblast specific loss of either *Bmpr1a* or *Bmpr1b* in mice is associated with low bone mass and apparently normal osteoblasts, although osteoblastic differentiation of marrow MSCs is compromised (Mishina et al. 2004; Shi et al. 2016).

Overall, these studies show that BMP signalling is an indispensable regulator of both osteoblastogenesis and adipocyte differentiation with convergence on either Runx2 and Osterix in osteoblasts or C/EBPs and PPARγ in adipocytes (James 2013).

Insulin and Insulin-like Growth Factor 1

Both insulin and insulin-like growth factor 1 (IGF-1) exert their physiological effects through interacting with cell membrane bound tyrosine kinase receptors, the insulin receptor (IR) and the IGF-1 receptor (IGF1R). Ligand mediated activation of the receptors results in phosphorylation of intracellular substrates including insulin receptor substrate 1 and -2 (IRS-1 and IRS-2) and downstream recruitment of phosphatidylinositol 3-kinase (PI 3-kinase), AKT (PKB), ERK1/2 and p42/44 signalling (Giorgetti et al. 1993; Grey et al. 2003; Raucci et al. 2008).

In vivo, osteoblast specific overexpression of IGF-1 is associated with double the BFR as compared to wildtype controls which leads to a higher bone mass and BMD values in these

mice (Zhao et al. 2011). *In vivo* disruption of IGF1R causes severe growth retardation associated with both bone and adipose tissue growth defects (Holzenberger et al. 2011). All trabecular parameters are deteriorated in these mice and osteoid mineralisation rate is severely decreased indicating a potential role for IGF-1 signalling in matrix mineralisation (Zhang et al. 2002). Further, IRS-1 and -2 null mice are osteopoenic and have significantly lower fat mass than the control mice which is accompanied by impaired osteoblastogenesis (Ogata et al. 2000; Miki et al. 2001; Akune et al. 2002).

In vitro, IGF-1 and -2 have a profound mitogenic and pro-survival effect on undifferentiated MSCs and osteoblasts and control the clonal expansion of committed preadipocytes (Rajkumar et al. 1999; Grey et al. 2003; Gaskinst et al. 2009; Thomas et al. 2011). Expression of IGF-1 in hMSCs upregulates collagen type I, Runx2 and ALP indicative of its role in early osteoblastogenesis (Koch et al. 2006). In contrast, mature osteoblasts and adipocytes respond to IGFs by increasing the expression of type I collagen and accumulation of triacylglycerol respectively indicating a role in late functional regulation of both cell types (Thomas et al. 2011).

Collectively, these observations demonstrate that IGF signalling is of paramount importance in the regulation of both osteoblastic and adipocytic differentiation. The effect is mediated via MAPK associated pathways that converge on Runx2, C/EBPα and PPARγ (James 2013).

Fibroblast Growth Factors

Interaction of fibroblast growth factors (FGFs) with the cognate FGF tyrosine kinase receptors (FGFR) results in the recruitment of two intracellular substrates and activation of Ras MAPK and PI 3-kinase-AKT signalling pathways (Beenken and Mohammadi 2009). There is evidence that FGF signalling may be involved in the regulation of both adipogenesis and osteoblastogenesis. Targeted deletions of *Fgf2* and *Fgf18* in mice cause a significant loss of trabecular bone as a result of impaired osteoblast differentiation and function (Montero et al. 2000; Liu et al. 2002; Ohbayashi et al. 2002). FGF-2 is an essential element of lineage determination in osteoblasts and required for PTH and BMP-2 to modulate their anabolic effects in bone (Hurley et al. 2006; Naganawa et al. 2008; Xiao et al. 2010). FGF1, -2 and -10 also promote adipogenic conversion of mesenchymal cells

by inducing expression of PPARγ (Sakaue et al. 2002; Neubauer et al. 2004; Hutley et al. 2004; Kyrou et al. 2017).

Notch Signalling

Notch signalling enables neighbouring cells to communicate through the reciprocal binding of their cell surface ligands and receptors. In mammals, two types of ligands, DLL-type ligands and JAG-type ligands, both transmembrane proteins, interact with a group of receptors, Notch1-4, to activate a variety of target genes such as Hess and Hey transcription factors (Cai et al. 2011). Notch signalling inhibits osteoblastogenesis and bone formation by suppression of canonical Wnt signalling and Runx2 activity (Hilton et al. 2008; Zanotti et al. 2008; Salie et al. 2010; Sciaudone et al. 2011). Notch signalling also appears to inhibit adipogenesis of MSCs (Ross et al. 2004; Song et al. 2015). Adipocyte specific activation of Notch *in vivo* results in dedifferentiation of adipocytes associated with lipodystrophy, insulin resistance and neoplasia (Chartoumpekis et al. 2015; Bi et al. 2016).

Other Regulatory Signals

The list of signalling pathways and biomolecules that govern the selective differentiation of osteoblasts and adipocytes is rather extensive. In addition to what has been discussed, other cell signalling mechanisms are also involved. For example the osteoinductive factor Nel-like protein 1 (Nell-1) signalling through integrinβ1, cross talks with both Wnt and HH signalling pathways to promote osteoblastogenesis and inhibit adipogenesis (James 2013). Factors such as sFRP-1 and Pref-1 have recently been proposed to actively participate in the control of MSC differentiation (reviewed by (Abdallah and Kassem 2012).

1.4 Protease-activated Receptor 2 (PAR_2)

1.4.1 Protease-activated Receptors as a family

Protease-activated receptors (PARs), designated as PAR_1, PAR_2, PAR_3 and PAR_4, are a family of seven transmembrane domain receptors from the superfamily of G protein coupled receptors (GPCRs) with similarities in their mechanism of activation. Protease-activated receptors are unique in that the receptor needs to be irreversibly cleaved by proteases (mostly serine) in order to be activated and transduce signal (Zhao et al. 2014). The first three members of PARs are encoded by a cluster of genes on chromosome 5q13 in human and 13D2 in mouse . This locus contains coagulation factor 2 receptor (*F2R*) for PAR_1, *F2R* like 1 (*F2RL1*) for PAR_2 and *F2RL2* for PAR_3. The fourth member, PAR_4 is encoded by *F2RL3* which maps to chromosome 19p12 in human and 8B3.3 in mouse (Kahn et al. 1998a).

All four genes span two exons with an intron in between. The first exon codes for the 5′-untranslated sequence, start codon, and the signal peptide; the second exon encodes the bulk of the mature receptor and the 3′-untranslated sequence (Kahn et al. 1998a). Each PAR consists of an extracellular amino terminus, three extracellular loops, three intracellular loops and an intracellular carboxyl terminus connected by seven transmembrane helices. The amino domain in PARs contains a signal peptide of between 17 and 26 residues and a propeptide of between 11 and 30 residues (Adams et al. 2011). The cleavage site is physically located in the extracellular amino terminal prodomain of the receptor and may contain subtype specific characteristics. For example, the amino domain of thrombin responsive PAR_1 and PAR_3 contains a high affinity hirudin-like motif that serves to facilitate thrombin binding and proteolysis resulting in a rapid intracellular Ca^{2+} influx, whereas PAR_4 exodomain lacks this sequence which results in different Ca^{2+} kinetics following thrombin activation (Nieman 2008).

Upon cleavage by proteases, the prodomain is detached from the receptor revealing a new amino terminus or tethered ligand. The tethered ligand then interacts with the second extracellular loop of the receptor (Figure 1.3) and possibly other intramolecular sites causing conformational changes within the receptor and canonical signal transduction which includes G protein dependent and independent signals (Soh et al. 2010). It is now believed that beside canonical cleavage, proteases may also produce alternative tethered

ligands with agonistic activities sometimes resulting in activation of a select platform of downstream signals (Zhao et al. 2014).

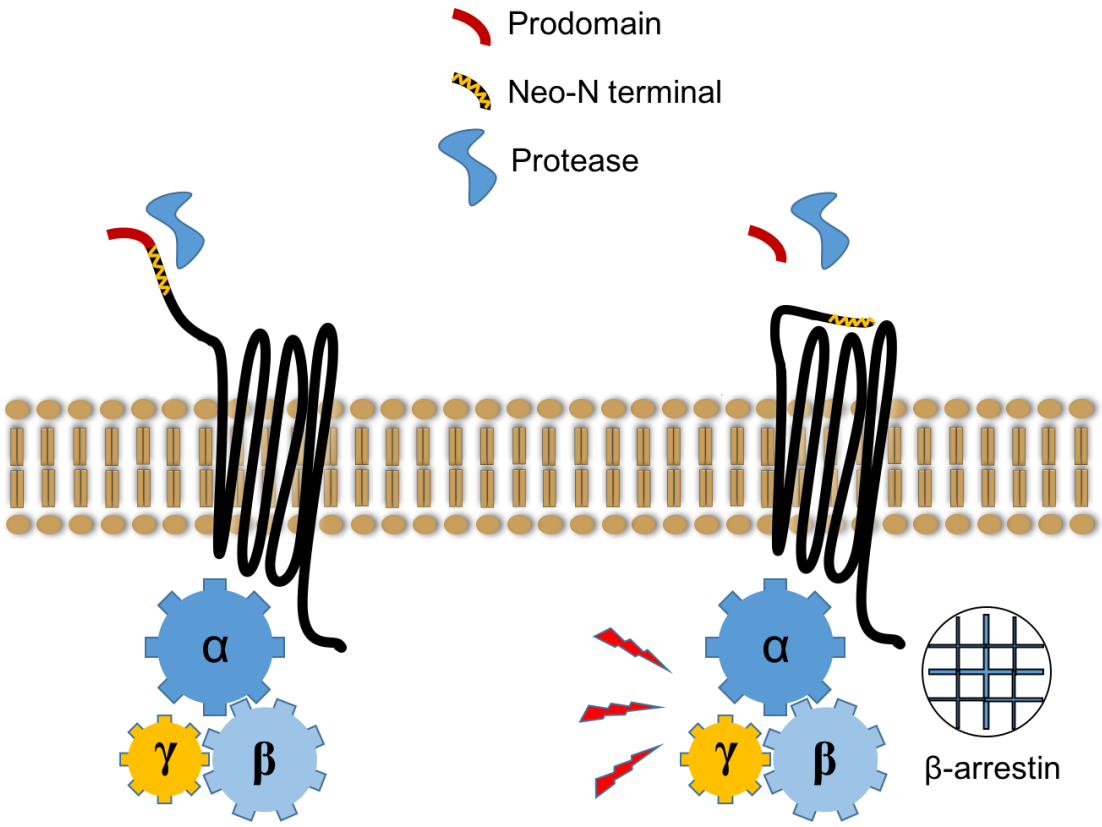


Figure 1.3 PAR activation and signal transduction.

Cleavage of the extracellular prodomain reveals a new N-terminus (tethered ligand) which interacts with the second extracellular loop of the receptor and other intramolecular sites to allow an allosteric change and signal transduction via G proteins and β-arrestin.

The ligand specific variation of downstream signalling through the same receptor is termed biased agonism (Urban et al. 2007). Biased signalling can also occur due to ligand independent conformational changes as a result of proteolysis alone. If proteolytic action creates a truncated amino terminus, the receptor is said to be inactivated or disarmed (Zhao et al. 2014). The released prodomain of the N terminus may also possess some biological activity as has been shown for PAR_1, nevertheless, whether the prodomain mediates any

effects of the other PARs remains to be fully elucidated (Furman et al. 2000a; Furman et al. 2000b; Zania et al. 2009).

Soon after their discovery, it was found that small peptides mimicking the sequence of the tethered ligand (called activating peptides or APs) could actually activate the receptors in a receptor specific manner and independently of proteases (Scarborough et al. 1992; Chen et al. 1994a; Lerner et al. 1996). However, PAR_3 is unresponsive to APs and is thought to function as a cofactor of the other thrombin receptors (Nakanishi-Matsui et al. 2000; Ruchika et al. 2015). This ability to activate the receptors without proteolysis has been exploited to study the functions of the PARs, especially where more than one receptor subtype is expressed and simultaneously present, e.g. platelets. However, at least in the case of PAR_2, APs may provoke intracellular mechanisms independently of the receptor and therefore their use in studying receptor function should be viewed with caution (McGuire 2002; Georgy et al. 2010).

Upon activation, the induced conformational changes within the alpha helices facilitates receptor interaction with the heterotrimeric membranous G proteins to form a high affinity receptor-G protein complex. Such interaction catalyses guanine nucleotide exchange within the alpha subunit of the G protein resulting in substitution of GTP for GDP. GTP bound G protein then dissociates from the receptor and breaks into α subunit and $\beta\gamma$ dimer (Morris and Malbon 1999; Gieseler et al. 2013). After activation, the bound GTP is gradually hydrolysed to GDP by the intrinsic GTPase activity of the α subunit. This triggers a turnoff mechanism by which subunits are reassembled and engaged with a new receptor. Both subunits are responsible for modulation of a variety of intracellular interactions through activation of downstream effector proteins and then secondary messengers (Hamm 1998). PAR_1 and PAR_2 affiliate with various heterotrimeric G protein subtypes including G_i, G_s, G_q and $G_{12/13}$ (Russo et al. 2009). PAR_4 couples with G_q and $G_{12/13}$ but not G_i (Kim et al. 2002). PAR_3 in contrast seems to rely on other PARs for mediation of its effects (Nakanishi-Matsui et al. 2000). PARs also interact with various adapter proteins, prominently, β-arrestins to mediate G protein independent signalling (Lefkowitz and Shenoy 2005; Walker and DeFea 2014).

Due to the irreversible nature of PAR activation and the inability of the tethered ligand to dissipate following receptor activation, PARs rely on prompt desensitisation and

internalisation of the receptor to shut off signalling. This depends on phosphorylation of the receptor and β-arrestin binding followed by internalisation of the receptor and degradation (DeFea et al. 2000; Stalheim 2005; Ricks and Trejo 2009). Like many other GPCRs, PARs also undergo various other posttranslational modifications which may include N-glycosylation, ubiquitination and palmitoylation. Such modifications can impact the function of the receptor in many ways from cell surface expression and G protein coupling to internalization, trafficking and degradation of the receptor (Adams et al. 2011).

As the name implies, PAR_1 was the first of the PARs to be discovered in 1991 (Vu et al. 1991). PAR_1 is mainly activated by thrombin which leads to cleavage of the exodomain of the receptor at position R41/S42 and exposure of the tethered ligand (Vu et al. 1991; Austin et al. 2013a). A number of other proteases act around this "hot spot" to mediate downstream canonical signalling; these include factor Xa (Camerer et al. 2002), granzyme A (Suidan et al. 1994) and plasmin (Kuliopulos et al. 1999).

Other proteases such as activated protein C (APC)-EPCR complex (Mosnier et al. 2012), MMP-1 (Austin et al. 2013b), MMP-13 (Jaffré et al. 2012), elastase and proteinase-3 (Mihara et al. 2013) also activate PAR_1 with potential induction of biased signalling mechanisms. Furthermore, a series of other proteases are also described that play their biological effect at least partly through activation of PAR_1; these include trypsin IV, KLK1, KLK4, KLK5, KLK6 and KLK14, cathepsin G, proatherocytin and the mold allergen pen C 13 a (Adams et al. 2011). PAR_1 may be disarmed and its activation prevented cleavage of its extracellular domain by KLK1 and KLK14, ADAM17, protease 3, trypsin, cathepsin G, elastase and finally plasmin (Adams et al. 2011).

Often regarded as the primary α-thrombin receptor in human, PAR_1 plays important roles in haemostasis and the cardiovascular system (Kahn et al. 1999; Derian et al. 2003; Cheung et al. 2011). Here, PAR_1 has been shown to play roles in platelet aggregation (Covic et al. 2000; Derian et al. 2003), vascular tone (Cicala et al. 2001), extravasation of plasma proteins during inflammation (Vergnolle et al. 1999b) and proliferation of vascular smooth muscle cells (McNamara et al. 1993). In the nervous system, PAR_1 activation contributes to the Ca^{2+} dependent excitation of glioma cells (Ubl and Reiser 1996) and astrocytes (Ubl and Reiser 1997). Moreover, PAR_1 agonists and antagonists are important

regulators of morphology of astrocytes (Cavanaugh et al. 1990; Beecher et al. 1994). PAR_1 also mediates survival and apoptosis of neuronal cells in response to various insults (Vaughan et al. 1995; Striggow et al. 2000) and may be involved in nociception (Asfaha et al. 2002; Tao et al. 2014). PAR_1 has been linked to multiple other functions such as gastrointestinal contractility (Al-Ani et al. 1995; Sung et al. 2015), protective secretion of mucus and PGE2 by the gastric epithelium (Toyoda et al. 2003), intestinal secretion of electrolytes (Buresi et al. 2002), proliferation of keratinocytes (Algermissen et al. 2000) and fibroblasts (Chen et al. 1994b; Lin et al. 2014), angiogenesis (Tsopanoglou and Maragoudakis 1999; Battinelli et al. 2014) and neoplasia (Jin et al. 2003; Lima and Monteiro 2013).

In osteoblasts, exposure to thrombin modulates an intracellular calcium response that is PAR_1 dependent (Jenkins et al. 1993). Either thrombin or AP dependent activation of PAR_1 in primary calvarial cells is associated with an increased rate of proliferation which is reversible upon use of blocking PAR_1 antibodies. Pretreatment of osteoblasts with TGF-β, which causes PAR_1 mRNA upregulation, increased the proliferative response of osteoblasts to thrombin (Abraham and Mackie 1999). Likewise, PAR_1 null marrow stromal cells and osteoblasts do not respond to thrombin whereas wildtype cells proliferate in response to thrombin (Song et al. 2005b; Song et al. 2005a). In line with these findings, it has been shown that PAR_1 null mice are not as competent as their wildtype cohorts in the healing of bony defects (Song et al. 2005a). Later studies have also shown that PAR_1 may be involved in the autocrine/paracrine regulation of osteoblasts by mediating cyclooxygenase dependent synthesis and release of multiple secreted factors, e.g. IL-6 mediated by PGE2 (Pagel et al. 2009).

In contrast, PAR_3, although a thrombin receptor, is only minimally expressed in human platelets whereas in mouse megakaryocytes, it is found at high levels (Ishihara et al. 1997). While necessary for normal haemostasis in mice, in the absence of other PARs, murine PAR_3 is unable to signal independently (Kahn et al. 1998b). As a result, it has been proposed that PAR_3 may be a part of a dual receptor system in conjunction with PAR_4 (Kahn et al. 1998b; Nakanishi-Matsui et al. 2000). Strikingly, unlike other PARs, APs are unable to activate PAR_3 even at high concentrations which has not been explained (Ishihara et al.

1997; Nakanishi-Matsui et al. 2000). The receptor is disabled by cathepsin G in both human and mouse, and by elastase only in human (Cumashi et al. 2001).

PAR_4, the last member to be identified, also responds to thrombin, however more slowly and less extensively than PAR_1 and PAR_3 (Nieman 2008). Trypsin, cathepsin G, trypsin IV, MASP-1, plasmin, factor Xa, bacterial gingipains and KLK1 and KLK14 are the other activating proteases for PAR_4. Cathepsin G and KLK14 can additionally disarm the receptor (Adams et al. 2011). PAR_4 is reported to be involved in the late phase of platelet activation (Covic et al. 2000), inflammatory vascular response (Hamilton et al. 2001), proliferation of vascular smooth muscle cells (Bretschneider et al. 2001), pathology of encephalitis (Suo et al. 2003), intestinal transit mechanisms (Kawabata et al. 2001b) and myenteric neuronal excitation (Gao et al. 2002).

1.4.2 PAR_2 Signalling, Agonism and Antagonism

PAR_2 was the second member of the PAR family to be identified during a high throughput screening of a mouse genomic library (Nystedt et al. 1994; Nystedt et al. 1995b; Nystedt et al. 1995a). Notably, the amino terminal of the receptor was found to contain a putative trypsin cleavage site $SKGR^{36}\downarrow S^{37}LIGRL$. Subsequently, it was shown that the receptor could be activated by trypsin and an activating peptide SLIGRL corresponding to the tethered ligand, but not by thrombin (Nystedt et al. 1994). Later, cloning and sequencing of human PAR_2, revealed 83% homology in the amino acid sequences between the two species. One great difference found was the substitution of the last two residues of the murine tethered ligand, arginine and leucine, with lysine and valine in human PAR_2 creating a slightly different canonical cleavage site $SKGR^{36}\downarrow S^{37}LIGKV$ (Nystedt et al. 1995a). Nevertheless, $hPAR_2$ was found to be responsive to both human and murine APs as well as trypsin (Nystedt et al. 1995a).

The canonical activation of the receptor initiates several downstream G protein dependent and independent pathways. Notably, PAR_2 recruitment of $G\alpha_q$ (also known as $G_{q/11}$) triggers phospholipase C β_1 (PLC β_1) to hydrolyse phosphatidylinositol 4,5-biphosphate to diacylglycerol and inositol 1,4,5-triphosphate (IP_3). IP_3 mediates release of Ca^{2+} from intracellular stores (Böhm et al. 1996a; Berridge 2009), a prototypic effect of PAR_2 that has been documented in various epithelial cell lines, astrocytes and tumour cells (Santulli

et al. 1995; Böhm et al. 1996b; Böhm et al. 1996a; Wang et al. 2002) as well as osteoblasts (Abraham et al. 2000). Diacylglycerol, on the other hand, activates PKC resulting in activation of MAP kinases (c-jun N-terminal kinase [JNK] and p38 MAP kinase) and inhibitory κB kinases (IKKα/β) with the latter stimulating NF κB and related cytokine production (Böhm et al. 1996a; Kanke 2001; Johnson et al. 2016). Additionally, recruitment of $G\alpha_s$ and $G\alpha_{12/13}$ by PAR_2 has been linked to formation of cAMP and activation of Rho kinase, respectively (Scott et al. 2003).

Desensitisation of the receptor is mainly achieved by means of protein kinase C (PKC) phosphorylation that facilitates the binding of β-arrestins. Binding of β-arrestins effectively dislodges the coupled Gα subunit and terminates signals distal to the G protein (Böhm et al. 1996a; DeFea et al. 2000; Ricks and Trejo 2009). Next, β-arrestin couples the receptor to clathrin coated pits and this initiates a GTPase rab51 mediated endocytosis and internalisaiton of PAR_2 (Déry et al. 1999; Roosterman et al. 2003). Whereas some of these β-arrestin scaffolded endosomes could be subjected to lysosomal targeting and receptor degradation (Böhm et al. 1996a; Déry et al. 1999), some form multiprotein signalling complexes by recruiting raf-1, cofilin, chronophin and ERK1/2 which leads to intracytosolic but not intranuclear ERK1/2 activity (DeFea et al. 2000; Zoudilova et al. 2007; Zoudilova et al. 2010). This phenomenon has been reported to be a prominent feature of PAR_2 promigratory effects in various immune cells (Ge 2003). Strikingly however, mutations of PAR_2 that lead to β-arrestin dissociation or lack of β-arrestin do not preclude activation of ERK1/2, but rather cause its nuclear localisation and promitogenic effects or otherwise more rapid inactivation (DeFea et al. 2000; Stalheim 2005). This β-arrestin independent activation of ERK1/2 seems to require GTPase Ras kinase, whereas in the presence of wildtype PAR_2, it is PKC dependent (DeFea et al. 2000). Due to the irreversible nature of receptor activation and subsequent internalization, resensitisation of PAR_2 is dependent on synthesis and redistribution of new receptor from the Golgi apparatus (Böhm et al. 1996a; Déry et al. 1999). GTPase rab11a contributes to this trafficking of PAR_2 to the cell membrane (Roosterman et al. 2003).

Other than trypsin, several endogenous proteases are capable of activating PAR_2 signalling (Table 1.1). PAR_2 can also be cleaved and activated by exogenous proteases such as bacterial gingipains (Lourbakos et al. 2001), mold allergen serine protease Pen c 13 (Chiu

et al. 2007), chitinase - from *Streptomyces griseus* (Hong et al. 2012) and multiple mite cysteine and serine proteases (Kato et al. 2009; Post et al. 2014). Additionally, it has been noted that in endothelial cells, PAR_2 could be transactivated by cleaved PAR_1 which can be of importance in thrombin induced signalling (O'Brien 2000).

Traditionally, it is thought that plasmin, protease 3 and calpain (Loew et al. 2000) as well as cathepsin G and elastase (Dulon et al. 2003; Dulon et al. 2005) disarm PAR_2 by truncation of the exodomain or degradation of the receptor (Dulon et al. 2005). In view of recent research however, emerging evidence suggests that many such proteases may in fact activate the receptor and produce biased signalling. For instance, the neutrophil protease, elastase, cleaves the amino terminus at position $S^{68}\downarrow V^{69}$ and removes the conserved tethered ligand. This however, triggers $G\alpha_{12/13}$ dependent activation of Rho and ERK phosphorylation without inducing the Ca^{2+} response, β-arrestin coupling or internalisation of the receptor (Ramachandran et al. 2011). The proof of the receptor's ability to initiate biased signalling is provided by the fact that some mutations of the tethered ligand or alternative AP analogs (e.g. SLAAAAA-NH_2) are associated with activation of MAP kinases but not Ca^{2+} mobilization (Ramachandran et al. 2009). Therefore, while it is still unclear whether some of these proteases initiate biased signals (Ramachandran et al. 2011), it may just be a matter of time before new ones are identified.

1.4.3 PAR_2 Expression and Pathophysiological Functions

PAR_2 is widely expressed in human and animal cells and tissues. It is highly expressed by enterocytes, keratinocytes, vascular endothelial and smooth muscle cells and is especially abundant in a wide variety of tissues including intestines, lungs, kidneys and liver. PAR_2 is important in the regulation of basic cell functions including cell proliferation and apoptosis, and a variety of physiological processes including embryonic development, inflammation and immunity (Adams et al. 2011).

Table 1.1 Endogenous activators of PAR_2.

Protease Name	Gene Name	Reference
acrosin	*Acr*	(Smith et al. 2000)
Airway trypsin-like protease (HAT)	*Tmprss11d*	(Miki et al. 2003)
Epitheliasin	*Tmprss2*	(Wilson et al. 2005)
granzyme A	*Gzma*	(Hansen et al. 2005)
Hepsin (activates matriptase)	*Hpn*	(Camerer et al. 2010)
Kallikrein 2	*Klk2*	(Mize et al. 2008)
Kallikrein 4	*Klk4*	(Ramsay et al. 2008)
Kallikrein 5	*Klk5*	(Oikonomopoulou et al. 2006)
Kallikrein 6	*Klk6*	(Oikonomopoulou et al. 2006)
Kallikrein 14	*Klk14*	(Oikonomopoulou et al. 2006)
Matriptase	*St14*	(Takeuchi et al. 2000)
Matriptase-2	*Tmprss6*	(Béliveau et al. 2009)
Tissue Factor: Factor Xa: Factor VIIa	*F3: F10: F7*	(Camerer et al. 2000)
Trypsin I	*Prss1*	(Nystedt et al. 1994)
Trypsin IV	*Prss3*	(Cottrell et al. 2004)
Tryptase Alpha/Beta 1	*Tpsab1*	(Molino et al. 1997)
Tryptase Beta 2	*Tpsb2*	(Molino et al. 1997)

In the cardiovascular system, activation of PAR_2 is associated with vascular relaxation and hypotension which is dependent on nitric oxide and prostaglandin mechanisms (Hamilton et al. 2002; Robin et al. 2003; Alberelli and De Candia 2014). In the airways, use of PAR_2 AP causes relaxation of trachea and bronchi through a prostaglandin dependent mechanism (Chow et al. 2000; Lan et al. 2001) and constriction of smaller bronchioles due to the direct activation of PAR_2 in the smooth muscle cells (Ricciardolo et al. 2000; Schmidlin et al. 2012). PAR_2 also plays a role in regulating gastrointestinal motility and transit (Corvera et al. 1997; Cocks et al. 1999; Sung et al. 2015) as well as pancreatic, salivary and gastric secretions (Kawabata et al. 2000; Kawabata et al. 2001a).

In the nervous system, the receptor has a prominent role in nociception. Intraplantar injection of PAR_2 APs, even at doses below those that cause oedema and inflammation, is

associated with a centrally mediated thermal and mechanical hyperalgesia and increased activity in the dorsal horn of the spinal cord all of which is absent in PAR_2 null mice (Vergnolle et al. 2001a; Cattaruzza et al. 2014; Tillu et al. 2015). In fact, PAR_2 is suggested as the target of a diverse range of algesic stimuli with potential to amplify and sustain the resulting inflammation and pain (Cattaruzza et al. 2014; Zhao et al. 2015). Not surprisingly, the receptor has also been implicated in the modulation of acute and chronic cancer associated pain. In cancer, activation of PAR_2 and its later upregulation in the peripheral nerves, in company with elevated levels of serine proteases in the cancer microenvironment, play a crucial role in the development and maintenance of nociception (Lam and Schmidt 2010; Lam et al. 2012; Liu et al. 2013).

PAR_2 is also involved in the development and function of various immune cells. Dendritic cells, for example, do not spontaneously form in PAR_2 null bone marrow cultures or following serine protease inhibition (Fields et al. 2003). PAR_2 null T-lymphocytes have lower IgE and IL-4 production and higher levels of intracellular JNK1 phosphorylation relative to those from wildtypes (Shichijo et al. 2006). Furthermore, in T lymphocytes, activation of intracytosolic ERK1/2 by β-arrestin bound PAR_2 following its internalisation is key to reorganization of the actin cytoskeleton, polarized pseudopodia extension, and chemotaxis (Ge 2003).

In fact, activation of PAR_2 is associated with production of various proinflammatory cytokines as shown by both loss of function studies and use of PAR_2 agonists and antagonists. Treatment of endothelial cells with the PAR_2 activator, matriptase, induces IL-6 and IL-8 expression and protein release (Seitz et al. 2006). Similar results are also reported in other cell types, including endometrial stromal cells (Hirota et al. 2005; Saito et al. 2011) and nasal epithelial cells (Shi et al. 2010). *In vivo,* administration of PAR_2 activating FVIIa in healthy human subjects induces a small but significant increase in both IL-6 and IL-8 plasma concentrations (de Jonge et al. 2003). Use of PAR_2 null mice indicates that the receptor is also crucial for the induction of IL-18 in response to bacterial antigens (Ikawa et al. 2005).

Local intraplantar administration of PAR_2 activators in rats, induced oedema and leukocyte rolling and extravasation (Vergnolle et al. 1999a) with the latter also observed in the

mesentery of rats and the cremaster muscle of mice (Vergnolle 1999; Lindner et al. 2000a). Moreover, PAR_2 null mice mount a less severe inflammatory response to surgical trauma in comparison with wildtype mice (Lindner et al. 2000a). Further observations in these mice indicate that the receptor is in fact a significant mediator of inflammation in several tissues.

Cartilage appears to be one such tissue where PAR_2 mainly plays a role as a pro-inflammatory receptor in the pathophysiology of osteoarthritis. Global PAR_2 deficient mice are significantly more resistant to chemical induction of osteoarthritis than wildtype controls. Also, intraarticular injection of PAR_2 activating peptide, ASKH95 results in joint swelling and synovial hyperaemia in wildtype mice but not in knockouts (Ferrell et al. 2003). Similarly, interfering with the PAR_2 upregulation that normally follows intra-articular administration of irritants substantially reduces the resulting inflammation. Studies with exogenous serine proteases, i.e. trypsin and tryptase in wildtype and PAR_2 deficient mice further support these observations (Kelso et al. 2006). Consistently, it has recently been shown that when osteoarthritis is induced by mechanical destabilisation of the stifle joint, PAR_2 null mice do not develop severe pathology up to 8 postoperative weeks unlike wildtypes where osteophyte formation and osteosclerosis are evident at 7 and 14 days, respectively (Jackson et al. 2014; Huesa et al. 2016).

PAR_2 has also been implicated in the pathology of periodontal disease and the associated bone resorption. In the periodontal tissue, PAR_2 is expressed by oral epithelial cells, osteoblasts, gingival fibroblasts and various inflammatory cells. It has been noted that the cysteine proteases produced by the human oral pathogen *Porphyromonas gingivalis*, are able to cleave PAR_2 and stimulate its downstream signalling and upregulation of inflammatory cytokines such as IL-6 (Lourbakos et al. 2001). Interestingly, topical application of PAR_2 AP, SLIGRL-NH_2 in rats causes prominent alveolar bone loss and gingival infiltration of inflammatory cells seemingly in a COX-1/2, MMP-2/9 dependent manner (Holzhausen et al. 2005). Expectedly, oral inoculation of wildtype mice with *P. gingivalis* caused the onset of periodontitis and subsequent alveolar bone loss, nevertheless, in the absence of PAR_2, no significant bone loss was observed, underlining the role of PAR_2 in the pathology of *P. gingivalis* induced periodontitis and bone loss (Holzhausen et al. 2006). PAR_2 knockout mice also show fewer mast cells in the periodontal tissues, and their

T lymphocytes, when exposed to *P. gingivalis* antigen, do not proliferate as much as their wildtype counterparts and have a milder cytokine profile (Wong et al. 2010).

1.4.4 PAR_2 and Bone

Prenatal expression of PAR_2 in osteoblasts is detected as early as E14 (Jenkins et al. 2000). Postnatally, murine and human PAR_2 is present at both mRNA and protein levels in osteoblasts (Jenkins et al. 2000; Kirilak et al. 2006). PAR_2 is also expressed by murine primary bone marrow stromal cells (Smith et al. 2004) and osteoblasts as well as human osteosarcoma cells (Abraham et al. 2000; Pagel et al. 2003).

In bone, although the cellular components contribute minimally to the production of PAR_2 activating proteases (Mackie et al. 2008b), nevertheless, the close proximity of bone and bone marrow means that exposure of osteoblasts to potential marrow proteases can be a possibility. The presence of several PAR_2 activating proteases, i.e. acrosin, trypsin IV, matriptase and KLK4 in bone marrow has been reported (Georgy et al. 2012). Various PAR_2 activators are also expressed by brown and white adipocytes as well as haematopoietic cells surrounding the marrow sinusoids (Su et al. 2004; Lattin et al. 2008). Furthermore, bone is a highly vascular organ and as such multiple proteases of circulatory and vascular origin can interact with osteoblasts especially after injury or inflammation (Koshikawa et al. 1997; Faurschou and Borregaard 2003).

Abraham *et al*., were the first to investigate the expression and functions of PAR_2 in osteoblasts (Abraham et al. 2000). In a series of experiments using trypsin, gingipain-R and PAR_2 APs, the authors reported that activation of PAR_2 did not cause any measurable effect on the proliferation rate of primary rat osteoblasts assessed by thymidine incorporation. Similarly, when murine PAR_2 wildtype and knockout calvarial cells were treated with PAR_2-activator-rich conditioned media (from prostate cancer cell lines), no difference in cell proliferation was observed between the genotypes (Kularathna et al. 2013). Consistently, in another series of experiments, no difference in the proliferation rate between wildtype and PAR_2 null calvarial osteoblasts was observed, however when these cells were cultured over 8 days there was a slightly more rapid increase in number of the PAR_2 null than the wildtype osteoblasts, which could be attributed to a decreased rate of apoptosis (Georgy et al. 2010).

PAR_2 is also involved in the differentiation and function of osteoclasts. In the presence of PTH, $1,25(OH)_2D_3$ and IL-11, PAR_2 activation in mouse bone marrow cultures inhibits osteoclastogenesis in association with suppression of various pro-osteoclastic factors including osteoblastic RANKL and RANKL/OPG ratio as well as expression of COX-2 and IL-6 (Smith et al. 2004).

In vivo, global PAR_2 knockout mice have significantly higher bone mass than wildtypes in both trabecular and cortical compartments at 7 weeks. However, this initial picture seems to even out at the age of 13 where both genotypes are comparable. Additionally, all osteoblastic and osteoclastic parameters are inferior in the absence of PAR_2 which suggest a possible role for the receptor in the determination phase and function of both cell lineages (Georgy et al. 2012). Accordingly, application of trypsin and PAR_2 activating peptides in primary calvarial cultures isolated from wildtype and knockout neonatal mice induces the expression of collagen type I in the wildtype osteoblasts but not in the knockouts (Georgy et al. 2010)

Later observations indicated that when primary osteoblastic cultures were kept under osteogenic conditions for long enough, some PAR_2 null cells started accumulating intracytosolic triacylglycerol and formed adipocytes (Kularathna et al. 2013). This was marked with a decrease in alkaline phosphatase activity, matrix mineralisation and expression of the osteoblastic markers *Runx2* and *Col1a1*. Knockout cells were also found to express significantly higher levels of *Pparγ* and *Lpl* transcripts. These observations suggested that PAR_2 promotes osteogenic conversion of mesenchymal progenitors at the expense of adipogenesis.

1.5 Aims of the study

There is still not much known about the role of PAR_2 in bone, but given what is known about the receptor itself and based on recent findings, it appears that it is important in two different aspects of bone biology: inflammatory states that can lead to bone loss, and regulation of the reciprocal relationship between osteogenesis and adipogenesis. Accordingly, the hypotheses of this study were set as 1) PAR_2 is a mediator of inflammation induced osteopoenia and as such its deletion will improve the resulting bone phenotype, and 2) PAR_2 activation regulates the determination of mesenchymal cell fate such that osteoblastogenesis is preferred over adipogenesis.

In addressing the first hypothesis, the mdx mouse model was selected. These mice develop a similar osteopoenic profile to those of the DMD patients which is suggested to be the result of their heightened inflammatory state (Novotny et al. 2011; Rufo et al. 2011). As PAR_2 has previously been shown to contribute to the pathology of arthritis and periodontitis related bone loss, it was considered desirable to further investigate the role of the receptor in another similar condition.

Activation of PAR_2 activates multiple MAP kinases such as ERK1/2 and p-38 all of which are crucial modifiers of Runx2 and Osterix signalling in osteoblasts (Xiao et al. 2000; Wang et al. 2007). These signals as well as others, are potentially common to both PAR_2 and BMP or Wnt signalling pathways (Figure 1.4). This, in addition to what is presented under section 1.4.4, suggests that PAR_2 is likely to be a pro-osteogenic and anti-adipogenic modifier. This needs to be further investigated using a properly controlled *in vitro* model.

A previous study demonstrated that while exhibiting a higher bone mass profile at 7 weeks, global PAR_2 deficient mice exhibit lower osteoblast and osteoclast surfaces than wildtype mice. This, as well as a relatively fast drop to values comparable to those of the wildtype group at 13 weeks, suggested that lack of PAR_2 may cause an osteopoenic profile at a later age. This needs to be tested using a similar global PAR_2 knockout model, while at the same time obtaining baseline information on bone mass in non-mdx PAR_2 knockout mice at the ages used for the study in mdx mice. Moreover, due to the limitations of global knockout models, osteoblast specific PAR_2 null mice needed to be generated to be able to distinguish

effects on bone structure of PAR_2 expressed by osteoblasts from those of PAR_2 expressed by other cell types. Accordingly, this study aimed to:

1. Identify the role of PAR_2 in the perceived bone loss associated with inflammatory conditions.
2. Confirm the prediction that global lack of PAR_2 results in loss of bone mass in ageing mice older than 13 weeks.
3. Establish an *in vitro* model to further study the role of PAR_2 in the regulation of the reciprocal relationship between osteogenesis and adipogenesis.
4. Achieve osteoblast specific deletion of the PAR_2 gene in an *in vivo* mouse model and evaluate the resultant bone phenotype.

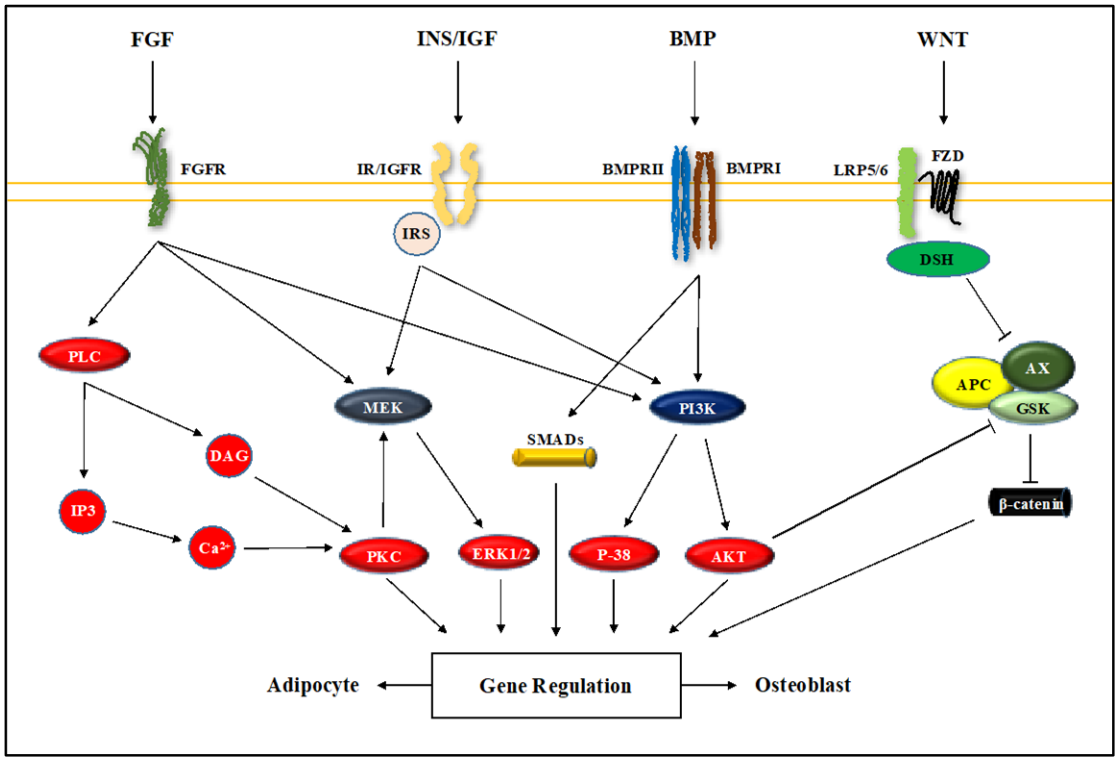


Figure 1.4 Extracellular regulating signals of osteo/adipogenesis.

Various extracellular signals appear to regulate both osteoblastic and adipocytic differentiation of MSCs. Here, only pathways with significant overlapping features have been demonstrated. Potential points of crosstalk with PAR_2 signalling are shown in red. Abbreviations: **AKT**, protein kinase B; **APC,** adenomatosis polyposis coli; **AX**, axin1/2; **DAG**, diacylglycerol; **DSH**, disheveled; **ERK**, extracellular signal regulated kinases; **GSK**, glycogen synthase kinase 3β; **IP3**, inositol 1,4,5-triphosphate; **MEK**, MAPK/ERK Kinase; **PI3K**, phosphatidylinositol-3-kinase; **PKC**, phosphokinase C; **PLC**, phospholipase C.

CHAPTER 2: MATERIALS AND METHODS

2.1 Materials

2.1.1 Animals

Mice used for this research were housed and maintained in the animal house facility at the Veterinary Preclinical Centre, Faculty of Veterinary and Agricultural Sciences, University of Melbourne. Weaning was carried out for animals 3 weeks of age or older and breeders were paired only after 6 weeks. The use of all animals in this study was approved by the Gene Technology and Biosafety Committee of the University of Melbourne and the Animal Ethics Committee of the Faculty of Veterinary and Agricultural Sciences (AEC ID 1413256, 1413381 and 1513784). Mice were housed in a controlled environment with free access to food and water, and all work was conducted in compliance with the Australian Code for the Care and Use of Animals for Scientific Purposes (2013) and the National Health and Medical Research Council's Guidelines for the Generation, Breeding, Care and Use of Genetically Modified and Cloned Animals for Scientific Purposes (2007).

2.1.1.1 Global PAR_2 Null Mouse

Global PAR_2 null mice (Lindner et al. 2000b) were kindly provided by Professor Shaun Coughlin of the Cardiovascular Research Institute, University of California, San Francisco. The colony was maintained as heterozygous breeding stock (*F2RL1*$^{+/-}$) on a C57BL/6J background (Lindner et al. 2000b). Male and Female wildtype (*F2RL1*$^{+/+}$) and knockout (*F2RL1*$^{-/-}$) mice generated from these breeders or their homozygous offspring were randomly allocated to experimental groups as described in chapter 3.

2.1.1.2 Dystrophin Deficient PAR_2 Null Mouse

Generation of PAR_2 null mdx mice was carried out as part of a separate project (Dr. Neda Taghavi, The University of Melbourne) where female C57BL10ScSn mdx mice (Bulfield et al 1984) were crossed with male global PAR_2 null mice (Taghavi 2016). The hemizygous mdx males of the first generation (that were also heterozygous for PAR_2 null allele - *F2rl1*$^{+/-}$

) were then backcrossed with female mdx mice to generate mdx mice that were heterozygous for the PAR_2 null allele (*F2rl1*$^{+/-}$). These mice were then crossed with each other to generate PAR_2 null and wildtype mdx mice, which were used as described in chapter 4. Genotyping was performed as per sections 2.2.9.1 and 2.2.9.3. The dystrophin-deficient phenotype of these mice was further confirmed by immunohistochemical staining of the muscle tissue obtained from a random littermate using anti-dystrophin antibody (Taghavi 2016).

2.1.1.3 Osteoblast specific PAR_2 null Mouse

Osteoblast specific PAR_2 null mice were generated using a Cre/lox system. Transgenic *Osx-Cre* mice [*Tg(Sp7-tTA,tetO-EGFP/cre)*] (Rodda 2006) were kindly provided by Dr. Andrew McMahon, University of Southern California. PAR_2 floxed mice (*F2rl1*$^{fl/fl}$), in which *F2rl1* is flanked by loxP sites, were generated by Dr. Charles N. Pagel (The FVAS, University of Melbourne). *Osx-Cre* and *F2rl1*$^{fl/fl}$ mice were backcrossed for over at least three generations to obtain breeding stocks of *Osx-Cre.F2rl1*$^{wt/\Delta}$ mice. Littermate osteoblast specific PAR_2 null mice (*Osx-Cre.F2rl1*$^{\Delta/\Delta}$) and appropriate controls (*Osx-Cre.F2rl1*$^{wt/wt}$, *F2rl1*$^{wt/wt}$ and *F2rl1*$^{fl/fl}$) were generated by crossing *Osx-Cre.F2rl1*$^{wt/\Delta}$ parents or their homozygous offspring. Osx-Cre negative mice (*F2rl1*$^{wt/wt}$ and *F2rl1*$^{fl/fl}$) used as controls were also similarly generated as Osx-Cre was not always present in the offspring. Use of control *Osx-Cre.F2rl1*$^{wt/wt}$ mice generated in the process was considered essential to control for the presence of the Osx-Cre transgene (Davey et al. 2011). Male and female mice of all genotypes were euthanised at 50 and 90 days as described in chapter 5.

2.1.2 Media and Reagents

All reagents including AEBSF, ascorbic acid, benzoyl peroxide, β-glycerophosphate, butyl/methyl methacrylate, Fura-2 AM, hexadimethrine bromide, probenecid and puromycin were obtained from Sigma Aldrich (St. Louis, Missouri, USA) unless otherwise specified. α-MEM, Dulbecco's Modified Eagles Medium (DMEM), trypsin and antibiotics were purchased from Gibco™-Life Technologies (Scoresby, Victoria, Australia). Foetal calf serum (USA origin) was purchased from Bovogen Biologicals (East Keilor, Victoria, Australia). Collagenase A for the isolation of murine primary osteoblasts was purchased from Roche Diagnostics (Indianapolis, Indiana, USA). MISSION™ shRNA lentiviral

transduction particles were acquired from Sigma Aldrich (St. Louis, Missouri, USA). All polymerase chain reaction (PCR) reagents, Wizard® Genomic DNA Purification kit, Wizard® SV Gel and PCR Clean-up kit, Total RNA Isolation system and GoScript™ reverse transcription mix were obtained from Promega (Madison, Wisconsin, USA). PRISM® BigDye® terminator v3.1 was from Applied Biosystems (Carlsbad, California, USA). Anti-IL-6 antibody and IL-6 ELISA kit were purchased from Thermo Fisher Scientific (Waltham, MA, USA). Experiment grade deionised water was produced by ion exchange and reverse osmosis in a MilliQ water purification system (Millipore, Darmstadt, Germany).

2.1.3 Equipment

Polymerase chain reactions were carried out in a Bio-Rad T100™Thermal Cycler (Hercules, CA, USA). Visualisation and image acquisition of the agarose gels was performed with use of a Chemi-Smart 2000 gel documentation system (VilberLourmat, Marne-la-Vallée, France). Micro Computed Tomographic images (micro CT) were acquired using a Scanco Micro CT 50 scanner (Scanco Medical AG, Bruettisellen, Switzerland). Resin embedded samples were trimmed and sliced with use of an IsoMet® 1000 precision saw (Buehler, Lake Bluff, IL USA) and a POLYCUT heavy duty sliding microtome (Meyer Instruments, Houston, TX, USA), respectively. An Olympus 1X70 inverted microscope (Tokyo, Japan) fitted with a ProgRes® C3 camera (Jenoptik, Thuringia, Germany) was used to acquire cell culture images. All colorimetric assays were performed using a Synergy H1 microplate reader (BioTek, Winooski, VT, USA). Intracellular calcium was measured using a BMG FLUOstar Galaxy microplate reader (BMG Lab Technologies, Germany). The quality and quantity of the DNA and RNA were determined by UV absorbance at 260 and 280 nm, respectively, using a Nanodrop spectrophotometer ND-100 (Thermo Scientific, Wilmington, DE, USA). DNA and RNA samples were concentrated in a Dynavac Medosjak DC40 Concentrator (Hingham, MA, USA) if required.

2.2 Genotyping and Polymerase Chain Reaction

2.2.1 Genomic DNA Isolation

When genomic DNA was needed for the genotyping of mice, ear biopsy samples acquired at weaning were processed using the HotSHOT method (Truett et al. 2000). Samples were placed in a 1.5 mL clear Eppendorf tube with 75 μL alkaline lysis buffer (NaOH [25 mM]; ethylenediaminetetraacetic acid [EDTA, 0.2 mM]), heated to 95°C for 30 minutes and then neutralised using 75 μL neutralisation buffer (Tris-HCL [40 mM], pH 5).

For any other purposes, genomic DNA was isolated using a Wizard® Genomic DNA Purification kit. Pulverised tissues were processed by placing them in 1.5 mL nuclease free Eppendorf tubes with 600 μL nuclear lysis buffer. For cell cultures, nuclear lysis buffer was directly applied to the wells and lysates transferred to Eppendorf tubes for further processing. If required, lysates were kept at -80°C until processed later. DNA was purified as per the manufacturer's instructions following by elution in 100 μL nuclease free water. Storage was carried out at 4°C if used within one week or at -20°C for long term purposes.

2.2.2 DNA Extraction from Agarose Gels

The band of the appropriate size was excised out of the agarose gel under direct visualisation with violet light, weighed in a nuclease free Eppendorf tube and then processed according to the Wizard® kit instructions. This entailed permanently liquefying the gel at 65°C using the membrane binding solution (10 μL per 10 mg agarose) followed by purification in a mini column by centrifugation (14,000 g). DNA was eluted in 50 μL nuclease free water.

2.2.3 Total RNA Isolation

Total RNA was isolated using the Total RNA Isolation mini columns according to the manufacturer's instructions (Promega). RNA was eluted in 50-100 μL nuclease free water and stored at -80°C if not used immediately.

2.2.4 Primer Design and Validation

PCR primers were designed in NCBI's native Primer-Blast environment (https://www.ncbi.nlm.nih.gov/tools/primer-blast/) and evaluated for the presence of secondary structures and homo/heterodimers using IDT Oligo Analyzer Version 3.1 (http://sg.idtdna.com/calc/analyzer) before being synthesized by Geneworks (Adelaide, Australia). For the comprehensive list of primers used in this work, please refer to Table 2.1. Where primers were being used for the first time, specificity was confirmed by product size measured on an agarose gel and DNA sequencing as described in section 2.2.8. For qPCR reactions, this was also evaluated at the end of each run by running a thermal melt profile cycle. To determine primer efficiency, first a standard curve was created by plotting the Ct (cycle threshold) value of each standard against the corresponding relative concentration or copy number. If $R^2 > 0.98$, then primer efficiency was calculated as $E = 10^{-1/slope}$ where E is efficiency. Only primer pairs with an E of 1.8-2.2 (90-110%) were selected to be used in this study.

2.2.5 Polymerase Chain Reaction

Polymerase chain reaction was conducted in a 20 µL reaction containing 100-400 ng of template, Taq DNA polymerase (0.5 U), forward and reverse primers (0.4 µM each), deoxynucleotide triphosphates mix (1 mM), magnesium chloride (1.5 mM) and 5x green PCR buffer (4 µl). Thermal cycling involved 35 cycles of denaturation at 95°C for 30 seconds followed by annealing at 50-60°C for 30 seconds and extension at 72°C for 30-40 seconds. This was optimised for each primer set before the experiments. PCR products were resolved on a 1-3% agarose gel (w/v) in Tris boric acid EDTA buffer at a constant voltage (4-8 V/cm) before being visualised in the gel documentation facility. SYBR safe DNA dye (Invitrogen, Carlsbad, CA, USA) was manually added to molten agarose before casting (4 µL per 100 mL gel).

Table 2.1 PCR primers.

Primers used for genotyping purposes have not been listed here. Refer to section 2.2.9 for details.

No.	Target Gene	Forward and Reverse Primers	Product Size (bp)	Design
1	*Acr*	5' GCGCTCTTGAAGATCACTCC 3' 5' ACAGGTCGAGGTCAATGAGG 3'	196	Georgy et al. 2012
2	*Arhgap22*	5' GAAGAACCTTCGCTGCCAGA 3' 5' CTGATCCCCTCGTAGCACAA 3'	188	R.S.†
3	*BMP7*	5' CACCCTCGATACCACCATCG 3' 5' GCAAGAAGAGGTCCGACTCC 3'	190	R.S.
4	*C1qtnf3*	5' GCCCCCGTATCAGGTGTGTAT 3' 5' GCTGAAGACTGTGTTGCCGT 3'	105	R.S.
5	*Cnr1*	5' TCTCATAGAGTCTGGGGGCAAAT 3' 5' CAGGCTCAACGTGACTGAGAA 3'	147	R.S.
6	*Col1a1*	5' GAGCGGAGAGTACTGGATCG 3' 5' GTTCGGGCTGATGTACCAGT 3'	142	Georgy et al. 2010
7	*Crct1*	5' GCCTAGCAGGTGTCAAGTTCC 3' 5' CTGTTGAGACATCTCGGCGTT 3'	97	R.S.
8	*Ctgf*	5' GGCATCTCCACCCGAGTTAC 3' 5' CAAACTTGACAGGCTTGGCG 3'	160	R.S.
9	*Cyp51*	5' GCCTATGTGCCATTTGGAGC 3' 5' GGGTTTTCTGGGGTGTGGAT 3'	170	R.S.
10	*Dhcr7*	5' CCCTTGCTATGGTGTGCCAA 3' 5' TCAAACCACTTCCCGATGCG 3'	167	R.S.
11	*Dhcr24*	5' GCCCAGCAAGCTGAATAGCA 3' 5' GAGGTAGCGGAAGATGGGGT 3'	196	R.S.
12	*Enpep*	5' GTGGGACGACTTGTGGCTAA 3' 5' TTGCACGGGGAACACATCTT 3'	124	R.S.
13	*F3*	5'CAAAATAGCCCAGGAAGCAG 3' 5'GGGGTGTTCTTCCCTTTCTG 3'	176	Taghavi 2016
14	*F7*	5' ACCAGTACTGCAGGGACCAT 3' 5' GGTATTCTCCCACACGGGTA 3'	121	Taghavi 2016
15	*F10*	5' TGAACTGCTCAACCTCAAG 3' 5' CCCACAGAACCCTTCATTGT 3'	142	Taghavi 2016
16	*Fabp4*	5' GGTGCAGAAGTGGGATGGAA 3' 5' GCCCTTGCATAAACTCTTGTGG 3'	114	Kularathna 2015
17	*F2rl1*	5' CTTCCTTTTCCGAACGAA 3' 5' ACAAGGTAGAGGGCGTAG 3'	687	Taghavi 2016

18	*F2rl1*	5’ GTCTCCTTGGCAATCTGGCT 3’ 5’ CCCCCACCAATACCTCCTCA 3’	133	R.S.
19	*F2rl1**	5’ AACATCACCACCTGTCACGA 3’ 5’ GGATAGCCCTCTGCCTTTTC 3’	196	R.S.
20	*Gapdh*	5’ CTGCACCACCAACTGCTTAG 3’ 5’ GTCTTCTGGGTGGCAGTG 3’	108	Kularathna 2015
21	*Gpr35*	5’ TGGACAGAGACCCGCATCTA 3’ 5’ GCAGTGACCAGGCTTATGCT 3’	176	R.S.
22	*Grem1*	5’ CACTCGTCCACAGCGAAGAA 3’ 5’ CTTGTCAGGAGGCGGAATGG 3’	159	R.S.
23	*Gzma*	5’ CACGGTTGTTCCTCACTCAA 3’ 5’ GAGTGAGCCCCAAGAATGAA 3’	153	Taghavi 2016
24	*Hmgn5*	5’ TCAGCCCGACTGTCTGCTAT 3’ 5’ ACATCTTCTGGCTTGGTTTCAGG 3’	152	R.S.
25	*Hpn*	5’ GAGTGACCAGGAGCCACTGT 3’ 5’ AGAAAGCCCATCTCCTCACA 3’	153	Georgy et al. 2012
26	*Hprt*	5’ GTTGGGCTTACCTCACTGCT 3’ 5’ GGTCCTTTTCACCAGCAAGC 3’	598	R.S.
27	*Hprt*	5’ AGTCCCAGCGTCGTGATTAG 3’ 5’ ATGGCCTCCCATCTCCTT 3’	168	R.S.
28	*Hprt**	5’ TGGAACTGGGCAGGACTAGG 3’ 5’ AGCATGGGGGCTAGAGAAGG 3’	139	R.S.
29	*Il6*	5’ GGATACCACTCCCAACAGACC 3’ 5’ GCAAGTGCATCATCGTTGTTCATA 3’	141	R.S.
30	*Insig1*	5’ TCTTCCCCGACGAGGTGATA 3’ 5’ CTAATTTGGCACTGGCGTGG 3’	207	R.S.
31	*Klk4*	5’ TGACCCTGTGTACCACCTCA 3’ 5’ TCATGTGGGCCTTGTAGTCA 3’	248	Georgy et al. 2012
32	*Klk5*	5’ GAAAGTCCTCCAGTGCCTGA 3’ 5’ ATTGCAGACCACAGGACCTC 3’	154	Georgy et al. 2012
33	*Klk6*	5’ GGTCCTATTGACCCACAGT 3’ 5’ TGGATTTTTCAGATGCACCA 3’	198	Georgy et al. 2012
34	*Klk14*	5’ CCTGTGTGGAGGAGTCCTGT 3’ 5’ GGTTGATACTGGGGATGTGG 3’	165	Georgy et al. 2012
35	*Lect1*	5’ GCTGTGAACAACTTGGAGACCT 3’ 5’ TCTTGCCTTCCAGTTCAGAGAT 3’	196	R.S.
36	*Lin7a*	5’ CCCGATTTACATCTCCCGCAT 3’ 5’ CCTTCCACACTCACTCCGTT 3’	105	R.S.

37	*Lpl*	5’ ACAACCAGGCCTTCGAGATT 3’ 5’ AGTCAGGCCAGCTGAAGTAG 3’	186	Kularathna 2015
38	*Mfi2*	5’ TGCTCAAAGCCGTTGGTGATT 3’ 5’ CTCCTTCCGCCAGGCAC 3’	183	R.S.
39	*Mmp8*	5’ TTTGGGACTCTCTCACTCCAC 3’ 5’ ATCAAATCTCAGGTGGGGGTC 3’	193	R.S.
40	*Mmp9*	5’ GCCATGCACTGGGCTTAGAT 3’ 5’ TCGGCTGTGGTTCAGTTGTG 3’	180	R.S.
41	*Mvd*	5’ GGACACTCTACCCCTCAGCC 3’ 5’ GGAGAGGTCTCCCTCAACCC 3’	151	R.S.
42	*Olr1*	5’ GGCTGAGGTCCTCGACTGT 3’ 5’ CCAGGCAGAGGATGACCAGA 3’	190	R.S.
43	*Prss1*	5’ TCTGTGGAGGTTCCCTCATC 3’ 5’ GTTGGGGTGCTTGATGATCT 3’	155	Georgy et al. 2012
44	*Pparg*	5’ ATCTCAGAGGGCCAAGGATT 3’ 5’ GGCGGTCTCCACTGAGAATA 3’	172	Kularathna 2015
45	*Ppia*	5’ TCAACCCCACCGTGTTCTTC 3’ 5’ TCCAGCTAGACTTGAAGGGGA 3’	649	R.S.
46	*Ppia*	5’ CACAAACGGTTCCCAGTTTT 3’ 5’ TTCACCTTCCCAAAGACCAC 3’	81	R.S.
47	*Ramp3*	5’ GTTGCTGCTTTGTGGTGAGT 3’ 5’ GTCTCCATCTCGGTGCAGTT 3’	186	R.S.
48	*Rgs2*	5’ ATGCAAAGTGCCATGTTCCTG 3’ 5’ CCAATCCTTTAAGAGTGTCCGCT 3’	123	R.S.
49	*Runx2*	5’ CTTCACAAATCCTCCCCAAG 3’ 5’ ATGCGCCCTAAATCACTGAG 3’	147	Georgy et al. 2010
50	*Scg2*	5’ AGCTGTCCGGTGCTGAAAC 3’ 5’ AACTGCTCCAAGTCGGTACG 3’	136	R.S.
51	*Snorc*	5’ CCATAAGACTGCTCACTCCCTG 3’ 5’ CCTTCACCAGAGGGCAATTCAA 3’	167	R.S.
52	*Tcea3*	5’ CGGAAGAAGACGGAAGGGG 3’ 5’ CCTTGTCTGAGCAGTGCTTG 3’	130	R.S.
53	*Tmprss2*	5’ ACATTGTCCAACGGAGAAG 3’ 5’ TCTCCCGTAGCTTCACTCC 3’	136	Georgy et al. 2012
54	*Tmprss6*	5’ ACAGCCATGACTACGACGTG 3’ 5’ GTCCTGAGGACCAGCTGTA 3’	206	Georgy et al. 2012
55	*Tmprss11d*	5’ GCCCTGGCAAGTCAGTCTTAC 3’ 5’ TGTCACGAGTTACGGAGCTG 3’	218	Georgy et al. 2012

56	*Tpsab1*	5’ GAGACCTTCCCCTCAGGAAC 3’ 5’ ATGTCCTTCATTCCCAGCAC 3’	213	Georgy et al. 2012
57	*Tpsb2*	5’ CTACCCATCTCCACCCCATA 3’ 5’ CCACAATGGGAACCTTCACT 3’	150	Georgy et al. 2012

* denotes primers that were designed to target genomic DNA. All other primers target cDNA reverse transcribed from isolated total RNA.
† **R.S.**, author.

2.2.6 Complementary DNA Synthesis

Up to 1 µg total RNA per sample was brought to 10 µL final volume by adding nuclease free water and incubated at 70°C for 5 minutes to break down potential secondary structures. This was followed by immediate chilling in iced water for at least 15 minutes before the addition of 10 µL GoScript™ reverse transcription mix which contained 4 µL nuclease free water, 4 µL GoScript™ Reaction Buffer & Oligo (dt) as well as 2 µL GoScript™ Enzyme Mix. The reverse transcription reactions were incubated in a thermal cycler at 25°C for 5 minutes to anneal primer followed by 42°C for 60 minutes to extend. At the last step, the reverse transcriptase was inactivated at 70°C for 15 minutes and cDNA stored at 4°C if used within a week or -80°C if later.

2.2.7 Quantitative Polymerase Chain Reaction

Relative DNA abundance, mRNA copy number and relative expression of a number of genes was measured by use of quantitative PCR (qPCR). Each PCR reaction contained 100-500 ng template in 10 µl 2x SYBR Green qPCR master mix (Applied Biosystems, California, USA) and 2 µl forward and reverse primers (250 nM each), brought to 20 µl with milliQ water. Following a 10 minute hot start at 95°C to activate Taq polymerase, amplifications were carried out by denaturing at 95°C (30 seconds), annealing at 60°C (30 seconds) and extending at 72°C (30 seconds) for a total of 40 cycles.

The linear range of the amplification plots was used by the software to automatically generate a threshold based on which Ct values were calculated. A thermal melt profile was

also generated for every sample between the temperatures of 70°C to 90°C at the conclusion of each run to evaluate primer specificity.

Mean normalised expression (MNE) or relative DNA abundance (RDA) was calculated using either *Ppia*, *Hprt* or *Gapdh* as the reference gene (Pfaffl et al. 2004). In chapter 5, the geometric mean of all these three genes (Best Keeper Index [BKI]) has been adopted as the reference (Pfaffl et al. 2004). MNE or RDA was calculated using the formula presented below (Muller et al. 2002).

$$\text{MNE or RDA} = \frac{(E_{\text{target}})^{Ct\text{target}}}{(E_{\text{reference}})^{Ct\text{reference}}}$$

E: primer efficiency
Ct: mean cycle threshold of technical replicates

To calculate PAR_2 mRNA copy number, first a relatively large target cDNA sequence (598-687 bp) was amplified using primer pairs no. 17, 26 and 45 (Table 2.1). The products were resolved on an agarose gel and then extracted and purified according to section 2.2.2 followed by sequencing as described under 2.2.8.
The number of copies per µL was calculated based on the concentration of the DNA, its molecular weight and Avagadro's constant using the formula shown below

Copy number = (concentration x 1000/Molecular weight) * 6 x 10^{23}

Products were then serially diluted by a ratio of 10:1 to generate the standard solutions. Using nested primer pairs no. 18, 27 and 46 (Table 2.1), Ct values were plotted against the copy number of the serially diluted standards and a standard curve was generated. Computed sample values (in copy number) were expressed as the number of copies of the gene of interest (PAR_2) to the number of copies of a reference gene (Hprt or Ppia).

For the purpose of calculating mRNA or RDA knockdown following the *Osterix* driven ablation of PAR_2 from osteoblasts (chapter 6), the following formula was used:

$$\text{knockdown } (\%) = \ 100\times(\bar{C}_{wt} - C_{\Delta})/\bar{C}_{wt}$$

$\bar{C}_{wt}$: mean PAR_2 relative copy number/RDA for the *Osx-Cre.F2rl1*$^{wt/wt}$ mice

C_{Δ}: PAR_2 mRNA relative copy number/RDA for the *Osx-Cre.F2rl1*$^{\Delta/\Delta}$ mice

2.2.8 DNA Sequencing

After amplification, PCR products were resolved on a 2% agarose gel, products of the correct size were excised and purified as described under 2.2.2. A sequencing reaction was carried out by adding 1-10 ng DNA to 1 µL ABI PRISM® BigDye® terminator v3.1 reaction mix, 3 µL 5x dilution buffer (Tris-HCL [400 mM], pH 9.0 and $MgCl_2$ [10 mM]) and either forward or reverse primer (4.2 µM) which was then brought to a total of 12 µL by adding milliQ water. The thermal profile used consisted of a 4 minute cycle at 94°C followed by 30 cycles at 96°C for 10 seconds, 50°C for 5 seconds and 60°C for 4 minutes. At completion, 8 µL milliQ water was added to the reaction mix and DNA was precipitated by adding 3 µL sodium acetate (3 M, pH 4.6), 62.5 µL 95% (v/v) ethanol and 14.5 µL milliQ water. The pellet was then washed with 70% (v/v) ethanol and dried in a Dynavac Medosjak DC40 Concentrator (Hingham, MA, USA). The DNA sequences were read by a capillary separation automated sequencer at the Australian Genome Research Facility (AGRF, Victoria, Australia). Sequencing data were viewed using Serial Cloner 2.6 (Frank Perez [SerialBasics]) and cross checked against reference databases using NCBI's standard nucleotide Basic Local Alignment Tool (BLAST® blastn suite: https://blast.ncbi.nlm.nih.gov/Blast.cgi).

2.2.9 Genotyping of Mice

2.2.9.1 Global PAR_2 Null Mice

Genomic DNA was extracted using the HotSHOT method as per section 2.2.1 and PCRs performed as described in 2.2.5. An annealing temperature of 55°C was selected for such amplification. A set of three primers designed and validated by Dr. Charles Pagel, (The

University of Melbourne) were used for this purpose which included PAR_2 forward primer (5' CTCTACCTTGTCGCCCTCTG 3'), PAR_2 reverse primer (5' CTTAGCCTTCTTGCCAGGTG 3') and pNTK (plasmid NTK) forward primer (5' GGGGAACTTCCTGACTAGGG 3'). Using these primers, a PCR product size of 599 bp, resolved on a 2% (w/v) agarose gel, is indicative of a wildtype allele ($F2RL^{+/+}$) whereas a 459 bp product indicates the knockout allele ($F2RL1^{-/-}$).

2.2.9.2 Osteoblast Specific PAR_2 Null Mice

The genotyping of osteoblast specific PAR_2 null mice involved a two step procedure to first identify the presence of Osx-Cre and then the floxed PAR_2 alleles. To identify Osx-Cre transgenes, a primer set of 5' GCCATGCCCGAAGGTTATGT 3' and 5' TG ATCCTGGCAATTTCGGCT 3' targeting the GFP::Cre construct was used. These primers were designed and validated by the author. An annealing temperature of 57°C was used to amplify a product of approximately 1000 bp size. Positive transgenes were identified by a single band on 1% (w/v) agarose gel whereas wildtypes were negative for any products (Figure 2.1).

The primer set used to distinguish floxed PAR_2 allele from the wild type allele included tm1c forward (5' CTGCCTTACTCACCAAAGACTCG 3') and reverse (5' CTTCT TCCTTTACTGTTGTTGC 3') primers, designed and validated by Dr. Charles Pagel (The University of Melbourne). An annealing temperature of 56°C was selected for amplifications. A product size of 556 bp on a 2% (w/v) agarose gel indicated the presence of the wildtype allele, and a 651 bp product the floxed PAR_2 allele (Figure 2.1).

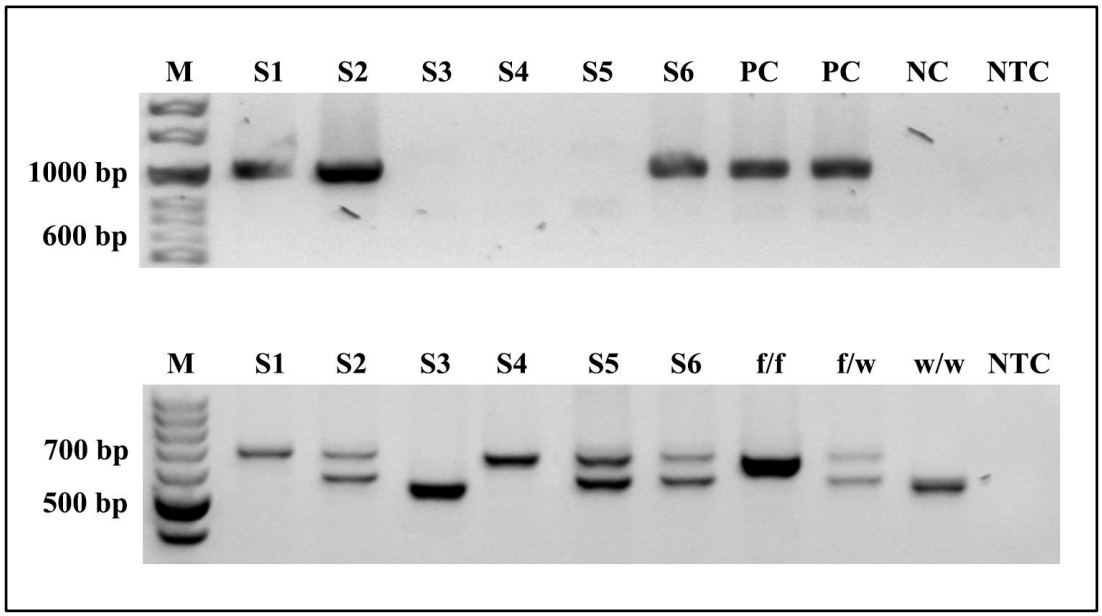


Figure 2.1 PCR based genotyping of osteoblast specific PAR_2 null mice.

The upper image demonstrates Osx-Cre genotyping where a single band is indicative of the presence of the transgene. In the bottom image, genotyping for floxed versus wildtype allele is demonstrated. **M**, molecular weight marker; **S**, sample; **PC**, Osx-Cre positive control; **NC**, Osx-Cre negative control; **f**, floxed allele; **w**, wildtype allele; **NTC**, no template control.

2.2.9.3 Dystrophin Deficient (mdx) Mice

The mdx mutation in the dystrophin gene was identified by competitive PCR for dystrophin using a set of three primers which included a common forward primer, DL1577 (5' GCGCGAAACTCATCAAATATGCGTGTTAGTGT 3'), a wild type reverse primer, DL1509 (5' GATACGCTGCTTTAATGCCTTTAGTCACTCAGATA GTTGAAGCCATTTT 3') and a mutant reverse primer, DL1573 (5' CGGCCTGTCA CTCAGATAGTTGGAAGCCATTTTA 3') as described (Shin et al. 2011). The thermal cycling comprised of two steps: PCR started by 5 cycles at 95°C for 20 seconds, 60°C for 20 seconds and 72°C for 20 seconds followed by 23 cycles at 95°C for 20 seconds, 64°C for 20 seconds and 72°C for 20 seconds. Products were resolved on a 3 % (w/v) agarose gel where a 134 bp product was associated with the wildtype genotype and a 117 bp as the mdx. Breeding and genotyping of this mouse colony was carried out by Dr. Neda Taghavi (The University of Melbourne).

2.3 Cell Culture

2.3.1 Kusa 4b10 Cell Line

Kusa 4b10 cells were kindly provided by Dr. Natalie Sims of the St. Vincent's Institute of Medical Research, Melbourne, Australia. Cells were maintained in α-modified Eagle's minimal medium (α-MEM) and 10% foetal calf serum (FCS) at 37°C under 5% CO_2 (Walker et al. 2008).

Osteoblast differentiation was carried out in α-MEM containing 15% heat inactivated FCS, ascorbic acid (50 μg/ml) and β-glycerophosphate (10 mM; Walker et al. 2008). If RNA isolation or Oil-Red O staining was planned, β-glycerophosphate was omitted. For adipogenesis, α-MEM containing 15% FCS, insulin (6.6×10^{-8} M), 3-isobutyl-1-methylxanthine (2.5×10^{-10} M) and dexamethasone (10^{-8} M) was used (Allan et al. 2003; Walker et al. 2008). A vehicle control medium comprised of α-MEM containing 15% HIFCS and water in the case of osteogenic and 15% FCS and DMSO in the case of adipogenic treatment was also used. Media were changed once every three days throughout both maintenance and differentiation stages.

For differentiation experiments, cells were subcultured and regularly maintained at a density of 3,000 cells/cm^2 (Allan et al. 2003) in 12-well plates (1.14×10^4 cells per well) if mineralisation assays or morphological measurements were to be performed or in 6-well plates for RNA isolation (2.85×10^4 cells per well). On day 3 (differentiation day 0), the medium was changed to either osteoblast or adipocyte differentiation medium.

2.3.2 Primary Osteoblast Cultures

Long bone osteoblasts were isolated using a modification of a procedure described by Bakker and Klein-Nulend (Bakker and Klein-Nulend 2011). Mice, nine weeks or older, were euthanised in a CO_2 chamber individually. Skin was aseptically prepared by soaking in 70% ethanol and removed by making an incision in the mid-abdominal region and pulling the skin edges cranially and caudally. Long bones (humeri, radii, ulnae and femora) were excised and placed in a petri dish with PBS. All soft tissues were then carefully removed and periosteum scraped off using a number 11 scalpel blade. Bones were then

washed three times in a 15 mL tube with PBS by vigorous shaking. Cleaned bones were taken to a new jar and their epiphyses removed using a pair of scissors immediately before flushing the marrow cavities using a 27-gauge hypodermic needle, a 5 mL syringe and PBS. Using scissors, bones were chipped into 1-2 mm pieces, washed three more times and immersed in 0.25% (w/v) collagenase A in DMEM for 2 hours at 37°C with vigorous agitation every 15 minutes to remove the remaining adherent cells and tissues. After this time, the bone chips were washed three times in complete culture medium which consisted of DMEM supplemented with penicillin (100 U/mL), streptomycin sulphate (100 μg/mL), L-glutamine (29 μg/mL), ascorbic acid (100 μg/mL) and 10% FCS. Chips were then dispersed across a 25 cm^2 flask and cultured at 37°C with 5% CO_2 for 4 to 6 weeks before splitting or experimentation.

2.3.3 Mycoplasma Screening

Mycoplasma screening of cultures was carried out using a protocol previously described (Uphoff and Drexler 2011). Briefly, following expansion and banking, cultures continuously grown for over two weeks were selected and media sampled. To ensure that the titer of mycoplasmas was higher than the assay threshold, media exchange was not carried out for three days prior to sampling. One millilitre of medium was then pelleted at 14,000 x g for 5 minutes. This was followed by removal of the supernatant and washing three times in PBS. After the final wash, pellet was resuspended in PBS (100 μL) and genomic DNA extracted using the technique described for cell culture under 2.2.1. The primers used (Table 2.2) provide an effective way of identifying known contaminating mycoplasmas and not airborne bacteria that could potentially cause false positive results (Uphoff and Drexler 2011). Template from previously known positive cultures was used as control.

Table 2.2 PCR primers used for mycoplasma screening.

A mix of both forward and reverse primers at 0.1 μM each was used in each reaction.

5' Primers	3' Primers
CGC CTG AGT AGT ACG TTC GC	GCG GTG TGT ACA AGA CCC GA
CGC CTG AGT AGT ACG TAC GC	GCG GTG TGT ACA AAA CCC GA
TGC CTG GGT AGT ACA TTC GC	GCG GTG TGT ACA AAC CCC GA
TGC CTG AGT AGT ACA TTC GC	
CGC CTG AGT AGT ATG CTC GC	
CAC CTG AGT AGT ATG CTC GC	
CGC CTG GGT AGT ACA TTC GC	

2.3.4 Intracellular Calcium Mobilisation Assay

Cells grown to full confluence in a 75 cm^2 tissue culture flask were lightly trypsinised, centrifuged at 175 x g for 5 minutes and resuspended in 30 mL medium. The suspension was stirred overnight (~15 hours) in small Techne® vessels (Cole-Parmer, UK) at minimum speed while being incubated at 37°C in 5% CO_2 to allow recovery of cells from trypsin. On the next day, cells were centrifuged and washed twice with 8-10 mL α-MEM. The pellet was then resuspended in 5 mL extracellular medium (NaCl [121 mM]; KCl [5.4 mM]; $MgCl_2.6\ H_2O$ [0.8 mM]; $CaCl_2$ [1.8 mM]; $NaHCO_3$ [6 mM]; glucose [5.5 mM]; HEPES [25 mM]; probenecid [2.5 mM]) with 0.1% (w/v) BSA and 5 μL 1 mM Fura-2 AM (1 μM final concentration) followed by incubation at room temperature while being protected from light and agitated for 45 minutes. After this time, cells were pelleted again and resuspended in 5 mL extracellular medium with BSA and agitated for another 15 minutes. Following centrifugation, the pellet was resuspended this time in extracellular medium without BSA and plated out into a 96 well plate, 100 μL per well at approximately 2 x 10^5 cells per well density. The plate was kept in the microplate reader for approximately 10 minutes to allow for temperature equilibration (37°C) whilst injectors were being primed with necessary reagents. Cells were treated with either trypsin (75 nM) or 2f-LIGRLO (10 μM), a PAR_2-activating peptide, followed by 5 μL 0.5% (v/v) Triton X-100 in PBS to confirm fluorochrome loading. Calcium responses were measured in a BMG FLUOstar Galaxy microplate reader. The ratio of fluorescence emission at 510 nm after excitation at

340 nm and 380 nm (340:380), which is directly proportional to intracytosolic calcium concentrations, was then plotted against time. To determine the extent of response to the agonists, area under the curve (AUC) was calculated and statistically analysed across groups.

2.4 Evaluation of the Role of PAR_2 in the Murine Bone Phenotype

2.4.1 Confirmation of Osteoblast Specific Deletion of PAR_2

This was carried out at both DNA and RNA levels. Whole bone DNA and RNA were used for this purpose. Bones were harvested from the same animals as used for micro CT and histomorphometric evaluations at the time of euthanasia. Humeri and femora were used for DNA and RNA isolation, respectively. Briefly, bones were excised, cleared of adherent soft tissues and marrow, snap frozen in liquid nitrogen and stored at -80°C until use. Cleared bones were cryopulverised using a mortar and pestle while submerged in liquid nitrogen. Pulverised tissue was lysed and processed according to sections 2.2.1 and 2.2.3. DNA level confirmation was also repeated using long bone primary osteoblast cultures (section 2.3.2). For the latter, after 4-6 weeks in culture, osteoblasts were trypsinised, washed twice with PBS and similarly processed for DNA extraction (section 2.2.1).

In order to demonstrate that PAR_2 deletion was in fact osteoblast specific and had not taken place in other cell types, spleens were also harvested at euthanasia, similarly cryopulverised and used for both DNA and RNA extraction which were then processed as described under section 2.2.7.

2.4.2 Micro Computed Tomography

For all *in vivo* studies, following euthanasia, the left tibiae were excised. For the evaluation of global PAR_2 null mice (chapter 3), the fifth lumbar vertebrae were additionally collected. The tibiae and vertebrae were placed in 70% ethanol and fixed for at least 96 hours at 4^oC prior to being sealed in small tubes filled with 70% ethanol (Figure 2.2) and subjected to micro CT. As bone lengths varied between individuals (based on sex, genotype and age), to avoid oversampling of shorter bones and undersampling of longer ones, the region of interest (ROI) to be scanned was defined as a percentage of bone length rather than a predefined fixed length, starting from particular anatomic landmarks all measured and

identified on the scout views (Lynch et al. 2011; Henriksen et al. 2011; William Lau et al. 2013). For tibiae, metaphyses of 20 and 32 week old mice were scanned starting at 3% full length of the tibia distal to the most cranial and proximal boundary of the proximal physeal plate for a total thickness equal to 10% of the bone length. In younger 7 and 13 week old specimens, it started at 5 % full length distal to the growth plate and acquired for a total thickness of 8% bone length. In determining the midshaft ROI, an area between 45% and 55% length of tibia was scanned in all specimens. For the fifth vertebrae, a thickness of the vertebral body equal to 70% of the total length of the vertebra was scanned starting at a distance equal to 15% of bone length from the cranial articular surface. All these criteria were determined by trial and error to avoid the primary spongiosa and assure reproducibility. For acquisition of all cancellous and cortical scans, an x-ray beam energy of 70 kVp, intensity of 200 μA, integration time of 500 ms and a frame averaging of 1 was adopted. Using the above settings, a final isometric voxel size of 3.4 μm was achieved when samples were scanned in an *ex vivo* Micro CT 50 (Scanco Medical AG, Brüttisellen Switzerland). Acquired images pertaining to chapters 3 and 4 were manually traced and analysed using Scanco's native evaluation program. Analysis of datasets in chapter 5 was performed using CT Analyser version 1.13.11.0 (Bruker Micro CT, Aartselaar, Belgium).

The mineral density of the bones was represented using two standard indices. Bone mineral density (BMD) reflects the radiographic opacity of the entire ROI without discriminating between marrow and bone material in units equivalent to milligrams of hydroxyapatite per cubic centimeter of standard phantoms (mg HA/cm^3). Tissue mineral density (TMD) refers to hydroxyapatite equivalent density of the bone tissue when the background marrow was not taken into account using a segmentation method. Using this technique also provided an indirect method for the estimation of marrow adiposity based on density, which was expressed as Hounsfield Units (HU). Due to the low X-ray attenuation coefficient of fat, higher fat content is expected to be associated with lower density (Schneider et al. 2000; Di Iorgi et al. 2008). This measure was adopted in the evaluation of osteoblast specific PAR_2 null mice in addition to routine histomorphometry (chapter 6). Scans used for the evaluation of the tibial metaphyseal trabeculae in 20 week old mdx mice were performed by another investigator, Dr. Neda Taghavi, who was trained by the author of this thesis following the same algorithm described above.

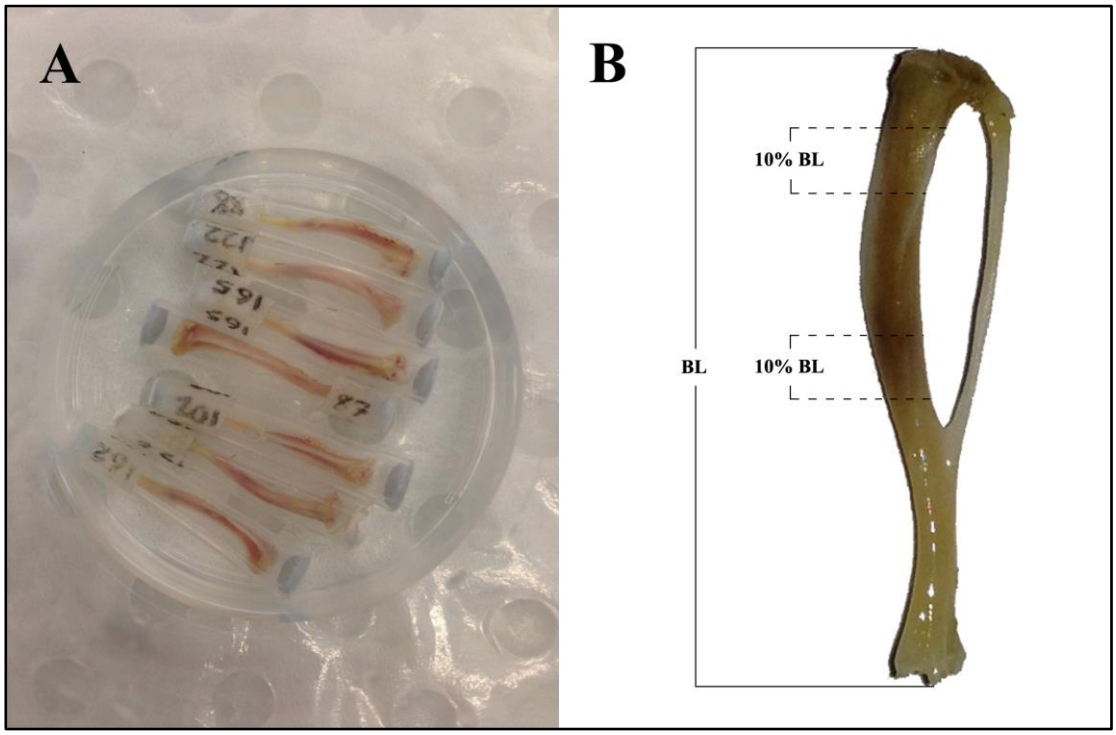


Figure 2.2 micro CT Evaluation of Tibiae.

A, Tibiae were enclosed in small plastic tubes with 70% (v/v) ethanol to prevent desiccation artifacts, improve positioning reproducibility and preserve bone samples for later histological evaluations. L5 vertebrae were similarly prepared for micro CT scans. ***B***, A proximal metaphyseal and a midshaft region were scanned per tibia each measuring 10% of the total bone length (**BL**).

2.4.3 Bone Histomorphometry

Undemineralised left tibiae were embedded in methyl methacrylate for histomorphometric evaluations. Sections obtained from proximal metaphyses were stained using toluidine blue for standard static histomorphometry. Bones were labelled *in vivo* using calcein for the purpose of dynamic histomorphometry. Evaluations were carried out by the author using a single section per staining method. Trabecular bone was evaluated in three adjacent rows, each equal in width to the width of the field of view at 20X. The first row started at a distance equal to half of the field of view away from the growth plate to avoid secondary spongiosa. The number of fields evaluated per row was variable and depended on the bone width.

2.4.3.1 Fluorochrome Labelling

For dynamic histomorphometric assessment of trabecular bone in osteoblast specific PAR_2 null and control mice, mice were labelled 3 and 1 days before euthanasia. The fluorochrome solution was prepared by dissolving 10 mg calcein per mL of 1.4% isotonic sodium bicarbonate (NaHCO3) adjusted to a pH of 7.7. Calcein solution was filter sterilised and administered subcutaneously at a dose of 20 mg/kg (approx. 0.02-0.08 mL per mouse) through a 27-gauge hypodermic needle. Animals were manually restrained for injections and sites varied to avoid multiple injections in the same location.

2.4.3.2 Preparation of Plastic Sections and Histomorphometry

Bones were embedded in a 4:1 ratio of butyl methacrylate to methyl methacrylate and cut into 7 μm thick serial sections parallel to their long axes. The secondary spongiosa of the proximal tibiae was evaluated using the Osteomeasure system (OsteoMetrics Inc., Atlanta, GA, USA). Static histomorphometry was performed on slides stained with toluidine blue. Histomorphometric measurement of dynamic parameters was performed on unstained slides. As micro CT indicated great variability of structure model index (SMI) across sexes and genotypes, a 2D approach was adopted for the calculation of many of the secondary indices (Dempster et al. 2012).

2.5 Evaluation of the Role of PAR_2 in Cultures of Kusa 4b10 Cells

2.5.1 Trypsin-like Amydolytic Activity

Kusa 4b10 cells were differentiated under adipogenic and osteogenic conditions for 5 days at which point media were replaced with low serum-containing medium (2% FBS in α-MEM). After 24 hours, conditioned media were collected and subjected to measurements. Trypsin-like amydolytic activity was assayed using Nα-benzoyl-L- arginine- p-nitroanilide dihydrochloride (BAPNA) as substrate (Erlanger et al. 1961).

The stock solution was prepared by dissolving 43.5 mg BAPNA (Sigma Aldrich, St. Louis, Missouri, USA) in 1 ml DMSO. At the time of the experiment, 200 μL of this solution was taken and made up to 5 ml with Tris-HCl buffer (0.05 M, pH 8.3) containing 0.02M CaCl2.

2H2O. The reaction mix was prepared by directly adding 80 µL conditioned medium and 100 µL of freshly prepared BAPNA working solution to a 96 well plate which was then incubated at 37ºC for 10 minutes (Chong et al. 2002). After stopping the reactions by adding 20 µL 30% acetic acid to each well, absorbance was read at 410 nm. A unit of trypsin-like activity was defined as the amount catalyzing the release of 1 µmol p-nitroanilide into the solution (Tsutsui et al. 1987). Trypsin-like activity was calculated using the following formula:

$$\text{Trypsin} - \text{like Activity (U/mL)} = \left[\frac{V}{v \times \varepsilon \times d}\right] F \times \frac{\Delta A}{\Delta T}$$

V = assay volume

v = sample volume

F = dilution factor

ε = 8.8 (mmol-1 × l × cm-1) = absorbance coefficient of p-nitroanilide at 405 nm (Erlanger et al. 1961)

d = light path in the microplate (0.62 cm)

ΔA/ΔT = ΔA/min = change in absorbance per minute

2.5.2 Kallikrein-like Activity

Preparation of the conditioned media was performed as discussed for the measurement of trypsin-like activity above. Kallikrein-like activity was measured using the chromogenic substrate Chromozym-pk (Benzoyl-Pro-Phe-Arg-4-nitranilide acetate; Roche Diagnostics, IN, USA). The method was adapted for use in a 96 well microplate. Prior to the assay, conditioned medium samples and the control medium (2% FBS in α-MEM) were activated by incubating with dextran sulphate (25 mg/mL) at 0 ºC for 7 minutes. Each reaction mixture consisted of 52 µL Chromozym-pk (1.3 mM), 152 µL incubation buffer (Tris-Imidazole buffer [0.33 M; pH 7.9], NaCl [0.33M]) and 50 µL activated sample at 37ºC. Immediately after loading the microplate, absorbance was read at 405 nm (0 minute) which was then repeated at one minute intervals for 5 minutes. The kallikrein-like activity of each sample was calculated using the same formula described before for trypsin-like activity (4.2.1). An absorbance coefficient of 10.4 ($mmol^{-1} \times l \times cm^{-1}$) was used here as per the manufacturer's instructions.

2.5.3 PAR_2 Knockdown

To evaluate the role of PAR_2 in osteogenic and adipogenic conversion of Kusa 4b10 cells, PAR_2 expression was stably knocked down using lentiviral small hairpin RNA (shRNA) constructs as explained below.

2.5.3.1 Lentiviral Transduction Particles

All five shRNA clones supplied by Sigma Aldrich (Table 2.3) were used to knockdown PAR_2 each at a multiplicity of infection (MOI) of 2 (a total cumulative MOI of 10). To control for the cellular effects of the transduction process as well as the RNA induced silencing complex (RISC) and RNA interference (RNAi) pathway, MISSION™ Non-Target shRNA Control Transduction Particles (Catalog Number SHC002V) were used at an MOI of 10 (vector control). Lentiviral particles also contained a puromycin resistance gene which was used to select for successfully transduced clones.

2.5.3.2 Puromycin Titration (Kill Curve)

Before the start of transductions, a puromycin kill curve was generated to be used later during the selection phase. Kusa 4b10 cells were plated at a density of 1.6×10^4 cells per well in a 96 well plate and incubated at 37°C in 5% CO_2 overnight. The next day, puromycin (500-10,000 ng/mL) was added to selected wells and changed once every 3 days. Cell viability was assessed every 2 days for a total period of 2 weeks. A concentration of 6,000 ng/mL was found to be conducive to complete cell death after 5 days which was used for the selection of successfully transduced cells.

Table 2.3 Small hairpin RNA constructs used for PAR_2 knockdown.

All five constructs were combined and delivered at a total MOI of 10.

TRC Id	Clone Name	Region	Target Sequence
TRCN0000026616	NM_007974.2-1198s1c1	CDS[1]	GCACTGTGAATCGCATGCAAA
TRCN0000026627	NM_007974.2-513s1c1	CDS	CATGGCAACAACTGGGTCTAT
TRCN0000026630	NM_007974.2-2279s1c1	3UTR	GCCAACTACAAATACTGCTTA
TRCN0000026643	NM_007974.2-1255s1c1	CDS	GCTCCTACTCTTCAAGCTCAA
TRCN0000026645	NM_007974.2-1025s1c1	CDS	CGTAGTGCATTATTTCCTAAT

[1] coding sequence of the mRNA

2.5.3.3 Transduction and Selection

On day 1, cells were plated at a density of 1.6 x 10^4 cells per well in a 96 well plate and incubated at 37°C in 5% CO_2 overnight. The next day, medium was removed and fresh medium containing hexadimethrine bromide (8 μg/mL) was added to cells followed by viral vectors at a total MOI of 10. Cells were then incubated overnight after which time medium was removed and fresh medium added to the wells. Cells were allowed to recover overnight and were then subjected to puromycin selection at a concentration of 6,000 ng/mL. Puromycin containing medium was replaced every 3-4 days until resistant colonies could be identified. Five resistant colonies were picked, expanded and assayed to confirm PAR_2 knockdown at both RNA and protein levels using RT-qPCR and intracellular calcium mobilization, respectively. Based on the results, a final clone from each knockdown and vector control group was selected and used for further experimentation.

2.5.4 Alizarin Red-S Mineralisation Assay

Cells cultured in 12 well plates were first washed three times with PBS, and fixed in ice cold 70% (v/v) ethanol for a minimum of 1 hour. Samples were then briefly washed with deionized water (x1 for 5 min) and stained by 40 mM Alizarin Red-S pH 4.2 (0.5 mL per well) for 10 min with rotation (Jacobson 1995; Allan et al. 2003). Excess dye was washed away in 5 changes of MilliQ water (2 minutes each with rotation) to prevent nonspecific staining. After photography, samples were destained using 5% (w/v) cetylpyridinium chloride (CPC) in MilliQ water (20 minutes with rotation at room temperature). Extracts were then diluted in 5% CPC solution (1 in 10) if required before being spectrophotometrically measured at 562 nm in a 96 well plate (Jacobson 1995). The concentrations were calculated by plotting the absorbance against concentration of a range of 0-2500 nM/mL solutions of Alizarin Red-S in 5% CPC (each mol of Alizarin Red-S binds 2 mols of Ca^{2+}).

2.5.5 Oil-Red O Staining and Cell Morphometry

To assess the extent of adiposity in the cultures of Kusa 4b10 cells under various experimental conditions, cultures in 12 well plates were stained using Oil-Red-O (ORO) and haematoxylin. Briefly, cells were first washed with PBS and fixed using 4% paraformaldehyde in PBS (w/v) at room temperature (1 mL per well for 5 minutes). Next, cells were irrigated three times with MilliQ water and stained with 1.8 mg/mL ORO solution in 60% (v/v) isopropanol (1 mL per well with rotation for 10 minutes). Excess dye was then washed away in tap water until water rinsed off clear. This was followed by staining with haematoxylin (1 mL per well for 1 minute) and bluing in tap water for at least 10 minutes. Cultures were then photographed at 40X magnification using an Olympus 1X70 inverted microscope (Tokyo, Japan) fitted with a ProgRes® C3 camera (Jenoptik, Thuringia, Germany). The number of mature adipocytes was manually counted using ImageJ software (National Institutes of Health, Bethesda, MD, USA) and expressed as a ratio of total cell counts.

2.5.6 Measurement of IL-6 Concentration in Cultures of Kusa 4b10 Cells

Measurement of IL-6 concentration in the supernatants of PAR_2 knockdown and vector control cells was carried out by enzyme linked immunosorbent assay (ELISA; Thermo Fisher Scientific, Waltham, MA, USA) according to the manufacturer's instructions. Supernatants were collected from days 1 to 7 from Kusa 4b10 cells cultured under osteogenic conditions and kept refrigerated at 4°C until use (3 replicates/day).

Upon use, undiluted samples and standards were added to the ELISA plate in duplicate (50 μL/well) and incubated for 2 hours at room temperature prior to washing of the plate in three changes of wash buffer. This was followed by an hour of incubation with biotinylated antibody reagent (50 μL/well) and irrigation with wash buffer. Next, streptavidin-horseradish peroxidase (HRP) solution was added to the wells (100 μL/well) and the plate was incubated for 30 minutes in the dark. Following a repeat of the wash step, premixed tetramethylbenzidine (TMB) substrate solution was added to the plate (100 μL/well) and allowed to develop in the dark for 30 minutes. Reactions were stopped by adding 100 μL/well of stop solution before measuring the absorbance at 450 and 550 nm. A standard curve was generated by plotting A_{450} minus A_{550} values versus the corresponding mouse IL-6 concentration (pg/ml) in standard solutions which was then used to interpolate sample absorbance values to IL-6 concentrations.

2.5.7 Neutralising IL-6 in Cultures of Kusa 4b10 Cells

To study the role of IL-6 in the adipogenic conversion of Kusa 4b10 cells, an IL-6 neutralising antibody (Thermo Fisher Scientific, Waltham, MA, USA) was added to the medium. An antibody to antigen molar ratio of 10:1 was used which equalled 17.2 ng of anti IL-6 neutralising antibody per mL of medium selected to neutralise maximum measured IL-6 concentrations (~250 picograms/mL on day 3). The selection of antibody concentration was based on the manufacturer's recommendation. Medium was changed every three days with freshly thawed antibody added just before each use.

2.6 Statistical Analysis

Sample size for animal studies was determined based on a priori power analysis using the micro CT BV/TV values of global PAR_2 null mice. Analysis suggested an N of 5 will provide a statistical power of 0.8 which was sufficient for the intended studies. Despite this, where possible, a larger number of samples was included to improve the power of the studies described in this thesis.

All sample assignments to experimental groups were randomised and analyses carried out blindly where possible. Results are expressed as mean ± standard error of the mean. A part of the micro CT data is presented as the difference between the means of two compared groups (chapters 3, 4 and 5), *viz*:

$$\bar{x}_{diff} = \bar{x}_2 - \bar{x}_1$$

$\bar{x}_{diff}$: difference between the means
$\bar{x}_1$: mean of control group
$\bar{x}_2$: mean of tested group

To calculate the standard error of the difference between means (SE_{diff}), the following formula was used (Burns and Dobson 1981):

$$SE_{diff} = \sqrt{\frac{\sigma_1^2}{N_1 - 1} + \frac{\sigma_2^2}{N_2 - 1}}$$

σ: standard deviation
N: sample size

The general approach to examining the data presented in this manuscript always involved an initial testing for normality. This was achieved via a Shapiro-Wilk test as well as a visual inspection of the histograms. Normally distributed continuous variables were analysed using either a t-test or a one-way analysis of variance (ANOVA) if multiple comparisons were required. With the latter, contrast analysis (planned comparisons) was adopted to determine group interactions (as opposed to post-hoc tests). In all instances, results were interpreted based on data heteroscedasticity as

determined by a Lavene's test of homogeneity of variance. In case of heteroscedasticity, the results of the Brown-Forsythe and Welch procedures were also inspected and results reconfirmed.

Non-normal data were analysed by either a Mann-Whitney U test if only two groups were to be compared or a Kruskal-Wallis test followed by Dunn's pairwise comparisons if multiple groups were compared. Due to variable patterns of distribution, micro CT and histomorphometric data were analysed using non-parametric tests so that all data could be uniformly processed. Additionally, in the evaluation of micro CT data, a one-way analysis of covariance (ANCOVA) was used after controlling for time (i.e. endpoint independent) to further test the effects of genotype on bone morphology.

In investigating the effect of ageing on micro CT indices, a simple linear regression was used to determine whether changes were significant. When the rate at which bone indices either deteriorated or improved over time was to be compared between the genotypes, the regression coefficient of each parameter was compared to that of the other group using a second multiple linear regression analysis. This essentially allowed assessment of the slope of changes that occur in a particular parameter over time between the two groups. A two tailed test was used for all such comparisons.

In all comparisons, *p* values less than 0.05 were considered statistically significant and have been denoted with an asterisk (*). If less than 0.01 or 0.001, two or three asterisks are used respectively. Depending on the hypothesis, a one tailed or two tailed test has been used. A † symbol marks comparisons analysed using a one tailed test. SPSS statistics version 23, (IBM Corp.©, Armonk, NY, USA) was used for analyses. Graphs were prepared using Graphpad prism v5 (GraphPad software Inc., La Jolla, CA, USA).

CHAPTER 3: EFFECT OF GLOBAL PAR_2 GENE ABLATION ON MURINE BONE PHENOTYPE IN CONTEXT OF AGE

3.1 Introduction and Aims

Given its universal expression and roles in the homeostasis of various tissues, it is no surprise that PAR_2 is also involved in the physiology of bone tissue and cells. Indeed, previous *in vitro* studies have shown that PAR_2 is expressed by osteoblasts and osteoclast precursors, and that it is involved in osteoblast apoptosis and protection of bone from osteoclastic resorption (Abraham et al. 2000; Smith et al. 2004; Georgy et al. 2010). In primary calvarial osteoblasts, not only is the activation of PAR_2 associated with proosteogenic gene expression, i.e. *ColIa1*, but also a higher rate of apoptosis (Georgy et al. 2010). In murine bone marrow cultures, treatment with PAR_2 activating peptides causes a reduced rate of osteoclastogenesis in response to treatment with PTH, $1,25(OH)_2D_3$ or IL-11. Additionally, these bone marrow cultures show significantly suppressed RANKL:OPG ratio (Smith et al. 2004).

A previous *in vivo* study in the laboratory, in which the current study was undertaken found that at 7 weeks PAR_2 null mice possessed more trabecular bone mass than their wildtype counterparts whereas at 13 weeks, both genotypes appeared similar. The study also reported slower healing in PAR_2 null mice (compared with wildtype mice) when a hole was drilled in the midshaft of tibiae. Interestingly, histomorphometric evaluations showed both osteoblast and osteoclast related values decline in response to the lack of PAR_2 (Georgy et al. 2012). These are all indications of a very complex role for PAR_2 in both osteogenesis and bone resorption rendering bone remodelling defective in its absence. The fact that trabecular bone mass in both genotypes appeared similar by the end of 13 weeks, the result of a possibly greater bone loss in PAR_2 null than in wildtype mice between 7 and 13 weeks, means that if continued, osteopoenia would be a likely outcome. However, this hypothesis was not tested at that time.

Accordingly, it was hypothesised that should PAR_2 be required for normal bone mass maintenance, then global loss of PAR_2 would result in more extensive changes in bone architectural and material properties over time. To test this hypothesis, mice were euthanised at 20 or 32 weeks with left tibiae and L5 vertebrae excised and subjected to micro CT evaluations. Both vertebral and tibial trabecular as well as tibial midshaft cortical structures were analysed and compared with wildtype sex and age controlled cohorts. Results indicated that PAR_2 is required for normal homeostasis of murine bone, however this effect was more pronounced in males.

3.2 Results

3.2.1 Body Weight and Bone Length

Global lack of PAR_2 did not result in any apparent phenotype aberrations although male knockout (KO) mice accrued weight at a faster rate and weighed more than their WT counterparts at 32 weeks (Figure 3.1). Bone lengths appeared to be quite uniform across genotypes of each sex and showed minimal variation although a slight increase from 20 to 32 weeks in female wildtype mice was noticed. There was a significant effect of sex on all these parameters with males having higher values than females ($p < 0.001$).

Analysis of regression coefficients of changes over time indicated that the rate at which male knockout mice accrued weight over time was faster than that of the wildtypes ($p < 0.05$). The change in the weight of females however, as well as bone length in either sex were similar between the two genotypes ($p > 0.05$). Despite the latter, simple linear regression indicated significant tibial length accrual in the female wildtype mice while this did not change significantly in the female knockouts.

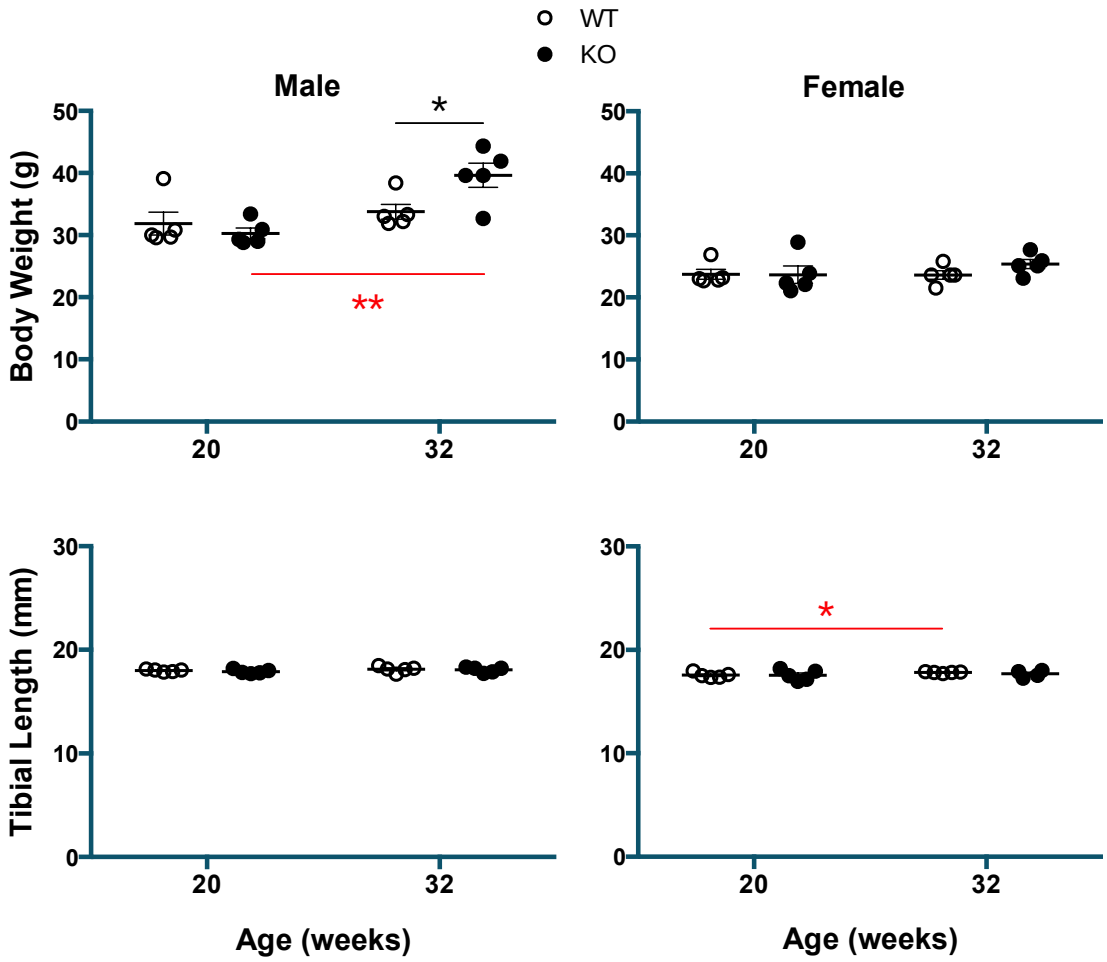


Figure 3.1 Body weight and tibial lengths in male and female mice.

Bone lengths were measured at the time of the micro CT scans using the scout views. **WT** - wildtype mice; **KO** - PAR_2 knockout mice. N = 5 for all groups except 32 week females where N = 4; * $p <$ 0.05 using two tailed independent samples t-test; * $p < 0.05$, ** $p < 0.05$ using simple linear regression indicating significant time related changes in sex-genotype controlled groups; error bars represent SEM.

3.2.2 Tibial Trabecular Bone

The total volume of tissue (TV) examined, ranged from 1.66 to 2.72 mm^3 in males and 1.26 to 2.28 mm^3 in females (Tables A.1 and A.2, Appendix A). Bone volume fraction (BV/TV) was found to be different only in males at 20 weeks where PAR_2 null mice appeared to have a smaller bone mass in comparison to their wildtype cohorts (Figures 3.2, 3.3 and 3.10). Further structural analysis indicated that most of such difference could be explained

by greater trabecular separation (Tb.Sp) in PAR_2 null mice than wildtypes. Additionally, trabecular number (Tb.N) was found to be significantly lower in PAR_2 null males of the 32 week age at $p = 0.01$ level. In contrast to the latter however, connectivity density (Conn.D) was too variable in all male groups to result in any statistically meaningful difference.

From other structural parameters measured, degree of anisotropy (DA) seemed to be the only parameter that corresponded to genotype differences however, only at 20 weeks where PAR_2 null bones appeared more isotropic. The structural inferiority of the PAR_2 null male mice was also found to be compounded by deficiency in their tissue mineral density (TMD) when compared to wildtype controls at both time points however more severely in the older 32 week old mice (13.2% difference). When controlled for time, using a one-way ANCOVA test, it was found that genotype in males had a significant effect on BV/TV and trabecular thickness (Tb.Th), $F(1, 17) = 6.57$ and 3.78, $p < 0.05$ as well as Tb.N, Tb.Sp, DA and TMD, $F(1, 17) = 12.24$, 12.29, 8.72 and 23.81, $p < 0.01$.

To understand whether or not the rate of bone structural changes over the 12 week period (from 20 to 32 weeks) varied between genotypes in the males, analysis of regression coefficients was carried out which found significantly higher rates of TMD loss in the lack of PAR_2 ($p < 0.05$). All other indices remained insignificant (Table 3.1).

Unlike the males, in females lack of PAR_2 did not seem to be associated with any significant difference in BV/TV values between the genotypes (Figures 3.2, 3.4 and 3.10). Of all structural indices evaluated, only DA, was found to be lowered by the absence of PAR_2 similar to males but here at 32 weeks. TMD was similar between the two genotypes at 20 weeks but it was found to be significantly inferior in PAR_2 null mice at the older age. In females, use of one-way ANCOVA when controlled for time indicated a significant effect of genotype on DA and TMD, $F(1, 16) = 9.10$ and 8.85, $p < 0.01$.

Regression analysis did not find any significant difference in the rate of architectural or material deterioration over time between the genotypes in the female mice (Table 4.1).

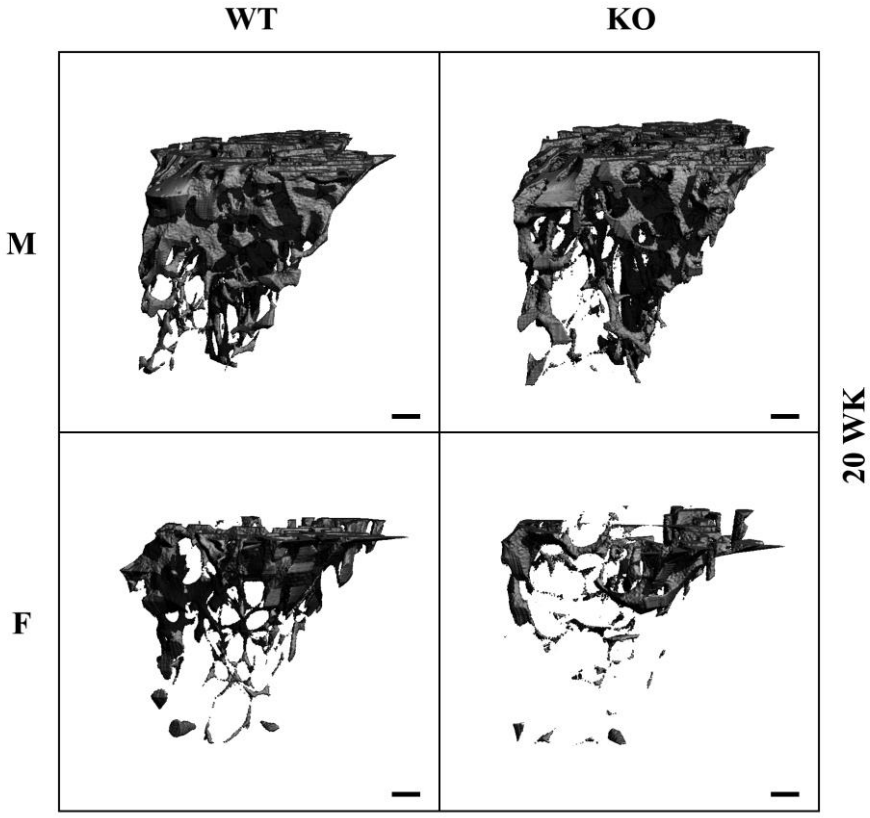


Figure 3. 2 3D models of the metaphyseal trabecular bone in KO and WT mice.

Male and female mice at 20 weeks of age are presented. The volumes of interest (VOIs) were defined using the native Scanco software by manually tracing the 2D images every few slices followed by interpolation in the three dimensional space. Rendering of the thresholded surfaces was then used to create the presented 3D images. The difference in BV/TV between the males of WT and KO genotypes is clearly noticeable. The difference in females was not statistically significant (see Figure 3.3). Lateral view, bar represents 200 μm.

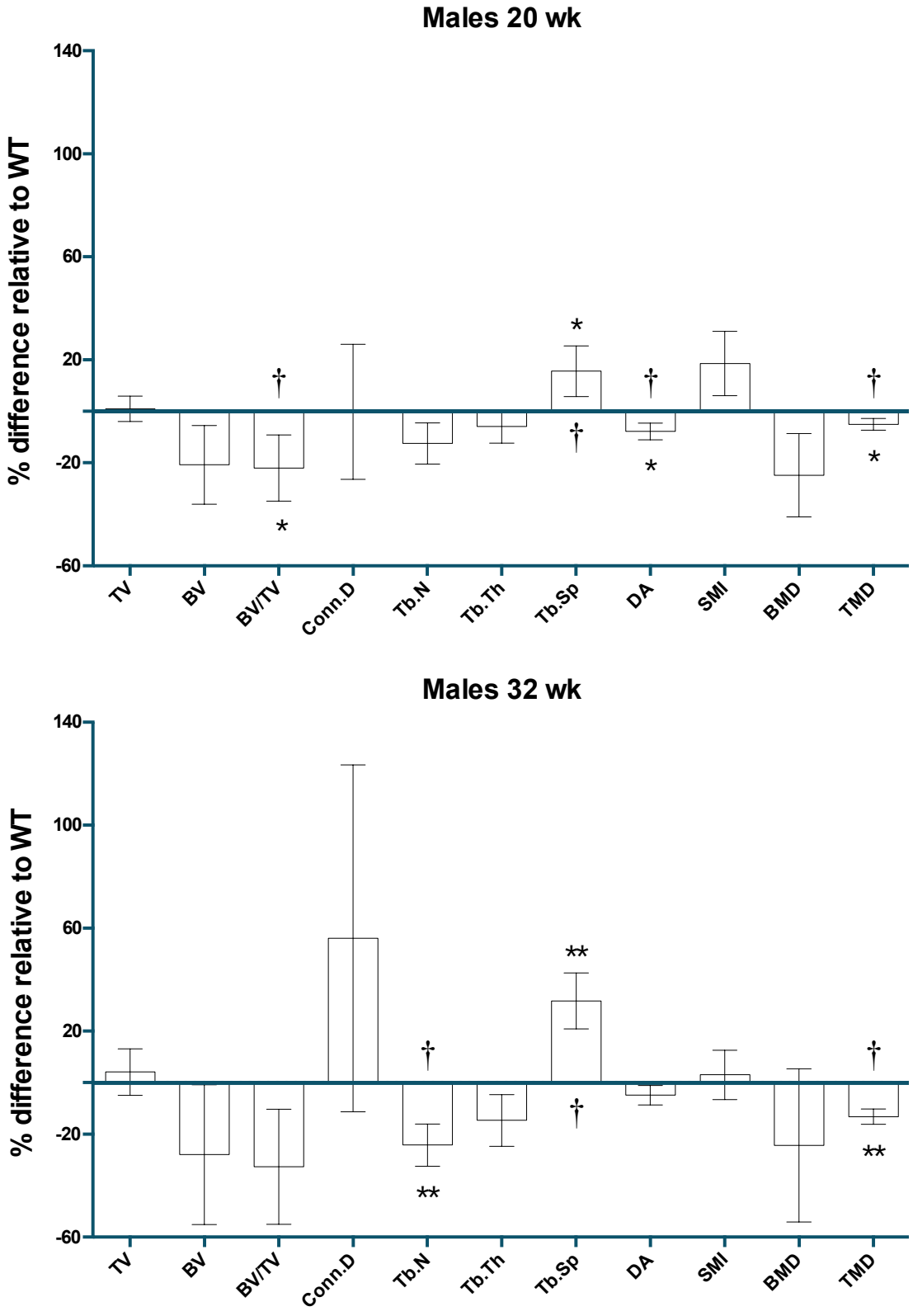


Figure 3.3 Percent difference in metaphyseal trabecular indices - males.

The difference between the KO and WT males at 20 and 32 weeks is presented as a percentage relative to the control WT mice. N = 5; * $p < 0.05$, ** $p < 0.01$ using Mann-Whitney U test; † one-tailed comparison; error bars represent SE_{diff}.

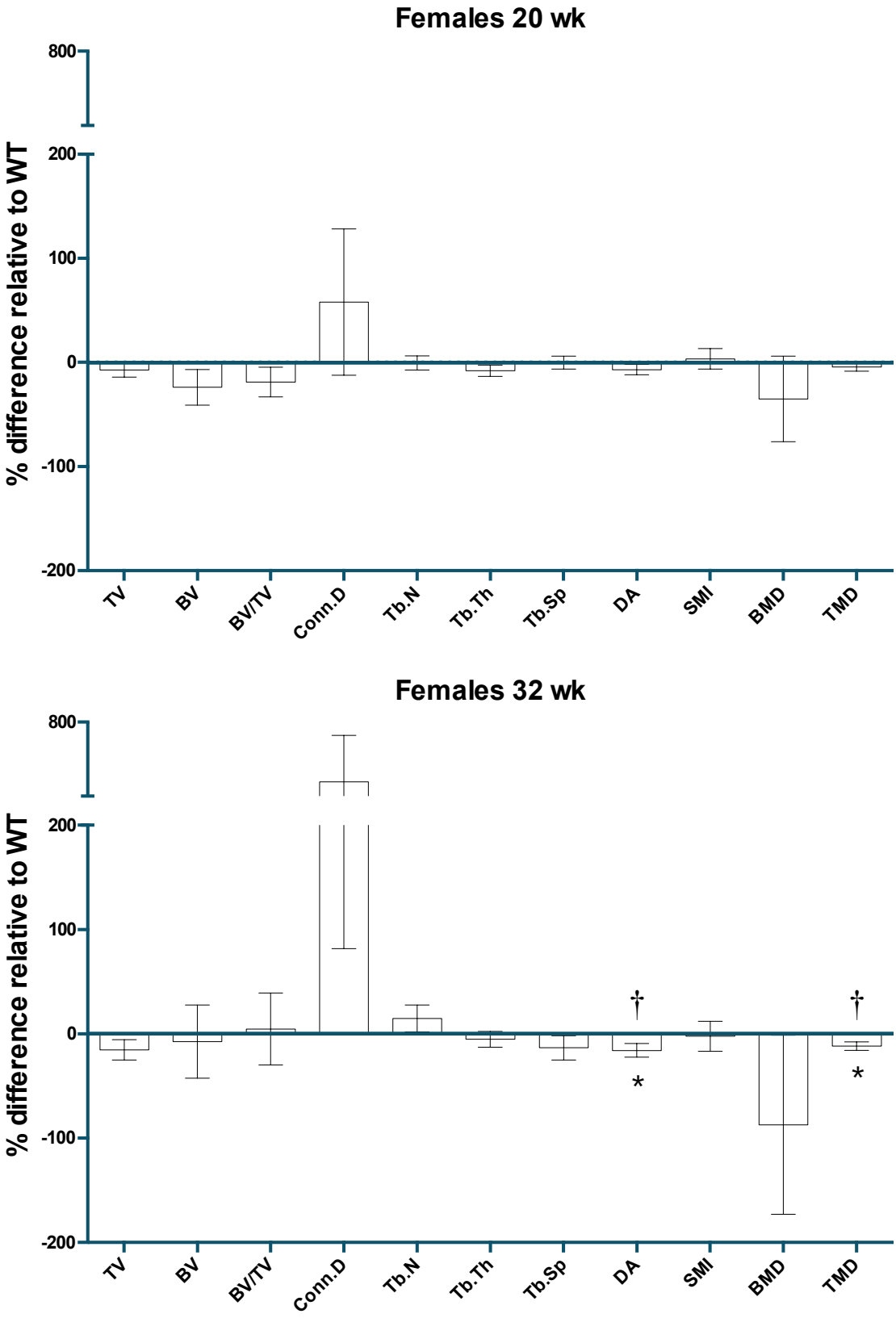


Figure 3.4 Percent difference in metaphyseal trabecular indices - females.

The difference between the KO and WT females at 20 and 32 weeks is presented as a percentage relative to the control WT mice. N = 4-5; * $p < 0.05$ using Mann-Whitney U test; † one-tailed comparison; error bars represent SE_{diff}.

Table 3.1 Time related change in the tibial metaphyseal trabecular bone.

Regression coefficients of time related changes in bone structural and material indices of PAR_2 wildtype and knockout mice are presented. Significant comparisons between the genotypes are highlighted.

	M			F		
Index	**B_{wt}[1]**	**B_{ko}[2]**	**p-value[3]**	**B_{wt}**	**B_{ko}**	**p-value**
TV	-0.022*	-0.017	0.755	0.010	-0.003	0.413
BV	-0.013*	-0.012	0.863	-0.003*	-0.002	0.409
BV/TV	-0.005*	-0.005	0.979	-0.002*	-0.001	0.328
Conn.D	3.526	17.546	0.390	-2.812*	0.402	0.468
Tb.N	-0.088**	-0.119**	0.460	-0.066**	-0.042*	0.284
Tb.Th	$1.12x10^{-4}$	$-2.72x10^{-4}$	0.410	0.000	0.000	0.755
Tb.Sp	0.005**	0.009**	0.126	0.014**	0.008*	0.235
DA	-0.023**	-0.017**	0.385	0.007	-0.008	0.214
SMI	0.049**	0.029	0.385	-0.009	-0.023	0.706
BMD	-3.889	-2.885	0.726	-2.852*	-1.300	0.172
TMD	-5.349*	-9.904***	0.044	0.619	-4.368	0.163

[1] Regression coefficient (slope) of changes over time in the wildtype group; a negative value depicts negative changes.

[2] Regression coefficient (slope) of changes over time in the PAR_2 KO group.

* $p < 0.05$, ** $p < 0.01$, *** $p < 0.001$ when values were regressed over time in each sex-genotype category indicating significant changes from 20 to 32 weeks.

[3] Regression coefficients were compared using a second multiple linear regression analysis.

3.2.3 Vertebral Trabecular Bone

In the vertebral body, findings were similar to those of the tibial metaphysis. Here, the total volumes evaluated ranged from 2.07 to 2.84 mm^3 in males and 1.99 to 2.90 mm^3 in females (Tables A.3 and A.4, Appendix A). In males, the lack of PAR_2 caused lower BV/TV values at 20 weeks, but not at 32 (Figures 3.5 and 3.10). This however was not explained by any significant changes in Tb.N, Tb.Th, Tb.Sp or Conn.D, thus all these parameters remained equivocal (Figures 3.6). DA of the vertebral trabeculae was also lower in PAR_2 null mice as well, here at both time points. Interestingly, the lack of PAR_2 also caused a significant increase in structural model index (SMI) again at both 20 (94.9%) and 32 (61.4%) weeks indicating a transition from plate shaped trabeculae in wildtype to more rod shaped trabeculae in PAR_2 null mice. Comparison of TMD values at both 20 and 32 weeks unveiled statistical significance between the genotypes at $p = 0.01$ level (Figures 3.6). When controlled for time, one-way ANCOVA showed a significant effect of genotype in males on BV/TV and Tb.Th, $F(1, 17) = 3.84$ and 6.06, $p < 0.05$ as well as SMI, DA and TMD, $F(1, 17) = 25.54$, 28.08 and 28.75, $p < 0.001$.

Using regression analysis, it was found that Conn.D increased at a significantly higher rate in PAR_2 null male mice than wildtypes over time (Table 4.2).

In females, TV at 20 weeks was more variable here than in the trabecular metaphyses, but at 32 weeks, it proved to be significantly lower than in the WT counterparts (Figures 3.7). As in the tibial metaphysis, TMD was similarly lower in PAR_2 null female mice of the 32 week age group as well (Figures 3.7). After controlling for time, one-way ANCOVA showed a significant effect of genotype on DA and TMD in females, $F(1, 16) = 3.23$ and 4.56, $p < 0.05$.

Genotype did not seem to have any significant effect on the rate of architectural deterioration over time in the female mice (Table 4.2).

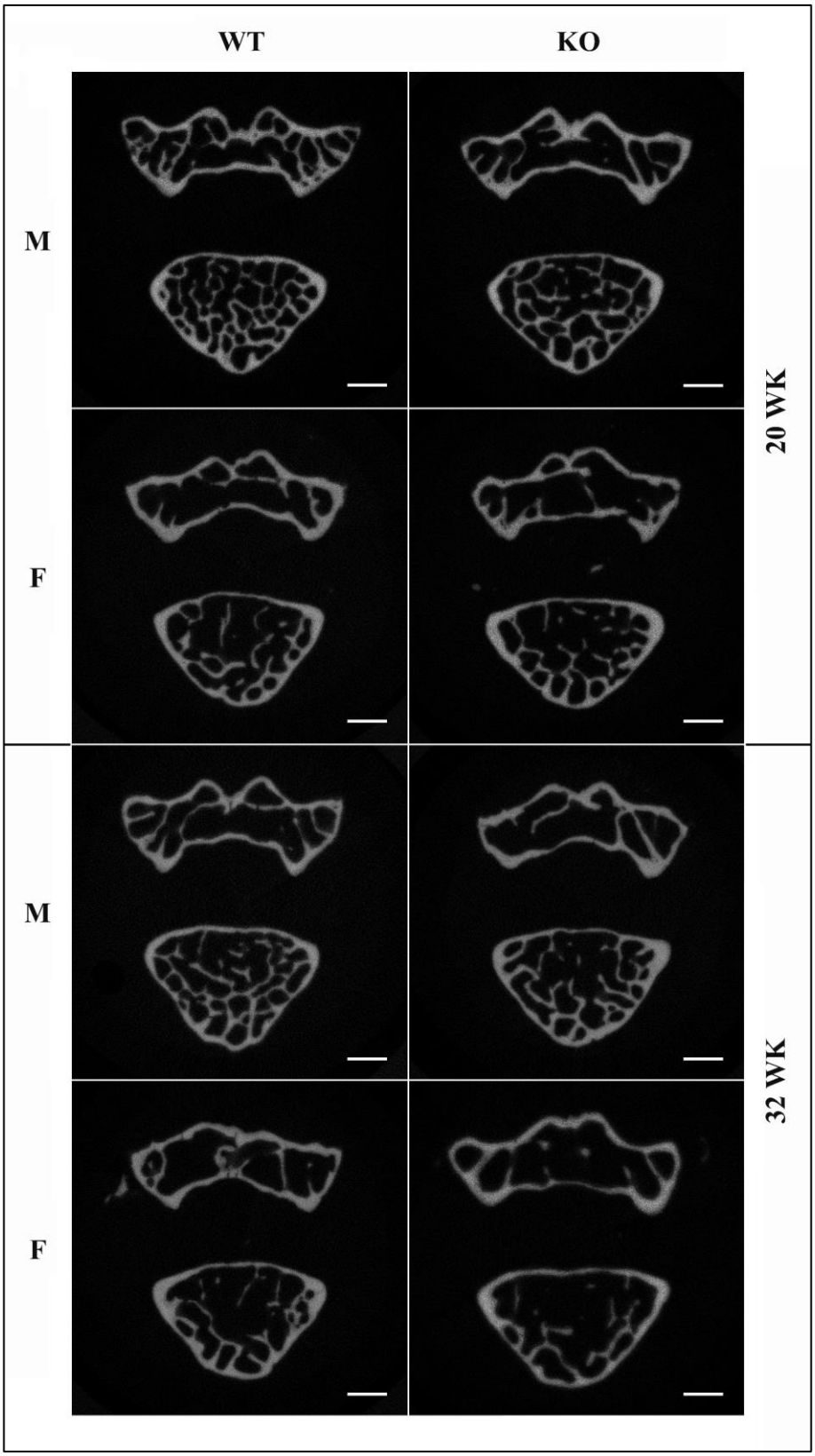


Figure 3.5 Representative micro CT slices from the L5 vertebrae of KO and WT mice.

Cross section of the vertebral bodies and laminae in male and female mice at 20 and 32 weeks of age are presented. Bar represents 400 μm.

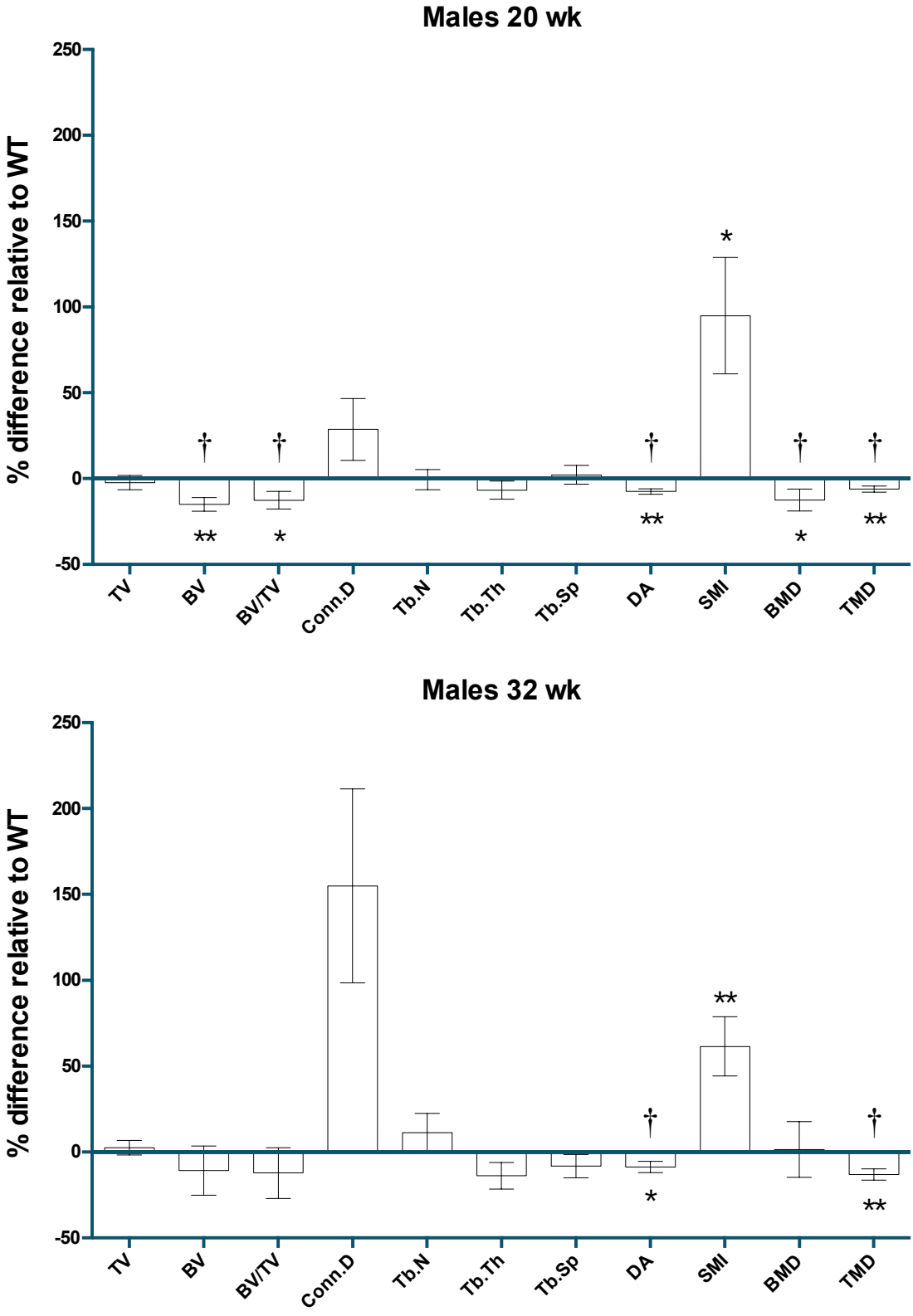


Figure 3.6 Percent difference in vertebral trabecular indices - males.

The difference between the KO and WT males at 20 and 32 weeks is presented as a percentage relative to the control WT mice. N = 5; * $p < 0.05$, ** $p < 0.01$ using Mann-Whitney U test; † one-tailed comparison; error bars represent SE_{diff}.

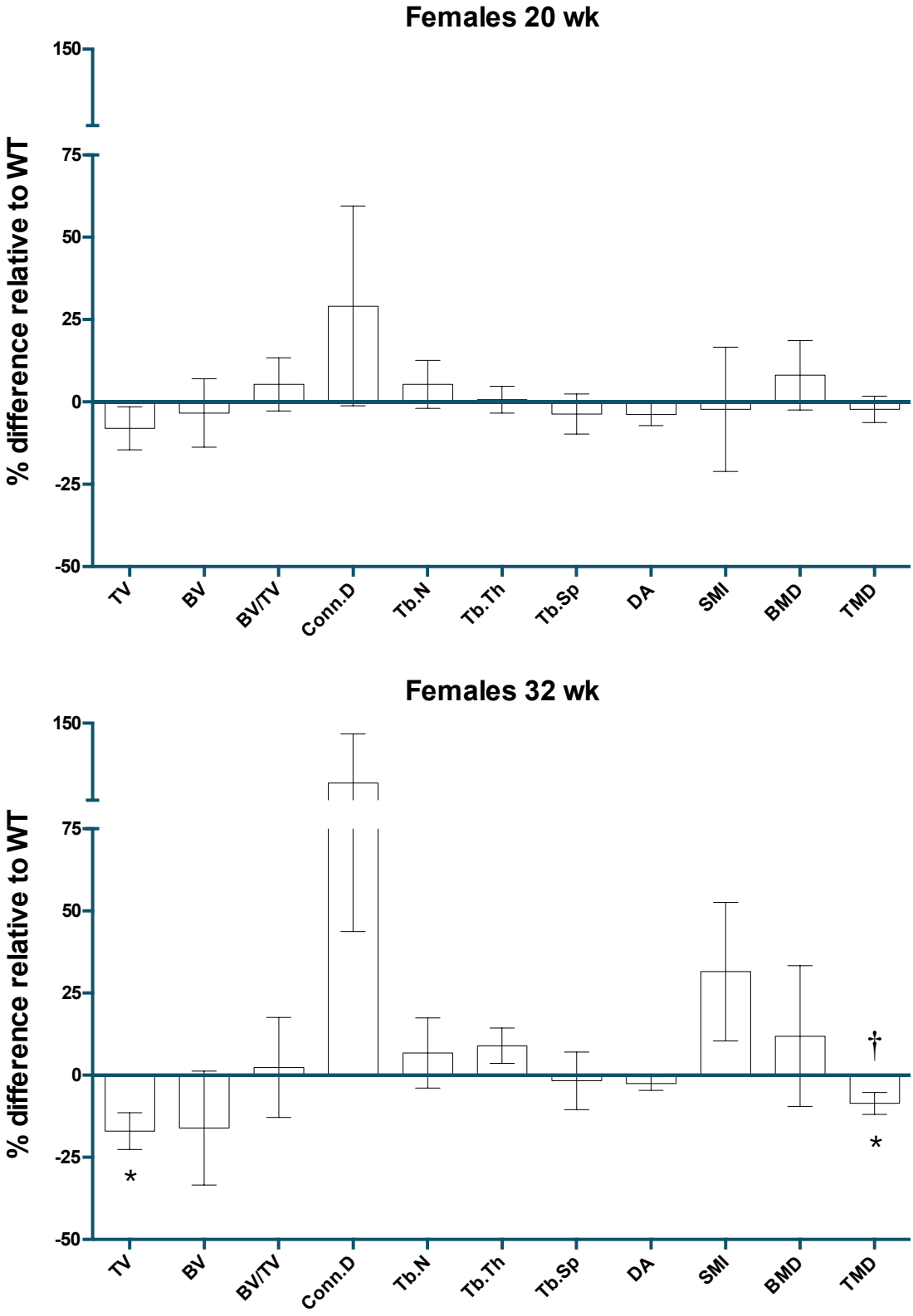


Figure 3.7 Percent difference in vertebral trabecular indices - females.

The difference between the KO and WT females at 20 and 32 weeks is presented as a percentage relative to the control WT mice. N = 4-5; * $p < 0.05$ using Mann-Whitney U test; † one-tailed comparison; error bars represent SE_{diff}.

Table 3.2 Time related change in the L5 trabecular bone.

Regression coefficients of time related changes in bone structural and material indices of PAR_2 wildtype and knockout mice are presented. Significant comparisons between the genotypes are highlighted.

	M			F		
Index	**B_{wt}[1]**	**B_{ko}[2]**	**p-value[3]**	**B_{wt}**	**B_{ko}**	**p-value**
TV	0.008	0.018	0.369	0.018	-0.003	0.228
BV	-0.007	-0.004	0.636	-0.003	-0.007	0.517
BV/TV	-0.004^{*}	-0.003	0.839	-0.002	-0.003^{*}	0.803
Conn.D	23.021	97.877^{**}	0.016	-3.940	6.336	0.285
Tb.N	-0.026	0.033	0.317	-0.061	-0.060^{*}	0.975
Tb.Th	-1.7×10^{-4}	-4.7×10^{-4}	0.432	3.5×10^{-5}	$3.9\times10^{-4*}$	0.206
Tb.Sp	0.002^{*}	-2.2×10^{-4}	0.193	0.004	0.004^{*}	0.878
DA	-0.019^{**}	-0.019^{***}	0.961	-0.006	-0.004	0.715
SMI	0.046^{***}	0.062^{**}	0.324	0.009	0.037^{*}	0.180
BMD	-3.279	-0.521	0.326	-2.530	-2.339	0.934
TMD	-6.550^{**}	-10.396^{***}	0.081	0.153	-3.855	0.206

[1] Regression coefficient (slope) of changes over time in the wildtype group; a negative value depicts negative changes.

[2] Regression coefficient (slope) of changes over time in the PAR_2 KO group.

* $p < 0.05$, ** $p < 0.01$, *** $p < 0.001$ when values were regressed over time in each sex-genotype category indicating significant changes from 20 to 32 weeks.

[3] Regression coefficients were compared using a second multiple linear regression analysis.

3.2.4 Tibial Cortical Bone

In the cortical region, the older PAR_2 null males had a smaller cortical area fraction (Ct.Ar/Tt.Ar) compared to controls (6.5%) which was compounded by a significantly lower (1.9%) tissue mineral density (TMD) value (Figures 3.8 and 3.10; Table A.5, Appendix A). There were also significant differences in the marrow cavity parameters indicating a greater diameter (Ma.Dm) at 20 weeks (5%) and a larger area (Ma.Ar) by 32 weeks (13.4%). Additionally, the extent of porosity was negatively affected by PAR_2 deficiency with all pore volume derived values (pore volume [Po.V] and average pore volume [Avg.Po.V]) significantly lower than wildtypes at 20 weeks (Figure 3.8). Using a One-way ANCOVA test, after controlling for time in the male mice, there was a significant effect of genotype on Ma.Ar, cortical thickness (Ct.Th), Avg.Po.V and pore density (Po.Dn), $F(1, 17) = 5.71$, 3.77, 7.19 and 6.68, $p < 0.05$ as well as Ct.Ar/Tt.Ar and Ma.Dm, $F(1, 17) = 8.22$ and 9.19, $p < 0.01$. This overall higher Po.Dn contrasted to the finding that pore volume derived values were lower in 20 week old PAR_2 null mice.

Regression analysis in males showed that whereas cortical porosity (Ct.Po), Po.V and Avg.Po.V declined over time in wildtypes, they increased in male PAR_2 null mice although slightly. Conversely, it was found that there was a significant difference between the groups in the rates of TMD changes over time where lack of PAR_2 induced a negative change in contrast to a gradual accrual in wildtypes.

In females, with the exception of the TMD measurements, the rest of the comparisons remained insignificant (Figures 3.9 and 3.10; Table A.6, Appendix A). Analysis of regression coefficients of change, did not show any significant differences in the females.

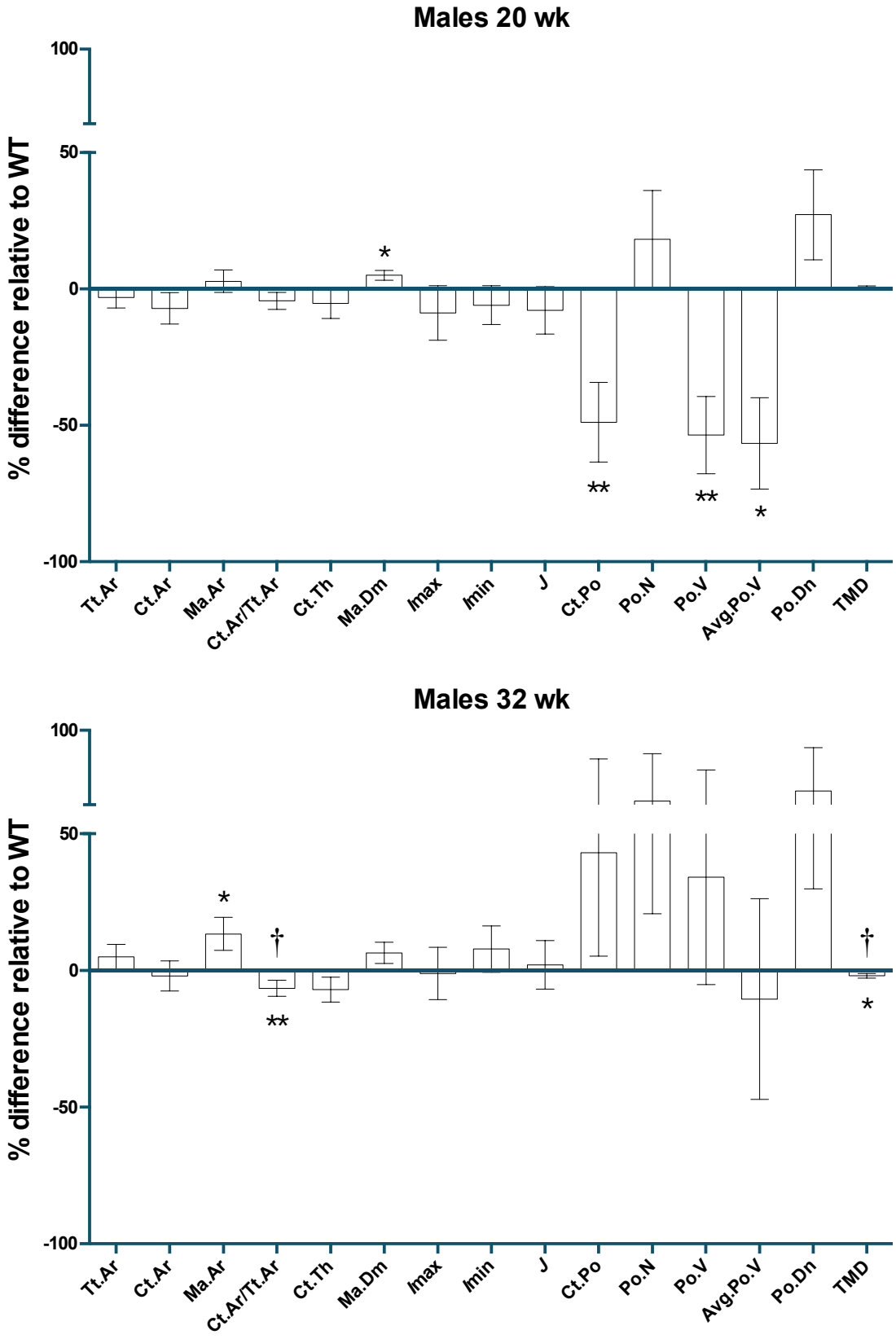


Figure 3.8 Percent difference in diaphyseal cortical indices - males.

The difference between the KO and WT males at 20 and 32 weeks is presented as a percentage relative to the control WT mice. N = 5; * $p < 0.05$, ** $p < 0.01$ using Mann-Whitney U test; † one-tailed comparison; error bars represent SE_{diff}.

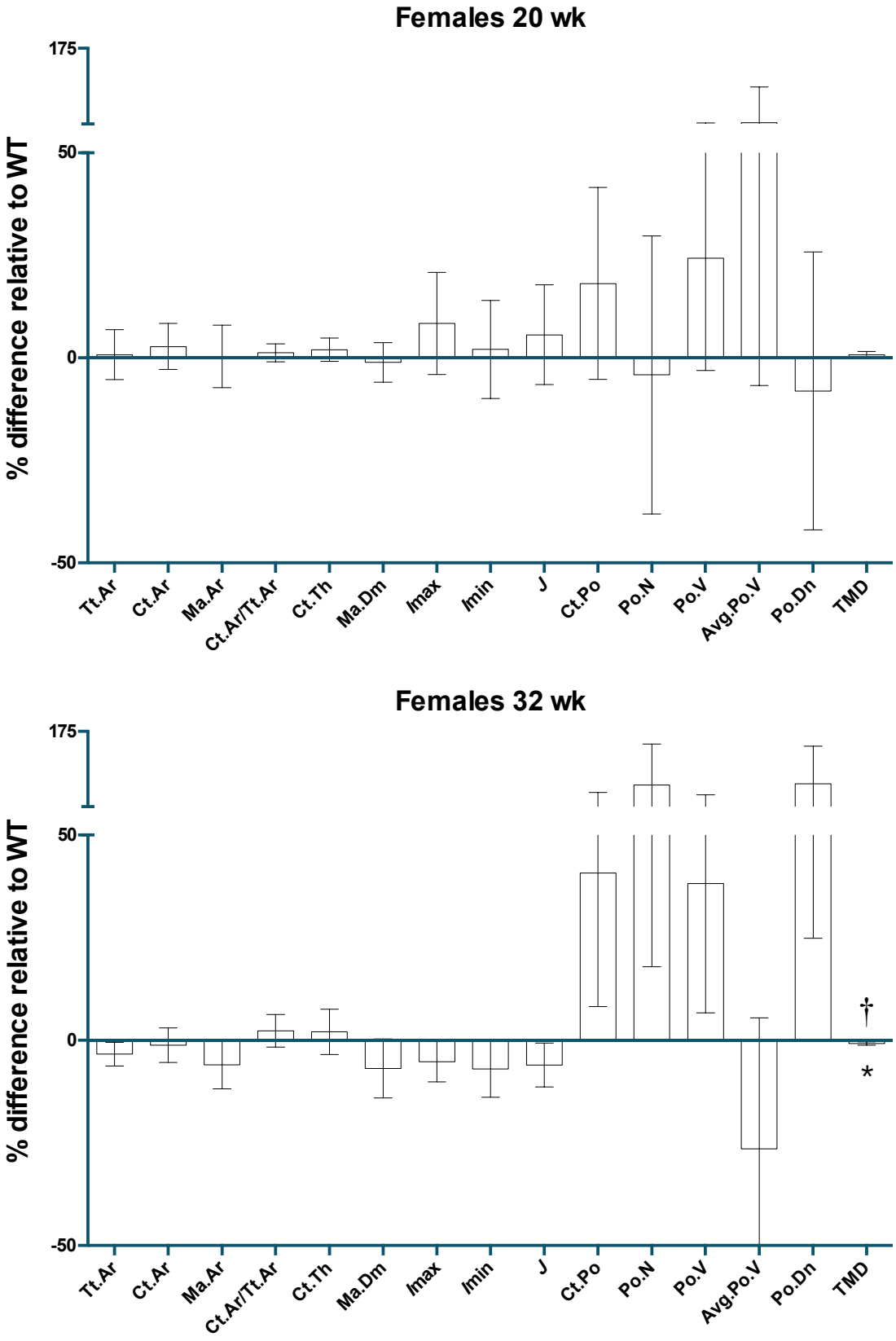


Figure 3.9 Percent difference in diaphyseal cortical indices - females.

The difference between the KO and WT females at 20 and 32 weeks is presented as a percentage relative to the control WT mice. N = 4-5; * $p < 0.05$ using Mann-Whitney U test; † one-tailed comparison; error bars represent SE_{diff}.

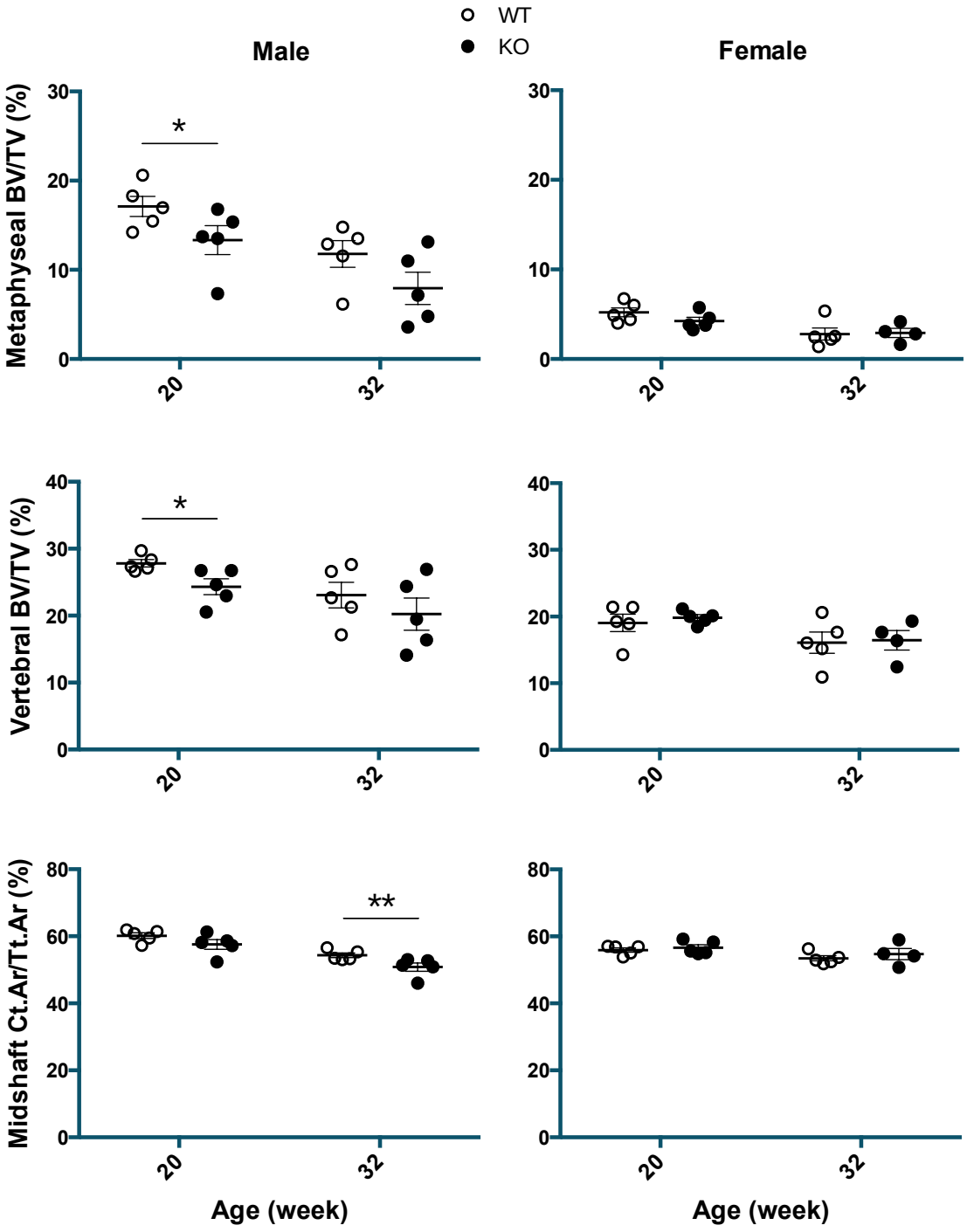


Figure 3.10 Main mass indices of the metaphyseal, vertebral and midshaft regions.

Only male PAR_2 null and wildtype mice showed statistically significant differences in the corresponding values. N = 4-5; * $p < 0.05$, ** $p < 0.01$ using one tailed Mann-Whitney U test; error bars represent SEM.

Table 3.3 Time related change in the tibial midshaft cortical bone.

Regression coefficients of time related changes in bone structural and material indices of PAR_2 wildtype and knockout mice are presented. Significant comparisons between the genotypes are highlighted.

	M			F		
Index	**B_{wt}[1]**	**B_{ko}[2]**	**p-value**	**B_{wt}**	**B_{ko}**	**p-value**
Tt.Ar	0.001	0.010^{*}	0.146	0.004	$-4.6x10^{-5}$	0.421
Ct.Ar	-0.005	-0.002	0.452	0.001	-0.001	0.541
Ma.Ar	0.007^{**}	0.012^{**}	0.099	0.003^{*}	0.001	0.448
Ct.Ar/Tt.Ar	-0.488^{**}	-0.562^{**}	0.691	-0.206^{*}	-0.159	0.780
Ct.Th	-0.002^{**}	-0.002^{*}	0.889	$-3.5x10^{-4}$	$-3.5x10^{-4}$	0.993
Ma.Dm	0.002	0.003	0.670	0.002	-0.001	0.426
/max	$6.0x10^{-5}$	0.001	0.539	0.001	$-2.3x10^{-4}$	0.289
/min	$-2.7x10^{-4}$	0.001	0.184	$3.0x10^{-4}$	$-1.2x10^{-4}$	0.470
J	$-2.1x10^{-4}$	0.002	0.383	0.001	$-3.5x10^{-4}$	0.352
Ct.Po	$-2.30x10^{-4}$	$2.8x10^{-4*}$	0.008	$-1.50x10^{-4}$	$-9.0x10^{-5}$	0.715
Po.N	5.900	11.933^{***}	0.182	-0.443	6.050	0.160
Po.V	$-3.40x10^{-4}$	$3.40x10^{-4*}$	0.009	$-1.30x10^{-4}$	$-1.10x10^{-4}$	0.910
Avg.Po.V	$-6.00x10^{-6}$	$-1.00x10^{-6**}$	0.014	$-1.00x10^{-6}$	$-6.00x10^{-6}$	0.246
Po.Dn	4.982	9.938^{***}	0.129	-0.693	6.571	0.120
TMD	1.403	-0.939	0.022	1.656^{*}	0.119	0.100

[1] Regression coefficient (slope) of changes over time in the wildtype group; a negative value depicts negative changes.

[2] Regression coefficient (slope) of changes over time in the PAR_2 KO group.

* $p < 0.05$, ** $p < 0.01$, *** $p < 0.001$ when values were regressed over time in each sex-genotype category indicating significant changes from 20 to 32 weeks.

[3] Regression coefficients were compared using a second multiple linear regression analysis.

3.3 Discussion

The finding that PAR_2 null mice initially develop high bone mass that gradually changes into a relatively normal phenotype by 13 weeks in a previous study by our laboratory (Georgy et al. 2012), led to the hypothesis that loss of PAR_2 causes a gradual loss of bone mass and density over time to lower than normal levels. Further support for this hypothesis came from the same report which indicated suboptimal osteoblastic and osteoclastic parameters in these mice as demonstrated by histomorphometry and cell differentiation studies as well as slower bone healing responses.

In addressing the above hypothesis, this chapter describes the micro CT findings of an *in vivo* experiment involving global PAR_2 null mice on the C57BL/6J background. Mice were compared to age and sex-matched normal wildtype controls (either littermates or offspring of littermates). It was found that in general, the lack of PAR_2 was associated with significant deficits in the trabecular and cortical indices, however in an age and sex dependent manner.

To evaluate both trabecular and cortical bones, proximal tibial metaphyses and midshafts as well as the fifth lumbar vertebrae were scanned in a Scanco Micro CT 50 facility using the technique described under section 2.4.2. All recommended indices are reported, nevertheless in evaluating the mineral density of trabecular bone, instead of the widely reported BMD, TMD values have been more heavily relied upon. Although it is often said that use of TMD may not be appropriate for murine trabecular bone, the use of 3.4 μm isometric voxel size allowed for the recommended minimum resolution (more than 3 voxels within trabeculae after edge peeling) for valid TMD measurements (Bouxsein et al. 2010). As BMD is reflective of both BV/TV and TMD values combined (and perhaps marrow mineral density), use of TMD provided more accurate information about the material properties of the examined bones while BV/TV was also separately and more reliably evaluated. This also explains the difference observed between the BMD and TMD measurements as reported by this study.

The tibial metaphysis was chosen so that the current observations could be directly comparable to those of the preceding studies (Georgy et al. 2012). To ensure that an early loss of trabecular bone in the tibial metaphyses was not going to be an issue, the L5 vertebrae, which retain more trabeculae over time, were also collected (Glatt et al. 2007).

As the amount of marrow adiposity in the murine vertebrae is expected to increase in a cranial to caudal direction (Naveiras et al. 2009), the choice of L5 also provided a middle ground, effectively avoiding the extreme range of either end. This was particularly important due to the mutually exclusive nature of adipogenesis and osteogenesis (Bethel et al. 2013), and the fact that emerging data from the laboratory suggested PAR_2 may be involved in the process (Kularathna et al. 2013).

The selection of the end points in this study was based on previous reports of the micro CT and histological findings in normal mice of the C57BL/6J background (Glatt et al. 2007) in conjunction with the practical time constraints of the project. Whilst it was intended to perform the evaluations at a relatively late time point, nevertheless, assuming a constant rate of bone loss per unit time, as individuals approach the final boundaries of bone loss, loss of even a few trabeculae in one group may result in a significant decrease in bone volume fraction that no longer corresponds to the magnitude of bone loss, eg. loss of only one trabecula out of two residual trabeculae in a week may be interpreted as a 50% change (Bouxsein et al. 2010). Also, too late a time point runs the risk of losing the window of opportunity for detecting greater bone loss in PAR_2 null mice, due to possible loss of all measurable bone particularly in females. To avoid the statistical implications of such a situation and based on available data on ageing of bone in C57BL/6J mice (Glatt et al. 2007), animals were not aged beyond 32 weeks.

With respect to the impact of genotype on each sex-age category, most of the differences observed concerned the trabecular indices. Here, the loss of PAR_2 was found to be associated with different BV/TV, however, in a sex dependent manner resulting in male PAR_2 null mice that had lower volume fractions at 20 weeks in both tibial and vertebral regions (Figures 3.3 and 3.8). This decrease in BV/TV was associated with corresponding changes in the underlying trabecular parameters but mostly an increased Tb.Sp (Figure 3.3). Tb.N was only lowered at 32 weeks whereas Tb.Th appeared unaffected. In contrast, analysis of bone volume fraction in females did not indicate much difference between the genotypes at any of the time points.

Degree of anisotropy (DA) also appeared to have been impacted by the lack of PAR_2 in males of the C57BL/6J background. In fact, the trabecular architecture in the tibial

metaphyses and vertebral bodies became more isotropic in these mice following the loss of PAR_2. A high degree of anisotropy is an inherent feature of trabecular bone which is arguably one of the most important predictors of its mechanical competence (Goulet et al. 1994). Thus, the fact that PAR_2 null male mice developed more isotropically incompetent bone than wildtypes suggests that PAR_2 is important in the normal response of trabecular bone to mechanical forces. Additionally, although not as severely affected, the female PAR_2 null mice had significantly lower DA and TMD as well as vertebral TV and TMD than their WT controls. Although mechanical evaluations were not included as a part of this study, nevertheless, these findings suggest that lack of PAR_2 could leave the trabecular bone more prone to mechanical failure in mice of the C57BL/6J background.

In the cortical bone, it was also noted that the impact of genotype more significantly affected the males causing a general architectural and material change evident by increased marrow diameter, marrow area and reduced Ct.Ar/Tt.Ar and TMD in response to the lack of PAR_2 in 32 week olds as well as lower Ct.Po in 20 week olds. PAR_2 null mice are known to have lower osteoclastic numbers and activity, at least in growing mice (Georgy et al. 2012), which may explain the latter finding. Except for a smaller TMD in PAR_2 null mice at 32 weeks, genotype did not determine any significant cortical changes in the females.

With respect to the effects of ageing on each sex-genotype category, micro CT measured indices generally deteriorated over the 12 week interval between 20 and 32 weeks (Tables 3.1-3). On occasion however, some parameters such as Tb.Th only showed little change particularly in the wildtypes. This is perhaps caused by the distribution of mechanical forces which remain rather unchanged despite ever shrinking bone mass. The result is a gradual loading of the remaining structural elements which acts to preserve integrity in order to overcome the increasing mechanical stress. The generic effect of ageing and sex on bone loss in mice of the C57BL/6J background has been published before and is consistent with the current findings (Glatt et al. 2007). Overall, the rate at which such age related changes occurred, reflected a significant effect of genotype on both architectural and material properties in trabecular and cortical compartments of male mice.

In the vertebral trabecular bone, however, the Conn.D value increased more rapidly over time in male PAR_2 null than in wildtype mice. This is the opposite of what is normally observed in the trabecular bone where Conn.D diminishes over time very much like Tb.N values (Chen et al. 2008; Chen et al. 2010). Specifically, since Conn.D reflects the number of trabecular connections per volume space (Toriwaki and Yonekura 2002), and given the lower TMD values in PAR_2 null mice, presence of any noise caused by deterioration of trabeculae over time (as a result of local areas of reduced TMD), can possibly imitate a high connectivity state. In light of other measured parameters particularly BV/TV and Tb.N, and given the general observed variability in Conn.D values, it seems likely that this increase could simply reflect technical artefacts.

Nevertheless, the fact that the increase in Conn.D is also associated with a lower DA in the knockouts is interesting. Assuming that the transverse trabeculae are resorbed first in the wildtypes, both a higher DA and a lower Conn.D would ensue whereas a lower rate of bone resorption overall, can leave most of these trabeculae intact and result in a higher state of connectivity and isotropy. Whether or not this higher connectivity in the knockouts compensates for their lower DA values, however, requires further mechanical evaluations.

Absence of PAR_2 seemed to have impacted the rate of bone material deterioration at the same time as architectural indices. Global loss of PAR_2 caused TMD values to decline at a higher rate in the tibial trabecular region of male mice and to lag behind in the face of gradually increasing cortical TMD values in the wildtype males. Whilst structural and BMD values could reflect a combination of resorptive and osteogenic parameters, TMD values, however, are more indicative of the quality of the osteoid deposited by the osteoblasts and the following mineralisation (Bouxsein et al. 2010; Kazakia et al. 2011). While TMD in wildtype mice showed the expected tendency to increase over time, in PAR_2 null mice it tended to decrease over time, which may be due to an inferior quality of bone formation by PAR_2 null osteoblasts. In fact, PAR_2 activation stimulates *Col1a1* expression by osteoblasts (Georgy et al. 2010). Moreover, PAR_2 null mice have lower osteoblast and osteoid derived parameters, which is in agreement with the current finding (Georgy et al. 2012).

The observed difference between males and females in response to the loss of PAR_2 is another noteworthy feature and may be explained in context of hormonal differences (Figure 3.10). Several studies have looked into the effects of androgens and estrogen in bone physiology and particularly in relation to age related bone loss and osteoporosis (Miyaura et al. 2001). Sex hormones overall appear to have a complicated role in the regulation of bone mass one of which is the later onset of puberty in males which results in significantly higher amounts of accumulated bone (Sidlauskas et al. 2014). Additionally, the greater muscle mass in males means higher mechanical forces which can also serve to protect bone from age related deterioration (Lang 2011). It has also been known for a long time that females experience an earlier onset of bone loss which can well result in lower bone mass than males of a similar age (Mazess 1982; Glatt et al. 2007).

Mechanistically, it has been suggested that most of the age related loss of bone mass could be explained by reduced formation in males and an increased resorption in females (Aaron et al. 1987). Thus, the finding that the absence of PAR_2 more profoundly affected the males in this study suggests that the role of the receptor is perhaps more significant in bone formation than resorption. However, it must be noted that previous histomorphometric evaluations in 7-week-old male mice have demonstrated the presence of defects in both features when PAR_2 is absent (Georgy et al. 2012). Thus, it is more logical to assume that a combination of both deficiencies, however at a certain ratio more likely to be attained in males, is a prerequisite of the observed phenotype.

Whatever the cause, the higher rate of bone loss in females means that it is possible for both WT and KO females to lose most of their trabeculae before 20 weeks of age. In essence, this means that due to a slower pace of bone loss in males over time, sufficient amounts of bone have been available throughout the timeline of this study to provide a medium in which lack of PAR_2 can be measured whereas in females, an earlier and more profound loss of bone results in a reduction of sampled bone, especially in the tibia (see absolute values shown in Figure 3.10). Despite this concern, the use of the L5 vertebra, which tends to retain its bone content for a longer time, provided sufficient confirmation of the current findings.

All in all, most of what has been described in this chapter could be explained by abnormalities of both bone formation and resorption in PAR_2 null mice. In the trabecular bone, lower BV/TV in PAR_2 null mice suggests either reduced formation or increased resorption. Based on the preceding study in 2012, PAR_2 null mice clearly demonstrated decreased resorption by their higher mass profile and reduced formation by a defective bone healing response, both of which correlated well with histomorphometric findings, i.e. lower osteoclast and osteoblast surfaces and higher volume of retained growth plate cartilage. These mice additionally formed lower numbers of osteoclasts in bone marrow cultures (Georgy et al. 2012). In support of this hypothesis, the significant increase of trabecular Conn.D over time in PAR_2 null mice could be explained by suboptimal resorption and residual connectivity. Additionally, lower TMD and its higher rate of deterioration in knockouts is indicative of defective bone formation features. This however, requires confirmation by means of dynamic histomorphometry.

In the cortical bone too, lower porosity values (Ct.Po and Po.V) in 20 week old PAR_2 null mice indicated lower resorption rate in the knockouts. This may be attributed to a deficit in osteoclastic function, as shown by Georgy et al. (2012), which itself may be indirectly caused by the effects of PAR_2 deletion on osteoblasts and osteocytes as regulators of osteoclastic formation and function. Despite the important role of osteocytes in the regulation of bone resorption, there is currently no data available on the expression and functions of PAR_2 in these cells. Further work should be undertaken to probe this possibility.

A rather counterintuitive finding in these mice, however, is a higher pore density (detected by ANCOVA). This could be explained by the compounding effect of reduced bone formation at the same time as reduced resorption. As resorption progresses slowly in PAR_2 null mice, as evident by lower pore volume, a reduced capacity to substitute any lost bone results in a higher number of detectable pores on a high resolution microCT scan whereas the majority of such minute pores could be quickly filled with new bone in the wildtypes and therefore remain undetectable. The result of such a situation would be a higher number of smaller pores as was observed in the knockouts.

These observations are in agreement with the prediction that global lack of PAR_2 leads to a bone deficient phenotype based on the preceding work (Georgy et al. 2012). The current study shows that PAR_2 is required for normal homeostasis and maintenance of bone postnatally and that its absence results in an altered rate of structural and material changes over time.

Regardless, global lack of PAR_2 from all mesenchymal and haematopoietic bone cellular units as well as potential hormonal and neurogenic aberrations in the absence of PAR_2 could all have affected the perceived results. For example, PAR_2 null mice have altered neuronal functions that affect the gastrointestinal system or perception of pain (Vergnolle et al. 2001b; Cuffe et al. 2002). The latter may have implications in bone as a result of altered weight bearing and distribution of mechanical forces. Various modulators of osteoclastogenesis and osteoblastogenesis such as IL-6 (Manolagas 1998) may also be affected by the absence or presence of PAR_2 (Smith et al. 2004) which may in turn impact the corresponding lineages (Kudo et al. 2003; Yoshitake et al. 2008; Kaneshiro et al. 2014). Thus, although not directly measured, such unrecognised factors could possibly be at play and affect the results.

The present chapter demonstrates the significance of PAR_2 in physiologic processes that govern bone tissue. It is important to note, however, that the described osteopoenic profile is the result of a global lack of PAR_2. Thus, generation of cell type specific PAR_2 null mice is required to further delineate the underlying mechanisms. Subsequently, experiments presented in chapter 6 have been designed to generate and use osteoblast specific PAR_2 null mice to shed light on the role of osteoblasts in the process.

CHAPTER 4: EFFECT OF GLOBAL PAR_2 GENE ABLATION ON BONE LOSS IN DYSTROPHIN - DEFFICIENT MICE

4.1 Introduction and Aims

Not only has PAR_2 been widely recognised as an important contributor to various homeostatic processes, a substantial body of evidence indicates that this receptor is also significant in the stimulation of inflammation (Rothmeier and Ruf 2011). Moreover, in the case of periodontal disease, it has been shown that PAR_2 is required for inflammation-induced bone loss (see section 1.4.3).

With regard to the possible roles of PAR_2 in mediating the pathological effects of inflammation on bone, the possibility of pharmacological targeting of PAR_2 is an attractive prospect. Accordingly, it was hypothesised that if PAR_2 is in fact involved in the inflammation related osteopoenia, then deletion of PAR_2 in the presence of a profound inflammatory condition (i.e. muscular dystrophy), must be protective. To test this hypothesis, C57BL/6J PAR_2 null mice were backcrossed on C57BL/10 mdx mice to generate PAR_2 null and wildtype mdx mice. These mice were then aged and their bones analysed using an identical time frame and setting as described in chapter 3 (see also section 2.1.1.2).

The mdx mouse is a model of DMD, which naturally lacks dystrophin due to a mutation in exon 23 of the dystrophin gene resulting in the absence of the protein (Sicinski et al. 1989). As a result, these mice develop an analogous phenotype to the human version of DMD (Coulton et al. 1988). Previous works have shown that mdx mice exhibit an increased inflammatory profile which is accompanied by increased osteoclastic parameters and bone resorption (Novotny et al. 2011; Rufo et al. 2011). This has been found to cause a significantly lower tibial metaphyseal BV/TV, Tb.N and a higher Tb.Sp than observed in the wildtype mice. These mice also have lower Tt.Ar and Ct.Ar in their tibial midshafts

with a consequent reduced moment of inertia and mechanical strength (Novotny et al. 2011; Rufo et al. 2011). All of these features made mdx mice a desired model for the purpose of this study.

PAR_2 null mdx mice were generated as a part of a separate project evaluating the possible roles of PAR_2 in the progression of muscle pathology in muscular dystrophy (Taghavi 2016). The tibiae from these mice were evaluated for the purpose of this chapter. Both trabecular and midshaft cortical parameters were assessed using micro CT evaluations. Comparison of values between PAR_2 null mdx and wildtype mdx mice showed that deletion of PAR_2 causes a substantial improvement in trabecular bone parameters in mdx mice.

4.2 Results

4.2.1 PAR_2 null mdx mice

These mice were generated in two steps by first crossing C57BL/6J PAR_2 null with C57BL10ScSn mdx mice to produce *F2rl1*$^{+/-}$ offspring (F1) that were homozygous for the dystrophin deficiency allele and then crossing the F1 mice with each other (section 2.1.1.2). Littermate wildtype mdx mice generated from the latter crossings were used as controls.

4.2.1.1 Weight and Bone Length

PAR_2 null mdx mice reproduced well and survived up to the designated age without any obvious problems. Body weight and bone length remained largely similar for both genotypes within each sex-age group (Figure 4.1). In investigating the effect of age within each sex-genotype category, it was found that apart from the male PAR_2 null mdx mice, values increased significantly from 20 to 32 weeks in all groups (Figure 4.1). Nevertheless, regression analysis, did not find any differences in the rate of change between the groups.

4.2.1.2 Tibial Trabecular Bone

A segment equal to 10% of the full length of the bone was scanned within the proximal tibial metaphyses (Figure 4.2). Evaluation of the trabecular bone in the male mice indicated

greater bone volume (BV) and bone volume fraction (BV/TV) with corresponding changes in the underlying connectivity density (Conn.D), trabecular number (Tb.N), trabecular thickness (Tb.Th) and trabecular separation (Tb.Sp) values in PAR_2 null mdx compared with wildtype mdx mice at 20 weeks (Figures 4.3 and 4.7). Degree of anisotropy (DA), bone mineral density (BMD) and tissue mineral density (TMD) were also found to be higher in PAR_2 null mdx males. None of the comparisons at 32 weeks were statistically significant (Figure 4.3; Table B.1, Appendix B). When a one-way ANCOVA was used while controlling for time, it was found that in general, the presence of PAR_2 had a significant effect on BV/TV, Conn.D, Tb.N and Tb.Th, $F(1, 24) = 4.38, 6.81, 3.64$ and 3.71, $p < 0.05$.

Despite the general superiority of the PAR_2 null group at the earlier time, comparison of regression coefficients across the endpoints in males revealed that BV, BV/TV, Conn.D and BMD deteriorated faster when PAR_2 was not present (Table 4.1).

In females, lack of PAR_2 was associated with greater BV and BV/TV at both time points (Figures 4.4 and 4.7). Both Tb.N and Tb.Sp also showed relevant changes with higher Tb.N and lower Tb.Sp values in PAR_2 null mdx mice. Conn.D was only different at 20 weeks whereas Tb.Th remained similar across the two time points. Structural model index was also reduced in the absence of PAR_2 but only at 20 weeks where TMD was found to be significantly higher (Table B.2, Appendix B). In females, when controlled for time, one-way ANCOVA indicated that presence of PAR_2 had a significant effect on BV/TV and Tb.N, $F(1, 34) = 23.73$ and 14.79, $p < 0.001$ as well as Tb.Sp and SMI, $F(1, 34) = 8.01$ and 5.61, $p < 0.05$.

In females, regression analysis showed a higher rate of Conn.D deterioration over time in PAR_2 null mice than in the wildtype controls (Table 4.1).

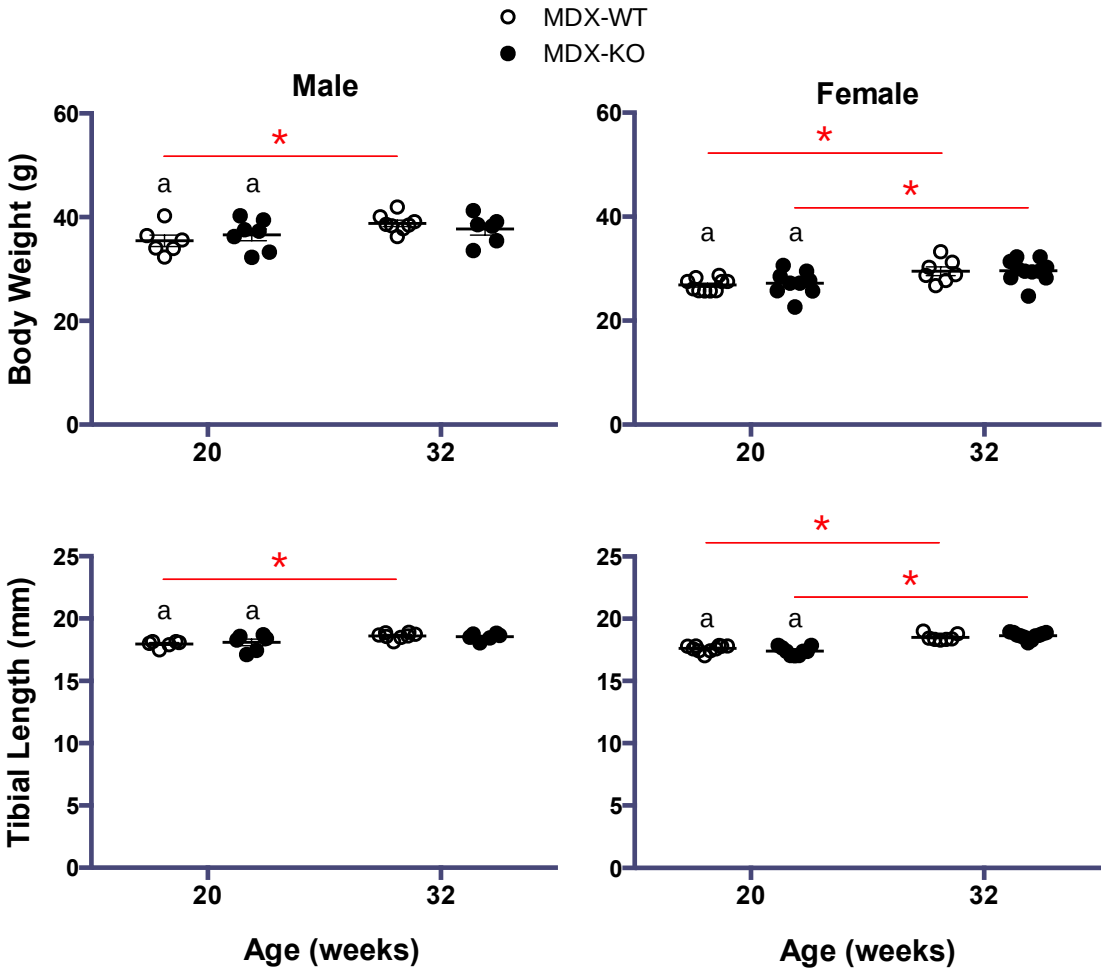


Figure 4.1 Body weight and tibial lengths in PAR_2 knockout and wildtype mdx mice.

Bone lengths were measured at the time of the micro CT scans using the scout views. **MDX-WT** - wildtype mdx mice; **MDX-KO** - PAR_2 knockout mdx mice. N = 6-11; no significant differences were found between sex-age controlled groups (between the genotypes) using two tailed independent samples t-test; * $p < 0.05$ using simple linear regression indicating significant time related changes in sex-genotype controlled groups; error bars represent SEM; [a] Data courtesy of Dr. Neda Taghavi (Taghavi 2016).

4.2.1.3 Tibial Cortical Bone

In the tibial midshaft, of all structural and material features evaluated in males, pore number (Po.N) and pore density (Po.Dn), which were lower in PAR_2 null mdx compared with wildtype mdx, were the only parameters to be altered by the absence of PAR_2. However, this only occurred in the 32 week old age group (Figure 4.5; Table B.3, Appendix B). One-way ANCOVA did not find any significant comparison in males after controlling for time.

In females, lack of PAR_2 only resulted in a significant improvement of maximum moment of inertia (/max) at 32 weeks but not any other indices (Figure 4.6; Table B.4, Appendix B). When controlled for time, using one-way ANCOVA, there was a significant effect of PAR_2 on /max and potent moment of inertia (*J*) in females, $F(1, 29) = 5.32$ and 3.16, $p < 0.05$.

Comparison of regression coefficients did not show any significant differences in the rate of change of cortical parameters over time between the genotypes of either sex (Table 4.2, $p > 0.05$).

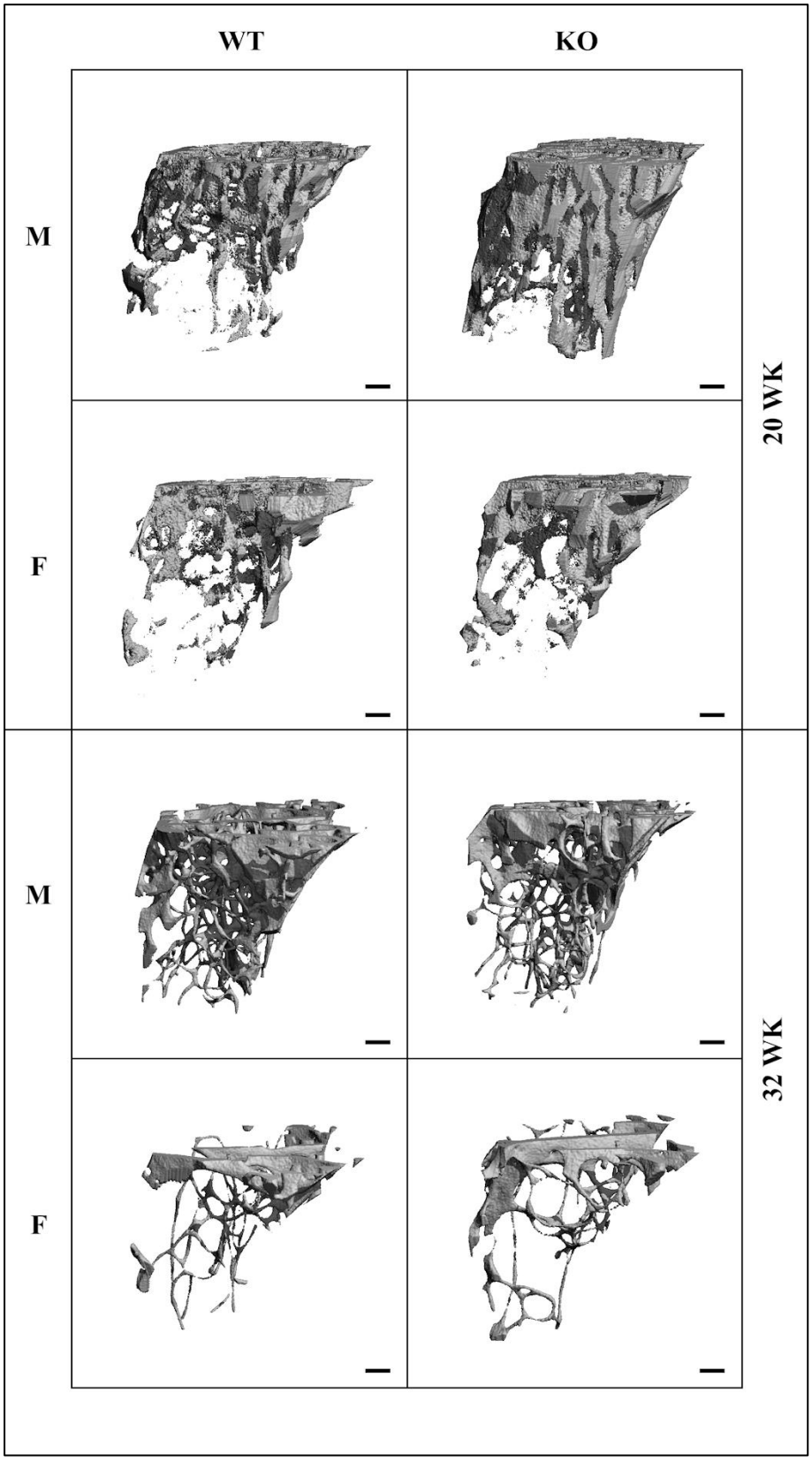


Figure 4.2 3D models of the metaphyseal trabecular bone in PAR_2 KO and WT mdx mice.
Male and female mice at 20 and 32 weeks of age are presented. Lateral view, bar represents 200 μm.

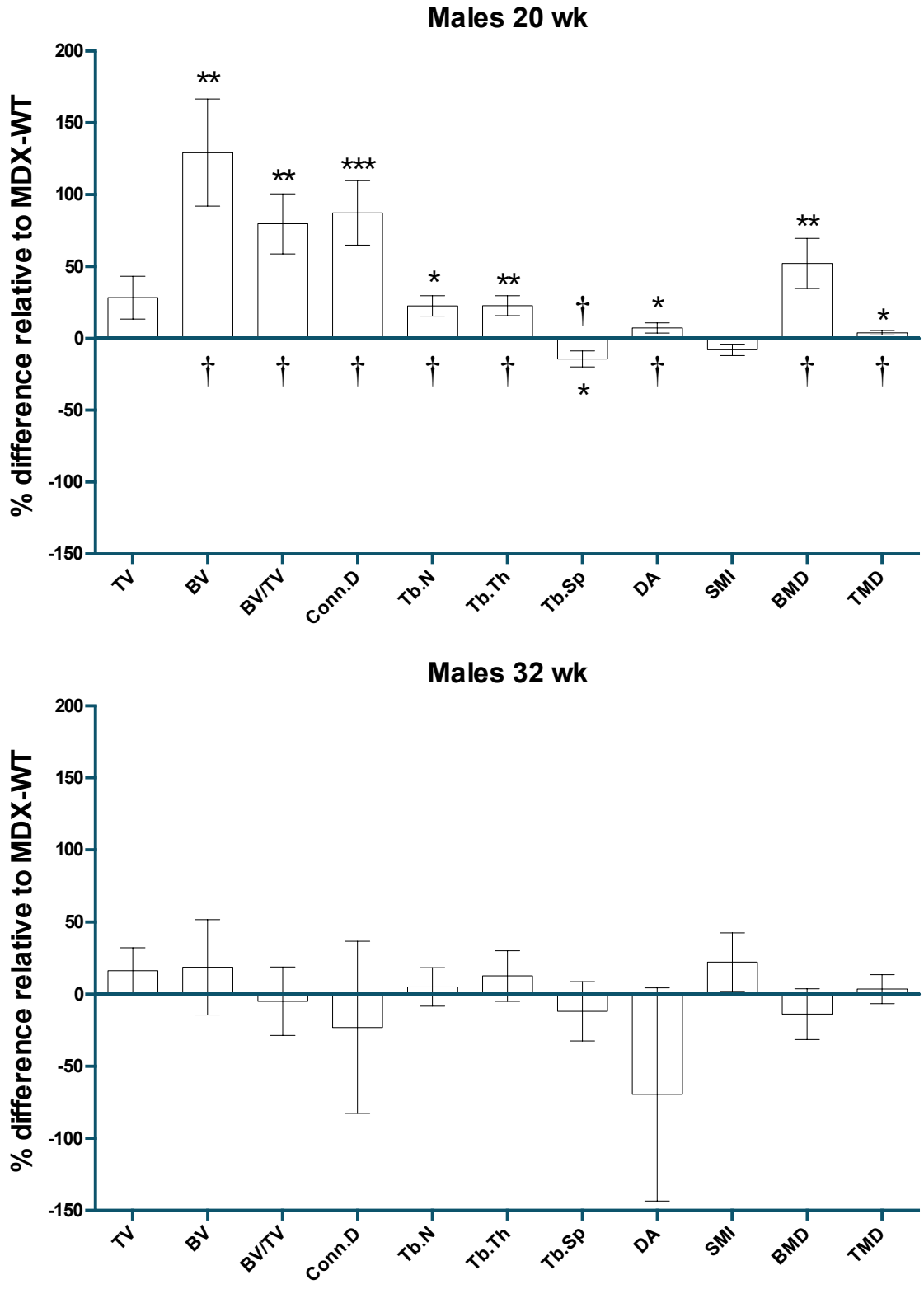


Figure 4.3 Percent difference in metaphyseal trabecular indices - males.

The difference between the KO and WT mdx males at 20 and 32 weeks is presented as a percentage relative to the control WT mdx mice. N = 6-8; * $p < 0.05$, ** $p < 0.01$, *** $p < 0.001$ using Mann-Whitney U test; † one-tailed comparison; error bars represent SE_{diff}.

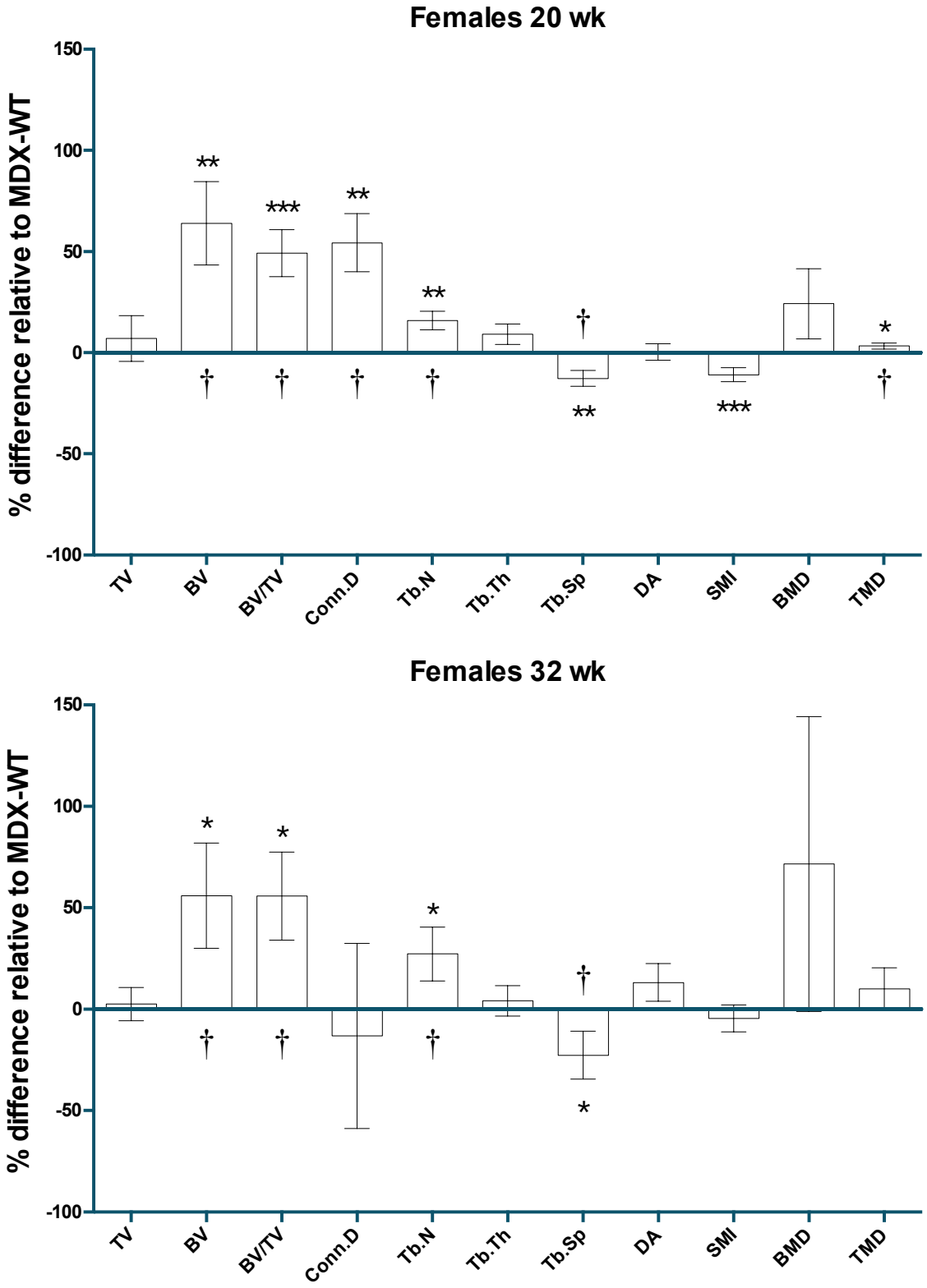


Figure 4.4 Percent difference in metaphyseal trabecular indices - females.

The difference between the KO and WT mdx females at 20 and 32 weeks is presented as a percentage relative to the control WT mdx mice. N = 7-11; * $p < 0.05$, ** $p < 0.01$, *** $p < 0.001$ using Mann-Whitney U test; † one-tailed comparison; error bars represent SE_{diff}.

Table 4.1 Time related change in the tibial metaphyseal trabecular bone.

Regression coefficients of time related changes in bone structural and material indices of PAR_2 null mdx and wildtype mdx mice are presented. Significant comparisons between the genotypes are highlighted.

	M			F		
Index	**B_{wt}[1]**	**B_{ko}[2]**	**P-value[3]**	**B_{wt}**	**B_{ko}**	**P-value**
TV	0.023	0.008	0.695	0.019	0.013	0.769
BV	0.001	-0.012*	0.042	0.005**	-0.008***	0.108
BV/TV	0.001	-0.005**	0.011	-0.003***	-0.004***	0.074
Conn.D	-49***	-105.79***	0.001	-9.811	-26.737***	0.049
Tb.N	-0.028	-0.082*	0.203	-0.107***	-0.109***	0.923
Tb.Th	-0.001	-0.001*	0.525	-.001	-0.001**	0.496
Tb.Sp	0.004	0.004	0.976	0.026***	0.017***	0.126
DA	0.0374	0.017*	0.403	-0.005	0.012	0.218
SMI	-0.058	-2.1x10^{-4}	0.132	0.003	0.018	0.344
BMD	-2.094	-6.812***	0.007	-4.321**	-4.746***	0.743
TMD	4.424	12.733**	0.476	-1.279	2.573	0.493

[1] Regression coefficient (slope) of changes over time in the wildtype group; a negative value depicts negative changes.

[2] Regression coefficient (slope) of changes over time in the PAR_2 KO group.

* $p < 0.05$, ** $p < 0.01$, *** $p < 0.001$ when values were regressed over time in each sex-genotype category indicating significant changes from 20 to 32 weeks.

[3] Regression coefficients were compared using a second multiple linear regression analysis.

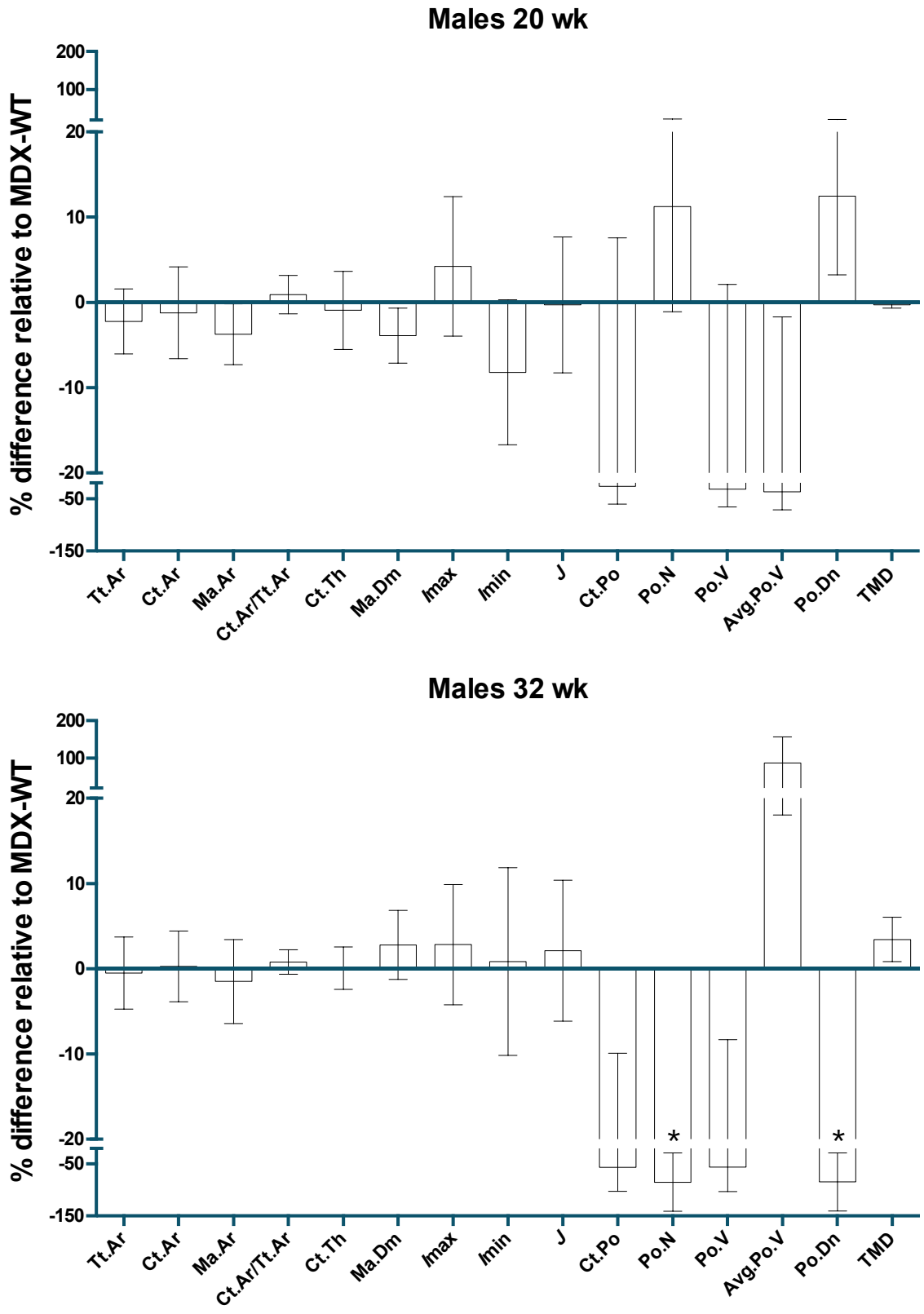


Figure 4.5 Percent difference in diaphyseal cortical indices - males.

The difference between the KO and WT mdx males at 20 and 32 weeks is presented as a percentage relative to the control WT mdx mice. N = 6-8; * $p < 0.05$ using Mann-Whitney U test; error bars represent SE_{diff}.

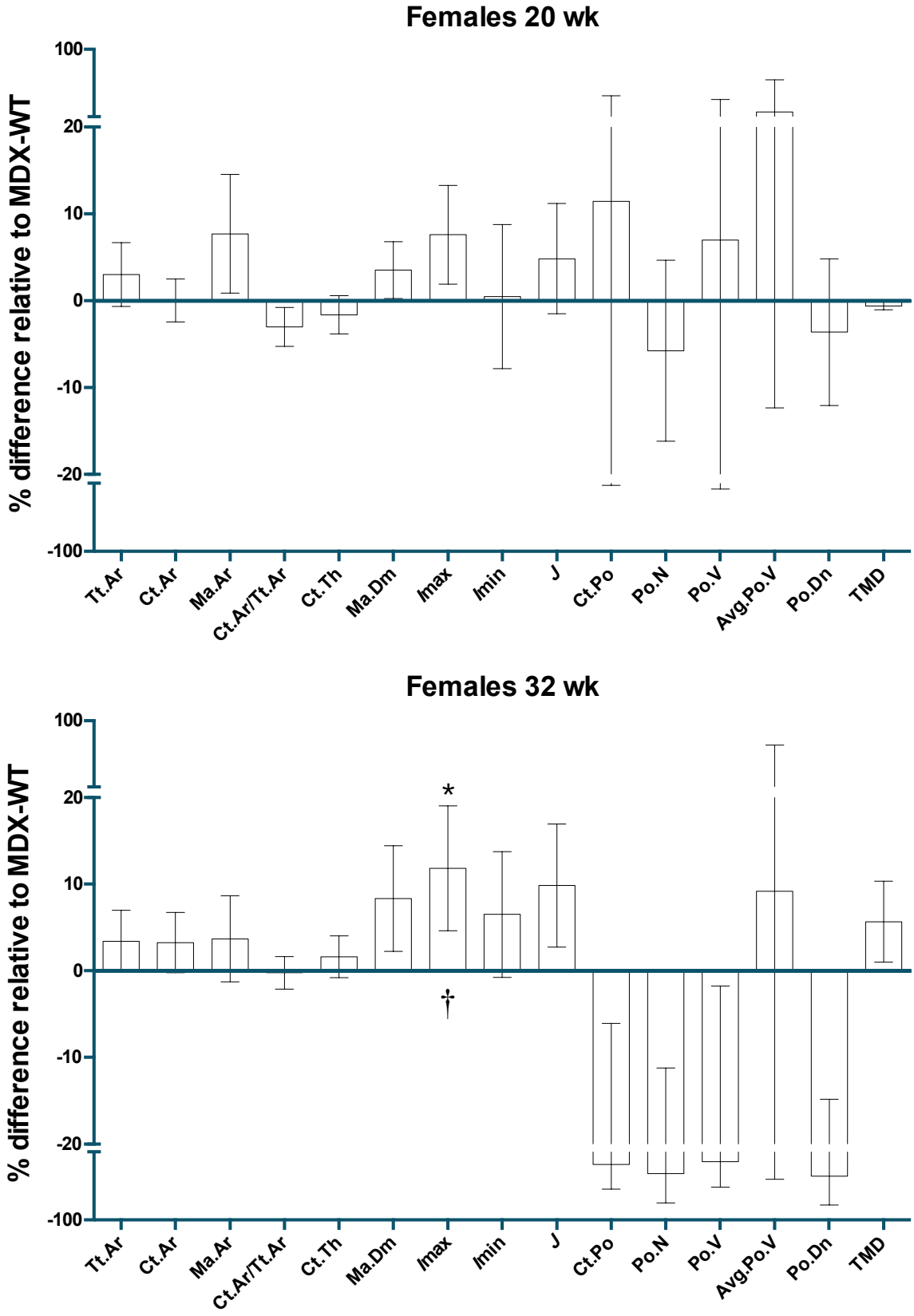


Figure 4.6 Percent difference in diaphyseal cortical indices - females.

The difference between the KO and WT mdx females at 20 and 32 weeks is presented as a percentage relative to the control WT mdx mice. N = 7-11; * $p < 0.05$ using Mann-Whitney U test; † one-tailed comparison; error bars represent SE_{diff}.

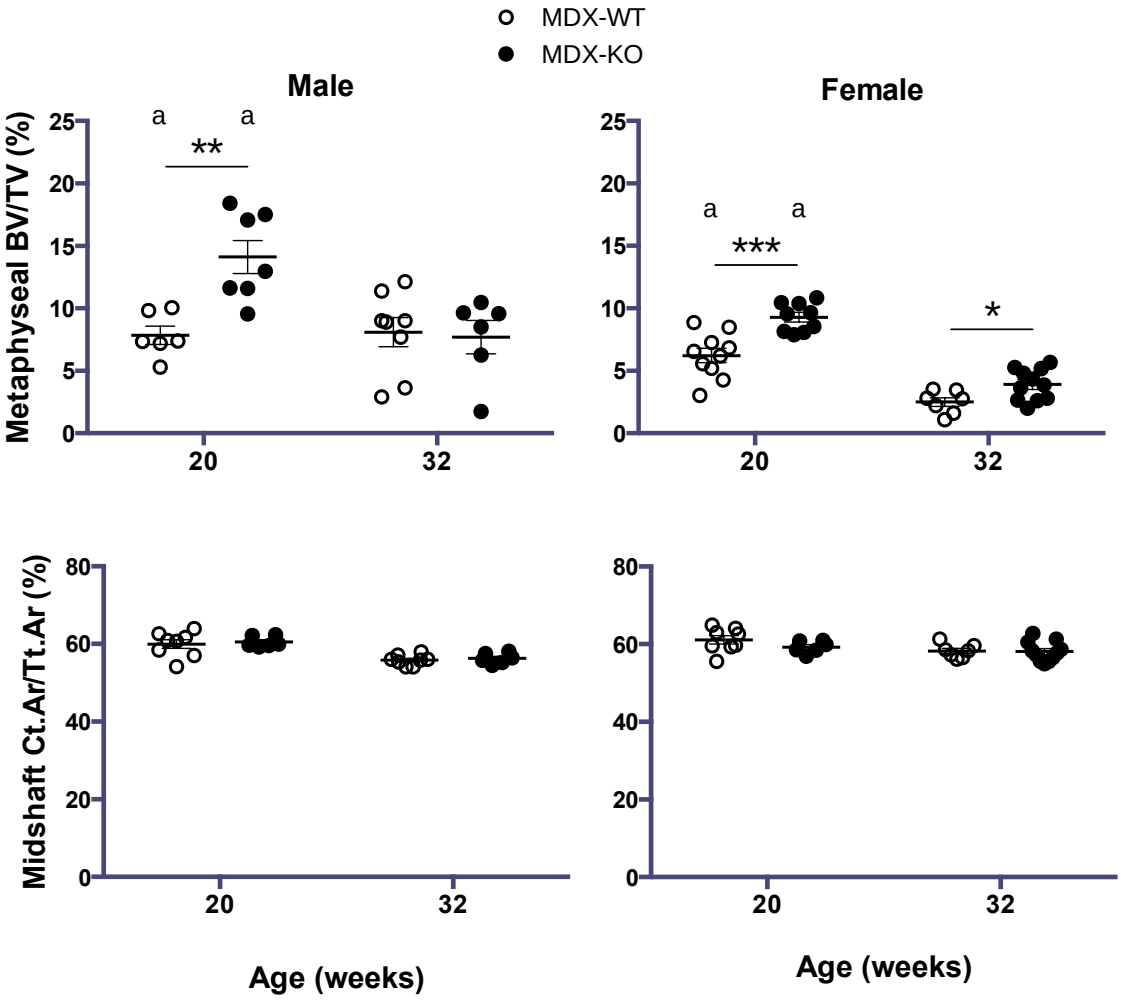


Figure 4.7 Main mass indices of the metaphyseal and midshaft regions in mdx mice.

Whereas trabecular mass improved by deletion of PAR_2 in males at 20 weeks and females across both endpoints, the distribution of midshaft Ct.Ar/Tt.Ar remained unchanged between the genotypes. * $p < 0.05$, ** $p < 0.01$, *** $p < 0.001$ using one tailed Mann-Whitney U test; error bars represent SEM; [a] Data courtesy of Dr. Neda Taghavi (Taghavi 2016).

Table 4.2 Time related change in the tibial midshaft cortical bone.

Regression coefficients of time related changes in bone structural and material indices of PAR_2 null mdx and wildtype mdx are presented. Significant comparisons between the genotypes are highlighted.

	M			F		
Index	**B_{wt}[1]**	**B_{ko}[2]**	**P-value[3]**	**B_{wt}**	**B_{ko}**	**P-value**
Tt.Ar	0.330	0.156	0.443	0.009^{*}	0.010^{**}	0.871
Ct.Ar	-0.003	-0.002	0.800	0.003	0.005^{**}	0.438
Ma.Ar	0.006^{**}	0.007^{**}	0.738	0.006^{*}	0.005^{*}	0.700
Ct.Ar/Tt.Ar	-0.004^{**}	-0.004^{***}	0.944	-0.002	-0.001	0.341
Ct.Th	-0.001^{*}	-0.001	0.836	-0.001	$-5.0\text{x}10^{-6}$	0.337
Ma.Dm	0.001	0.005^{*}	0.183	-0.003	-0.001	0.523
/max	$2.9\ \text{x}10^{-4}$	$1.2\ \text{x}10^{-4}$	0.887	0.001^{*}	0.002^{**}	0.503
/min	$-3.0\text{x}10^{-6}$	0.001	0.445	0.001	0.001^{*}	0.515
J	0.001	0.001	0.803	0.002^{*}	0.003^{**}	0.493
Ct.Po	$9.9\ \text{x}10^{-5}$	$-4.8\ \text{x}10^{-5}$	0.524	0.001^{**}	$3.3\text{x}10^{-4}$	0.224
Po.N	8.740	-2.236^{**}	0.165	21.819^{**}	10.311	0.211
Po.V	$1.2\ \text{x}10^{-4}$	$-5.1\ \text{x}10^{-5}$	0.600	0.001^{**}	$4.9\ \text{x}10^{-4}$	0.308
Avg.Po.V	$-4.0\text{x}10^{-6}$	$6.0\text{x}10^{-6}$	0.102	3.7585E-7	-7.2546E-7	0.817
Po.Dn	6.333	-1.593^{***}	0.160	17.496^{**}	7.421	0.166
TMD	-1.426	2.367^{***}	0.206	-9.490^{**}	-3.533	0.211

[1] Regression coefficient (slope) of changes over time in the wildtype group; a negative value depicts negative changes.

[2] Regression coefficient (slope) of changes over time in the PAR_2 KO group.

* $p < 0.05$, ** $p < 0.01$, *** $p < 0.001$ when values were regressed over time in each sex-genotype category indicating significant changes from 20 to 32 weeks.

[3] Regression coefficients were compared using a second multiple linear regression analysis.

4.3 Discussion

PAR_2 is a well known proinflammatory receptor (Rothmeier and Ruf 2011). As inflammation can potentiate bone loss due to the impact of various cytokines on the bone microenvironment, we decided to study the role of PAR_2 in this process. At the time, another project in our laboratory was investigating the role of PAR_2 in the pathogenesis of muscular dystrophy. A mouse colony was created by backcrossing the C57BL/6J PAR_2 null mice with a C57BL/10 background mdx colony which provided an opportunity to examine the effects of PAR_2 deletion on the osteopoenic feature of mdx mice previously reported (Nakagaki et al. 2011; Novotny et al. 2011; Rufo et al. 2011).

It was observed that in general, lack of PAR_2 resulted in a significant improvement of trabecular bone indices in mdx mice, nevertheless cortical bone remained mostly unaffected. Age seemed to moderate the perceived effect such that differences were more prevalent at 20 weeks. Like the previous chapter, here too an attempt has been made to outline these changes from two perspectives: first, by noting the effect of genotype on bone architecture and material parameters at each time point and second, by viewing the impact of genotype on age related bone loss. The first view concerns the direct effect of genotype on bone when age and sex are controlled whereas the second view attempts to answer the question of whether age related changes are a function of genotype when sex is controlled.

With respect to the impact of genotype on each sex-age category, most of the differences observed occurred in the trabecular bone, however small changes were also noticeable in the cortical bone. In contrast to the non-mdx mice (chapter 3), mdx mice demonstrated thoroughly different trabecular features. Here, the lack of PAR_2 significantly improved BV, BV/TV, Conn.D, Tb.N, Tb.Sp and TMD values of the 20 week old males and females. Tb.Th and DA were additionally improved in the males. At 32 weeks, only females demonstrated improvement in their structural parameters i.e. BV, BV/TV, Tb.N and Tb.Sp, nonetheless, as in males, TMD was not affected at this later time point.

In the cortical region, like the non-mdx mice, male PAR_2 null mdx mice also exhibited a decrease in porosity related features. Nevertheless, these changes contrasted from those reported in chapter 3 in that here, pore number derived indices were found to be affected as opposed to volume related parameters and this only occurred at the later 32 week time point

rather than at 20 weeks. This was evident by a lower Po.N and Po.Dn measurements. Apart from a higher maximum moment of inertia at 32 weeks in PAR_2 null mice, genotype did not determine any significant cortical changes in the females.

In the mdx mice, the data presented here indicate that there is an immense improvement of trabecular bone architectural and material properties in the absence of PAR_2 particularly at the earlier 20 week time point across both sexes. In light of the recent findings from a concurrent study on the muscle pathology in these mice (Taghavi 2016), the pathophysiology involved in this observation will be discussed briefly here.

The recent study in our laboratory has demonstrated that knocking out PAR_2 from mdx mice has a limiting effect on the pathology of murine muscular dystrophy. It has been found that PAR_2 null mdx mice have a significantly superior performance to their WT counterparts in both grip strength and fatigue tests. Additionally, the cumulative histological percentage of the damaged muscle fibres was significantly higher in WT animals than the knockouts. Regardless of the mechanism involved, improvement of muscle pathology in essence signifies the possibility of higher mechanical loading of the skeleton in these mice partly explaining these results.

It is well known that mechanical forces play an essential role in the maintenance and remodelling of osseous tissue. The intrinsic mechanoreceptor system of the bone mainly consists of osteocytes that are thought to sense even the slightest of change in the mechanical forces being applied to the bone and translate it into soluble signals (Robling 2017). It has also been suggested that mechanical forces through β-catenin can control lineage allocation of mesenchymal cells and inhibit adipogenesis (Case and Rubin 2010). Thus, it is possible that improvement of muscle pathology in PAR_2 null mdx mice could be held at least partly responsible for the observed bony changes.

Aside from the mechanical factors, the close proximity of muscle and bone as a working skeletal unit could raise the possibility of direct biochemical interactions in a paracrine manner culminating in enhanced bone resorption in muscular dystrophy (Guo et al. 2017). Inflammation and fibre damage in muscles immediately adjacent to bone provides a unique opportunity for inflammatory cytokines to come into contact with the bone

microenvironment and activate osteoclasts (Redlich and Smolen 2012). Histological evaluations of various muscles show that global lack of PAR_2 from mdx mice improves muscle damage and myositis (Taghavi 2016). Damaged muscle fibres express myostatin which promotes RANKL induced osteoclastogenesis *in vitro* (Dankbar et al. 2015). Moreover, use of myostatin inhibitors *in vivo* has been associated with reduced bone turnover and increased mass (Bialek et al. 2014). Inflammatory cells in muscle tissue such as T cells can also contribute to the expression of IL-6 and RANKL (Kong et al. 1999; Naka et al. 2002). Moreover, PAR_2 null mice had significantly lower levels of apparent mast cell degranulation in their skeletal muscles, which can release a range of inflammatory cytokines such as TNF-α and mast cell tryptase (Taghavi 2016).

In fact, another possible explanation for these findings arises from the perceived changes in the systemic biochemical profile of mdx mice following PAR_2 deletion. Recent findings have clearly shown that deletion of PAR_2 from the mdx mice is associated with a significant decrease in the serum IL-6 and RANKL levels and the RANKL/OPG ratio (Taghavi 2016). The association of PAR_2 with IL-6 is perhaps the key to understanding of the reported observations. It is likely that IL-6 from the inflamed muscles acts on the osteoblasts increasing the RANKL/OPG ratio which in turn results in an increased osteoclastogenesis and bone loss. Indeed, the serum level of CTX-1, a marker of bone resorption, was also significantly lower in PAR_2 null mdx than in wildtype mdx mice, indicating that bone resorption rates in mdx mice are higher in the presence of PAR_2 (Taghavi et al. 2017). Whether IL-6 is the only cytokine responsible is unclear; the possibility of other known and unknown proinflammatory factors at play cannot be ruled out at this time and requires further research.

Another piece of evidence suggestive of such osteoclast dependent rescue of bone mass in PAR_2 null mdx mice comes from the reduced porosity parameters in these mice. Cortical porosity is a measure of resorptive processes in bone and as such, lower pore number in KO mice points to the lower rates of bone resorption in these mice. This feature was also evident in the non-mdx PAR_2 null mice where Ct.Po, Po.V and Avg.Po.V were lower than normal. These findings are further supported by the finding that global PAR_2 null mice have lower osteoclast numbers (Georgy et al. 2012). This finding per se could indeed explain our observations of improved bone phenotype in mdx mice following deletion of

PAR_2. It might be that lower osteoclast numbers in PAR_2 null mice serve as a limiting factor rendering the heightened inflammatory cytokine levels in the mdx mice ineffective in reaching maximum possible bone resorption.

Despite the initially superior quality and quantity, the trabecular bone phenotype declined at a relatively faster rate in the PAR_2 null mdx mice (particularly males) to values no longer different from the wildtype mdx mice at 32 weeks (Figure 4.3). Although this may mean that given enough time, PAR_2 null mdx mice may eventually fall behind wildtypes, nevertheless, the differences between the two genotypes at 32 weeks shows superior values at least in the case of females. Whether or not the slope of changes would remain the same after the 32 week mark however, requires further long term experimentation and may not be simply deduced from this finding. The slower decline in trabecular parameters in wildtype mdx mice is likely to stem from the gradual improvement in the inflammatory signature of the muscle pathology in the wildtype mdx mice beyond 8 weeks of age (Porter et al. 2002; Apolinário et al. 2015). This could potentially ameliorate the impact of DMD on bone turnover, hence a slower more normal rate of bone loss. Subsequently, having lost its advantage, lack of PAR_2 may eventually result in an inferior bone phenotype similar to that of the non-mdx PAR_2 null mice. Indeed, the BV/TV values for male PAR_2 null mdx mice were similar to those of male non-mdx PAR_2 null mice at both time points examined, although no direct comparisons were made since the backgrounds of the two strains were not the same. DMD causes progressive weakness, loss of ambulation, restrictive respiratory disease, cardiomyopathy, osteopoenia and scoliosis in addition to other cognitive and educational deficits (Yiu and Kornberg 2015). Standard care for DMD patients has largely aimed at preservation of ambulation as long as possible. Historically, this has been mainly achieved via the use of corticosteroids due to their potent anti-inflammatory characteristics. Randomised clinical trials have shown that these agents slow the progression of the disease and onset of its fatal consequences (Matthews et al. 2016). Unfortunately however, prolonged use of corticosteroids is associated with severe side effects and worsening of the preexisting osteopoenia and osteoporosis which has been shown in both humans and mdx mice (Morgenroth et al. 2012; Novotny et al. 2012).

Attempts to find a substitute for these drugs has led to the development of a new category of agents that target the aetiology of the condition, i.e. dystrophin deficiency. Eteplirsen is

an example of such agents that has been recently approved by the FDA for use in the United States. The drug acts by inducing skipping of exon 51 in DMD pre-RNA, restoring the open reading frame and production of functional dystrophin. However, this is only possible in a fraction of patients (approximately 13%) who have amenable deletions in their exon 51 (Mendell et al. 2013; Mendell et al. 2016). *In vivo* genome editing tools such as the CRISPR-Cas9 system have also been recently described and successfully used in mdx mice (Nelson et al. 2016). Regardless, due to the fact that not all patients benefit equally from these methods, and whilst other agents are being developed, anti-inflammatory therapy will perhaps remain a viable option for the time being. In this respect, the fact that loss of PAR_2 improves not only muscle pathology (Taghavi 2016) but also bone phenotype even at such markedly late time points, supports the idea that PAR_2 antagonism may provide a better therapeutic option than corticosteroid treatment. As improving ambulation is one of the final goals of any DMD treatment, and because mdx mice also demonstrate clear ambulation deficits like the human patients, future inclusion of a six-minute ambulation assay and myoglobinuria testing as further endpoint measures would be beneficial in better assessing the efficacy of anti PAR_2 treatment and translatability of these findings (Kobayashi et al. 2012).

This study demonstrates that the global lack of PAR_2 is beneficial for the bone phenotype of mdx mice. Thus, in line with our hypothesis, it can be concluded that PAR_2 is a mediator of the impact of dystrophin deficiency and presumably muscle inflammation on murine bone. Whether or not the same could be said about the other inflammatory conditions, however, remains to be elucidated by further investigations. As mentioned earlier (section 3.3), due to the limitations of global knockout models, generation of cell type specific PAR_2 null mice is required to further delineate the underlying mechanisms. Nevertheless, given the present evidence, it seems likely that PAR_2 antagonists may be of value in the current treatment of patients with DMD.

CHAPTER 5: ROLE OF PAR_2 IN THE RECIPROCAL RELATIONSHIP BETWEEN OSTEOBLASTOGENESIS AND ADIPOGENESIS

5.1 Introduction and Aims

In the bone marrow milieu, MSCs give rise to both osteoblasts and adipocytes, as well as other lineages (Owen 1988; Minguell et al. 2001). This differentiation is said to be mutually exclusive such that one can predominate only at the expense of the other lineage (Bethel et al. 2013). Current evidence suggests that this process may contribute to the pathology of various bone conditions (Berendsen and Olsen 2014). For instance, the increase in the adiposity of bone marrow and gradual bone loss with ageing has been attributed to a decrease in osteogenesis in favour of adipogenesis (Kawai et al. 2009). Despite this, the phenomenon is still poorly understood and the role of many mediators and genes remain to be fully elucidated.

In determining MSCs' fate, various molecules interact and activate multiple signalling pathways. These converge on the lineage specific transcription factors, e.g. RUNX2 and PPARγ which results in the respective lineage specific phenotype (Berendsen and Olsen 2014). Being a G protein coupled receptor, activation of PAR_2 initiates several downstream signalling pathways, some of which may interact with lineage specific signals (see Figure 1.3). PAR_2 is expressed by osteoblasts both prenatally (Jenkins et al. 2000) and postnatally (Abraham et al. 2000) and its activation in calvarial cells induces the expression of collagen type I (Georgy et al. 2010). Additionally, PAR_2 null primary bone marrow cultures have significantly lower numbers of ALP positive colony forming units indicating the role of PAR_2 in the cellular niche and the osteogenic differentiation of marrow stromal cells (Georgy et al. 2012).

A recent study in the laboratory in which the current work was undertaken has shown that when PAR_2 null calvarial osteoblasts are treated with the highly osteogenic medium

conditioned by human prostate cancer cells (MDA-PCa-2b), they become more adipogenic than their wildtype controls (Kularathna 2015). These cultures express higher levels of *Pparγ* and *Lpl* and contain more Oil Red-O-positive cells. Consistently, knockout cells also partially lose their osteogenic abilities as demonstrated by reduced ALP activity and mineralisation as well as lower expression of osteoblastic markers *Runx2* and *Col1a1* (Kularathna 2015).

In light of these findings and based on the phenotype of global PAR_2 null mice, it was hypothesised that PAR_2 is involved in the regulation of MSC fate such that in its absence, adipogenesis is favoured over osteoblastogenesis. To test this hypothesis, PAR_2 was stably knocked down in a mesenchymal cell line model, i.e. Kusa 4b10 cells, using shRNA constructs delivered via a lentiviral transduction system and the resulting phenotype was evaluated. Kusa 4b10 is a bipotential murine bone marrow stromal cell line, capable of differentiating into both osteoblasts and adipocytes (Walker et al. 2008). The particular characteristic of this cell line is that unlike its parent cells (Kusa O cells), they appear to only differentiate into either osteoblasts or adipocytes in the corresponding cell type specific differentiation medium (Allan et al. 2003). In line with the goals of this study to establish an *in vitro* model for this purpose, this also made it possible to take advantage of an immortalised cell line avoiding the disadvantages associated with use of primary cultures, including, importantly, animal welfare considerations.

Next, RNA sequencing data generated by the preceding study on PAR_2 KO and WT calvarial osteoblasts were used to select a number of genes for further analyses (Kularathna 2015). The data were filtered and sorted in order to identify highly regulated genes (at least 2-fold up- or downregulation) following treatment with MDA-PCa-2b conditioned medium, which were also differentially expressed between treated cells of the two genotypes ($p < 0.001$). This was followed by a PubMed search of the literature for any evidence of previous association with adipogenesis and osteogenesis. Genes not previously associated with the reciprocal relationship between osteogenesis and adipogenesis were shortlisted for further analysis (Table C.1, Appendix C). Twenty-seven genes of interest (GOIs) selected this way were then organised in three categories as follows. Category 1 GOIs were those that were upregulated by MDA-PCa-2b-conditioned medium in WT but not KO cultures; only genes for which the endpoint expression levels

were significantly higher in WT than in KO cells were included. Category 2 GOIs were those that were downregulated in the KO but not WT cultures, and showed lower expression levels in KO than in WT cells following treatment with the conditioned medium. Category 3 GOIs included genes that were upregulated uniquely in the KO cells, and more highly expressed at the endpoint in the KO cultures. None of the genes downregulated in the wildtype group were selected for such analysis based on the criteria set. Following the knockdown of PAR_2 in Kusa 4b10 cells, the expression of these genes was measured using RT-qPCR and compared with that of vector control cells.

5.2 Results

5.2.1 Expression of PAR_2 by Kusa 4b10 Cells

Expression of PAR_2 mRNA by Kusa 4b10 cells was confirmed under both maintenance and differentiation conditions and at multiple time points (Figure 5.1). While some variations in *F2rl1* band intensity can be seen in Fig. 5.1, transcript levels were not quantitated. Results clearly demonstrated that PAR_2 was expressed by Kusa 4b10 cells under all conditions examined.

5.2.2 Expression of PAR_2 Activators and Spontaneous Protease Activity in Cultures of Kusa 4b10 Cells

5.2.2.1 Expression of PAR_2 activators

The expression of PAR_2 activators (or their activators, e.g. tissue factor) was also evaluated under maintenance and differentiation conditions. Reverse transcription PCR studies indicated that a variety of these factors are expressed by Kusa 4b10 cells, however, this varied based on the treatment and time point (examples shown in Figure 5.1). Under basic maintenance condition, Kusa 4b10 cells expressed tissue factor (*F3*), Factor VII, hepsin, kallikrein-4, -6 and -14, matriptase-2 and tryptase β2 (Table 5.1). Depending on time, cells treated with the adipogenic medium expressed tissue factor, Factor VII, hepsin, kallikrein-6 and -14 and matriptase 2 whereas under osteogenic condition, tryptase α/β1 and tryptase β2 were additionally expressed (Table 5.1). Of the 16 proteases investigated, acrosin, Factor X, granzyme A, Kallikrein-5, trypsin type I, epitheliasin and human

airway trypsin-like protease (HAT) were not expressed by Kusa 4b10 cells under any of the tested conditions at any of the time points.

5.2.2.2 Endogenous Protease Activity

On further examination of Kusa 4b10 cultures, media conditioned for 6 days under adipogenic and osteogenic treatments (see section 2.3.1) were tested for the presence of proteolytic activity using colorimetric assays as per sections 2.5.1 and 2.5.2. Trypsin-like amydolytic and kallikrein-like activities were positive in both cultures, but no statistically significant differences between adipogenic and osteogenic treatments were identified (Figure 5.2).

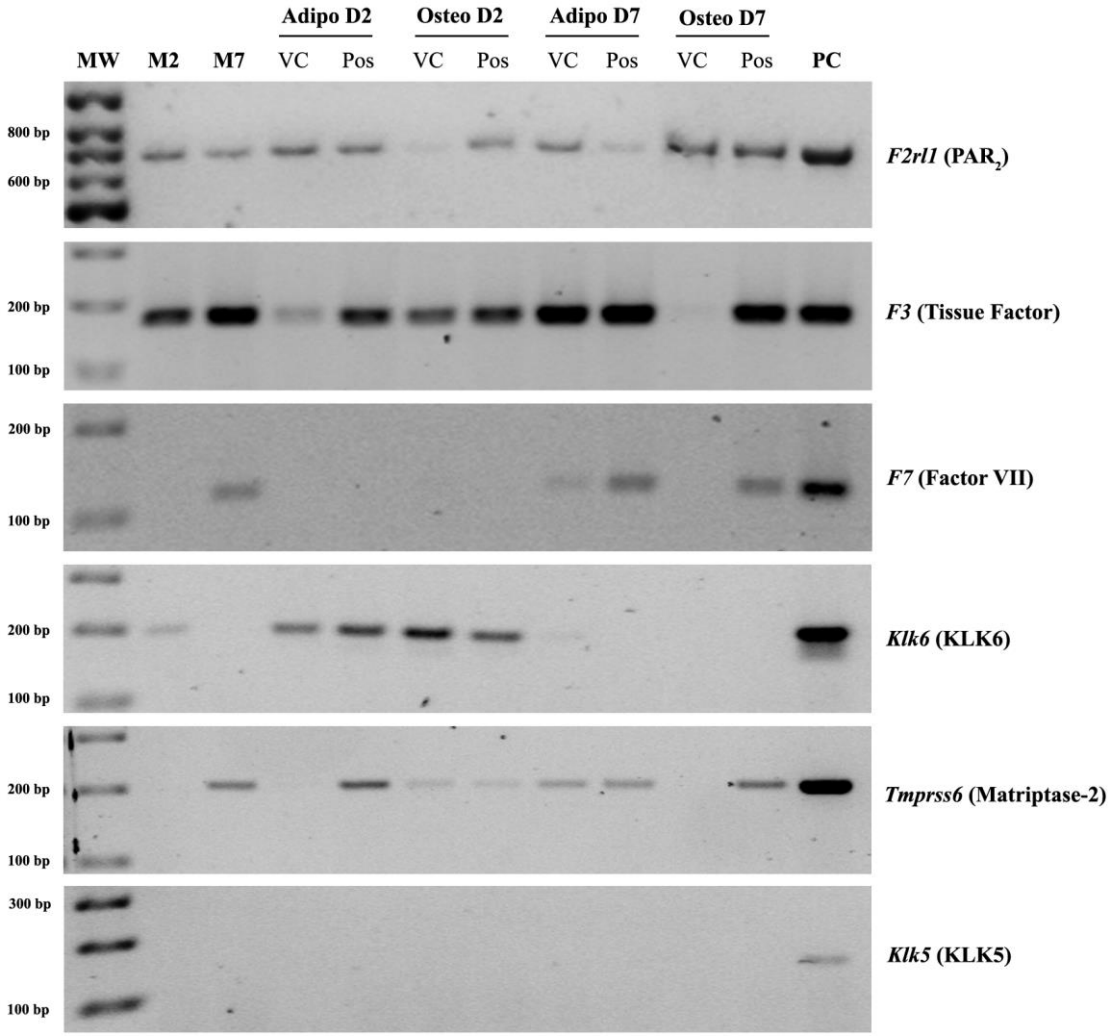


Figure 5.1 Expression of PAR_2 mRNA and some of its activators by Kusa 4b10 cells.

Cells were sampled at 2 and 7 days under maintenance (**M2** and **M7**) and both adipogenic (Adipo D2 and Adipo D7) and osteogenic (Osteo D2 and Osteo D7) conditions. Complementary DNA generated from extracted mRNA was investigated by PCR for the presence of PAR_2 activators. **MW** - molecular weight, **VC** - vehicle control medium, **Pos** - positive adipogenic/osteogenic medium, **PC** - positive control (see Table 5.1).

Table 5.1 Expression of PAR_2 activating proteases by Kusa 4b10 cells.

Complementary DNA from 3 biological replicates was investigated by PCR at 2 and 7 days. Where two or more samples are positive, a positive result is reported.

Protease	Positive Control	Maintenance		Adipogenic				Osteogenic			
		Day 2	Day 7	Day 2		Day 7		Day 2		Day 7	
				VC[1]	Pos[2]	VC	Pos	VC	Pos	VC	Pos
Acr	Testis	-	-	-	-	-	-	-	-	-	-
F3	Lung	+	+	+	+	+	+	+	+	-	+
F7	Liver	-	+	-	-	-	+	-	-	-	+
F10	Liver	-	-	-	-	-	-	-	-	-	-
Gzma	NK cell	-	-	-	-	-	-	-	-	-	-
Hpn	Pancreas	-	+	-	-	+	+	-	-	-	+
Klk4	Brain	-	+	-	-	-	-	-	-	-	-
Klk5	Stomach	-	-	-	-	-	-	-	-	-	-
Klk6	Brain	+	-	+	+	-	-	+	+	-	-
Klk14	Testis	+	+	+	+	-	-	-	-	-	+
Prss1	Pancreas	-	-	-	-	-	-	-	-	-	-
Tmprss6	Liver	-	+	-	+	+	+	+	+	-	+
Tmprss2	Lung	-	-	-	-	-	-	-	-	-	-
Tmprss11d	Testis	-	-	-	-	-	-	-	-	-	-
Tpsab1	Pancreas	-	-	-	-	-	-	-	-	+	-
Tpsb2	Lung	-	+	-	-	-	-	-	-	+	+

[1] **VC** - vehicle control medium

[2] **Pos** - positive differentiation medium

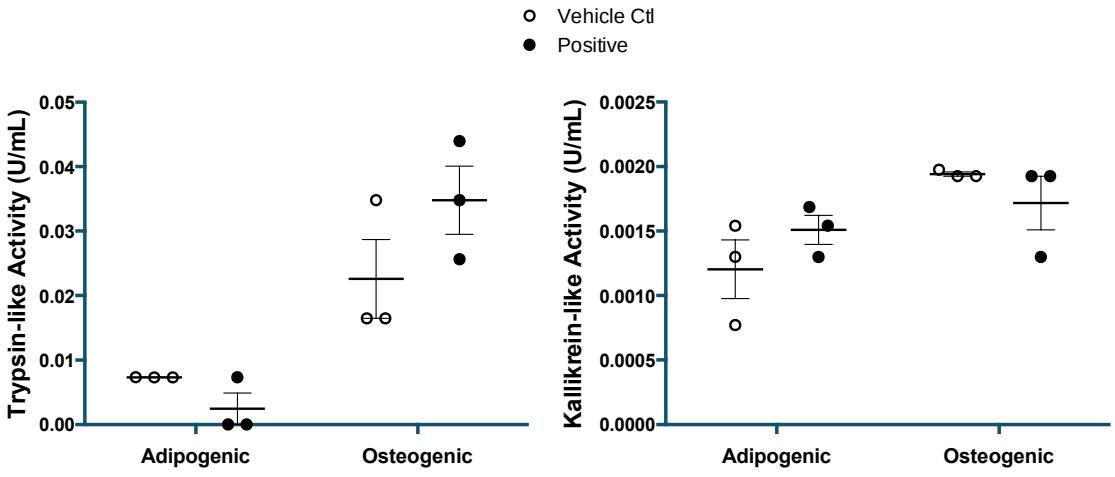


Figure 5.2 Trypsin-like and kallikrein-like activity in cultures of Kusa 4b10 cells.

Trypsin-like and kallikrein-like activities were detected under both adipogenic and osteogenic conditions on day 6. N = 3; Kruskal-Wallis test was used to compare adipogenic or osteogenic media with their corresponding vehicle controls, and adipogenic medium with osteogenic medium, and the two vehicle controls with each other ($p > 0.05$); error bars represent SEM.

5.2.3 Effects of PAR_2 Deficiency on Osteoblastogenesis and Adipogenesis

5.2.3.1 PAR_2 knockdown

To study the role of the receptor in the differentiation of Kusa 4b10 cells, PAR_2 expression was stably knocked down using lentiviral small hairpin RNA (shRNA) constructs as described under 2.5.3. Following an initial expansion, storage and testing, selected cultures were maintained for 21 days and subjected to total RNA extraction using the protocol described in section 2.2.3 followed by complementary DNA synthesis (section 2.2.6). Knockdown was then confirmed at both mRNA and protein levels using RT-qPCR (section 2.2.7) and intracellular calcium mobilization assay (section 2.3.4) respectively (Figure 5.3).

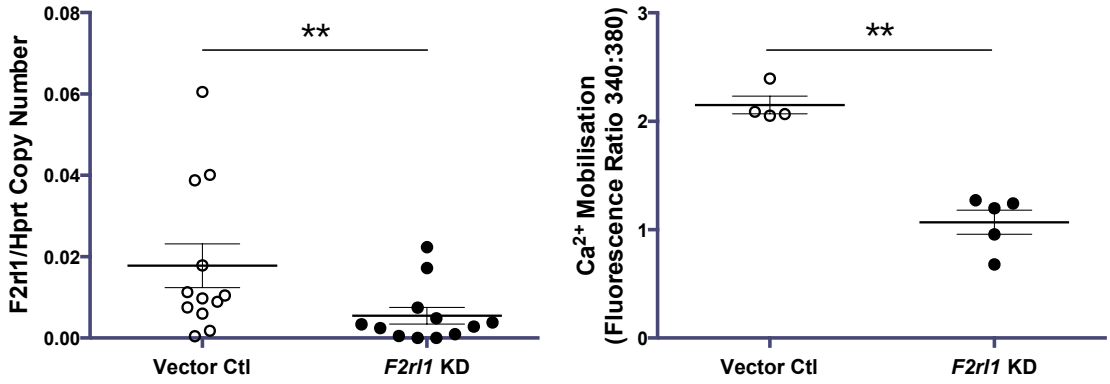


Figure 5.3 Confirmation of PAR_2 knockdown following shRNA lentiviral transduction.

Reverse transcription qPCR analysis as well as intracellular Ca^{2+} mobilisation in response to trypsin after knockdown of PAR_2 from Kusa 4b10 cells. Area under the curve is shown for Ca^{2+} mobilisation assay. **Vector Ctl** - vector control; ***F2rl1* KD** - PAR_2 knockdown. N = 12 (*F2rl1*/Hprt copy number); N = 4-5 (calcium mobilisation assay); ** $p \leq 0.01$. Data were analysed using Mann-Whitney U test; error bars represent SEM.

5.2.3.1 Adipogenesis in Cultures Under Osteogenic Conditions

Following the confirmation of knockdown, cells were placed under osteogenic conditions (see section 2.3.1) in 12-well plates and maintained for 7, 14, 17 and 21 days. Study groups consisted of the original Kusa 4b10 as well as the vector control and knockdown (*F2rl1* KD) cells. For each designated endpoint, a new batch of frozen cells was thawed,

expanded and subcultured. At the endpoints, adipogenesis was assessed by counting Oil Red-O positive cells following the protocol described in section 2.5.5 (Figures 5.4-5.6).

On conclusion, analysis showed that PAR_2 deficiency in Kusa 4b10 cells resulted in lower total cell counts (Tt.N) in days preceding day 21 and an increased adiposity at all time points evident by higher absolute adipocyte number (Ad.N) and Ad.N/Tt.N (Figures 5.5 and 5.6). Adipocyte area normalised to Tt.N (Ad.Ar/Tt.N) agreed with these observations except at 21 days.

Introduction of control lentiviral particles also appeared to lower the total number of cells at all time points and also slightly increase the adiposity of cultures at days 7, 14 and 21 (Figures 5.4, 5.5 and 5.6).

5.2.3.2 Mineralisation of Cultures Under Osteogenic Conditions

To assess mineralisation, parallel cultures were treated with osteogenic medium for similar time periods to those used for the evaluation of adipogenesis. Alizarin Red-S mineralisation assays were performed using the protocol described in section 2.5.4.

PAR_2 deficiency caused a significant reduction in the concentrations of Alizarin Red-S recovered from *F2rl1* KD cultures in comparison to vector control at all time points. A similar effect was also observed after normalisation of values to Tt.N (Alizarin Red-S/Tt.N), however not at 17 days (Figures 5.4, 5.5 and 5.6).

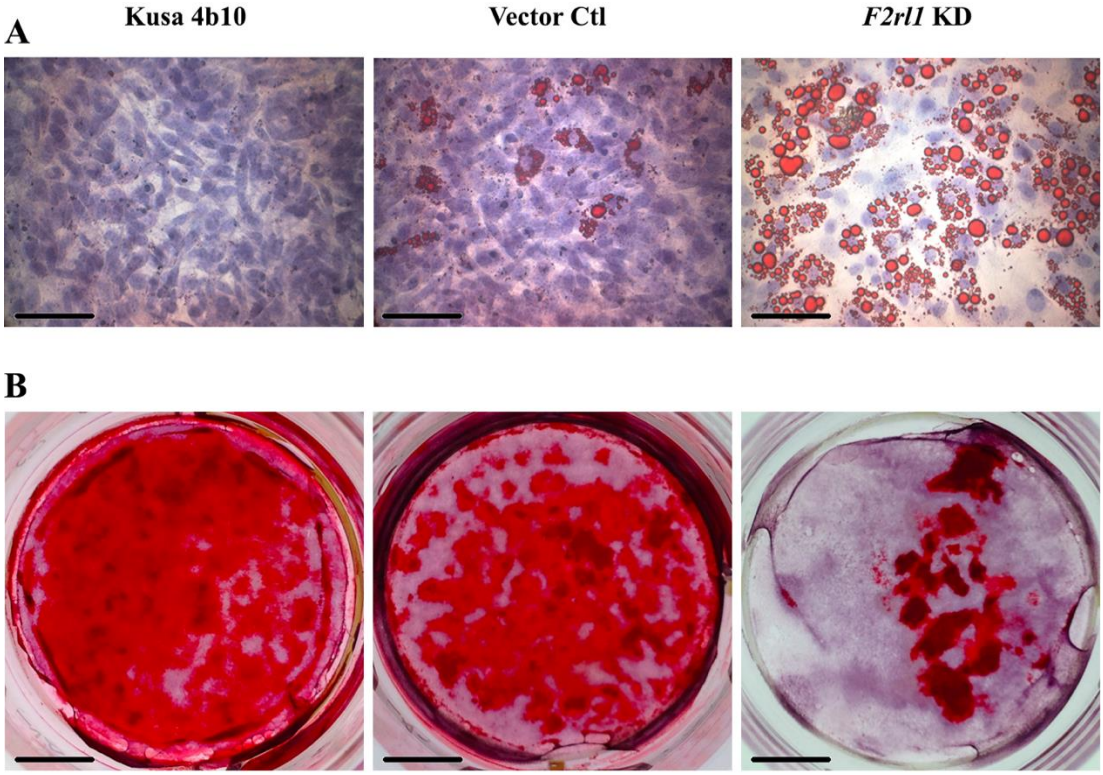


Figure 5.4 The extent of adipogenesis and mineralisation following PAR_2 knockdown.

Kusa 4b10, vector control (**Vector Ctl**) and PAR_2 knockdown (***F2rl1* KD**) cells treated with osteogenic medium. **A.** Oil Red-O and haematoxylin staining at day 14, scale bar = 100 μm; **B.** Alizarin Red-S staining at day 17; scale bar = 5 mm.

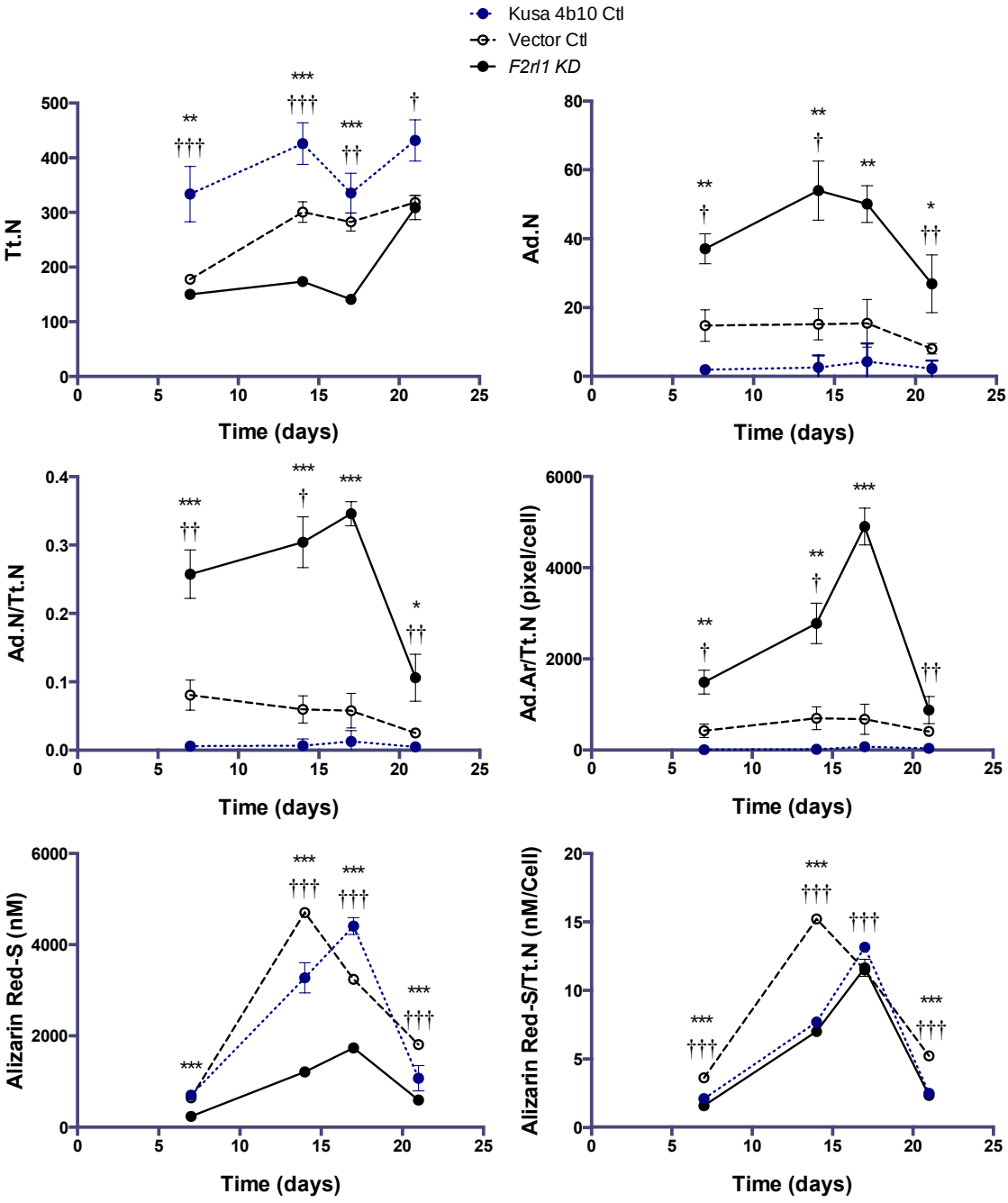


Figure 5.5 Effect of PAR_2 deficiency on differentiation of Kusa 4b10 cells - time course.

All cultures were treated with osteogenic medium. Following fixation, cultures were either stained with Oil Red-O and haematoxylin for cell counts or assayed with Alizarin Red-S for calcium content. **Vector Ctl** - vector control; ***F2rl1* KD** - PAR_2 knockdown; **Tt.N** - total number of cells; **Ad.N** - number of adipocytes; **Ad.Ar** - total adipocyte area; N = 8-12; * $p \leq 0.05$, ** $p \leq 0.01$, *** $p \leq 0.001$ depicts significant differences between the vector control and PAR_2 knockdown subclones; † $p \leq 0.05$, †† $p \leq 0.01$, ††† $p \leq 0.001$ depicts significant differences between the original Kusa 4b10 and vector control subclones. Data were analysed using one-way ANOVA preplanned (contrast) tests; the comparison between the two control groups was undertaken separately from the comparison between the vector control and *F2rl1* KD groups; error bars represent SEM.

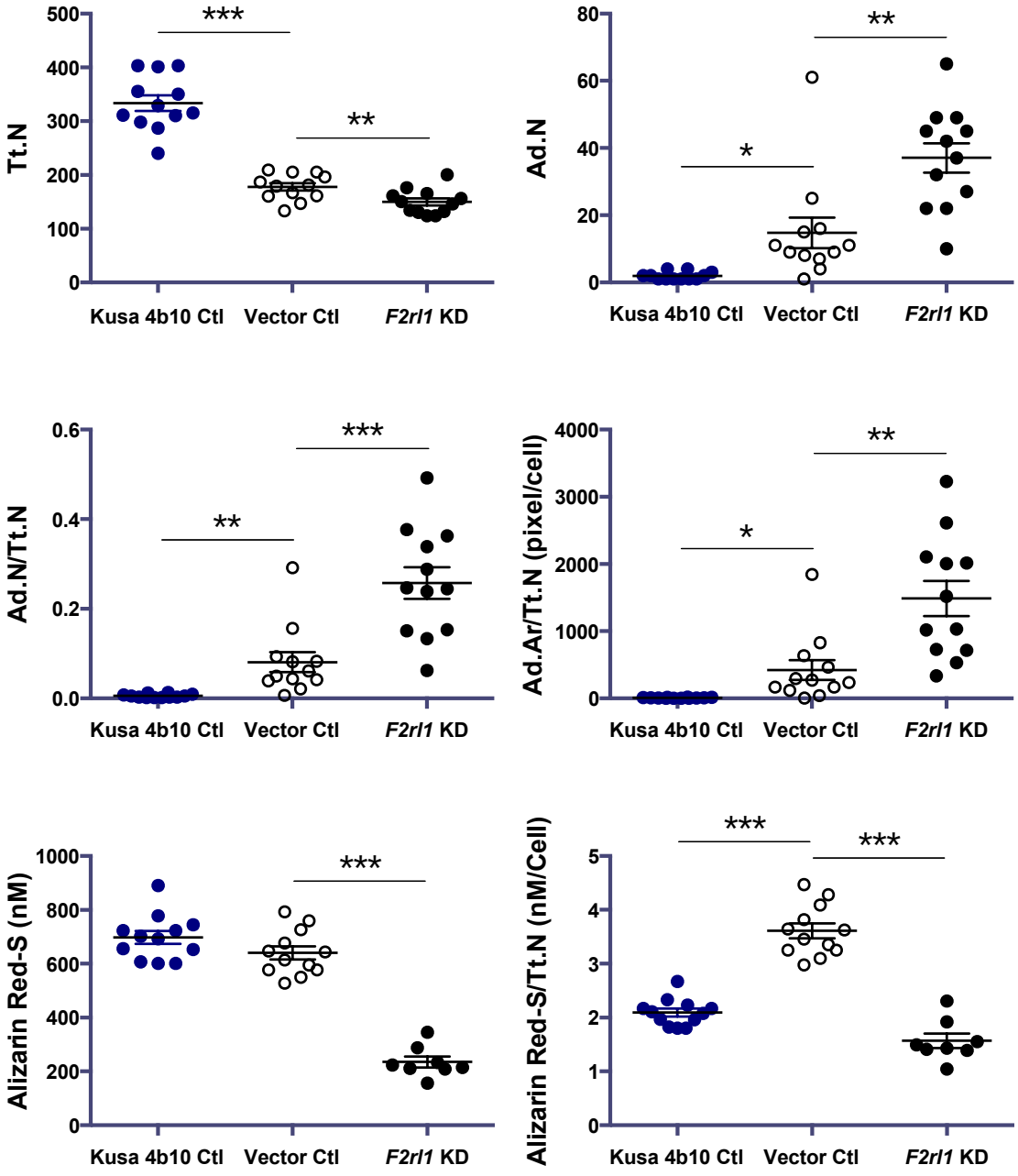


Figure 5.6 Effect of PAR_2 deficiency on differentiation of Kusa 4b10 cells at day 7.

All cultures were treated with osteogenic medium. **Vector Ctl** - vector control; ***F2rl1* KD** - PAR_2 knockdown; **Tt.N** - total number of cells; **Ad.N** - number of adipocytes; **Ad.Ar** - total adipocyte area; N = 8-12; * $p \leq 0.05$, ** $p \leq 0.01$, *** $p \leq 0.001$ using one-way ANOVA preplanned (contrast) tests; the comparison between the two control groups was undertaken separately from the comparison between the vector control and *F2rl1* KD groups; error bars represent SEM.

5.2.3.3 Effects of PAR_2 Deficiency on Expression of Differentiation-Associated Genes

Evaluation of cell lineage-associated genes across four relatively early time points also demonstrated that deficiency of PAR_2 in the Kusa 4b10 cells was associated with higher adipogenic and lower osteogenic characteristics (Figure 5.7). Using RT-qPCR, we found that *Pparg* expression was significantly higher in *F2rl1* KD cells during the first three time points at 0, 1 and 3 days. The values dropped between days 3 and 5, when no difference was observed. Levels of $Runx_2$ expression, on the other hand, appeared higher in the vector control cells only at 5 days. The relatively later adipogenic biomarker, lipoprotein lipase (*Lpl*) was minimally expressed until day 5, when its expression was significantly higher in the *F2rl1* KD group. *Col1a1* demonstrated some variability with values higher in *F2rl1* KD at day 1, lower at day 3 and not significantly different at day 5. Based on these results, day 5 was selected for further experimentation.

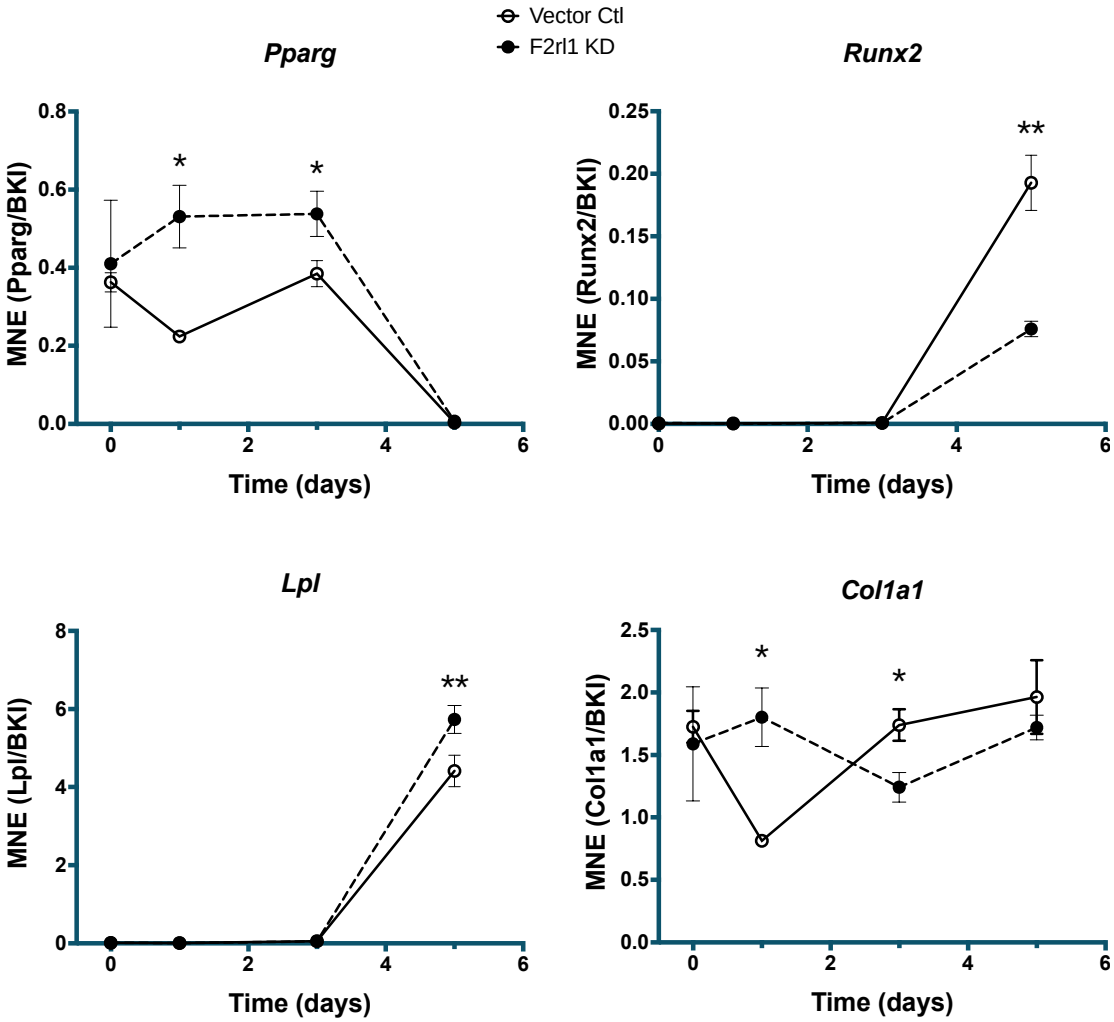


Figure 5.7 Effects of PAR2 deficiency on the expression of differentiation-associated genes.

In order to understand the phenotypical changes observed following PAR_2 knockdown, a number of differentiation-associated genes were examined from day 0 to day 5 in cells cultured in osteogenic medium. **Vector Ctl** - vector control; ***F2rl1* KD** - PAR_2 knockdown; **MNE** - mean normalised expression; N = 6; * $p \leq 0.05$, ** $p \leq 0.01$. Data were analysed using Mann-Whitney U test; error bars represent SEM.

5.2.4 Identification of Molecular Mediators of PAR_2 Action in Kusa 4b10 Cells

5.2.4.1 RT-qPCR Analysis of GOI Expression Under Osteogenic Conditions

Cultures were evaluated 5 days after the introduction of osteogenic medium or vehicle control.

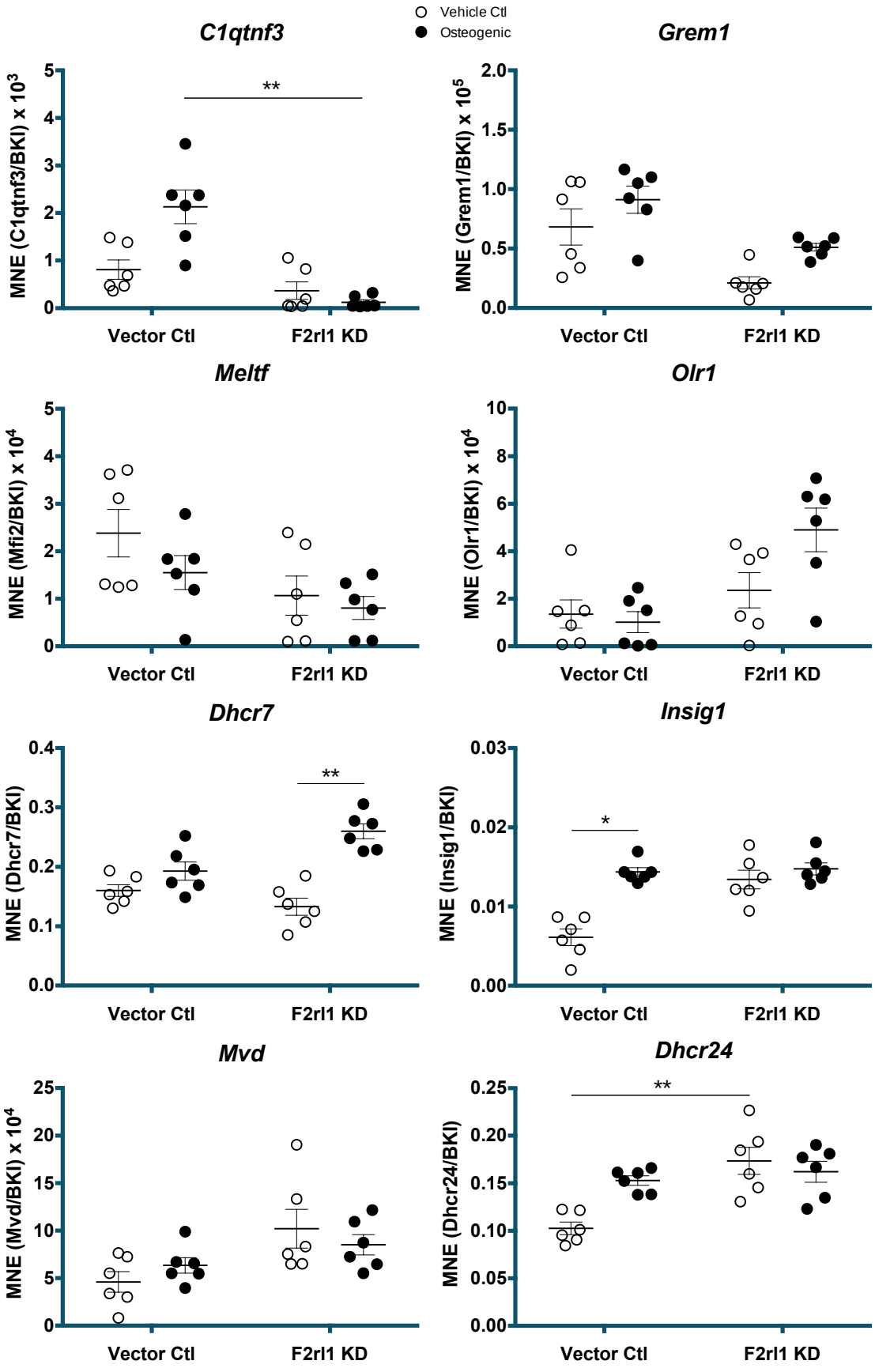
Out of 13 genes examined in category 1, only *C1qtnf3* was consistently expressed at higher levels in vector control than in *F2rl1* KD cells (Figure 5.8). *Arhgap22*, one of the GOIs originally found to be upregulated in the WT osteoblasts was completely undetectable in all groups using the methods described.

In category 2 GOIs, 6 genes were evaluated out of which *Snorc* and *Gpr35* were found to be consistently lower in expression in the PAR_2 deficient cultures (Figure 5.9).

The category 3 GOIs included 8 genes that had previously been found to be more highly expressed in the PAR_2 null calvarial osteoblastic cultures. Here, *Cnr1*, *Il6*, *Ramp3* and *Enpep* demonstrated higher levels of expression in response to PAR_2 deficiency (Figure 5.10).

Of the rest of the GOIs examined, some showed no differential expression between vector control and *F2rl1* KD cells, while others showed differential expression in the opposite direction to that predicted on the basis of the earlier RNA sequencing study (Figures 5.8-10).

From the list of GOIs that were differentially expressed following PAR_2 knockdown, *Il6* was selected for further examination. This was accomplished by ELISA investigation of IL-6 levels in the media obtained from vector control and *F2rl1* KD cultures at various time points, and by investigation of the effect on these cultures of treatment with anti-IL-6 neutralising antibody.



Cont'd over page..

Cont'd Figure 5.8..

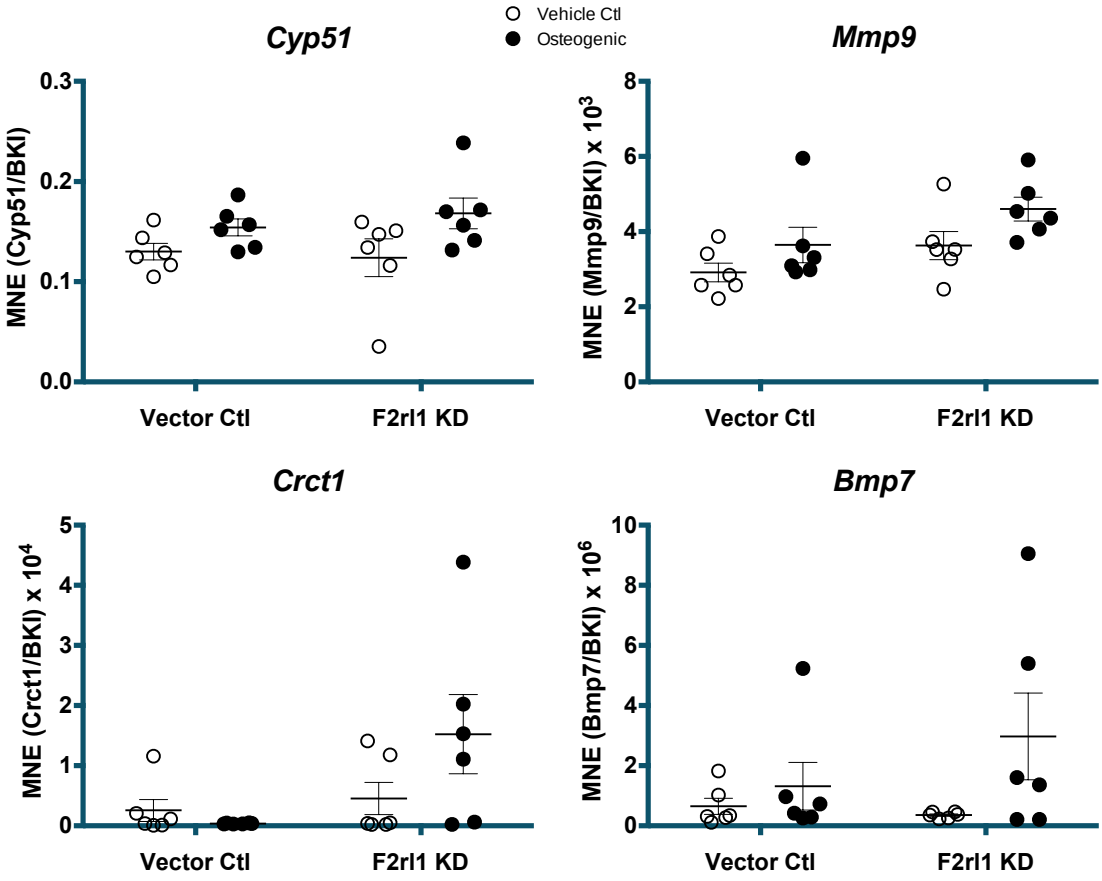


Figure 5.8 RT-qPCR analysis of the category 1 GOIs.

Arhgap22 is not presented as it was not detectable in any of the groups. **Vector Ctl** - vector control; ***F2rl1* KD** - PAR_2 knockdown; **MNE** - mean normalised expression. N = 6; * $p \leq 0.05$, ** $p \leq 0.01$. Data were analysed using Kruskal-Wallis test; error bars represent SEM.

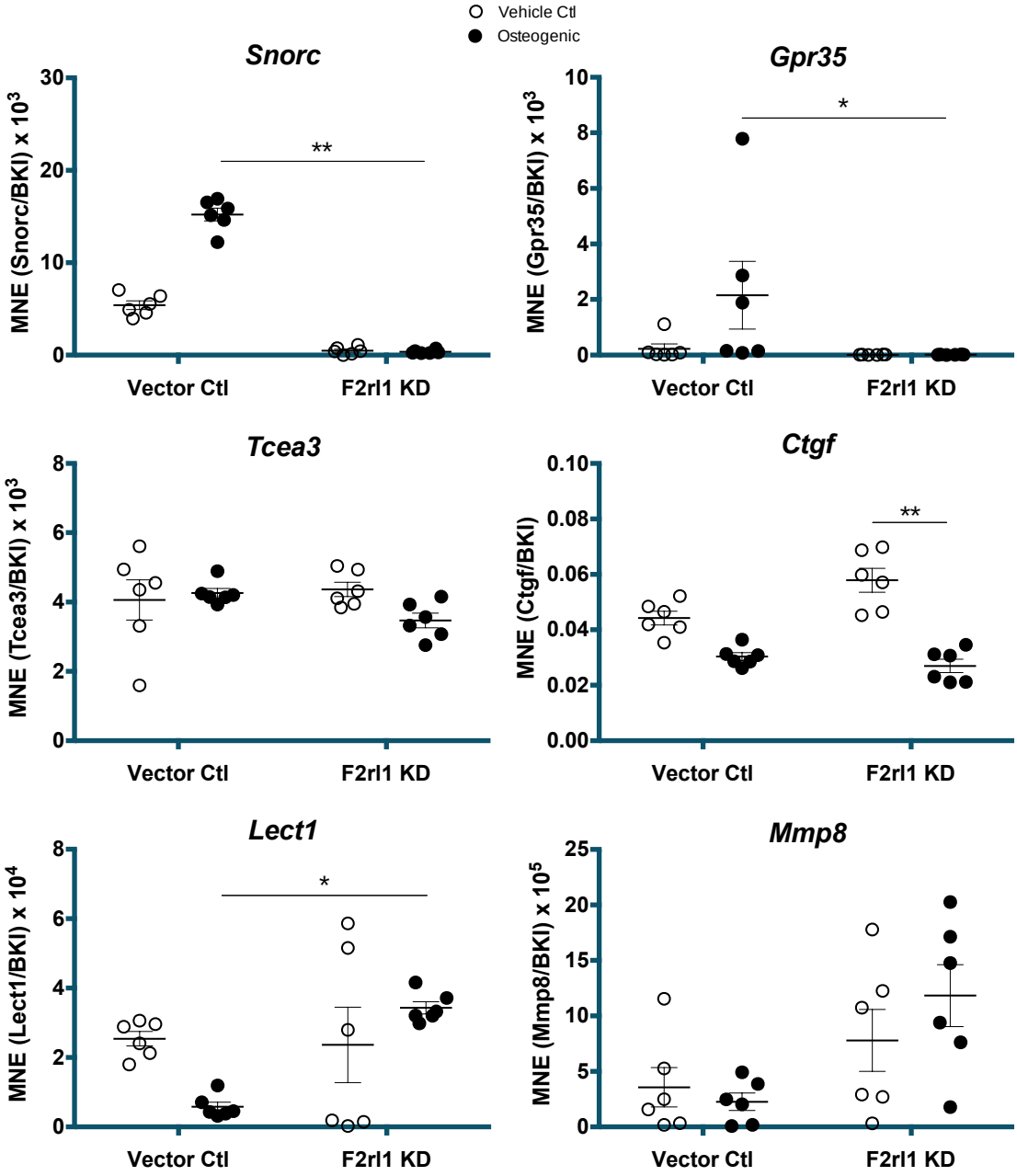


Figure 5.9 RT-qPCR analysis of the category 2 GOIs.

These are genes that were previously reported to be downregulated in the KO osteoblasts and have lower final expression levels. N = 6; * $p \leq 0.05$, ** $p \leq 0.01$. Data were analysed using Kruskal-Wallis test; error bars represent SEM.

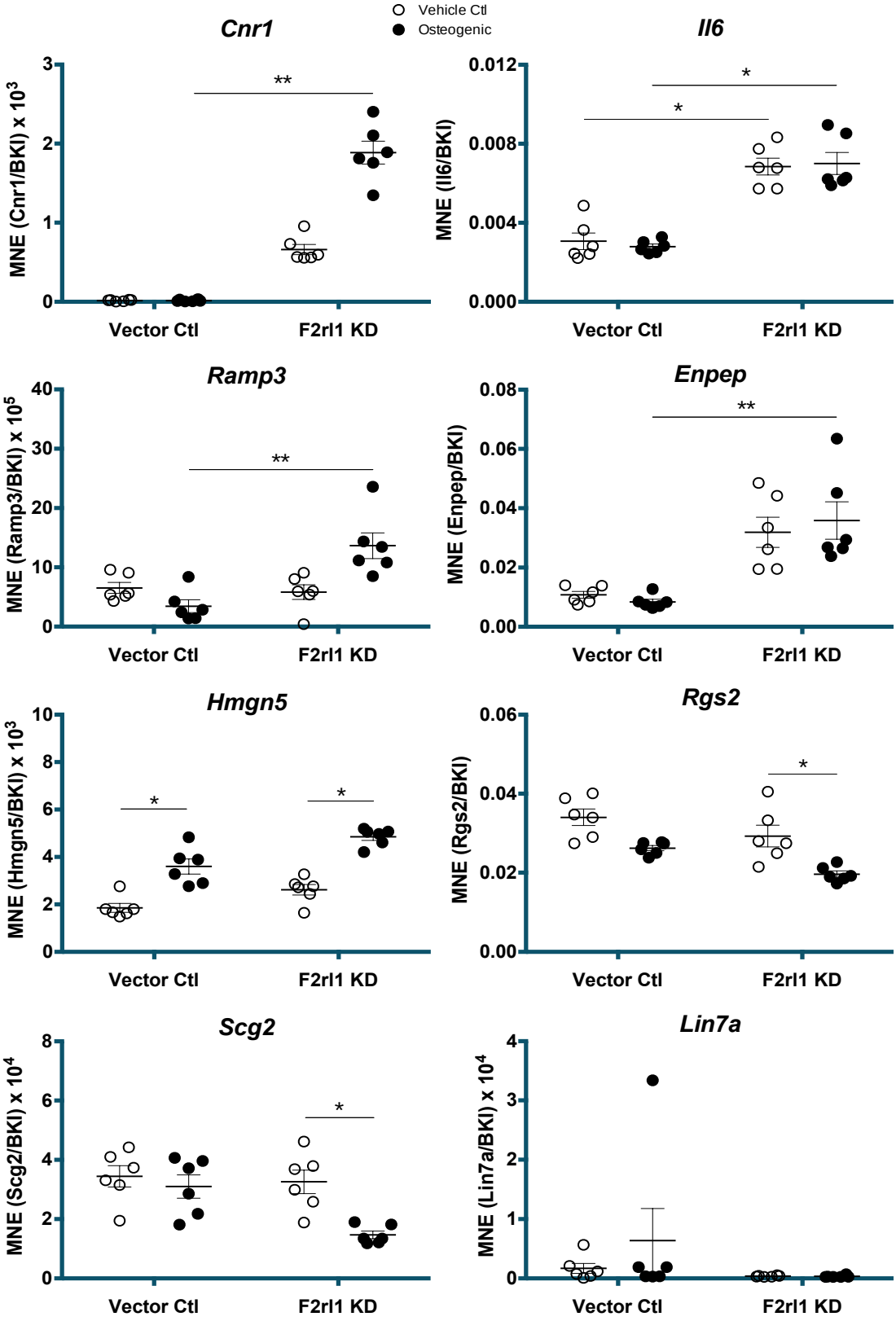


Figure 5.10 RT-qPCR analysis of the category 3 GOIs.

These are genes that were previously reported to have a higher expression in KO osteoblasts. N = 6; * $p \leq 0.05$, ** $p \leq 0.01$. Data were analysed using Kruskal-Wallis test; error bars represent SEM.

5.2.4.2 Interleukin-6 ELISA

Media were collected every 24 hours from days 1-7 from vector control and *F2rl1* KD cells cultured in osteogenic medium, and IL-6 levels determined using the method described in section 2.5.6. These experiments indicated that IL-6 was always found at significantly higher concentrations in the *F2rl1* KD cultures throughout the whole culture period (Figure 5.11). The magnitude of this difference was found to be greatest during the first three time points. Change of medium at day 3 resulted in significant reduction of IL-6 concentrations in both cultures, however, values remained higher in the *F2rl1* KD conditioned medium.

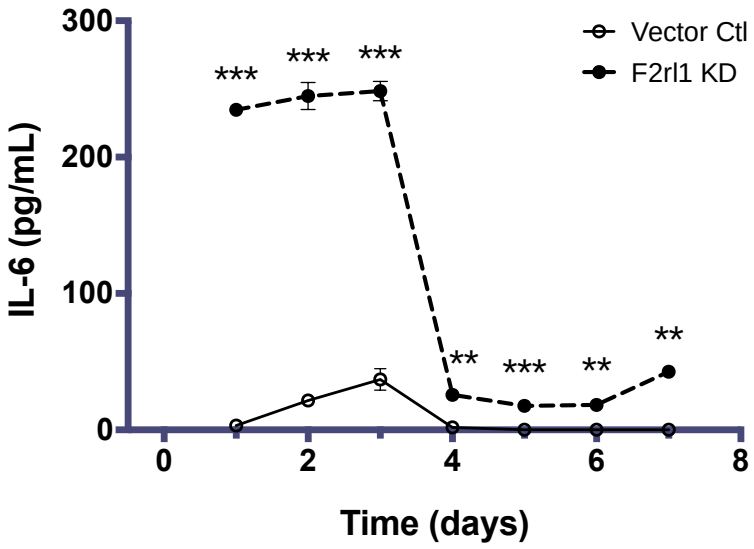


Figure 5.11 ELISA investigation of IL-6 in vector control and *F2rl1* KD cultures.

ELISA measurement of IL-6 concentrations in the media at days 1 to 7 under osteogenic conditions. The sharp decrease is caused by a change of medium on day 3 after which point concentrations appear to gradually rise again despite the second change on day 6. N = 3; ** $p \leq 0.01$, *** $p \leq 0.001$. Data were analysed using Mann-Whitney U test; error bars represent SEM.

5.2.4.3 Interleukin-6 Neutralisation

Use of anti-IL-6 antibody in the osteogenic medium (see section 2.5.7) resulted in partial reversal of the effects of PAR_2 deficiency in Kusa 4b10 cells. This involved a significant reduction in adipocyte numbers to values that were no longer statistically different to

untreated and antibody treated vector control cultures (Figure 5.12). Moreover, mineralisation in both *F2rl1* KD and vector control cultures also appeared to respond to the presence of anti-IL-6 antibody in the medium resulting in significantly greater values. However, the difference in mineralisation between the antibody treated *F2rl1* KD and the untreated vector control cells remained highly significant (Figure 5.12). Tt.N did not show any changes following the use of antibody (data not shown).

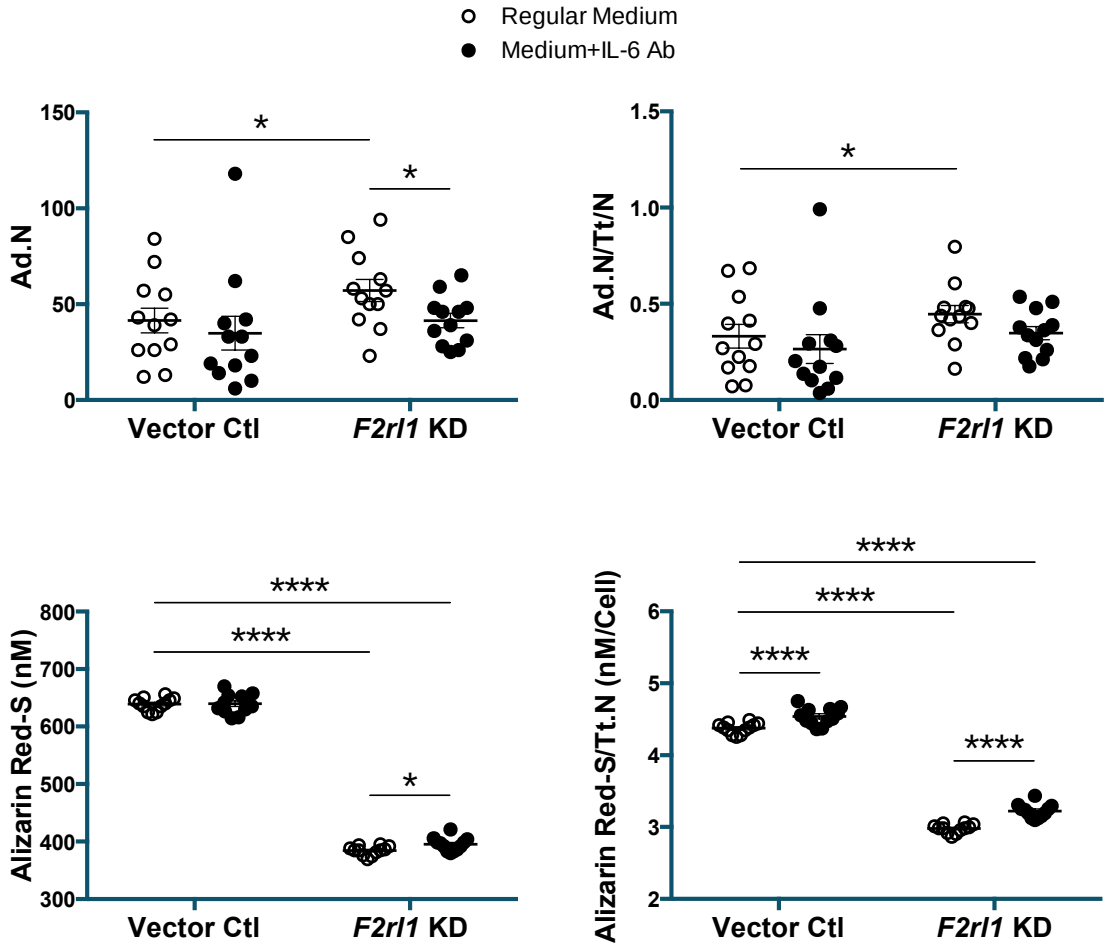


Figure 5.12 Effect of Anti IL-6 antibody on the differentiation of Kusa 4b10 cells.

Cells were grown for 7 days under osteogenic conditions in the presence of anti IL-6 antibody (17.2 ng/mL). N = 12; * $p \leq 0.05$, **** $p \leq 0.0001$. Data were analysed using One-way ANOVA preplanned (contrast) test; error bars represent SEM.

5.3 Discussion

Data from past *in vivo* experiments (Georgy et al. 2012) as well as those described in the previous chapters suggest that PAR_2 may be involved in the differentiation or function of osteoblasts. In a recent *in vitro* model, when treated with conditioned media obtained from prostatic cancer cells, PAR_2 null primary osteoblasts started accumulating intracytosolic fat droplets and acquired adipocytic features (Kularathna 2015). Corresponding changes in alkaline phosphatase activity, matrix mineralisation and expression of various differentiation-associated genes clearly supported these observations pointing towards a role for the receptor in the relationship between the two cellular niches.

In view of these findings, the current study was undertaken to test the hypothesis that PAR_2 has a role in the reciprocal relationship between the osteogenic and adipogenic lineages, stimulating the former at the expense of the latter. To address this hypothesis, Kusa 4b10 cells, a murine bone marrow mesenchymal stem cell line able to differentiate into either lineage was used (Allan et al. 2003). Characterisation of the phenotype of the cells treated with an osteogenic medium, following the knockdown of PAR_2, supported the suggestion that PAR_2 plays a role in the coordination of adipogenesis and osteoblastogenesis. The effect also appeared to be partly dependent on IL-6 related mechanisms.

Before the start of the experiments, it was first confirmed that PAR_2 was indeed expressed by the Kusa 4b10 cells. It was also shown that various direct and indirect activators of PAR_2 are transcriptionally expressed by the Kusa 4b10 cells at least up to day 7 and under various culture conditions. The proteolytic activity of two groups of these activators (trypsin-like and kallikrein-like activity) was consistently demonstrated to be present in the conditioned media as well. Expression of PAR_2 by primary bone marrow stromal cells has been demonstrated before (Georgy et al. 2012). Presence of PAR_2 activating proteases has also been previously demonstrated in the bone marrow (Georgy et al. 2012). Overall, these findings render the experimental setting of this chapter relevant to the *in vivo* conditions and confirm the appropriateness of Kusa 4b10 cell line for the intended studies. To study the role of the receptor in the differentiation of Kusa 4b10 cells, PAR_2 was stably knocked down using a lentiviral transduction system. For efficient silencing of PAR_2 in

Kusa 4b10 cells, all 5 available shRNA variants were simultaneously used. This assured that in the event of an shRNA having a lower efficacy than the rest, PAR_2 would still be sufficiently knocked down (Taxman et al. 2010). Gene knockdown of PAR_2 was assessed by both mRNA expression and functional studies, i.e. RT-qPCR and Ca^{2+} mobilization assay. To ensure that PAR_2 knockdown was stable and that expression of the integrated shRNAs would not be inactivated during the experiments, the assessments were performed following an initial clonal expansion and banking in addition to a period of maintenance in culture for up to 21 days after thawing. This corresponded to the longest period cultures would be grown during the following trials.

The sole choice of osteogenic conditions for the purpose of this study stemmed from the observations that PAR_2 null calvarial cells undergo adipogenesis when treated with the highly osteogenic medium conditioned by MDA-PCa-2b cells (Kularathna 2015). The fact that *F2rl1* KD cells formed adipocytes when treated with an osteogenic medium signifies that the mechanism involved in PAR_2's suppression of adipogenesis of MSCs requires a trigger that normally leads to their differentiation into osteoblasts. It has been noted that some degree of plasticity still exists following the initial stages of differentiation. For instance, osteoblasts derived from human trabecular bone fragments can differentiate into adipocytes in the presence of adequate hormonal stimuli (Nöth et al. 2002). In this regard, the study model used is directly in line with the goals of this investigation.

This adipogenic conversion of *F2rl1* KD cells cultured under osteogenic conditions is also significant because the adipogenic induction of most clonal MSCs requires strict culture conditions. Measurement of differentiation specific genes also showed significantly higher *Pparg* and lower *Runx2* levels in *F2rl1* KD cultures than those of the vector control cells (Figure 5.7). Although a potential off-target effect triggered by the lentiviral transduction itself could have affected the cells, as suggested by a slightly more adipose nature of vector control cells than the original Kusa 4b10 cells (Figure 5.5), the most relevant comparisons are those drawn between the vector control and *F2rl1* KD cells.

Additionally, the simultaneous inhibition of osteogenesis in the *F2rl1* KD cultures underpins the mutual exclusiveness of adipo/osteogenesis and further supports the notion

that PAR_2 is crucial in the process. Measurement of molecular markers of osteoblastogenesis demonstrated lower expression of *Runx2* in *F2rl1* KD cells at day 5 (Figure 5.7). *Runx2* is a crucial transcription factor of the osteoblast specific genes and its presence is a strong indicator of osteoblastic differentiation (Komori 2017). *Col1a1*, another biomarker of osteoblastogenesis, however showed some variability and was transiently more highly expressed in *F2rl1* KD cells at day 1, before reversal of this situation by day 3 (Figure 5.7).

The finding that *F2rl1* KD cultures have lower total cell numbers (Tt.N) is another interesting finding that initially appears to contrast with those reported in previous studies. In a series of experiments using trypsin, gingipain-R and PAR_2 APs, Abraham *et al*. reported that activation of PAR_2 did not cause any measurable effect on the proliferation rate of primary rat osteoblasts assessed by thymidine incorporation (Abraham et al. 2000). Similarly, when murine PAR_2 wildtype and knockout calvarial cells were treated with PAR_2-activator-rich prostate cancer conditioned media, no difference in cell proliferation was observed between the genotypes (Kularathna 2015). Yet in another study, the authors reported a more rapid increase in the number of PAR_2 null osteoblasts which they explained in the context of a decreased rate of apoptosis rather than increased proliferation (Georgy et al. 2010). During early adipogenesis, proliferating preadipocytes must first permanently lose their ability to undergo mitosis before entering the final stage of differentiation (Pairault and Green 1979; Sugihara et al. 1988; Rosen and MacDougald 2006). In this regard, the contrasting finding observed in the current model may be explained by either a higher adiposity of *F2rl1* KD cultures and therefore earlier cessation of proliferation or a direct effect of PAR_2 deficiency on restricting the rate of proliferation and hence more adiposity. Nevertheless, the fact that cell numbers in *F2rl1* KD cultures still increase from day 17 to 20 tends to contradict such interpretations. On the other hand, it is worthwhile to note that direct comparisons between the mesenchymal cells described in the current model and those of the osteoblasts reported previously may be inappropriate due to the physiological differences between the two cell types. Additionally, as suggested before by Georgy *et al.* (2010), there still exists a possibility that PAR_2 affects the final cell numbers by its role in cell survival and inhibition of apoptosis. Any further clarification in this regard, therefore, requires investigation of such possibilities.

To evaluate the PAR_2 related downstream mediators of the observed phenotype, the transcriptional levels of a number of genes previously associated with the complete lack of PAR_2 in calvarial osteoblasts (Kularathna 2015) was investigated. Due to the greater difference in the observed Runx2 mRNA levels at day 5, this time point was selected for such analyses. A total of 27 genes selected were then evaluated in three categories based on their expression patterns following treatment with media conditioned by human prostate cancer cells (in the previous study). Not all these genes were similarly regulated in the Kusa 4b10 cells and therefore, emphasis was placed on those that were consistently regulated across the two studies.

In the category 1 GOIs, *C1qtnf3* was the only one that in the osteogenic medium was higher in expression in the vector control cells than in *F2rl1* KD cells consistent with the observations in the WT and PAR_2 KO osteoblasts reported by the preceding study. In category 2, in osteogenic medium the expression of *Snorc* and *Gpr35* was found to be lower in the *F2rl1* KD cells than in vector control cells consistent with values observed in PAR_2 KO osteoblasts relative to WT osteoblasts. These category 1 and 2 GOIs had a common feature in that they both had higher final values in the WT osteoblasts and vector control cells than the PAR_2 KO or *F2rl1* KD cultures respectively. This could simply mean that the effect of PAR_2 in promoting osteoblastogenesis is through stimulating the expression of these genes. In category 3, in osteogenic medium, *Cnr1*, *Il6*, *Ramp3* and *Enpep* were found to be more highly expressed in the more adipose *F2rl1* KD cultures than in vector control cells similar to PAR_2 KO compared with WT calvarial cells. This suggests that not only is the effect of PAR_2 on osteogenesis dependent on its ability to promote expression of some genes, but also on its ability to inhibit adipogenesis by suppressing a number of other GOIs. Overall, these findings suggest a role for these GOIs in the regulation of adipo/osteogenic differentiation of MSCs as well as mediating the effect of PAR_2 in the process.

Due to the availability of commercial reagents and neutralising antibodies, amongst all other GOIs, *Il6* was selected for further investigations. ELISA showed that IL-6 concentrations in the conditioned media obtained from *F2rl1* KD and vector control cultures followed the same pattern as the transcriptome, being higher after knockdown.

The major increase in IL-6 occurred within the first 24 hours following the initial change to osteogenic medium. The fact that PAR_2 deficiency causes an increased expression of IL-6 in Kusa 4b10 cells contrasts with several studies on the role of the receptor in inflammation. Multiple studies on various cell types have shown that activation of PAR_2 can induce the expression of various cytokines including IL-6. As examples, treatment of endothelial cells by the PAR_2 activator, matriptase, induces *Il6* expression and protein release (Seitz et al., 2006). Similar results have also been reported in endometrial stromal cells (Hirota et al., 2005; Saito et al., 2011) and nasal epithelial cells (Shi et al., 2010). Another study, however, using primary murine bone marrow cultures treated with osteoclastogenesis-promoting factors, showed that the expression of IL-6 is significantly decreased following the use of PAR_2 activating peptide, which is in keeping with the current finding (Smith et al. 2004). Based on these results, it seems that in Kusa 4b10 mesenchymal cells, PAR_2 deficiency causes a surge in IL-6 expression and secretion into the medium where it potentially stimulates adipogenic differentiation.

This view is further supported by the observation that use of anti-IL-6 antibody in the medium partly abolishes the difference between the two subclones by suppressing adipogenesis in the *F2rl1* KD subclone and stimulating mineralisation in both knockdown and control cultures. This finding suggests that IL-6 stimulates the adipogenic conversion of MSCs and inhibits osteoblastogenesis or osteoblastic function when released from suppression by PAR_2. A number of studies have been undertaken on the role of the IL-6 family of cytokines in bone formation (Sims 2016). Global deletion of IL-6 in mice causes no apparent structural abnormalities (Poli et al. 1994) and conveys resilience to the adverse effects of high fat diet on trabecular bone (Wang et al. 2016a). However, *in vitro* experiments show that osteoblasts express IL-6 receptor subunits and respond to its presence in the medium by increasing ALP activity (Bellido et al., 1997; 1996). Similar findings are also reported when adipose-derived stem cells are treated with IL-6 and its soluble receptor (Fukuyo et al. 2014; Bastidas-Coral and Bakker 2016). In contrast, a recent work showed that IL-6 and its soluble receptor inhibit the osteoblastic differentiation of murine calvarial cells by suppressing the expression of osteoblast specific genes, e.g. *Runx2* and *Osx* and ALP activity in a dose dependent manner (Kaneshiro et al. 2014) which is consistent with the current finding and those of the *in vivo* observations (Wang et al. 2016a). It seems likely that these contradictory results are

driven by the physiological context in which the experiments are performed, e.g. use of the receptor subunit or marrow versus adipose stem cells or calvarial osteoblasts.

It is possible that the IL-6 released into the medium, as reported here, will exert some paracrine action on the neighboring cells as bone marrow MSCs are known to express functional IL-6 receptors (Tondreau et al. 2009). Although other IL-6 class cytokines are known to suppress adipogenesis and promote osteogenesis which has also been shown in Kusa 4b10 cells (Walker et al. 2008; Poulton et al. 2012; Sato et al. 2014), specific data on the role of IL-6 itself in the process is elusive. Treatment of subcutaneous preadipocytes from insulin sensitive obese individuals with exogenous IL-6 *in vitro*, reduces their adipogenic capacity to levels comparable to insulin resistant obese patients who happen to exhibit elevated IL-6 plasma levels as well (Almuraikhy et al. 2016). Moreover, in 3T3-L1 preadipocytes, exogenous IL-6 inhibits adipogenic differentiation (Xie et al. 2010). It has also been noted that under physiologic conditions, IL-6 null primary osteoblasts express higher levels of both *Runx2* and *Pparg* than WT osteoblasts (Wang et al. 2016a). These finding are, however, different to those reported by the current study where IL-6 seemed to be linked with higher culture adiposity and lower osteogenic capacity after PAR_2 knockdown. Because IL-6 could potentially induce the signal transducer and activator of transcription 3 (STAT3; Niemand et al. 2003), and because in preadipocytes (3T3-L1), STAT3 regulates adipogenesis through regulation of PPARγ and C/EBPβ (Wang et al. 2010; Zhang et al. 2011), it is possible for the IL-6-STAT3 signal to be responsible for the current observation. This, however, remains to be determined by further investigations.

These results demonstrate that PAR_2 is required for the normal differentiation of osteoblasts and suppression of adipogenesis in murine mesenchymal stem cells. The findings indicate that PAR_2 promotes osteoblastogenesis by stimulating the expression of *C1qtnf3*, *Snorc* and *Gpr35* whilst inhibiting the differentiation of adipocytes by suppressing *Cnr1*, *Il6*, *Ramp3* and *Enpep*. These genes are therefore suggested as novel putative regulators of the reciprocal relationship between the adipogenic and osteogenic differentiation of MSCs. This study also indicates that these genes are novel PAR_2 regulated genes. Further experiments using anti-IL-6 antibody clarified that IL-6 is required for maximal adipogenic differentiation and suppression of osteoblastogenesis of

F2rl1 KD Kusa 4b10 cells. In this regard, a potential caveat of this study was the lack of an IgG matched control group to confirm these results were in fact caused by IL-6 neutralisaiton and not the presence of the IgG in the medium. Future experiments are required to include this control group to confirm these results. Due to the time constraints, amongst all putative regulators identified, only IL-6 was further examined by this study. Confirmation of the role of those other regulators in the process of adipogenic-osteogenic differentiation of MSCs, however, remains to be further investigated in the future.

CHAPTER 6: EFFECT OF OSTEOBLAST-SPECIFIC ABLATION OF PAR_2 GENE ON MURINE BONE PHENOTYPE

6.1 Introduction and Aims

In chapter 3, it was shown that the global PAR_2 null mice undergo a significant phenotypic transformation during ageing; turning from the high bone mass phenotype, as previously reported (Georgy et al. 2012), to one that is clearly inferior to that of the wildtype mice. Due to the global expression of PAR_2 and its multiple roles in different cell types within bone as well as multiple body systems, it is likely that a part of the phenotype developed by the global PAR_2 null mice would be due to local and systemic processes that are initiated in other tissues and affect bone indirectly. Therefore, use of a cell type specific knockout model is advantageous in that it allows for a more precise delineation of the role of the receptor in that particular cell type.

Previously, histomorphometry of samples from 7 week old PAR_2 null mice demonstrated that both osteoblastic and osteoclastic features were impacted by the lack of the receptor (Georgy et al. 2012). These observations in addition to those described in chapter 5, led to the hypothesis that lack of PAR_2 from pre-osteoblasts is perhaps responsible for the phenotypic changes observed in global PAR_2 null mice as a result of a cell fate shift towards adipogenesis. To test this hypothesis, wildtype mice expressing *Cre* under the *Osx* promoter (*Osx-Cre.F2rl1*$^{wt/wt}$) were compared with *Cre* expressing mice in which PAR_2 had been floxed (*Osx-Cre.F2rl1*$^{\Delta/\Delta}$). Non-*Osx-Cre* wildtype (*F2rl1*$^{wt/wt}$) and floxed (*F2rl1*$^{fl/fl}$) mice were also separately evaluated to control for the potential confounding effects of the LoxP sequences; the results pertaining to these mice are presented first in this chapter. In order for the results to be directly relevant to those of the original work on the global PAR_2 null mice, similar ages were examined here, with comparisons made at 7 and 13 weeks (50 and 90 days respectively).

Accordingly, micro CT images from the proximal tibial metaphyseal and the midshaft diaphyseal regions of interest (ROIs) were acquired and analysed for all four genotypes. The cortical shells of the metaphyseal ROIs as well as the bone marrow in both ROIs were additionally analysed and presented. Static histomorphometry of the trabecular bone was also carried out and complemented by dynamic histomorphometry of calcein labels as described in section 2.4.3.

6.2 Results

6.2.1 Phenotype of *F2rl1*$^{wt/wt}$ and *F2rl1*$^{fl/fl}$

6.2.1.1 Body Weight and Bone Length

Whilst otherwise normal, the presence of the targeted allele sites caused an increase in body weight and tibial lengths of the male mice which was evident at 13 weeks. Females at both time points and males of the earlier time point were unaffected (Figure 6.1).

Linear regression analysis indicated that all groups were still growing with an average bone length increase of 5.9% in males and 5.4% in females (Figure 6.1). Body weights also increased during this time. Analysis of regression coefficients, however, did not reveal any differences between the genotypes.

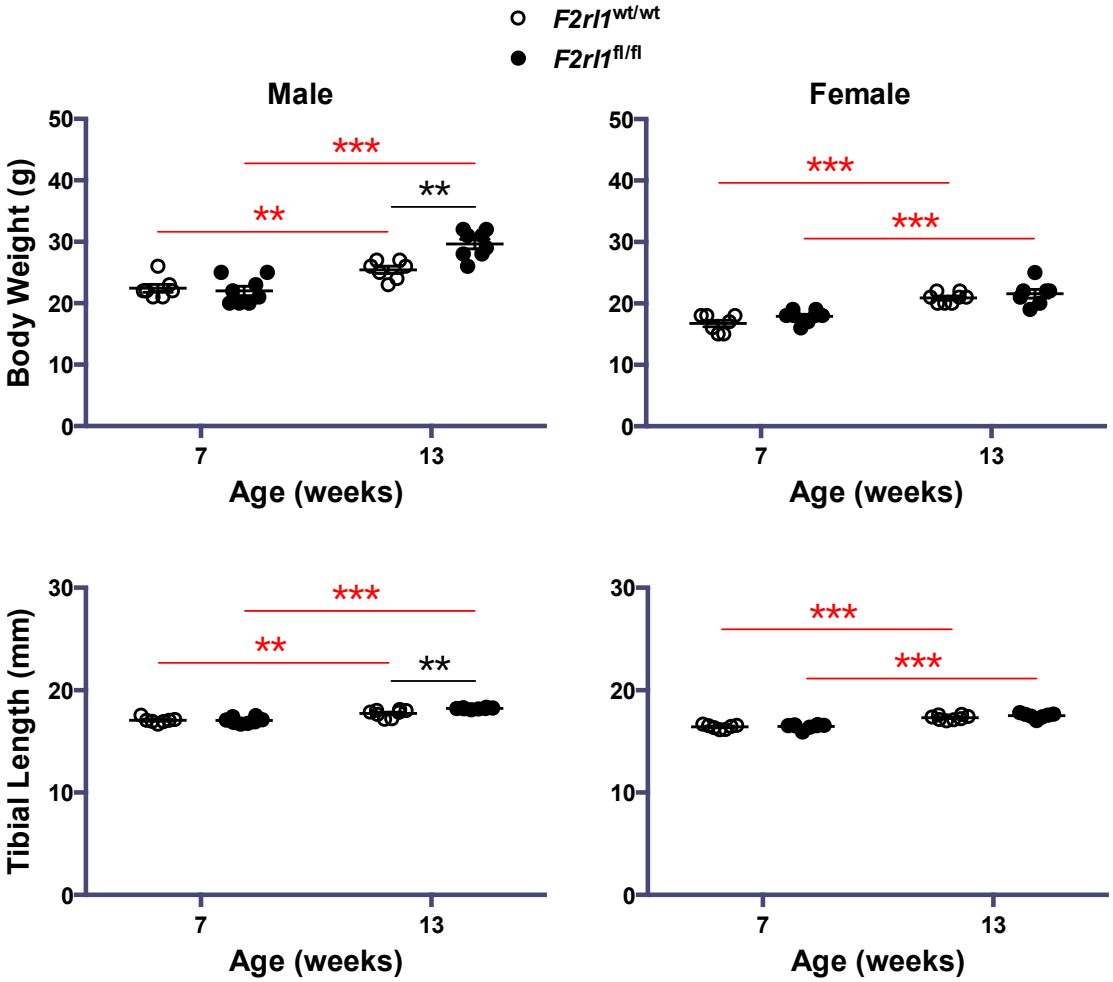


Figure 6.1 Body weight and tibial length in *F2rl1*$^{wt/wt}$ and *F2rl1*$^{fl/fl}$ mice.

Bone lengths were measured at the time of the micro CT scans using the scout views. N = 7-8; ** $p < 0.01$ using two tailed independent samples t-test; ** $p < 0.01$, *** $p < 0.001$, using simple linear regression indicating significant time related changes in sex-genotype controlled groups; error bars represent SEM.

6.2.1.2 Tibial Metaphyseal Trabecular Bone

The total volume of the metaphyseal trabecular compartment (TV) evaluated by micro CT ranged from 1.27 to 2.49 mm^3 in males and 1.00 to 1.78 mm^3 in females (Tables D.5 and D.6, Appendix D). Assessment of the trabecular bone showed that at 7 weeks, male *F2rl1*$^{fl/fl}$ mice had higher DA values than the *F2rl1*$^{wt/wt}$ group. Females of the 7 week age group demonstrated a comparatively higher BMD than the wildtype controls (Figure 6.2; Table 6.1).

At 13 weeks, males of the *F2rl1*$^{fl/fl}$ mice had a significantly higher mass profile than the *F2rl1*$^{wt/wt}$ mice with all BV, BV/TV, Tb.N and Tb.Sp different to those of the wildtype genotype. The measurements appear similar between the genotypes in the 13 week old females (Table 6.1).

Analysis of regression coefficients of changes from 7 to 13 weeks indicated a higher rate of gain in BV and BV/TV with corresponding significant changes in Conn.D and Tb.N. in the male *F2rl1*$^{fl/fl}$ mice than in the wildtype counterparts (Table 6.2).

In histology, a total tissue area (T.Ar) of 0.65 to 1.57 mm^2 in males and 0.58 to 1.45 mm^2 in females was evaluated. The bone perimeter (B.Pm) measured ranged from 4.35 to 12.48 mm in males and 1.86 to 10.89 in females. At 7 weeks, male *F2rl1*$^{fl/fl}$ mice had lower osteoid area (O.Ar/T.Ar) and osteoid perimeter (O.pm/B.Pm) than *F2rl1*$^{wt/wt}$ mice. Seven week old female *F2rl1*$^{fl/fl}$ mice, on the other hand, demonstrated higher bone area fraction (B.Ar/T.Ar) and B.Pm/T.Ar than the wildtype mice (Table 6.3).

At 13 weeks, male *F2rl1*$^{fl/fl}$ mice possessed a relatively higher number of osteoblasts (N.Ob/B.Pm) and osteoblast perimeter (Ob.pm/B.Pm) whilst females maintained their higher B.Pm/T.Ar relative to controls (Table 6.3).

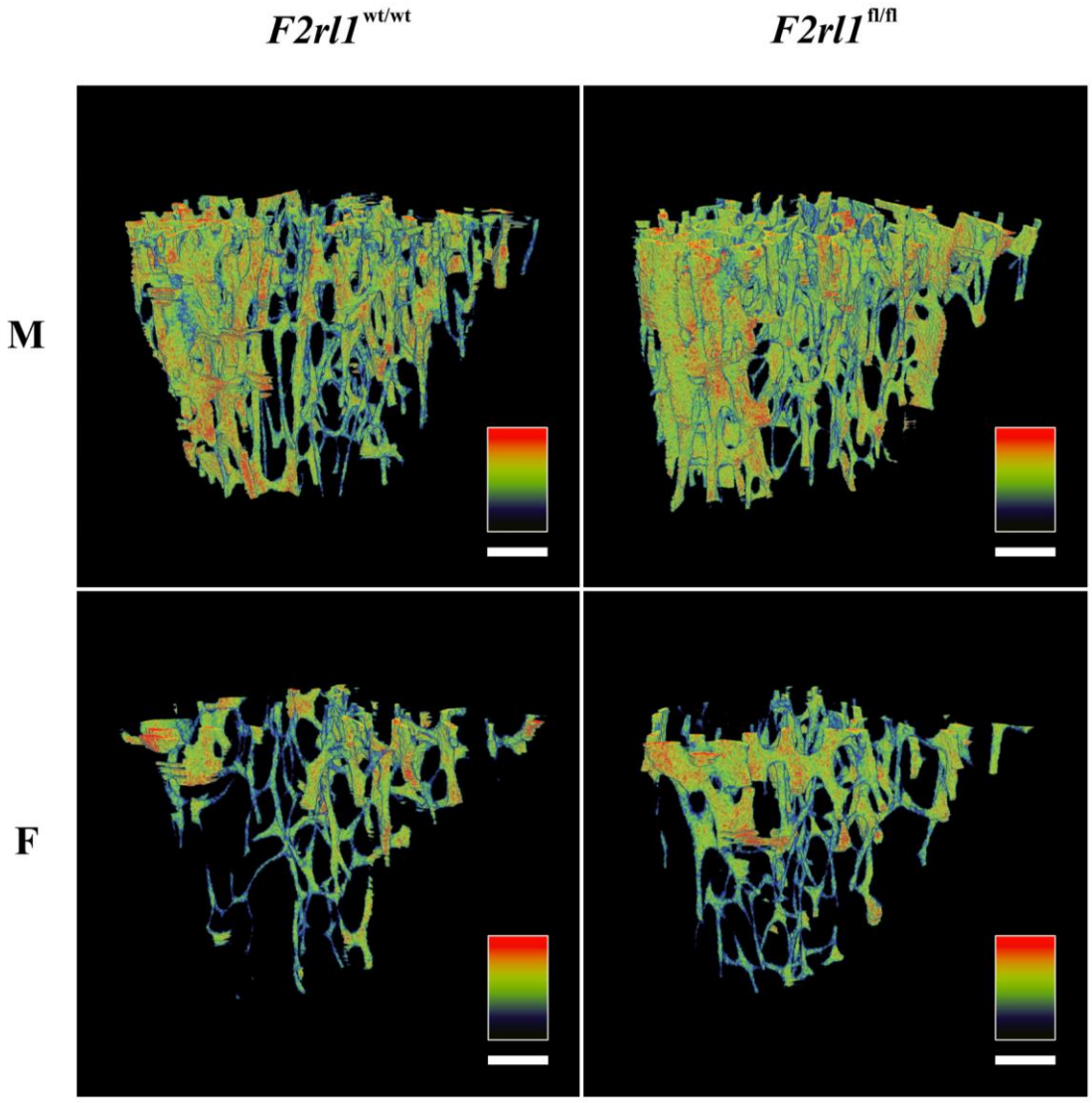


Figure 6.2 3D models of the metaphyseal trabecular bone in *F2rl1*$^{wt/wt}$ and *F2rl1*$^{fl/fl}$ mice.

Representative micro CT images at 13 weeks of age, lateral view; bar represents 200 μm; heat bar represents increasing opacity from black to red (may be used to estimate mineralisation within each figure - different figures are not to be compared).

Table 6.1 Metaphyseal trabecular indices determined by micro CT - *F2rl1*$^{wt/wt}$ and *F2rl1*$^{fl/fl}$ mice.

The difference in micro CT indices between the *F2rl1*$^{wt/wt}$ and *F2rl1*$^{fl/fl}$ mice (Mean diff) is presented as a percentage relative to the control *F2rl1*$^{wt/wt}$. N = 7-8; significant differences are highlighted.

	Male						Female					
	7 wk			13 wk			7 wk			13 wk		
	Mean diff (%)	SE $_{diff}$ (%)	*p*-value[1]	Mean diff (%)	SE $_{diff}$ (%)	*p*-value	Mean diff (%)	SE $_{diff}$ (%)	*p*-value	Mean diff (%)	SE $_{diff}$ (%)	*p*-value
TV	-0.48	7.32	0.536	1.65	6.02	0.798	0.18	6.22	0.955	-3.38	5.94	0.463
BV	-20.96	15.65	0.281	31.21	15.28	0.021	10.47	9	0.232	12.16	20.49	0.189
BV/TV	-22.53	16.24	0.232	29.13	13.11	0.049	11.19	9.32	0.189	19.15	16.83	0.121
Conn.D	-29.6	18.68	0.189	22.16	20	0.279	13.31	15.26	0.463	14.4	18.16	0.336
Tb.N	-11.36	14.71	0.613	31.66	11.87	0.015	10.52	8.84	0.189	21.61	14.87	0.121
Tb.Th	-11.66	5.22	0.072	-2.37	4.77	0.721	0.63	3.04	0.779	-0.44	3.59	1.000
Tb.Sp	2.99	10.32	0.867	-12.33	4.73	0.021	-8.48	5.32	0.152	-9.89	5.26	0.121
DA	19.84	7.88	0.021	-1.39	8.28	0.959	12.08	6.77	0.336	-4.94	5.45	0.694
SMI	-7.01	3.62	0.054	-4.22	4.55	0.382	-3.35	2.08	0.232	-1.96	1.35	0.152
BMD	-21.61	16.29	0.152	22.64	16.28	0.161	64.59	17.3	0.006	21.23	27.74	0.397
TMD	-3.95	6.44	0.694	-2.8	5.67	0.798	9.43	5.85	0.189	-0.38	5.14	0.649

[1] Two tailed Mann-Whitney U test

Table 6.2 Time related change in the metaphyseal trabecular bone assessed by micro CT - *F2rl1*$^{wt/wt}$ and *F2rl1*$^{fl/fl}$ mice.

Regression coefficients of time related changes in bone structural and material indices of *F2rl1*$^{wt/wt}$ and *F2rl1*$^{fl/fl}$ mice are presented. Significant differences between the genotypes are highlighted.

	M			F		
Index	**B_{wt}[1]**	**B_{fl}[2]**	**p-value[3]**	**B_{wt}**	**B_{fl}**	**p-value**
TV	-0.030	-0.024	0.814	-0.059***	-0.066***	0.709
BV	-0.001	0.014**	0.016	-0.006**	-0.007***	0.821
BV/TV	0.058	0.918**	0.011	-0.250	0.221*	0.845
Conn.D	-21.100	26.183	0.043	-16.926*	-18.745*	0.865
Tb.N	-0.011	0.170**	0.021	-0.089*	-0.076**	0.736
Tb.Th	4.8 x10^{-4}	0.001***	0.182	2.9x10^{-4}	2.3x10^{-4}	0.817
Tb.Sp	-0.001	-0.006*	0.169	0.002	0.002	0.793
DA	0.013	-0.036*	0.064	0.005	-0.035*	0.056
SMI	-0.018	-0.005	0.580	0.016**	0.021*	0.592
BMD	1.943	9.065**	0.053	-0.093	-2.449*	0.178
TMD	5.099	6.387	0.901	11.463	0.917	0.225

[1] Regression coefficient (slope) of changes over time in *F2rl1*$^{wt/wt}$ mice; a negative value depicts negative changes.
[2] Regression coefficient (slope) of changes over time in the *F2rl1*$^{fl/fl}$ mice.
[*] $p < 0.05$, [**] $p < 0.01$, [***] $p < 0.001$ when values were regressed over time in each sex-genotype category indicating significant changes from 7 to 13 weeks.
[3] Regression coefficients were compared using a second multiple linear regression analysis.

Table 6.3 Trabecular histomorphometric indices - *F2rl1*$^{wt/wt}$ and *F2rl1*$^{fl/fl}$ mice.

Both static and dynamic histomorphometric parameters of the *F2rl1*$^{wt/wt}$ and *F2rl1*$^{fl/fl}$ mice are presented (mean ± SEM). N = 4-6.

	Male						Female					
	7 wk			13 wk			7 wk			13 wk		
	F2rl1$^{wt/wt}$	*F2rl1*$^{fl/fl}$	*p*[1]	*F2rl1*$^{wt/wt}$	*F2rl1*$^{fl/fl}$	*p*	*F2rl1*$^{wt/wt}$	*F2rl1*$^{fl/fl}$	*p*	*F2rl1*$^{wt/wt}$	*F2rl1*$^{fl/fl}$	*p*
B.Ar/T.Ar	11.5 ± 1.98	12.1 ± 2.62	NS	21.1 ± 3.54	13.8 ± 1.55	NS	6.65 ± 1.07	12.4 ± 0.56	**	3.19 ± 0.5	8.31 ± 1.62	NS
B.Pm/T.Ar	6.45 ± 0.71	6.92 ± 0.95	NS	9.73 ± 0.85	7.67 ± 0.31	NS	4.17 ± 0.48	6.89 ± 0.37	**	2.51 ± 0.35	4.84 ± 0.64	*
O.Ar/B.Ar	1.29 ± 0.23	0.34 ± 0.04	*	0.19 ± 0.09	0.81 ± 0.33	NS	2.51 ± 0.81	1.88 ± 0.49	NS	2.11 ± 1.07	1.51 ± 0.53	NS
O.Pm/B.Pm	7.22 ± 0.95	1.99 ± 0.08	*	1.82 ± 0.83	5.09 ± 2.06	NS	12.1 ± 3.83	10.3 ± 2.28	NS	9.82 ± 4.2	9.08 ± 2.83	NS
O.Th	3.15 ± 0.43	2.79 ± 0.26	NS	2.05 ± 0.37	2.69 ± 0.72	NS	2.94 ± 0.13	3.23 ± 0.28	NS	2.24 ± 0.4	2.33 ± 0.28	NS
Ob.Pm/B.Pm	2.51 ± 1.19	0.41 ± 0.15	NS	0.25 ± 0.08	1.68 ± 0.31	**	3.28 ± 1.53	6.7 ± 1.97	NS	4.91 ± 3.24	3.37 ± 1.94	NS
N.Ob/B.Pm	1.91 ± 0.82	0.3 ± 0.11	NS	0.27 ± 0.09	1.61 ± 0.51	*	2.61 ± 1.14	6.33 ± 1.77	NS	3.37 ± 2.2	2.76 ± 1.65	NS
Oc.Pm/B.Pm	0.43 ± 0.13	0.17 ± 0.12	NS	0.36 ± 0.11	1.39 ± 0.67	NS	0.38 ± 0.17	1.49 ± 0.41	NS	1.46 ± 0.95	1.04 ± 0.51	NS
N.Oc/T.Ar	1.26 ± 0.42	0.57 ± 0.36	NS	2.14 ± 0.83	3.71 ± 1.82	NS	0.78 ± 0.31	3.9 ± 1.08	NS	1.31 ± 0.84	1.57 ± 0.78	NS
Ad.Ar/Ma.Ar	1.05 ± 0.81	0.23 ± 0.13	NS	0.03 ± 0.03	0.31 ± 0.22	NS	0.43 ± 0.26	0.25 ± 0.03	NS	1.11 ± 0.74	0.53 ± 0.23	NS
Ad.Ar/T.Ar	0.92 ± 0.70	0.22 ± 0.13	NS	0.02 ± 0.02	0.28 ± 0.20	NS	0.40 ± 0.24	0.22 ± 0.02	NS	1.09 ± 0.73	0.49 ± 0.21	NS
N.Ad/Ma.Ar	18.9 ± 14.77	4.57 ± 2.96	NS	0.69 ± 0.69	4.72 ± 3.1	NS	9.3 ± 4.82	8.74 ± 1.08	NS	17.93 ± 10.74	11.92 ± 5.47	NS
N.Ad /T.Ar	16.6 ± 12.73	4.25 ± 2.83	NS	0.5 ± 0.5	4.25 ± 2.87	NS	8.71 ± 4.47	7.66 ± 0.96	NS	17.56 ± 10.62	11.08 ± 5.17	NS
MS/BS	13.84 ± 1.82	14.5 ± 1.87	NS	5.45 ± 1.13	10.35 ± 2.6	NS	19.15 ± 3.04	13.28 ± 2.24	NS	16.48 ± 3.37	17.91 ± 1.5	NS
MAR	2.85 ± 0.17	2.99 ± 0.22	NS	2.32 ± 0.36	2.23 ± 0.1	NS	3.47 ± 0.23	3.65 ± 0.28	NS	2.93 ± 0.44	2.94 ± 0.16	NS
BFR/BS	0.4 ± 0.06	0.44 ± 0.08	NS	0.14 ± 0.04	0.24 ± 0.07	NS	0.66 ± 0.11	0.47 ± 0.06	NS	0.49 ± 0.13	0.53 ± 0.06	NS
BFR/BV	2.5 ± 0.48	2.99 ± 0.53	NS	0.67 ± 0.2	1.14 ± 0.28	NS	5.03 ± 1.03	2.64 ± 0.3	NS	3.44 ± 1.22	2.89 ± 0.28	NS

[1] Two tailed Mann-Whitney U test; * $p < 0.05$, ** $p < 0.01$.

6.2.1.3 Tibial Metaphyseal Cortical Bone

The total volume of metaphyseal cortical compartment evaluated by micro CT ranged from 2.77 to 4.03 mm^3 in males and 2.29 to 3.50 mm^3 in females (Tables D.7 and D.8, Appendix D). At 7 weeks, no differences were found between the male *F2rl1*$^{fl/fl}$ and *F2rl1*$^{wt/wt}$ mice in any of the parameters evaluated. Female *F2rl1*$^{fl/fl}$ mice, however, showed a significantly higher overall cortical porosity (Ct.Po) with both pore number and volume related values greater than in the wildtype group (Table D.1, Appendix D). At 13 weeks, the only difference observed was a lower Ma.Dm in male *F2rl1*$^{fl/fl}$ mice. All other measurements remained similar between the genotypes of either sex (Table D.1, Appendix D).

Analysis of regression coefficients of time related changes indicated a greater reduction in Ma.Dm in the male *F2rl1*$^{fl/fl}$ mice which explained their lower values at 13 weeks (Table D.2, Appendix D).

6.2.1.4 Tibial Diaphyseal Cortical Bone

The total volume of midshaft cortical compartment evaluated by micro CT ranged from 1.39 to 2.35 mm^3 in males and 1.13 to 1.60 mm^3 in females (Tables D.9 and D.10, Appendix D). At 7 weeks, whereas males remained similar, females diverged significantly in Ma.Ar and Ma.Dm, with the *F2rl1*$^{fl/fl}$ mice showing greater values than the *F2rl1*$^{wt/wt}$ mice.

At 13 weeks, a similar feature was observed, this time affecting only males whilst female genotypes showed no difference at all. Male *F2rl1*$^{fl/fl}$ also demonstrated significantly greater cortical porosity with all pore number and volume related variables affected (Table D.3, Appendix D).

Analysis of regression coefficients indicated a faster rate of increase in Tt.Ar, Ma.Ar, Ma.Dm and Po.N for males in *F2rl1*$^{fl/fl}$ mice than in the *F2rl1*$^{wt/wt}$ mice. In females, Ma.Dm showed a greater reduction in *F2rl1*$^{fl/fl}$ mice than in the *F2rl1*$^{wt/wt}$ mice (Table D.4, Appendix D).

The overall bone mass profile of *F2rl1*$^{wt/wt}$ and *F2rl1*$^{fl/fl}$ mice has been summarised in Figure 6.3.

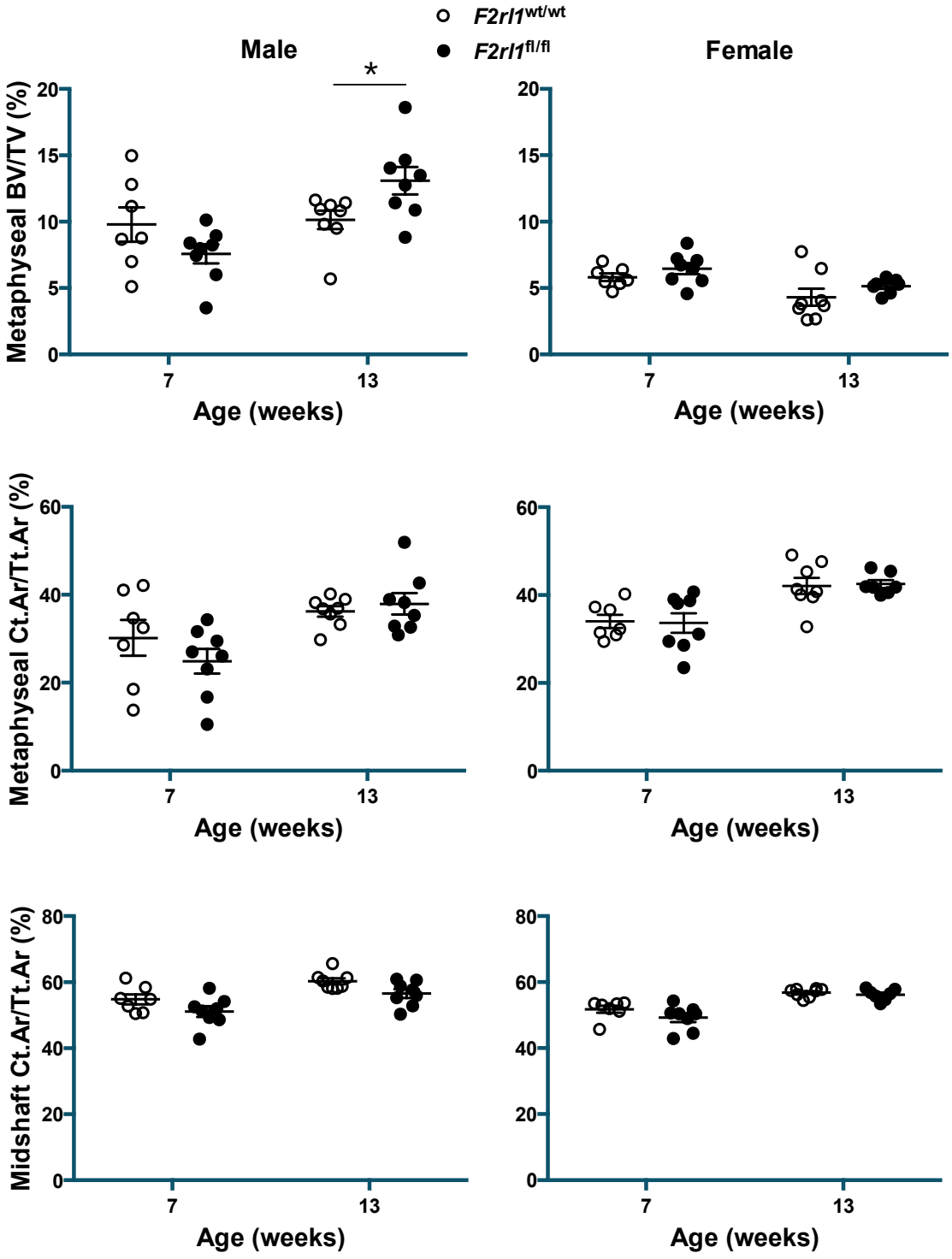


Figure 6.3 Main mass indices of metaphyseal and diaphyseal regions - *F2rl1*$^{wt/wt}$ and *F2rl1*$^{fl/fl}$ mice.

N = 7-8; * $p < 0.05$ using two tailed Mann-Whitney U test; error bars represent SEM.

6.2.1.5 Bone Marrow Adiposity

Micro CT measurement of bone marrow densities in both metaphyseal and diaphyseal regions indicated that whereas male mice of both genotypes were similar, females varied slightly. However, the latter varied across the two ROIs with the female *F2rl1*$^{fl/fl}$ mice possessing higher marrow density (suggestive of lower adiposity) than the *F2rl1*$^{wt/wt}$ mice in the metaphyseal region at 7 weeks and a lower density than the *F2rl1*$^{wt/wt}$ mice in the diaphyseal region at 13 weeks (Figure 6.4). Analysis of regression coefficients did not show any difference in the rate of change between the genotypes.

Histomorphometry of the metaphyseal region, however, did not indicate any differences between the genotypes in adipocyte derived values at any of the time points (Table 6.3; Figure D.1, Appendix D).

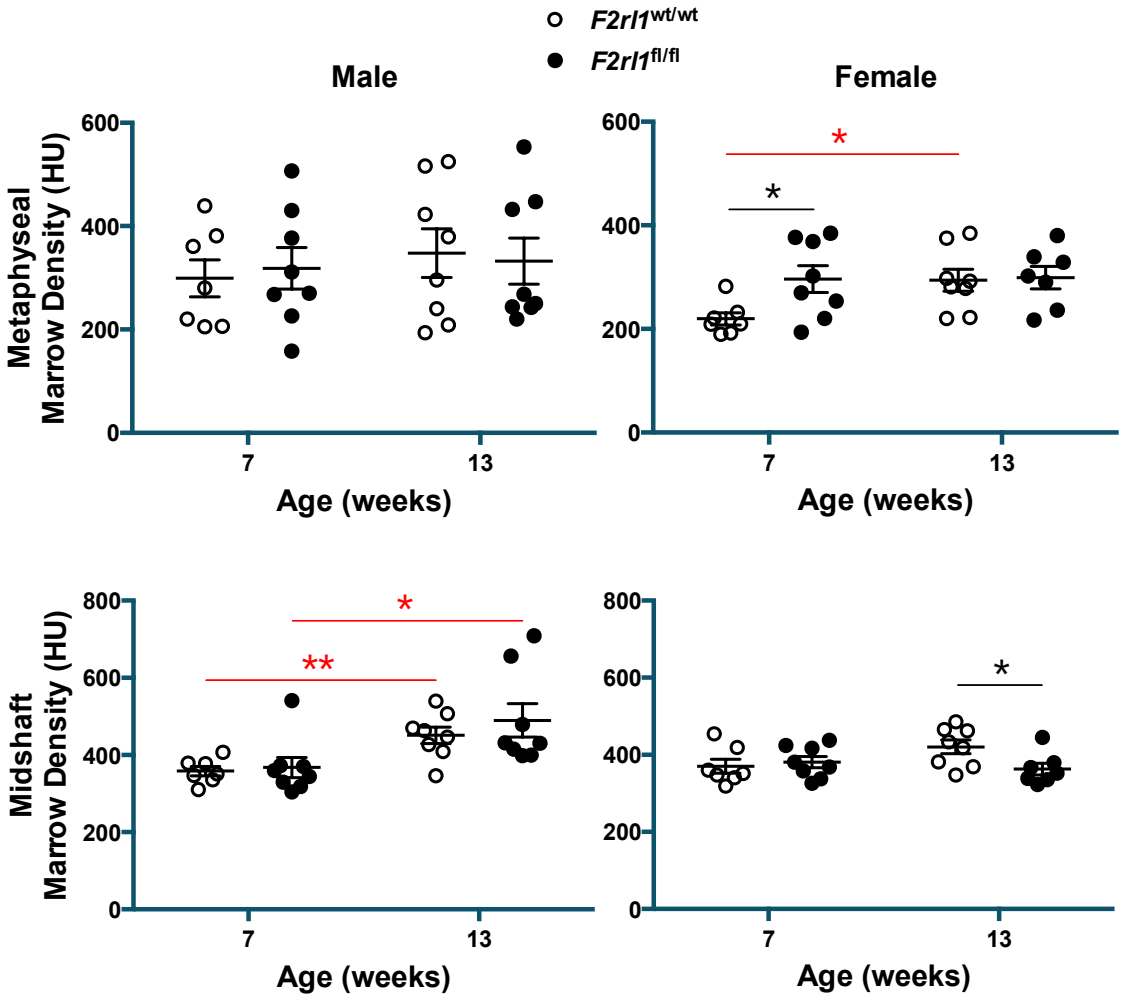


Figure 6.4 Marrow density of the metaphyseal and diaphyseal ROIs - *F2rl1*$^{wt/wt}$ and *F2rl1*$^{fl/fl}$ mice.

Density of the marrow tissue in both micro CT ROIs was measured and expressed in Hounsfield Units (HU). N= 7-8; * $p < 0.05$ using the Mann-Whitney U test; * $p < 0.05$, ** $p < 0.01$ using simple linear regression indicating significant time related changes in sex-genotype controlled groups; error bars represent SEM.

6.2.2 Phenotype of *Osx-Cre.F2rl1*$^{wt/wt}$ and *Osx-Cre.F2rl1*$^{\Delta/\Delta}$ mice

6.2.2.1 Confirmation of Osteoblast Specific PAR$_2$ deletion

To ascertain osteoblast specific deletion of PAR_2 from *Osx-Cre.F2rl1*$^{\Delta/\Delta}$ mice, DNA and RNA were extracted from a number of tissues and quantitatively evaluated by means of a qPCR. DNA from whole bones (femora) and long bone primary osteoblasts (see section 2.3.2) showed a significantly lower abundance of PAR_2 in *Osx-Cre.F2rl1*$^{\Delta/\Delta}$ mice in comparison to controls (Figure 6.5). To rule out the possibility of any non-specific loss of PAR_2 from other cell types, DNA from spleen was similarly assessed which confirmed the specificity of deletion to the osteoblasts (Figure 6.5).

Analysis of PAR_2 mRNA levels in whole bone and spleen from the two genotypes agreed with the results of the DNA quantification analyses (Figure 6.5).

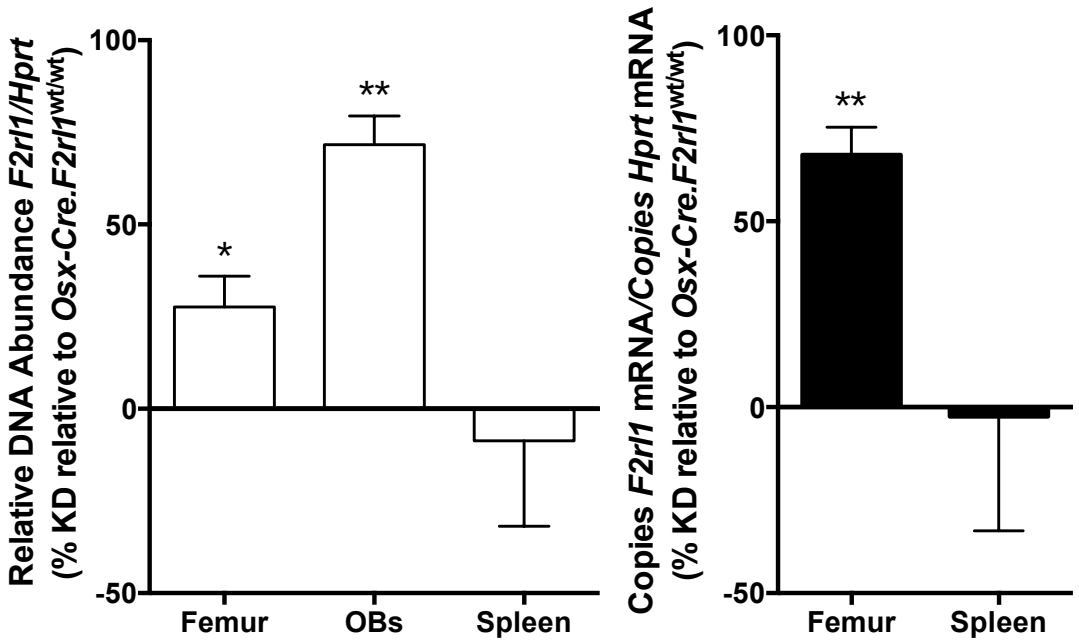


Figure 6.5 Knockdown (KD) of PAR_2 DNA and mRNA.

Abundance of PAR_2 gene and transcript in osseous and non-osseous sources, expressed as percentage knockdown in *Osx-Cre.F2rl1*$^{\Delta/\Delta}$ relative to *Osx.Cre.F2rl1*$^{wt/wt}$ mice. Primary osteoblasts (**OB**) were isolated from long bones using a protocol described in section 2.3.2. N = 4 for OBs and 8-16 for femur and spleen samples; * $p < 0.05$, ** $p < 0.01$ using the Mann-Whitney U test, compared to *Osx-Cre.F2rl1*$^{wt/wt}$ controls; error bars represent SEM.

6.2.2.2 Body Weight and Bone Length

Comparison of body weight and bone lengths revealed that the male *Osx-Cre.F2rl1*$^{\Delta/\Delta}$ mice weighed less than the *Osx-Cre.F2rl1*$^{wt/wt}$ mice at 13 weeks with all other measurements remaining similar between the genotypes of either sex (Figure 6.6). Due to the impact of the floxed allele on these values in the 13 week old male *F2rl1*$^{wt/wt}$ and *F2rl1*$^{fl/fl}$ mice (Figure 6.1), these values were re-analysed following normalisation to non-Osx-Cre values. This revealed a significantly lower body weight and bone length in the *Osx-Cre.F2rl1*$^{\Delta/\Delta}$ mice than the *Osx-Cre.F2rl1*$^{wt/wt}$ mice (Figure 6.7).

Simple linear regression analysis indicated that whereas male *Osx-Cre.F2rl1*$^{\Delta/\Delta}$ and *Osx-Cre.F2rl1*$^{wt/wt}$ mice both gained weight from 7 to 13 weeks, the weight of the females remained relatively static. However, bone length increased in both genotypes over time with an average bone length increase of 9.5% in males and 7.1% in females (Figure 6.6). Analysis of regression coefficients of these changes over time did not indicate any difference between the genotypes ($p < 0.05$).

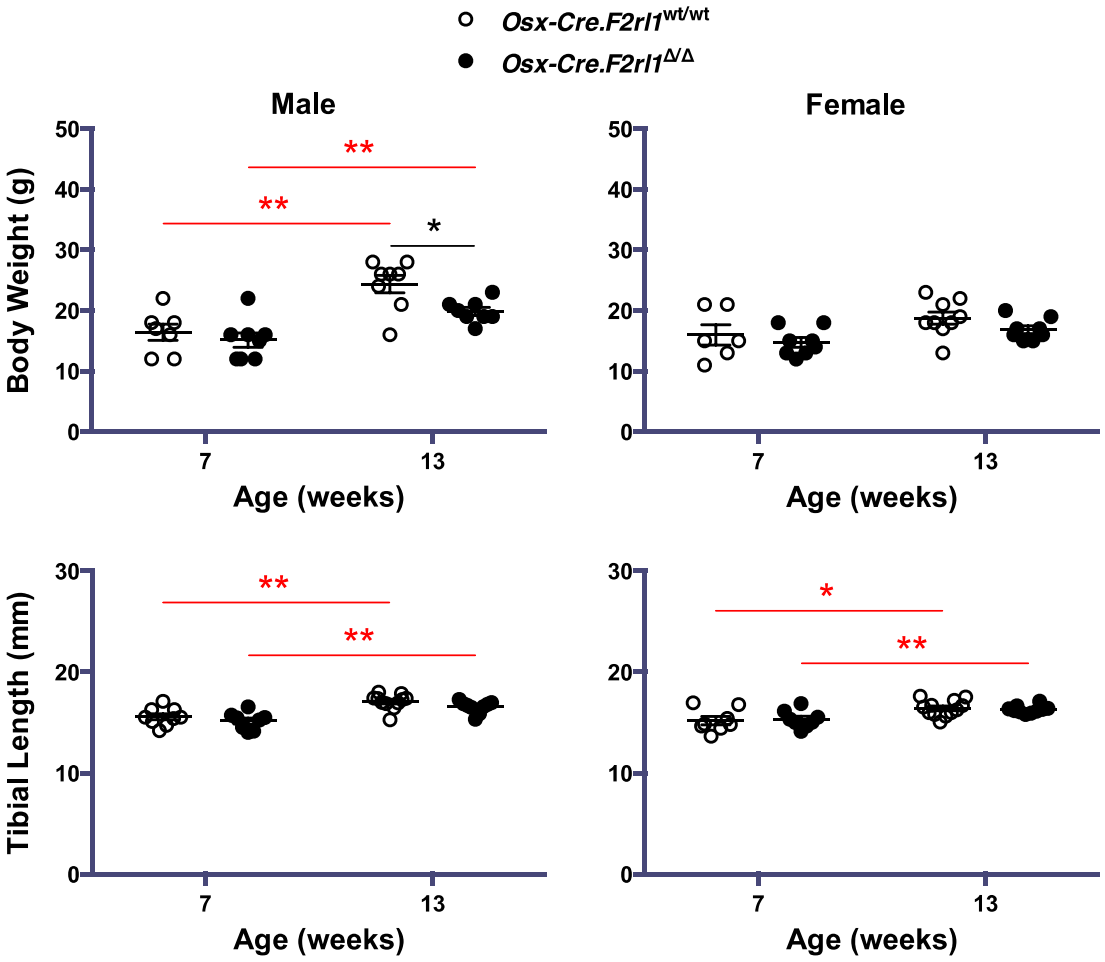


Figure 6.6 Body weight and tibial lengths in *Osx-Cre.F2rl1*$^{wt/wt}$ and *Osx-Cre.F2rl1*$^{\Delta/\Delta}$ mice.

Bone lengths were measured at the time of the micro CT scans using the scout views. N = 8-12; * $p < 0.05$ using two tailed independent samples t-test; * $p < 0.05$, ** $p < 0.01$ using simple linear regression indicating significant time related changes in sex-genotype controlled groups; error bars represent SEM.

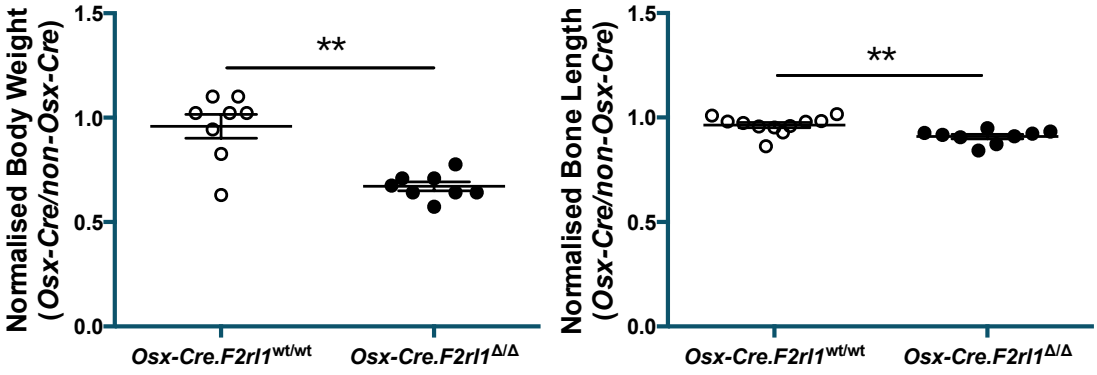


Figure 6.7 Corrected body weight and bone length in 13 week old male *Osx-Cre* mice.

Due to the significant difference observed between the 13 week old male *F2rl1*$^{wt/wt}$ and *F2rl1*$^{fl/fl}$ mice in body weight and bone length, these measurements were corrected by normalisation of values from the *Osx-Cre* to their respective non-*Osx-Cre* group. N = 8-12; ** $p < 0.01$ using two tailed Mann-Whitney U test; error bars represent SEM.

6.2.2.3 Tibial Metaphyseal Trabecular Bone

The total volume of metaphyseal trabecular compartment evaluated by micro CT ranged from 1.05 to 2.01 mm^3 in males and 0.91 to 2.08 mm^3 in females (Figure 6.8; Tables E.1 and E.2, Appendix E). Analysis did not show any differences between the two genotypes in males at either of the two time points or in females at 7 weeks (Figures 6.8-10). However, 13 week old female *Osx-Cre.F2rl1*$^{\Delta/\Delta}$ mice exhibited a significantly higher bone mass profile than controls with all BV, BV/TV, Conn.D, Tb.N, Tb.Sp and BMD values in keeping with the observation (Figures 6.8 and 6.10).

Due to the differences observed between the *F2rl1*$^{wt/wt}$ and *F2rl1*$^{fl/fl}$ mice in some of the parameters (Table 6.2), values from the *Osx-Cre* mice (only for those particular sex, genotype and time specific observations) were normalised to their respective values in *Osx-Cre* negative mice. This way, values from the *Osx-Cre.F2rl1*$^{\Delta/\Delta}$ mice were expressed as a ratio to those of the *F2rl1*$^{fl/fl}$ mice, and values from *Osx-Cre.F2rl1*$^{wt/wt}$ mice expressed as a ratio to those of the *F2rl1*$^{wt/wt}$ mice. Statistical analysis then revealed that male *Osx-Cre.F2rl1*$^{\Delta/\Delta}$ mice had significantly lower Tb.N than the *Osx-Cre.F2rl1*$^{wt/wt}$ mice (Table 6.4). All other comparisons were similar to those before normalisation (Figure 6.9 and 6.10).

Analysis of regression coefficients of changes in micro CT parameters over time in males revealed a higher rate of decrease in SMI towards a more planar configuration, however, this change was very small. In females, such analysis showed that BV/TV and Tb.N increased in the *Osx-Cre.F2rl1*$^{\Delta/\Delta}$ mice over time whereas values in the *Osx-Cre.F2rl1*$^{wt/wt}$ mice generally declined. Analysis of DA values indicated a relatively quick decline towards a more isotropically incompetent configuration in the *Osx-Cre.F2rl1*$^{\Delta/\Delta}$ group (Table 6.5). Despite this faster rate, DA at 13 weeks remained similar in both genotypes.

In histology, a T.Ar of 0.58 to 1.82 mm^2 in males and 0.58 to 1.44 mm^2 in the females was evaluated. The B.Pm measured ranged from 2.27 to 10.14 mm in males and 1.22 to 10.46 in females. Statistical analysis did not detect any difference between the genotypes in males at any of the time points (Table 6.6).

At 7 weeks, female *Osx-Cre.F2rl1*$^{\Delta/\Delta}$ mice showed a > two-fold higher rate of bone formation (BFR/BS) than the *Osx-Cre.F2rl1*$^{wt/wt}$ mice and at 13 weeks higher B.Pm/T.Ar values (Table 6.6). Analysis of normalised values for those parameters that were found to be different between *F2rl1*$^{wt/wt}$ and *F2rl1*$^{fl/fl}$ mice, did not reveal any different comparisons than those reported in Table 6.6. These are not presented.

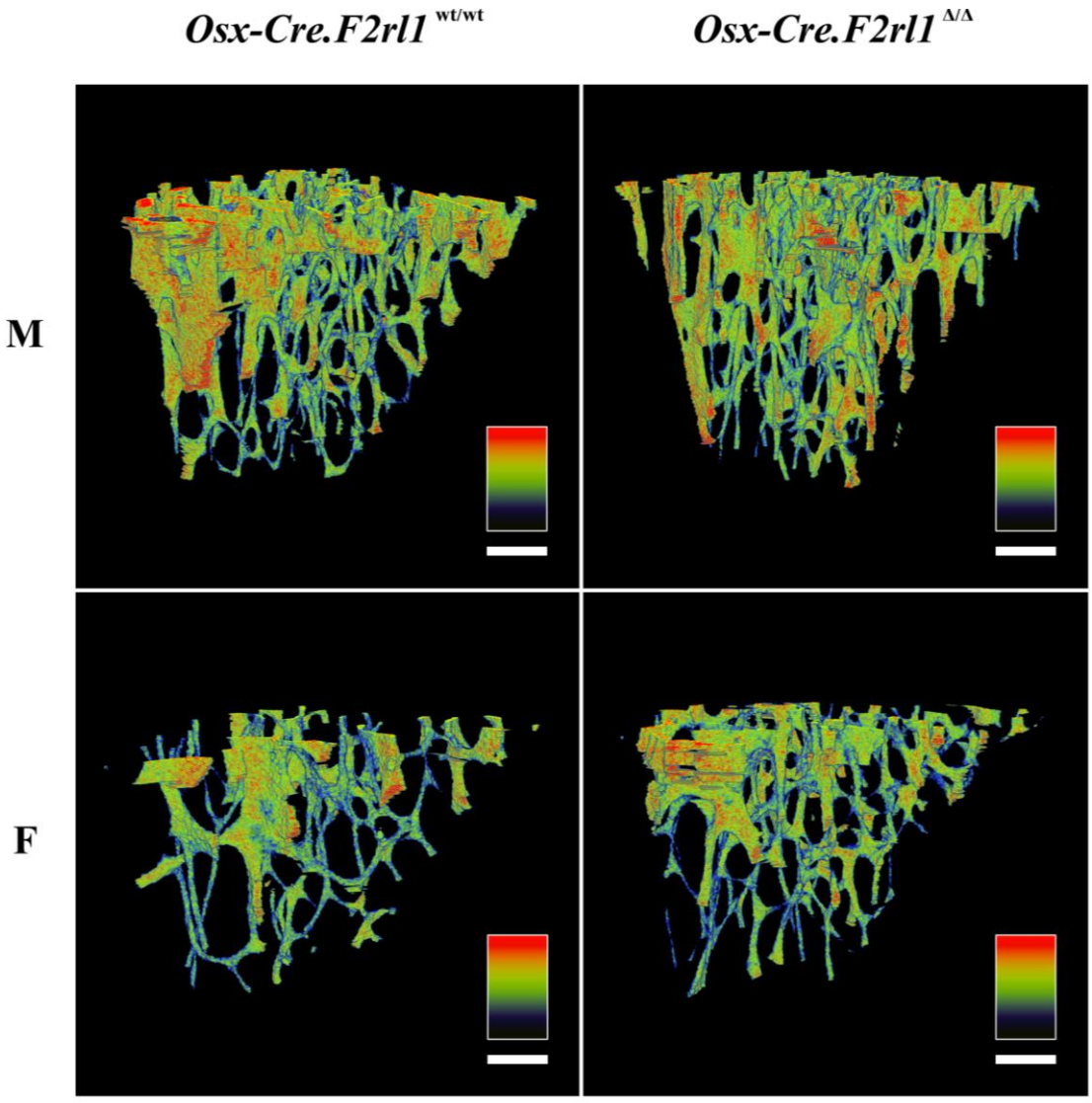


Figure 6.8 3D models of the metaphyseal trabecular bone in *Osx-Cre* mice.

Representative micro CT images at 13 weeks of age, lateral view; bar represents 200 μm; heat bar represents increasing opacity from black to red (may be used to estimate mineralisation within each figure - different figures are not to be compared).

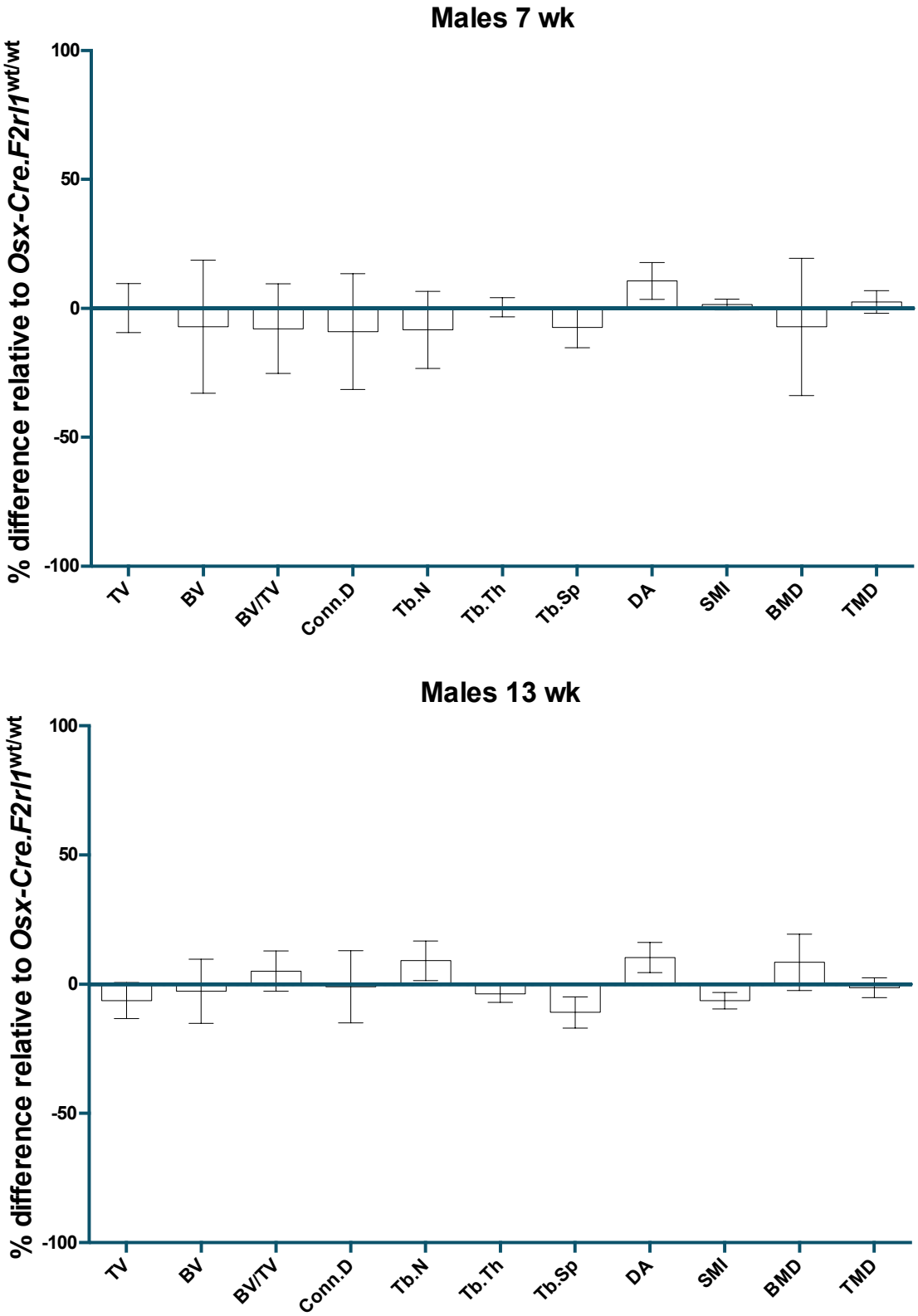


Figure 6.9 Percent difference in metaphyseal trabecular indices - male *Osx-Cre* mice.

The difference between the male *Osx-Cre.F2rl1*$^{wt/wt}$ and *Osx-Cre.F2rl1*$^{\Delta/\Delta}$ mice at 7 and 13 weeks is presented as a percentage relative to the control *Osx-Cre.F2rl1*$^{wt/wt}$. N = 8-11; Mann-Whitney U test did not show any statistically significant differences; error bars represent SE_{diff}.

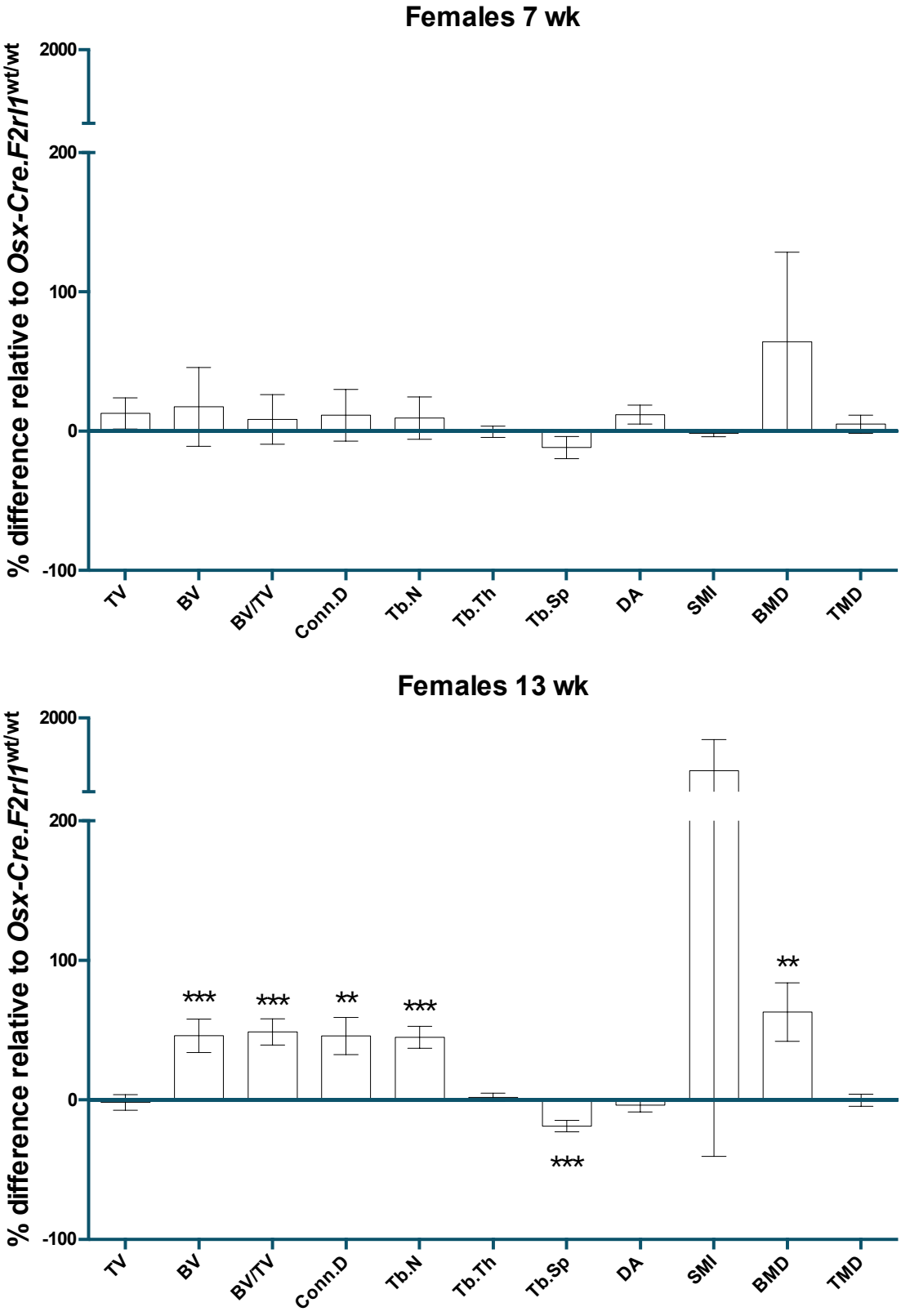


Figure 6.10 Percent difference in metaphyseal trabecular indices - female *Osx-Cre* mice.

The difference between the female *Osx-Cre.F2rl1*$^{wt/wt}$ and *Osx-Cre.F2rl1*$^{\Delta/\Delta}$ mice at 7 and 13 weeks is presented as a percentage relative to the control *Osx-Cre.F2rl1*$^{wt/wt}$. N = 8-12; ** $p < 0.01$, *** $p < 0.001$ using Mann-Whitney U test; error bars represent SE_{diff}.

Table 6.4 Analysis of trabecular indices affected by the presence of the floxed allele.

Where comparison of micro CT values between the *F2rl1*$^{wt/wt}$ and *F2rl1*$^{fl/fl}$ indicated a potential non-specific effect for the floxed PAR_2 allele, values from the *Osx-Cre* mice were normalised to their respective non-*Osx-Cre* group and re-analysed.

Sex	Age	Index	Mean (wt)[1]	Mean (Δ)[2]	*p*-value[3]
M	7	DA	1.04 ± 0.03	0.96 ± 0.05	0.527
M	13	BV	1.02 ± 0.13	0.82 ± 0.06	0.145
M	13	BV/TV	1.18 ± 0.08	0.96 ± 0.03	0.067
M	13	Tb.N	1.20 ± 0.08	0.99 ± 0.03	0.046
M	13	Tb.Sp	0.97 ± 0.05	0.99 ± 0.02	0.292
F	7	BMD	-8.12 ± 10.33	-13.45 ± 10.28	1.000
F	7	Ma.Dn^{m}	0.73 ± 0.11	0.74 ± 0.12	0.854
F	13	Ma.Dn^{d}	0.88 ± 0.06	1.22 ± 0.08	0.007

[1] Normalised mean of *Osx-Cre.F2rl1*$^{wt/wt}$ mice ± SEM.
[2] Normalised mean of *Osx-Cre.F2rl1*$^{\Delta/\Delta}$ mice ± SEM.
[3] Two tailed Mann-Whitney U test.
[m & d] Metaphyseal and diaphyseal marrow densities

Table 6.5 Time related change in metaphyseal trabecular bone - *Osx-Cre* mice.

Regression coefficients of time related changes in bone structural and material indices of *Osx-Cre.F2rl1*$^{wt/wt}$ and *Osx-Cre.F2rl1*$^{\Delta/\Delta}$ mice are presented. Significant differences between the genotypes are highlighted.

	M			F		
Index	**B_{wt}[1]**	**B_{Δ}[2]**	**p-value[3]**	**B_{wt}**	**B_{Δ}**	**p-value**
TV	0.013	-0.004	0.542	-0.011	-0.043*	0.195
BV	0.013**	0.013**	0.932	-0.002	0.000434	0.413
BV/TV	0.722**	0.924***	0.440	-0.076	0.272*	0.036
Conn.D	19.976	25.818	0.772	-7.938	8.185	0.156
Tb.N	0.115*	0.193**	0.241	-0.039	0.046	0.044
Tb.Th	0.001***	0.001**	0.352	$4.4x10^{-4}$*	0.001**	0.609
Tb.Sp	-0.007*	-0.007**	0.849	$-3.2x10^{-4}$	-0.003	0.387
DA	-0.012	-0.014	0.922	-0.005	-0.042*	0.047
SMI	-0.007	-0.040**	0.040	0.002	0.004	0.871
BMD	10.227***	12.387***	0.464	1.655	2.651	0.686
TMD	19.371***	15.094**	0.513	12.898*	7.510	0.509

[1] Regression coefficient (slope) of changes over time in *Osx-Cre.F2rl1*$^{wt/wt}$ mice; a negative value depicts negative changes.
[2] Regression coefficient (slope) of changes over time in the *Osx-Cre.F2rl1*$^{\Delta/\Delta}$ mice.
[*] $p < 0.05$, [**] $p < 0.01$, [***] $p < 0.001$ when values were regressed over time in each sex-genotype category indicating significant changes from 7 to 13 weeks.
[3] Regression coefficients were compared using a second multiple linear regression analysis.

Table 6.6 Trabecular histomorphometric indices - *Osx-Cre* mice.

Both static and dynamic histomorphometric parameters for the *Osx-Cre.F2rl1*$^{wt/wt}$ (Cre-wt) and *Osx-Cre.F2rl1*$^{\Delta/\Delta}$ (Cre-Δ) mice are presented (mean ± SEM). N = 5-6; significant differences are highlighted.

	Male						Female					
	7 wk			13 wk			7 wk			13 wk		
	Cre-wt	*Cre*-Δ	*P* [1]	*Cre*-wt	*Cre*-Δ	*p*	*Cre*-wt	*Cre*-Δ	*p*	*Cre*-wt/wt	*Cre*-Δ	*p*
B.Ar/T.Ar	9.53 ± 2.47	8.12 ± 1.68	NS	13.27 ± 0.7	13.71 ± 1.19	NS	5.39 ± 1.28	5.52 ± 0.95	**	7.12 ± 0.83	11.78 ± 2.65	NS
B.Pm/T.Ar	6.08 ± 1.24	5.49 ± 0.83	NS	7.74 ± 0.4	8.65 ± 0.5	NS	3.49 ± 0.48	3.84 ± 0.71	**	4.66 ± 0.54	6.83 ± 0.8	*
O.Ar/B.Ar	0.68 ± 0.23	0.69 ± 0.4	NS	0.61 ± 0.37	0.49 ± 0.23	NS	0.89 ± 0.61	1.35 ± 0.43	NS	0.85 ± 0.2	0.94 ± 0.33	NS
O.Pm/B.Pm	4.1 ± 1.42	3.52 ± 1.86	*	4.53 ± 2.34	3.5 ± 1.58	NS	4.97 ± 2.52	7.38 ± 1.71	NS	5.22 ± 0.94	6.51 ± 2.31	NS
O.Th	2.54 ± 0.37	2.39 ± 0.18	NS	2.01 ± 0.27	2.22 ± 0.19	NS	2.03 ± 0.24	2.29 ± 0.28	NS	2.43 ± 0.33	2.42 ± 0.28	NS
Ob.Pm/B.Pm	0.91 ± 0.6	0.62 ± 0.17	NS	1.64 ± 1.29	1.77 ± 0.87	**	1.09 ± 0.45	0.94 ± 0.48	NS	2.02 ± 0.52	1.47 ± 0.82	NS
N.Ob/B.Pm	0.87 ± 0.64	0.55 ± 0.15	NS	1.31 ± 0.97	1.36 ± 0.63	*	1.19 ± 0.44	0.68 ± 0.31	NS	1.36 ± 0.36	1.23 ± 0.69	NS
Oc.Pm/B.Pm	0.22 ± 0.14	0.24 ± 0.14	NS	0.26 ± 0.2	0.42 ± 0.1	NS	0.83 ± 0.54	0.63 ± 0.23	NS	0.78 ± 0.26	0.39 ± 0.17	NS
N.Oc/T.Ar	0.63 ± 0.39	0.77 ± 0.4	NS	0.7 ± 0.47	1.12 ± 0.25	NS	2.86 ± 1.61	0.77 ± 0.25	NS	1.25 ± 0.51	1.15 ± 0.51	NS
Ad.Ar/Ma.Ar	5.05 ± 1.92	3.08 ± 2.11	NS	1.58 ± 1.14	1.26 ± 0.69	NS	4.86 ± 1.89	2.27 ± 0.8	NS	2.34 ± 0.67	2.19 ± 0.66	NS
Ad.Ar/T.Ar	4.70 ± 1.79	2.85 ± 1.97	NS	1.38 ± 1.00	1.09 ± 0.60	NS	4.61 ± 1.80	2.14 ± 0.75	NS	2.17 ± 0.63	1.89 ± 0.53	NS
N.Ad/Ma.Ar	116.7 ± 45.3	70.6 ± 42.7	NS	27.2 ± 17.6	28.2 ± 14.16	NS	92 ± 28.5	60.5 ± 19.1	NS	58.1 ± 16.2	49.01 ± 13.9	NS
N.Ad/T.Ar	108.4 ± 42.1	65.5 ± 39.9	NS	23.8 ± 15.45	24.5 ± 12.21	NS	87 ± 26.56	56.92 ± 17.8	NS	53.9 ± 15.2	42.32 ± 10.9	NS
MS/BS	12.06 ± 1.3	12.7 ± 1.6	NS	9.1 ± 1.78	7.87 ± 1.95	NS	11.93 ± 1.8	18.8 ± 2.84	NS	14.25 ± 1.8	16.03 ± 2.72	NS
MAR	2.6 ± 0.16	2.8 ± 0.29	NS	2.68 ± 0.48	2.1 ± 0.1	NS	2.45 ± 0.22	3.09 ± 0.28	NS	2.52 ± 0.18	2.54 ± 0.27	NS
BFR/BS	0.31 ± 0.03	0.38 ± 0.08	NS	0.28 ± 0.11	0.16 ± 0.04	NS	0.28 ± 0.03	0.59 ± 0.14	*	0.35 ± 0.04	0.43 ± 0.12	NS
BFR/BV	2.07 ± 0.32	2.44 ± 0.41	NS	1.48 ± 0.49	1.02 ± 0.25	NS	2.2 ± 0.41	4.16 ± 0.93	NS	2.14 ± 0.35	2.2 ± 0.29	NS

[1] Two tailed Mann-Whitney U test; * $p < 0.05$, ** $p < 0.01$.

6.2.2.4 Tibial Metaphyseal Cortical Bone

The total volume of metaphyseal cortical compartment evaluated by micro CT ranged from 1.72 to 3.89 mm^3 in males and 1.78 to 3.47 mm^3 in females (Tables E.3 and E.4, Appendix E). The only difference found here was at 13 weeks, where minimum and polar moments of inertia (/min and *J*) were found to be lower in the *Osx-Cre.F2rl1*$^{\Delta/\Delta}$ males (Figure 6.11). Both genotypes remained similar in all other time and sex controlled comparisons (Figures 6.11 and 6.12). Moreover, the rate of time related changes was not found to be different between the genotypes of either sex (Table 6.7).

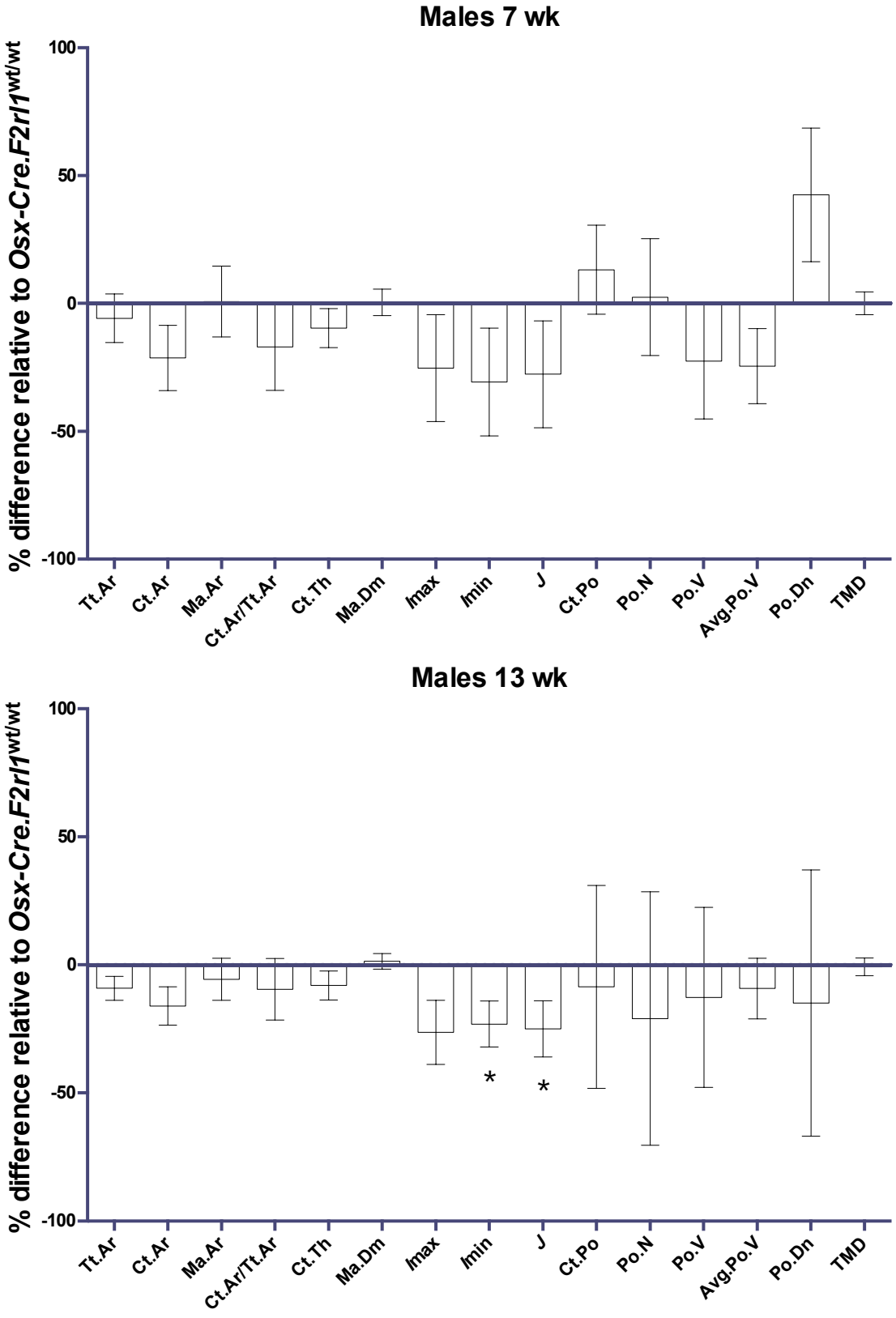


Figure 6.11 Percent difference in metaphyseal cortical indices - male *Osx-Cre* mice.

The difference between the male *Osx-Cre.F2rl1*$^{wt/wt}$ and *Osx-Cre.F2rl1*$^{\Delta/\Delta}$ mice at 7 and 13 weeks is presented as a percentage relative to the control *Osx-Cre.F2rl1*$^{wt/wt}$. N = 8-11; * $p < 0.05$ using Mann-Whitney U test; error bars represent SE_{diff}.

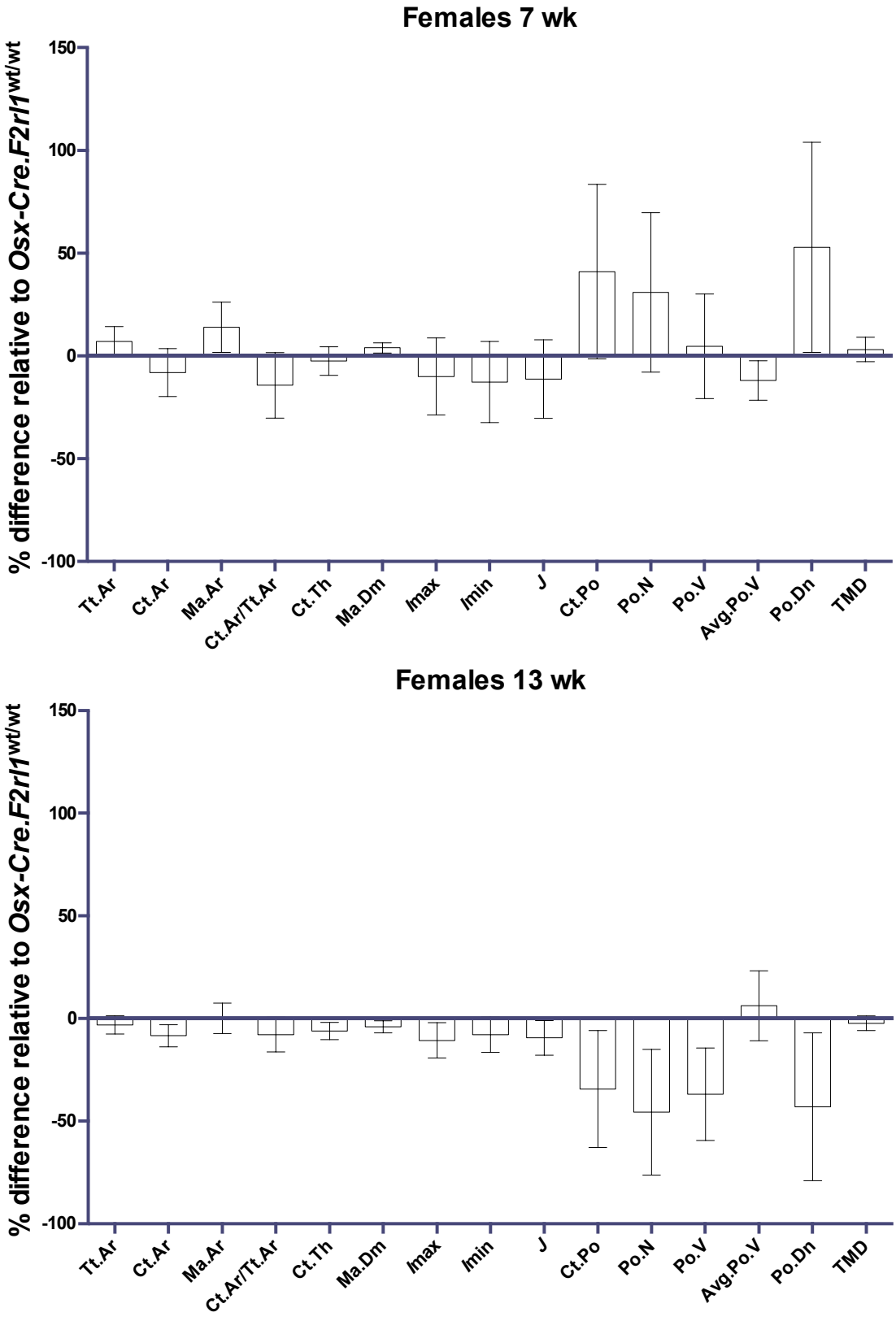


Figure 6.12 Percent difference in metaphyseal cortical indices - female *Osx-Cre* mice.

The difference between the female *Osx-Cre.F2rl1*$^{wt/wt}$ and *Osx-Cre.F2rl1*$^{\Delta/\Delta}$ mice at 7 and 13 weeks is presented as a percentage relative to the control *Osx-Cre.F2rl1*$^{wt/wt}$. N = 8-12; Mann-Whitney U test did not show any statistically significant differences; error bars represent SE_{diff}.

Table 6.7 Time related change in metaphyseal cortical bone assessed by micro CT - *Osx-Cre* mice.

Regression coefficients of time related changes in bone structural and material indices of *Osx-Cre.F2rl1*$^{wt/wt}$ and *Osx-Cre.F2rl1*$^{\Delta/\Delta}$ mice are presented. Comparisons were statistically insignificant.

	M			F		
Index	**B_{wt}[1]**	**B_{Δ}[2]**	**p-value**	**B_{wt}**	**B_{Δ}**	**p-value**
Tt.Ar	0.016	0.002	0.693	-0.004	-0.038*	0.201
Ct.Ar	0.020	0.022	0.879	0.022*	0.020	0.872
Ma.Ar	-0.004	-0.020	0.667	-0.026	-0.057**	0.278
Ct.Ar/Tt.Ar	0.635	0.961	0.761	1.177	1.430*	0.794
Ct.Th	0.004*	0.004*	0.969	0.004**	0.003	0.558
Ma.Dm	-0.011**	-0.010	0.869	-0.008*	-0.018***	0.050
/max	0.013*	0.009	0.676	0.008	0.007	0.867
/min	0.005	0.006	0.880	0.005	0.006	0.871
J	0.018	0.015	0.850	0.013	0.013	0.986
Ct.Po	-4.4×10^{-4}	-0.005	0.639	-0.002	-0.018*	0.131
Po.N	34.759	2.398	0.695	14.410	-89.379*	0.133
Po.V	1.9×10^{-5}	3.1×10^{-5}	0.864	1.8×10^{-5}	-5.5×10^{-5}	0.228
Avg.Po.V	1.4×10^{-8}	4.8×10^{-8}	0.432	4.3×10^{-8}	8.3×10^{-8}	0.418
Po.Dn	17.371	-61.480	0.402	-11.105	-162.738*	0.122
TMD	21.626**	20.188**	0.865	25.247**	16.634*	0.406

[1] Regression coefficient (slope) of changes over time in *Osx-Cre.F2rl1*$^{wt/wt}$ mice; a negative value depicts negative changes.

[2] Regression coefficient (slope) of changes over time in the *Osx-Cre.F2rl1*$^{\Delta/\Delta}$ mice.

* $p < 0.05$, ** $p < 0.01$, *** $p < 0.001$ when values were regressed over time in each sex-genotype category indicating significant changes from 7 to 13 weeks.

[3] Regression coefficients were compared using a second multiple linear regression analysis.

6.2.1.5 Tibial Diaphyseal Cortical Bone

The total volume of midshaft cortical compartment evaluated by micro CT ranged from 0.69 to 2.10 mm^3 in males and 0.66 to 1.66 mm^3 in females (Tables E.5 and E.6, Appendix E). None of the differences at 7 weeks were found to be statistically significant in either sex. At 13 weeks, Avg.Po.V and Ma.Ar were significantly lower in the male and female *Osx-Cre.F2rl1*$^{\Delta/\Delta}$ mice than in their *Osx-Cre.F2rl1*$^{wt/wt}$ counterparts, respectively (Figures 6.13 and 6.14).

Analysis of regression coefficients indicated a small discrepancy in the time related rate of change in Avg.Po.V between the male genotypes, however, the difference was negligible. Instead, female *Osx-Cre.F2rl1*$^{\Delta/\Delta}$ mice showed a substantial 9.6-fold faster rate of TMD accumulation than the controls (Table 6.8). Despite the latter, TMD values were not significantly different between the genotypes at either time point (Figure 6.14).

Figure 6.15 summarises the main mass indices of the trabecular and cortical bones in the *Osx-Cre* mice.

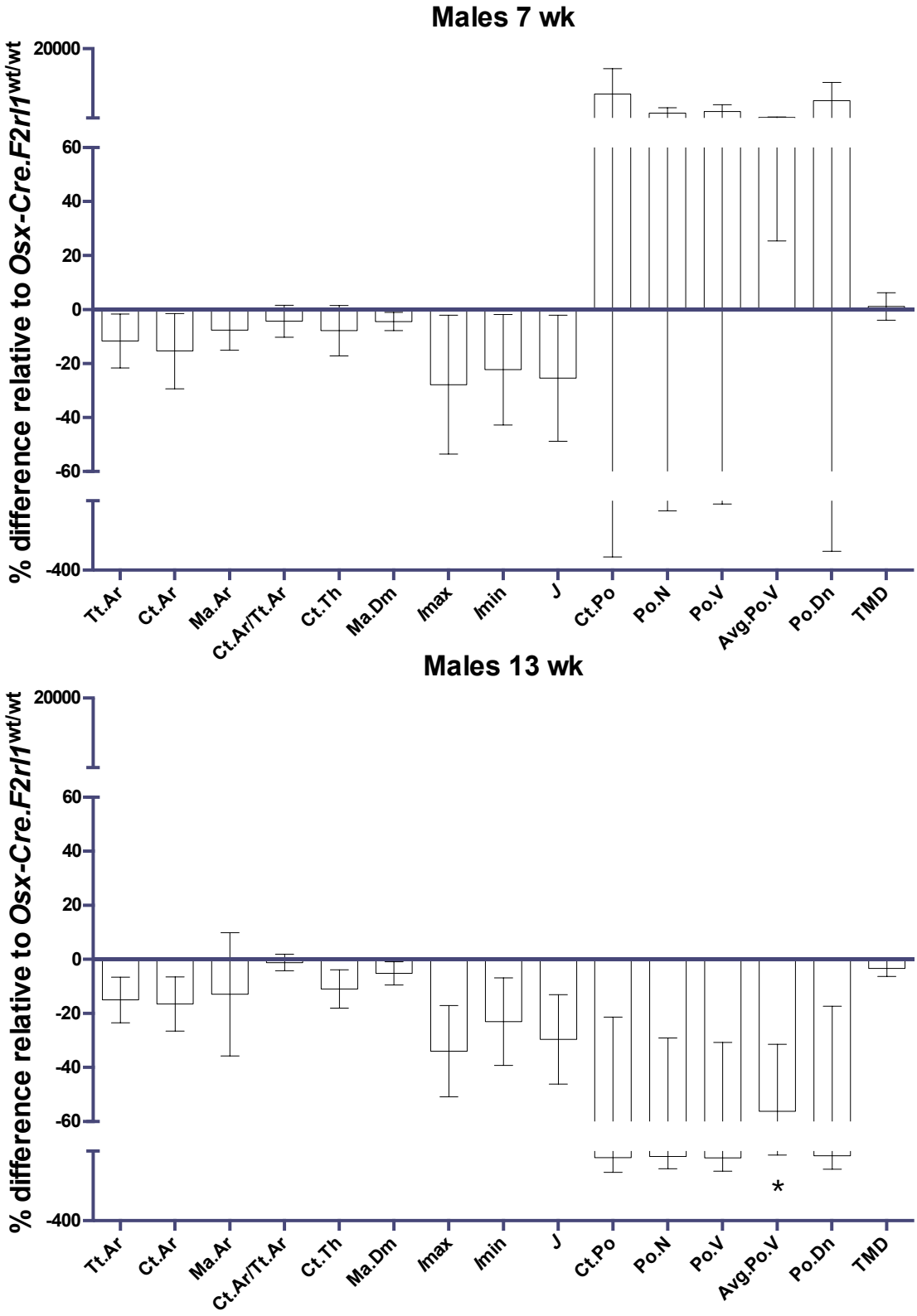


Figure 6.13 Percent difference in diaphyseal cortical indices - male *Osx-Cre* mice.

The difference between the male *Osx-Cre.F2rl1*$^{wt/wt}$ and *Osx-Cre.F2rl1*$^{\Delta/\Delta}$ mice at 7 and 13 weeks is presented as a percentage relative to the control *Osx-Cre.F2rl1*$^{wt/wt}$. N = 8-11; * $p < 0.05$ using Mann-Whitney U test; error bars represent SE_{diff}.

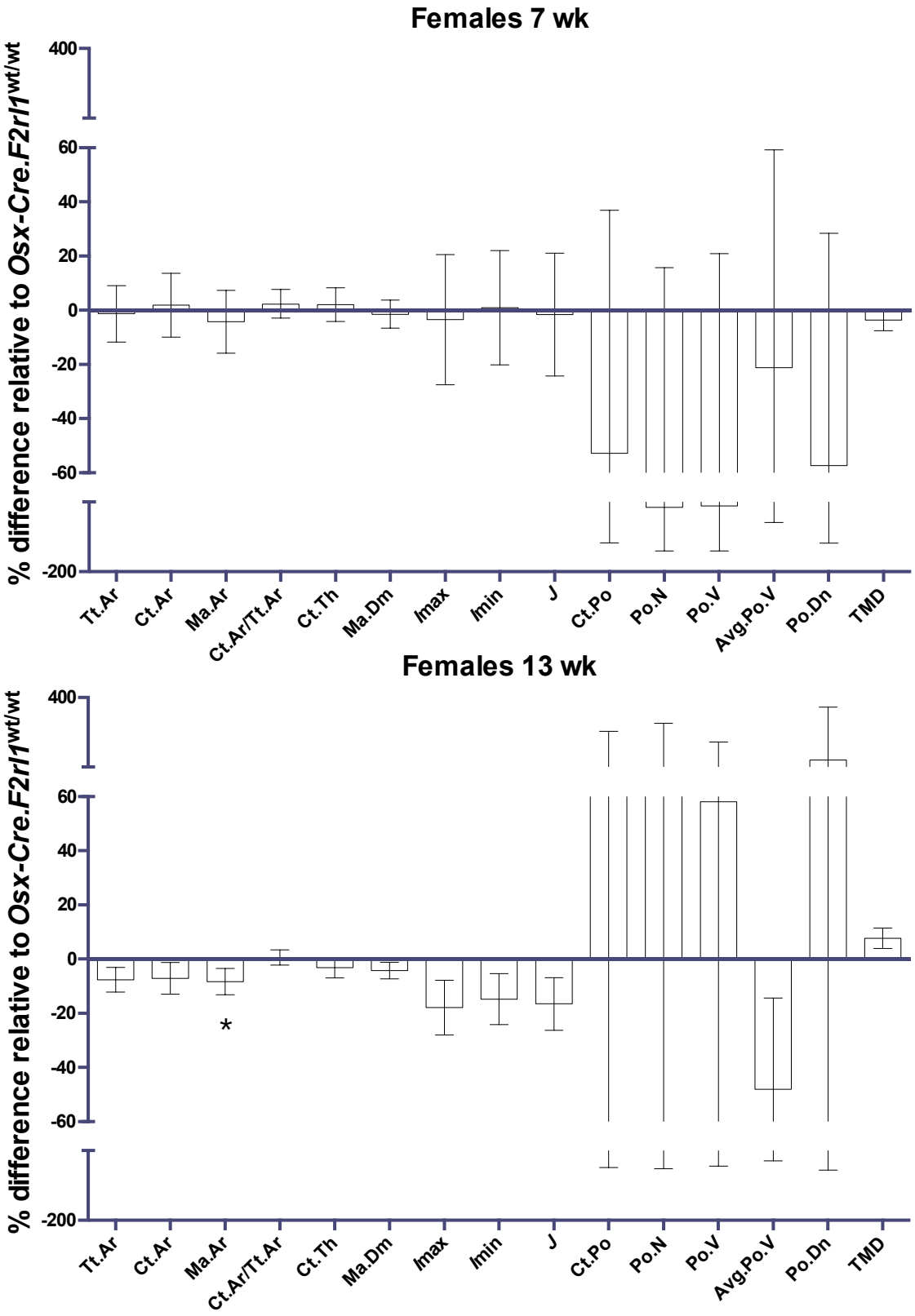


Figure 6.14 Percent difference in diaphyseal cortical indices - female *Osx-Cre* mice.

The difference between the female *Osx-Cre.F2rl1*$^{wt/wt}$ and *Osx-Cre.F2rl1*$^{\Delta/\Delta}$ mice at 7 and 13 weeks is presented as a percentage relative to the control *Osx-Cre.F2rl1*$^{wt/wt}$. N = 8-12; * $p < 0.05$ using Mann-Whitney U test; error bars represent SE_{diff}.

Table 6.8 Time related change in diaphyseal cortical bone assessed by micro CT - *Osx-Cre* mice.

Regression coefficients of time related changes in bone structural and material indices of *Osx-Cre.F2rl1*$^{wt/wt}$ and *Osx-Cre.F2rl1*$^{\Delta/\Delta}$ mice are presented. Significant differences between the genotypes are highlighted.

	M			F		
Index	**B_{wt}[1]**	**B_{Δ}[2]**	**p-value**	**B_{wt}**	**B_{Δ}**	**p-value**
Tt.Ar	0.041**	0.031*	0.568	0.020*	0.012	0.470
Ct.Ar	0.031**	0.025**	0.469	0.019**	0.013*	0.390
Ma.Ar	0.010	0.006	0.808	0.001	-0.002	0.704
Ct.Ar/Tt.Ar	0.998*	1.260*	0.636	1.189***	1.052**	0.759
Ct.Th	0.009**	0.008**	0.603	0.006***	0.005**	0.412
Ma.Dm	0.004	0.003	0.855	-0.001	-0.004	0.625
/max	0.006**	0.004*	0.350	0.003*	0.001	0.378
/min	0.004**	0.003*	0.581	0.002**	0.001	0.334
J	0.010**	0.007*	0.428	0.005*	0.003	0.357
Ct.Po	0.004	-0.001	0.141	-0.004	-0.002	0.429
Po.N	14.827	-1.368	0.132	-10.847	-1.462	0.271
Po.V	$4.0x10^{-5}$**	$-2.0x10^{-6}$	0.167	$-2.3\ x10^{-5}$	$-5.0x10^{-6}$	0.319
Avg.Po.V	$2.1\ x10^{-7}$**	$1.6\ x10^{-9}$	0.019	$1.6\ x10^{-7}$	$5.8\ x10^{-8}$	0.402
Po.Dn	14.371	-10.369	0.118	-21.293	-5.934	0.347
TMD	18.703	8.817	0.405	2.825	27.133**	0.048

[1] Regression coefficient (slope) of changes over time in *Osx-Cre.F2rl1*$^{wt/wt}$ mice; a negative value depicts negative changes.
[2] Regression coefficient (slope) of changes over time in the *Osx-Cre.F2rl1*$^{\Delta/\Delta}$ mice.
* $p < 0.05$, ** $p < 0.01$, *** $p < 0.001$ when values were regressed over time in each sex-genotype category indicating significant changes from 7 to 13 weeks.
[3] Regression coefficients were compared using a second multiple linear regression analysis.

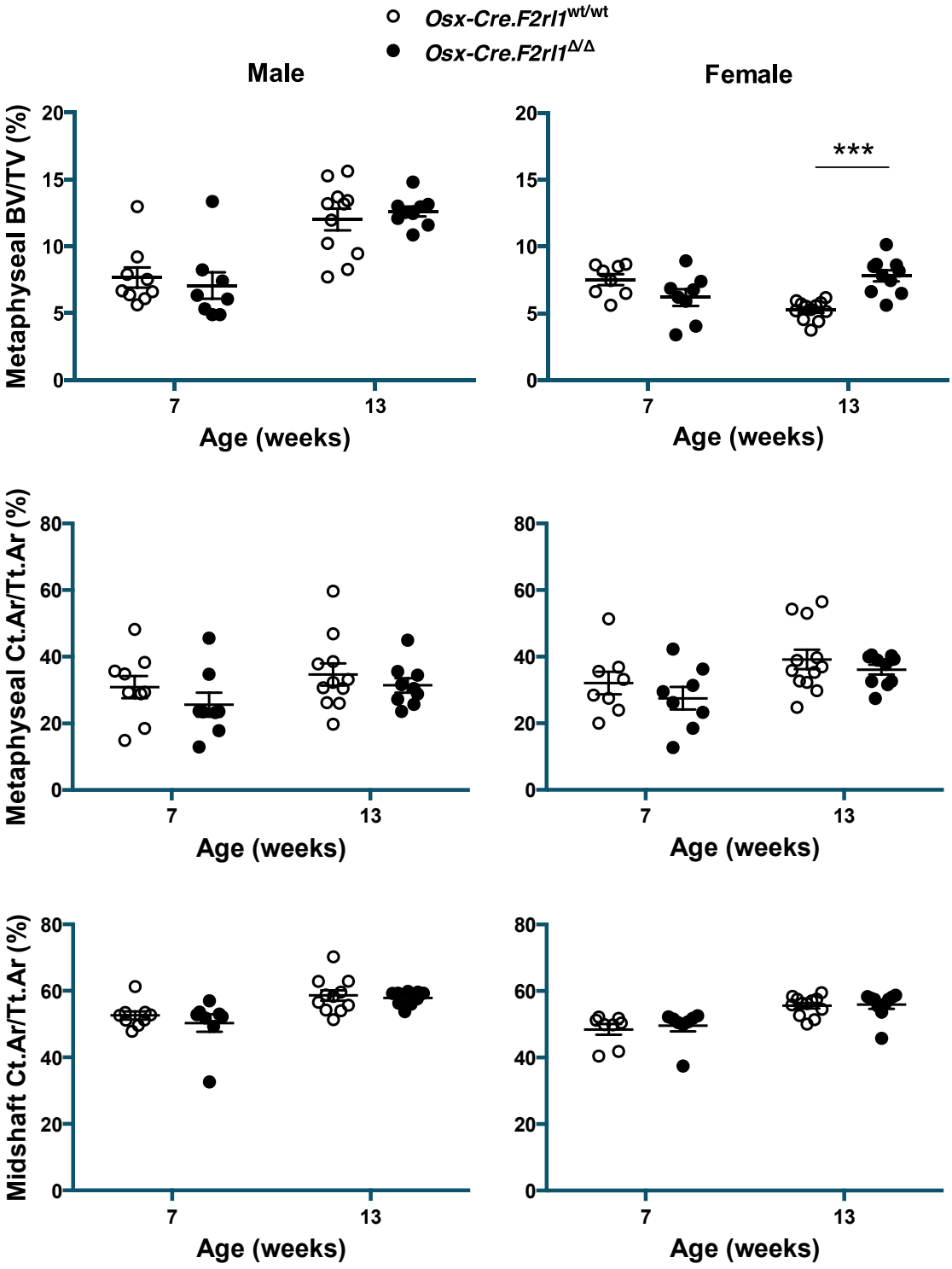


Figure 6.15 Main mass indices of the metaphyseal and midshaft regions in *Osx-Cre* mice.

N = 8-12; *** $p < 0.001$ using two tailed Mann-Whitney U test; error bars represent SEM.

6.2.2.5 Bone Marrow Adiposity

Analysis of micro CT derived metaphyseal and diaphyseal marrow densities showed that male *Osx-Cre.F2rl1*$^{\Delta/\Delta}$ mice had a lower value for diaphyseal marrow density than the *Osx-Cre.F2rl1*$^{wt/wt}$ counterparts at 13 weeks, but no other differences between genotypes were observed (Figure 6.16). Due to the observed difference between the *F2rl1*$^{wt/wt}$ and *F2rl1*$^{fl/fl}$ females at 7 and 13 weeks, a normalisation approach was also attempted which revealed a higher Ma.Dn in the diaphyseal ROI of 13-week-old female *Osx-Cre.F2rl1*$^{\Delta/\Delta}$ mice than in that of the *Osx-Cre.F2rl1*$^{wt/wt}$ counterparts (Table 6.4). Time related changes in all groups also occurred at relatively similar rates ($p < 0.05$).

Histomorphometrically, analysis of adipocyte number or area related values did not reveal any difference between the genotypes of either sex-age group (Figure D.2, Appendix D). Analysis of the rates at which changes occurred over time, also, did not show any significance ($p < 0.05$).

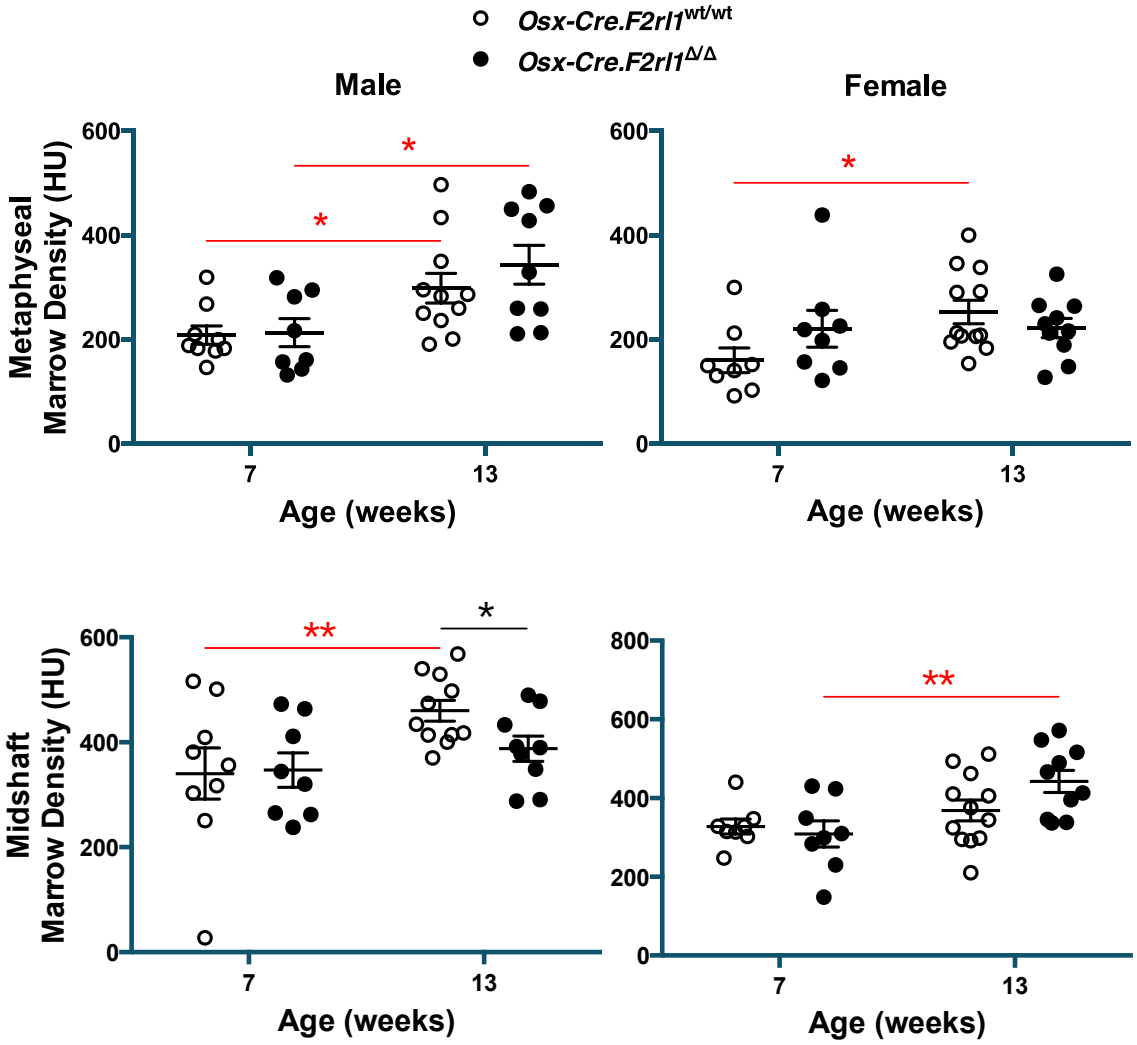


Figure 6.16 Marrow density of the metaphyseal and diaphyseal ROIs - *Osx-Cre* mice.

Density of marrow tissue in both micro CT ROIs was measured and expressed in Hounsfield Units (HU). N= 8-12; * $p < 0.05$ using the Mann-Whitney U test; * $p < 0.05$, ** $p < 0.01$ using simple linear regression indicating significant time related changes in sex-genotype controlled groups; error bars represent SEM.

6.2.3 The Effect of *Osx-Cre* Transgene on the Phenotype of C57BL/6J Mice

Characterisation of the phenotype of the *Osx-Cre* line in the past indicated an abnormally slow rate of growth and smaller body and bone size in these mice (Davey et al. 2011). In the current model, slower growth of *Osx-Cre* mice was also evident using the bone length measurements where values remained constantly below those of the non-*Osx-Cre* counterparts regardless of ageing (Figure 6.17). Overall, the presence of the *Osx-Cre* transgene resulted in a significantly lower body weight at weaning (Figure 6.18). This, however, was compensated over time in the *Osx-Cre.F2rl1*$^{wt/wt}$ mice such that values were no longer statistically different to those of the *F2rl1*$^{wt/wt}$ mice at 13 weeks in either sex. In contrast, the difference in weight between the *Osx-Cre.F2rl1*$^{\Delta/\Delta}$ and *F2rl1*$^{fl/fl}$ persisted over time in both males and females and reached statistical significance at all three time points (Figure 6.18).

Analysis of regression coefficients of change over time revealed a significantly higher rate of weight accrual in the male *Osx-Cre.F2rl1*$^{wt/wt}$ mice than the normal wildtype control. All other comparisons in this regard remained insignificant.

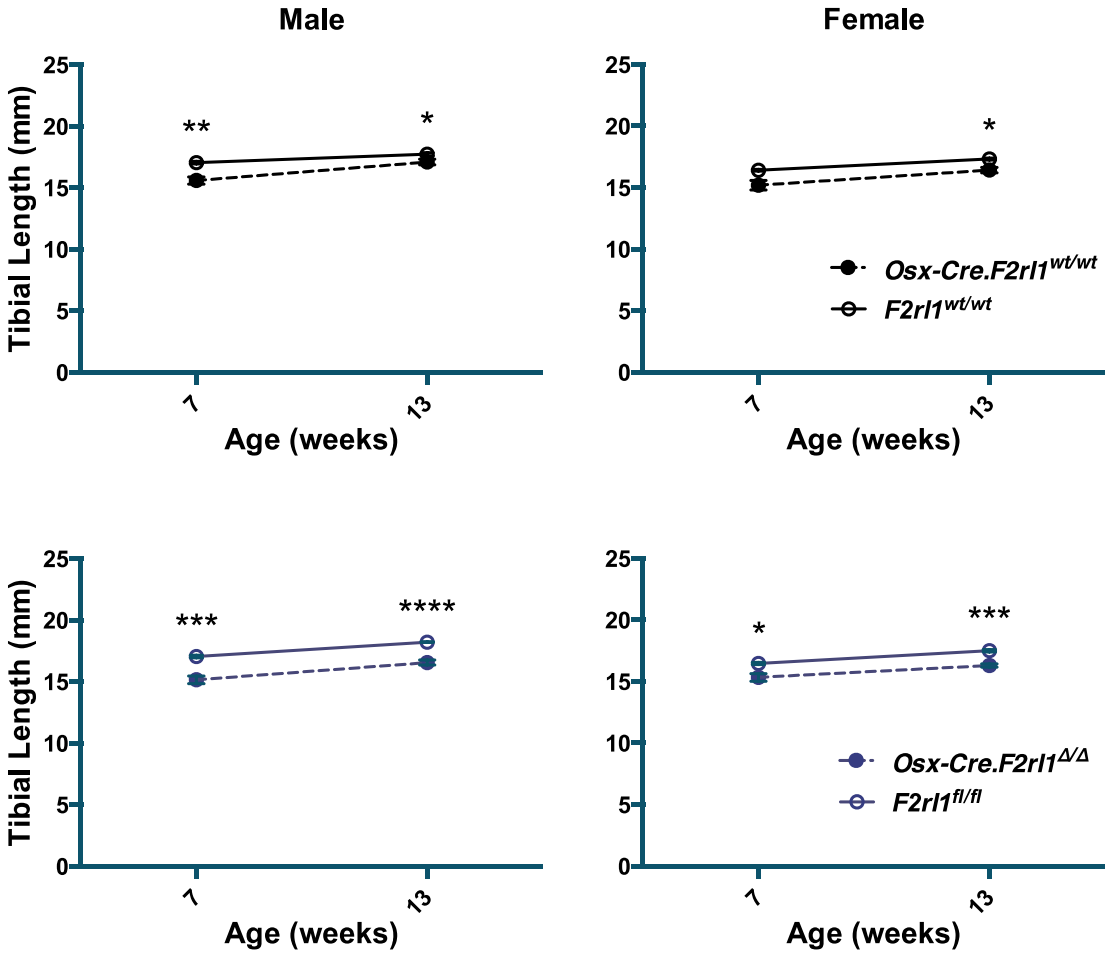


Figure 6.17 Comparison of tibial lengths between *Osx-Cre* positive and negative mice. Measurements were carried out at the time of micro CT scans at the end points (weeks 7 and 13). N = 7-12; * $p < 0.05$, ** $p < 0.01$, *** $p < 0.001$, **** $p < 0.0001$ using two tailed Mann-Whitney U test; analysis of regression coefficients of change over time did not show any difference between the *Osx-Cre* and non-*Osx-Cre* mice ($p < 0.05$); bars represent SEM.

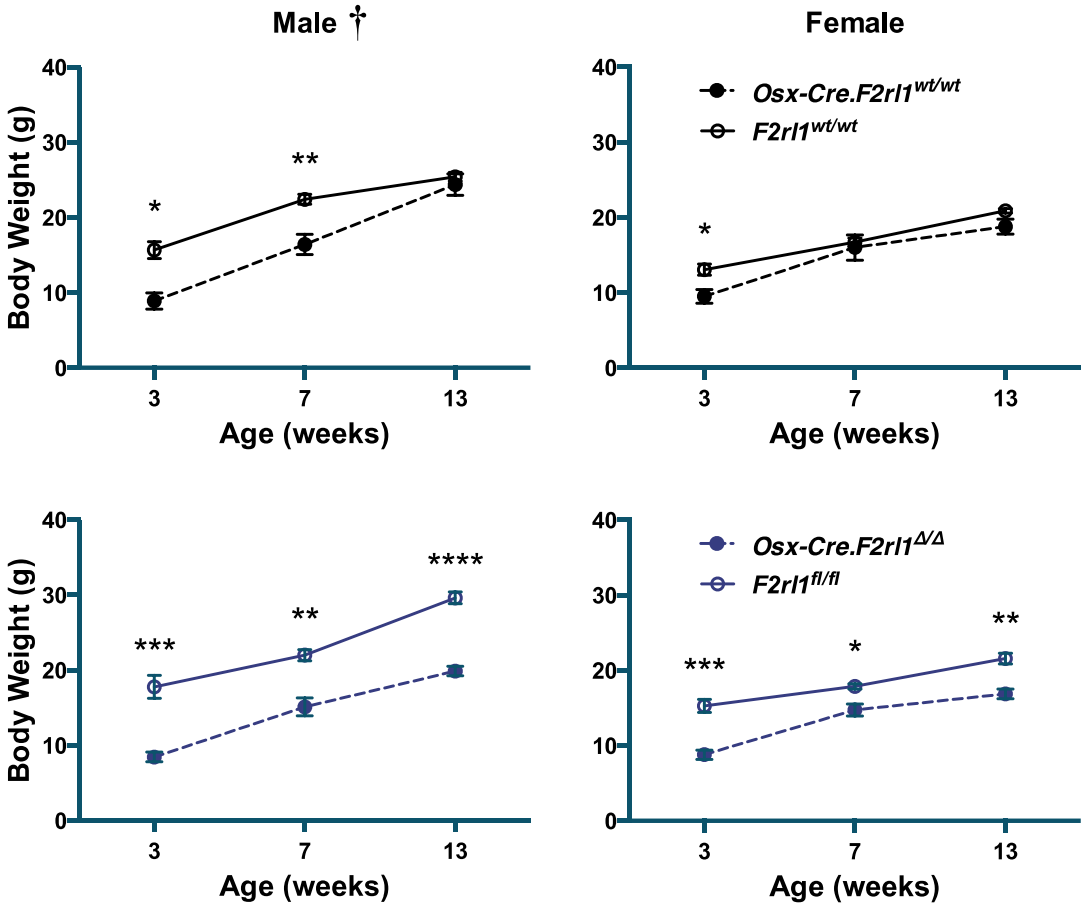


Figure 6.18 Comparison of body weight between *Osx-Cre* positive and negative mice.

Measurements were carried out once at weaning (week 3) and once before collection of samples at the end points (weeks 7 and 13). N = 7-15; * $p < 0.05$, ** $p < 0.01$, *** $p < 0.001$ using two tailed independent samples t-test; † $p < 0.05$ when regression coefficients of change over time were significantly different between the groups; error bars represent SEM.

6.3 Discussion

Due to the inherent limitations of global knockout models, this study undertook to achieve an osteoblast specific ablation of PAR_2 in C57BL/6J mice in order to further delineate the role of the receptor in the differentiation and function of osteoblasts and the related impact on bone phenotype. Accordingly, *Osx-Cre* wildtype and PAR_2 floxed mice were examined at 7 and 13 weeks of age and their differences identified. To ascertain the differences were not caused by the presence of the floxed alleles, non-*Osx-Cre* mice were similarly evaluated.

This study reports the use of the *Osx-Cre* mouse line to achieve the desired osteoblast specific deletion of PAR_2. Osterix is an osteoblast specific transcription factor downstream of Runx2 (Nishio et al. 2006) and Dlx5 (Ulsamer et al. 2008; Hojo et al. 2016). Other choices that are currently available for osteoblast specific gene ablation include, *Runx2-Cre, Paired related homeobox 1-Cre* (*Prx1-Cre*), *Col1a1-Cre* and *Osteocalcin-Cre* (*Ocn-Cre*) mice. As *Osx* is expressed earlier than either *Col1a1* (Ortuño et al. 2013) or osteocalcin (Rashid et al. 2014) and because the adipocytic/osteoblastic lineage plasticity has been reported in *Osx* expressing osteoblasts (Song et al. 2012), this transgene was selected for the purpose of this study. In this respect, use of *Runx2-Cre* and *Prx1-Cre* lines would have been advantageous, however, these lines had not been yet fully characterised at the time this study was initiated (Elefteriou and Yang 2011). Moreover, depending on the gene flanked by LoxP sites, *Prx1-Cre* mice can potentially exhibit sex-specific penetrance patterns, which made them inappropriate for the current model (Logan et al. 2002).

Comparison of bone length and body weight of the *Osx-Cre* mice to those of the non-*Osx-Cre*, showed an overall lower body size due to the presence of the *Osx-Cre* transgene (Figure 6.17 and 6.18). The bone length measurements clearly indicate that the *Osx-Cre* transgene impedes longitudinal bone growth in both sexes. The effects also seem to persist up until 13 weeks of age which is longer than was reported previously (Davey et al. 2011). Whether, this lag in growth is later compensated was not determined in the current study. As the *Osx-cre* mice were only compared to each other, this lag of growth should not affect the validity of the reported outcomes. Nevertheless, because of the implications of any non-

specific effects being introduced due to the presence of the targeted allele, the phenotype of these mice was also evaluated.

Evaluation of non-*Osx*-*Cre* control mice indicated that the PAR_2 floxed genotype had a slightly different phenotype to that of the wildtype counterparts. Most of the differences observed by micro CT in the trabecular bone were detected at week 13 when male *F2rl1*$^{fl/fl}$ mice were characterised by a higher bone mass and also body weight (Table 6.1; Figure 6.1). This coincided with an increase in osteoblastic number and surface parameters which can explain the finding (Table 6.3). Histomorphometric analysis of the trabecular bone also indicated that female *F2rl1*$^{fl/fl}$ mice had a higher bone area fraction than the wildtype controls (Table 6.3), which did not agree with the micro CT evaluations. Due to the more stereologically sound nature of micro CT measurements, the discrepancy is potentially the result of the spacial limitations of histological methods.

Evaluation of the cortical bone in both ROIs demonstrated a general tendency for an increased porosity in the *F2rl1*$^{fl/fl}$ mice, however the sexes were affected in a location specific manner (Tables D.1 and D.3, Appendix D). This in combination with an inclination towards having an increased marrow diameter and area in the diaphyseal region suggests a potentially higher rate of bone resorption in the *F2rl1*$^{fl/fl}$ mice. Nonetheless, Ct.Th did not vary across the genotypes and therefore the increase in marrow parameters is likely to have other explanations.

Female *F2rl1*$^{fl/fl}$ mice also demonstrated a higher metaphyseal Ma.Dn at 7 weeks suggesting lower marrow adiposity than their wildtype counterparts, nevertheless, increase in the wildtype Ma.Dn over time led to values that were no longer different between the genotypes at 13 weeks. Moreover, this finding was not supported by the histomorphometric assessments of the metaphyses where no histological indices of adiposity showed differences (Figure D.1, Appendix D). In contrast, measurements in the midshaft ROI indicated a lower Ma.Dn in the female *F2rl1*$^{fl/fl}$ at 13 weeks hinting at the possibility of a higher marrow adiposity, but as histomorphometric evaluations were not performed for the diaphyseal region, this remained unclear. The significance of these observations, therefore, was not determined.

Due to the observed differences discussed above and their potential implications in interpreting the results of the *Osx-Cre* mice, a normalisation approach was further undertaken to assure validity of the reported comparisons using the absolute values (Table 6.4). Such analysis however did not undermine the reported results and apart from a slight difference in Tb.N between the male *Osx-Cre.F2rl1*$^{\Delta/\Delta}$ and *Osx-Cre.F2rl1*$^{wt/wt}$ mice, all other comparisons remained unchanged. The same approach was also adopted in verifying the results of the histomorphometric analyses with no significant outcome.

This study illustrates a clear sex specific distribution of phenotypical changes in response to PAR_2 loss from the cells of the osteoblastic lineage. Bone mass parameters in the female *Osx-Cre.F2rl1*$^{\Delta/\Delta}$ mice showed a significantly higher rate of increase over time (Table 6.5) than the *Osx-Cre.F2rl1*$^{wt/wt}$ leading to a definitive gap in bone mass at 13 weeks (Figure 6.10). It is interesting that coincident with such findings, Ma.Dn was also higher in these mice at 13 weeks suggesting lower adiposities although this was not shown in histology (Table 6.4). Analysis of the bone fluorochrome labels indicated that this was likely the result of a higher rate of bone formation at 7 weeks (Table 6.6). The fact that DA deteriorated at a higher rate over time in this group (Table 6.5) may also be reflective of a sudden expansion of bone volume at such a rate that surpasses that of the remodelling leaving trabeculae primitively arranged. Other possibilities such as unresponsiveness of osteoblasts to mechanical signals, or a disarray of mechanoreceptor mechanisms due to the loss of PAR_2 from osteocytes and bone lining cells cannot be ruled out using the current model. Female *Osx-Cre.F2rl1*$^{\Delta/\Delta}$ mice also showed a significantly higher rate of mineral accrual in their midshaft cortical bone, although this did not lead to any significantly higher values at the later time point.

In contrast, the male *Osx-Cre.F2rl1*$^{\Delta/\Delta}$ mice appeared relatively similar to their *Osx-Cre.F2rl1*$^{wt/wt}$ counterparts in both metaphyseal and diaphyseal ROIs. Nevertheless, indications of a subtle negative impact for PAR_2 loss was evident in a few areas. Of these, bone length was found to be shorter in the male *Osx-Cre.F2rl1*$^{\Delta/\Delta}$ mice than the *Osx-Cre.F2rl1*$^{wt/wt}$ mice at 13 weeks (Figure 6.7). Whilst this might be reflective of less efficient endochondral ossification due to osteoblast related changes, it could also be the result of *Cre* expression (and thus PAR_2 ablation) in hypertrophic chondrocytes (Nakashima et al. 2002). Additionally, despite the insignificance of comparisons in the trabecular bone, upon

normalisation of values from the *Osx-Cre.F2rl1*$^{\Delta/\Delta}$ and *Osx-Cre.F2rl1*$^{wt/wt}$ mice to their respective non-*Osx-Cre* counterparts, a drop in the Tb.N was noted (Table 6.4). Lower values were also observed in */min* and *J* values in the metaphyseal cortical bone of the *Osx-Cre.F2rl1*$^{\Delta/\Delta}$ males (Figure 6.11). Interestingly, evaluation of the marrow densities pointed toward a higher adiposity of midshaft marrow in the males of the 13 week old age group. Nonetheless, the latter failed to correlate with the results of the static histomorphometry (Figure D.2, Appendix D).

Based on the description of the 7 week old global PAR_2 null line (Georgy et al. 2012), the finding that *Osx-Cre.F2rl1*$^{\Delta/\Delta}$ female mice exhibited a high bone mass phenotype may not seem surprising. However, the results of this study otherwise depart from any possible predictions drawn based on the global model. Firstly, unlike the sex independence of findings in the global PAR_2 model, here, the high bone mass attributes were only apparent in the females and not the males. Additionally, this occurred at the later 13 week time point, later than that reported by the previous study on global knockouts. Most importantly however, a strong relationship existed in the current model between a higher rate of bone formation in the female *Osx-Cre.F2rl1*$^{\Delta/\Delta}$ group and a higher rate of mass accumulation over time. This contrasted to the observation that global PAR_2 null mice had a lower osteoblastic surface and osteoid volume at 7 weeks (Georgy et al. 2012). And finally, no difference was observed here between the genotypes with respect to static osteoblastic and osteoclastic parameters and they remained unchanged following PAR_2 ablation (Table 6.6).

In explaining the results observed, it is useful to note a few fundamental differences between the two studies. Firstly, global lack of a gene may prevent development of the processes in the tissue of interest that otherwise might not be disrupted by the lack of the gene in that particular cell lineage per se, especially if the gene spans a variety of embryonic or developmental phenomena. In other words, global targeting of a gene, may lead to the formation of complex lesions if the gene of interest plays roles in several stages of ontogeny and in different cell types, which might be difficult to interpret (Rajewsky et al. 1996; Hofker and Van Deursen 2003). In this context, as PAR_2 has been shown to be ubiquitously expressed and functional in a variety of tissues both prenatally and postnatally, the phenotype of global PAR_2 null mice may not be necessarily reflective of the role of the receptor expressed by bone cells. In fact, PAR_2 activation can stimulate the release of

various pro-inflammatory cytokines that are important for osteoclastogenesis. This may help explain the lower osteoclast surface measurements reported in the global PAR_2 null mice as well as the fewer osteoclast precursors in their bone marrow cultures (Georgy et al. 2012). The use of a conditional knockout model reported herein, was indeed an effort to overcome such shortcomings.

Secondly, *Osx* dependent deletion of PAR_2 certainly means that PAR_2 is initially expressed and present during the early stages of osteoblastogenesis. Thus, unlike the global PAR_2 null model, here, PAR_2 is being deleted from the mesenchymal cells only after their early commitment to the osteoblastic lineage and after when they become committed osteoprogenitor cells. In this regard, unlike the finding that PAR_2 is essential for osteoblastogenesis and inhibition of adipogenic differentiation of MSCs (chapter 5), deletion of PAR_2 in *Osx* expressing osteoprogenitor cells seems to stimulate the osteoblastic formation of new bone. This however, appears to require female specific factors, whether steroids or other factors, as the phenotype was not observed in males.

Thirdly, the general phenotypical characteristics and background of mice used in the current model differ significantly to those of the global PAR_2 null studies. The original work by Georgy *et al.* (2012) used mice of the 129/Sv background that were also negative for *Osx-Cre*. Given that the mass attributes of the global PAR_2 null mice decline significantly from 7 weeks to 32 weeks (Chapter 3), and in light of the subtle tendencies of the male *Osx-Cre.F2rl1*$^{\Delta/\Delta}$ mice to have inferior bone characteristics in comparison to controls (Table 6.4, Figure 6.11), it is possible that a similar osteopoenic profile occurs at a later stage. The fact that *Osx-Cre* expressing mice exhibit a phenotype of their own as reported by a previous study (Davey et al. 2011) and shown here (Figures 6.17 and 6.18) suggests that the temporal pattern of changes observed in comparison to that of the non-*Osx-Cre* counterparts may vary considerably. Moreover, the sampling in this study took place while the mice were still growing as is evident from the bone length measurements (Figure 6.6). These results highlight the possibility of substantial shifts over time which may consequently affect the bone phenotype when mice are sufficiently aged. Further longer term investigations are therefore warranted.

The substantial differences observed between the sexes in the context of osteoblast specific PAR_2 deletion highlight the significance of factors that regulate the sex specific occurrence

of bone traits. Of all, the positive change noted in the bone formation rate in females is particularly interesting. This may be the result of a direct osteoblast mediated response to female hormones, e.g. oestrogen. Although most of the effect of oestrogen on bone in females is caused by its anti-resorptive properties (Windahl et al. 2013), nevertheless, it is also known that oestrogen might stimulate bone formation (Chow et al. 1992; Kondoh et al. 2014). If such a dependency on oestrogen is somewhat enhanced in PAR_2 null osteoblasts, then the lower oestrogen values in males can explain the current results. The only known PAR_2-oestrogen interaction is the PAR_2 dependency of oestrogen induced breast cancer cell proliferation which seems to support the opposite of this notion. Regardless, this requires further investigation of hormonal variables in the preceding weeks, i.e. before week 7. It may also be that other factors that themselves depend on sex hormones, e.g. muscle mass and the resulting biomechanical variables are responsible for the observation.

All in all, the higher observed mass of bone in the female *Osx-Cre.F2rl1*$^{\Delta/\Delta}$ mice suggests an anti-osteogenic effect for PAR_2 in the regulation of bone formation by mature *Osx* expressing osteoblasts, however, in a sex dependent fashion. This work also highlights the importance of cell type specific loss of function studies in conjunction with global loss of function models in the understanding of physiological processes.

CHAPTER 7: CONCLUSIONS AND FUTURE DIRECTIONS

Bone loss is considered a multifactorial pathology with complex aetiology. The current work examines two common mechanisms involved in the pathophysiology of the condition, i.e. ageing and inflammation. Both mechanisms ultimately impact bone mass through uncoupling of bone formation and resorption causing a gradual loss of net bone mass over time (Hardy and Cooper 2009; Drake et al. 2015). This study produces evidence that PAR_2 is significant in both ageing and inflammation related bone loss due to its role in early osteoblastogenesis and cytokine induced bone resorption.

7.1 Main Findings and Implications of the Research

It is currently understood that the osteogenic and adipogenic differentiation of MSCs is mutually exclusive (Bethel et al. 2013). Evidence suggests that this reciprocal relationship may be critical in the pathology of some of the clinical conditions affecting bone (Berendsen and Olsen 2014). Importantly, the increase in the adiposity of bone marrow observed in patients affected by age related osteoporosis has been linked to a decrease in osteogenesis in favour of adipogenesis (Moerman et al. 2004; Kawai et al. 2009). This view is further supported by the observation that the osteopoenia associated with conditions of disuse or mechanical unloading, such as that caused by microgravity, is often coincident with an increased marrow adiposity (Minaire et al. 1974; Wronski et al. 1981; Ahdjoudj et al. 2002).

Despite more than four decades of research, the role of a large number of factors and genes in this adipo/osteogenic lineage relationship remains to be fully elucidated. Recent studies in the laboratory in which the current work was carried out, indicate that PAR_2 may be involved in this process. Although experiments with mice have described a high bone mass phenotype in global PAR_2 null mice at 7 weeks, lower osteoblast and osteoclast parameters as well as phenotypical changes observed over time suggested that this may be reversed by ageing (Georgy et al. 2012). Subsequent studies using PAR_2 null

primary calvarial osteoblasts demonstrated that when kept under the highly osteogenic medium conditioned by MDA-PCa-2b cells, some PAR_2 null cells start accumulating intracytosolic triacylglycerol and form adipocytes (Kularathna et al., 2015). This is accompanied by a decrease in the expression of osteoblastic markers, *Runx2* and *Col1a1* and an increase in the adipogenic *Pparg* and *Lpl* transcripts. These observations led to the hypotheses that PAR_2 promotes osteogenic conversion of mesenchymal progenitors at the expense of adipogenesis and that its *in vivo* loss, given enough time, should result in osteopoenia.

To investigate if the lack of PAR_2 induces osteopoenia in the context of ageing, this work undertook to evaluate the phenotype of 20 and 32 week old global PAR_2 null mice. Comparison of micro CT derived structural and material indices from these mice to those of the wildtype controls provided evidence that lack of PAR_2 is associated with significant deficits in the trabecular and cortical indices, however in an age and sex dependent manner. Whilst the effect of ageing is evident in both genotypes, the rate at which such age related change occurred was significantly higher in the PAR_2 null male mice. Genetic polymorphisms that affect the coding sequence, downstream signalling or expression of PAR_2 have been described (Compton et al. 2000; Lamba et al. 2008; Ma and Burstein 2013). Although not directly associated with any disease phenotype so far, these observations highlight the possibility of PAR_2's involvement in the pathology and occurrence of age related osteopoenia and osteoporosis.

To further investigate the role of the receptor in the differentiation of MSCs, PAR_2 expression was silenced in the bipotential murine Kusa 4b10 cells. Whereas regular or vector control cells treated with osteogenic medium mainly developed osteoblastic features, PAR_2 deficient cultures demonstrated a highly adipogenic profile. In essence, these observations are in keeping with a pro-osteogenic/anti-adipogenic function of the receptor in the regulation of MSC niche and lineage commitment. This conclusion offers a plausible explanation for the observation that global PAR_2 null mice exhibit lower osteoblast surface and osteoid volume than normal wildtype mice (Georgy et al. 2012). It also explains the osteopoenia observed in the ageing PAR_2 null mice as is reported by this study.

To better understand the PAR_2 regulation of the adipogenic/osteogenic relationship, the mRNA expression of a number of putative novel genes was quantitatively analysed. Consistent with previously reported findings (Kularathna 2015), *Cnr1*, *Il6*, *Ramp3* and *Enpep* were found to be more highly expressed following PAR_2 knockdown whereas the expression of *C1qtnf3*, *Snorc* and *Gpr35* was suppressed. The similarity of these observations across the two studies suggests that these genes are highly regulated and significant in the reciprocal relationship between adipogenesis and osteogenesis. This also proposes a lower place for these GOIs than PAR_2 in the hierarchy of signalling regulators of adipo/osteogenesis. The results indicate that further study of the roles of these GOIs in the temporal and hierarchical control of MSC differentiation is warranted.

Investigation of IL-6 protein concentrations in the *F2rl1* KD and vector control cultures further demonstrated its higher expression as well as secretion by the PAR_2 deficient cells very early during differentiation. Use of anti-IL-6 antibody in the medium revealed a paracrine mechanism in which PAR_2 exerted its anti-adipogenic/pro-osteogenic effect at least in part through suppression of IL-6. This also suggested an anti-osteogenic/pro-adipogenic function for IL-6 itself. The latter finding contrasted to those previous works where an anti-adipogenic role for IL-6 has been demonstrated (Xie et al. 2010). However, this is likely to be the result of differences in the physiological context of the various studies.

Although not directly investigated, it is possible that there is an interaction between PAR_2 signalling and pathways that are known to regulate adipogenesis and osteogenesis. The possibility of PAR_2-β-catenin crosstalk in osteoblasts has previously been ruled out (Kularathna et al., 2015). However, as PAR_2 has been shown to activate ERK1/2 and P38 MAPK in some cell types, crosstalk with BMP, FGF or IGF signalling is probable (Figure 1.4) Moreover, an indirect route via some of the aforementioned GOIs, i.e. *C1qtnf3* and *Snorc*, may link PAR_2 to such pathways. Complement 1q tumour necrosis factor-related protein-3 is a novel adipokine and an adiponectin paralogue (Kishore et al. 2004). It is known to exert several biological roles such as stimulating adipokine secretion (Wölfing et al. 2008), inhibiting systemic inflammation (Schmid et al. 2014), and stimulating cell proliferation (Akiyama et al. 2009). In fact, C1qtnf3 mediates the proliferation response of vascular smooth muscle cells to TGF-β1, which belongs to the same family of proteins

as BMPs (Maeda and Wakisaka 2010). Interestingly, exogenous C1qtnf3 also causes phosphorylation of ERK1/2 and P38 MAPK in both vascular smooth muscle (Maeda and Wakisaka 2010) and endothelial cells (Akiyama et al. 2007). As C1qtnf3 was found to be upregulated in the vector control Kusa 4b10 cells in the current model, such signalling mechanism via kinases may be relevant in the osteoblastic differentiation of MSCs. Small Novel Rich in Cartilage, is a type I single-pass transmembrane chondroitin sulfate proteoglycan that was first identified in mouse limb cartilage during embryogenesis (Heinonen et al. 2011) and has been since connected to chondrocyte maturation and endochondral ossification (Heinonen et al. 2017). Like C1qtnf3, Snorc was also found to be more highly expressed in the osteoblastic vector control cells. Somewhat consistent with C1qtnf3, Snorc expression in chondrocytes is stimulated by BMP-2 (Heinonen et al. 2011; Heinonen et al. 2017). Taken together, there seems to be an association between PAR_2 and the previously known signalling pathways that regulate adipogenic and osteogenic differentiation of MSCs, which might be worth investigating. On the other hand, the IL-6-STAT3 signalling pathway as was noted in chapter 5, may be a novel pathway that regulates the adipogenic conversion of MSCs (Wang et al. 2010; Zhang et al. 2011). If so, the effect of PAR_2 on adipogenesis may be conveyed by its interactions with this pathway through inhibition of IL-6 expression.

Despite the findings implying a mandate for the presence of PAR_2 during osteoblastogenesis, osteoblast specific ablation of the receptor in growing mice not only resulted in an increased rate of bone formation in 7 week old females, but also culminated in a higher bone mass profile at 13 weeks. Perhaps, the key factor explaining these results lies in the reliance of osteoblast specific ablation of PAR_2 in *Osx-Cre.F2rl1*$^{\Delta/\Delta}$ mice on *Osx* expression. The expression of *Osx* is relatively late in the temporal hierarchy of transcriptional regulators of osteoblastogenesis (Nishio et al. 2006; Ulsamer et al. 2008; Hojo et al. 2016). Whereas MSCs in the global PAR_2 null mice and *F2rl1* KD cultures constitutively lack PAR_2 at the start of their osteogenic differentiation, loss of PAR_2 in *Osx-Cre.F2rl1*$^{\Delta/\Delta}$ mice only occurs after cells are committed preosteoblasts at a later stage.

Taken together, these findings suggest that the requirement of PAR_2 for osteoblastogenesis only applies during the early stages of differentiation before *Osx* is

expressed. In this context, the paradox that female *Osx-Cre.F2rl1*$^{\Delta/\Delta}$ mice have higher rates of bone formation and accrual than controls is, therefore, indicative of a dual time and sex dependent role of the receptor in the differentiation and function of osteoblasts (Figure 7.1).

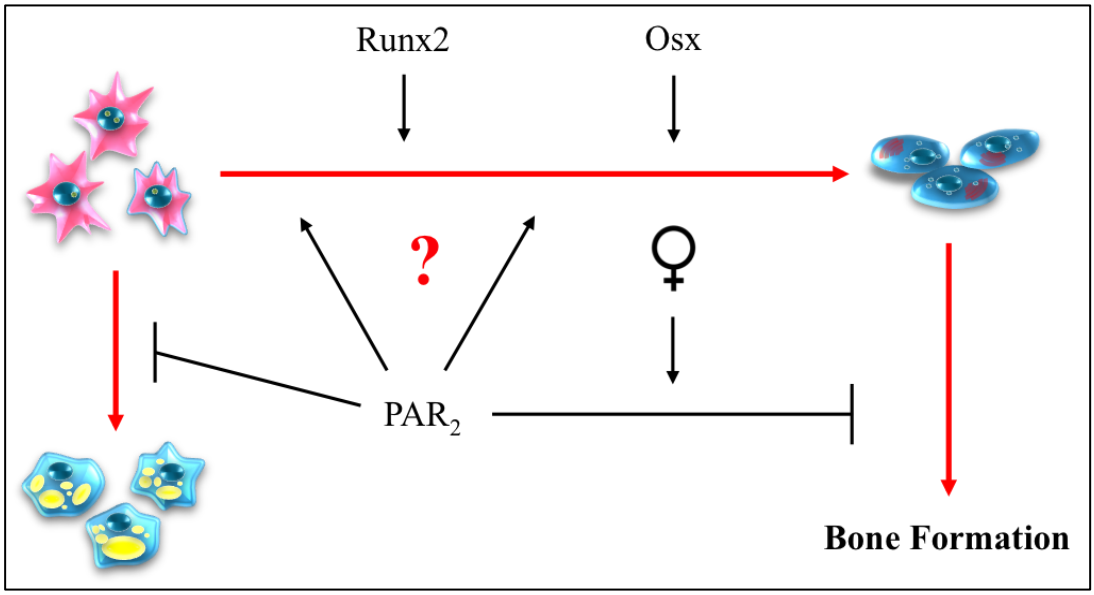


Figure 7.1 The dual role of PAR_2 in differentiation and function.

The receptor appears to regulate both differentiation and function at different times with respect to the expression of *Osx* during the ontogeny of osteoblasts with the latter being prominent in females.

Due to the significance of PAR_2 in inflammation and its possible role in inflammation induced osteopoenia, this study also undertook to investigate the latter in the mdx mice. Mdx mice are dystrophin-deficient and have been previously shown to exhibit low bone mass features analogous to those of the human DMD patients (Novotny et al. 2011; Rufo et al. 2011). Examination of PAR_2 null mdx mice revealed that these mice have an improved trabecular architecture even at relatively late time points. Further investigations (Taghavi 2016) suggested that such improvement is perhaps due to reduced circulating IL-6 levels, which tends to have a limiting effect on osteoclastogenesis and bone resorption. In contrast to these findings, results reported in chapter 5 indicated that PAR_2 deficiency is associated with a higher expression and release of IL-6 by mesenchymal cells which appears to be somewhat paradoxical. It must be noted, however, that these

apparently opposite effects of PAR_2 activation on IL-6 secretion are associated with two different cell types, i.e. MSCs versus inflammatory cells and, therefore, are not necessarily incongruent.

In addition to the improvements observed in the bone phenotype of PAR_2 null mdx mice, lack of PAR_2 also led to a significant reduction in the severity of muscle disease, i.e. improved strength, histopathology, systemic inflammatory profile, etc. (Taghavi 2016). These observations suggest that PAR_2 antagonism may be of value in patients with muscular dystrophy. Although the advent of modern gene editing technology such as CRISPR-Cas9 system and the relatively recently developed exon skipping agents, e.g. eteplirsen hold much promise for the future of DMD treatment, a large fraction of patients still continue to receive glucocorticoids. Due to the apparently safer nature of PAR_2 deficiency, it seems tangible that PAR_2 antagonists will be able to at least partially substitute for steroids in the near future. Currently, due to potential benefits of PAR_2 antagonism in the treatment of various inflammatory, neurological and metabolic conditions, a number of such agents are under investigation and new ones are being developed (Boitano et al. 2015; Yau et al. 2016a; Yau et al. 2016b). It is, therefore, plausible to take advantage of the great wealth of this existing knowledge in the treatment of DMD.

7.2 Limitations of the Research and Future Work

As has been mentioned before, *in vivo*, the compounding impact of global loss of PAR_2 across all mesenchymal and haematopoietic bone cellular units as well as endocrine and nervous systems could make the interpretation of any resulting phenotype challenging. The study of the phenotype of cell type specific PAR_2 null mice was therefore considered appropriate, in this case using the *Osx-Cre* line.

The study of *Osx-Cre.F2rl1*$^{\Delta/\Delta}$ mice proved to be informative in that it provided insight into the osteoblast specific functions of PAR_2 with regard to the overall bone architecture and homeostasis. Nevertheless, introduction of loxP sites itself appeared to induce phenotypical attributes that need be taken into account. In the case of this study, a normalisation approach was adopted in which the ratio of values from each *Osx-Cre* and

non-*Osx-Cre* group was used for analyses. This underpins the significance of the use of appropriate controls in the conduct of such cell type specific studies.

Dynamic histomorphometry indicated that a high BFR/B.S likely explained the positive mass accrual of the female *Osx-Cre.F2rl1*$^{\Delta/\Delta}$ mice from 7 to 13 weeks. However, this difference was no longer present at the later 13 week time point. This, as well as a tendency in males to develop a slightly inferior bone phenotype to that of the *Osx-Cre.F2rl1*$^{wt/wt}$ suggests that over time, these mice may become osteopoenic. Studies of older mice, therefore, are necessary to rule out this possibility.

The high bone mass profile of the female *Osx-Cre.F2rl1*$^{\Delta/\Delta}$ mice may also be the result of a rather late gene deletion. Whilst informative per se, this caused limitations in the ability to confirm results obtained in the previous and current *in vitro* experiments. Thus, studies using other osteoblast specific transgenic lines such as *Runx2-Cre* would be advantageous to further resolve the temporal functionality of PAR_2 relative to the transcriptional regulators of *in vivo* osteoblastogenesis and osteoblastic function. The future use of CRISPR-Cas9 technology in this respect, may prove to be invaluable.

To better understand the anti-osteogenic effect of PAR_2 in *Osx-Cre.F2rl1*$^{\Delta/\Delta}$ females, an *in vitro* model using primary osteoblasts or marrow cultures separately derived from male and female mice, would be useful to confirm these findings. Further knockdown or inducible conditional knockout models using committed clonal osteoblastic cultures may also be of value. Treatment of cultures with hormonal stimuli, e.g. oestrogen, etc. may help narrow down the factors that result in the high bone profile of the *Osx-Cre.F2rl1*$^{\Delta/\Delta}$ females. Likewise, ovariectomised (OVX) *Osx-Cre.F2rl1*$^{\Delta/\Delta}$ female mice may be advantageous in further delineating the effect of sex steroids in the process and its implications in post-menopausal osteoporosis. The results may provide insight into the processes that govern bone mass which may be useful in the future development of anabolic therapeutics.

Use of the bipotential Kusa 4b10 cells demonstrated an anti-adipogenic/pro-osteogenic role for PAR_2 in the process of MSC differentiation. Due to the mutually exclusive nature of adipogenesis and osteogenesis, however, one may not be able to confidently deduce

an equal effect on both lineages. It may be that a single process, either the inhibition of adipogenesis, or stimulation of osteoblastogenesis, would be all that it is required for PAR_2 to regulate MSC fate. Further experiments using committed unipotential cell lines will be necessary to confirm the lineage specificity of these roles.

Finally, the proinflammatory role of PAR_2 in the pathogenesis of DMD is one with significant implications. It would be interesting to undertake further loss of function or drug targeting experiments in the context of inflammation induced bone disease. The implications of such studies, if successful, could potentially impact the future treatment of bone inflammatory and autoimmune conditions such as chronic recurrent multifocal osteomyelitis, Majeed syndrome and SAPHO syndrome. These disorders are all marked with chronic recurrent non-infectious inflammation of bone and associated tissues and are, with the exception of Majeed syndrome, of unknown aetiology (Falip et al. 2013; Stern and Ferguson 2013). The possibility of using agents that induce PAR_2 biased signalling provides a unique opportunity to manipulate disease specific signals which lends itself to both studying the pathophysiology involved and development of disease specific pharmacological agents (Yau et al. 2016a).

This work demonstrated that PAR_2 is an important regulator of both physiological and pathological processes that govern bone tissue. From the physiological standpoint, these results provide evidence for the receptor's involvement in the regulation of MSC fate which favours osteoblastogenesis at the expense of adipogenic differentiation. This role seems to be prominent during the earlier stages of differentiation before *Osx* is expressed. Global loss of PAR_2 in ageing mice is associated with trabecular and cortical bone impairment suggesting possible involvement of the receptor in the pathophysiology of age related bone loss. Moreover, osteoblast specific loss of function studies *in vivo* demonstrated an anti-osteogenic effect for PAR_2 in committed osteoblasts, however, only in the females. Data from the mdx mice link PAR_2 to the pathophysiology of inflammation induced osteopoenia with potential implications in the future treatment of the disease Duchenne muscular dystrophy.

REFERENCES

Aaron JE, Makins NB, Sagreiya K (1987) The microanatomy of trabecular bone loss in normal aging men and women. Clinical Orthopaedics and Related Research 215:260-271.

Abdallah BM, Kassem M (2012) New factors controlling the balance between osteoblastogenesis and adipogenesis. Bone 50:540–545.

Abou Khalil R, Yang F, Mortreux M, et al (2014) Delayed bone regeneration is linked to chronic inflammation in murine muscular dystrophy. Journal of Bone and Mineral Research 29:304–315.

Abraham LA, Chinni C, Jenkins AL, et al (2000) Expression of protease-activated receptor-2 by osteoblasts. Bone 26:7–14.

Abraham LA, Mackie EJ (1999) Modulation of osteoblast-like cell behavior by activation of protease-activated receptor-1. Journal of Bone and Mineral Research 14:1320–1329.

Acampora D, Merlo GR, Paleari L, et al (1999) Craniofacial, vestibular and bone defects in mice lacking the Distal-less-related gene Dlx5. Development 126:3795–3809.

Adams MN, Ramachandran R, Yau M-K, et al (2011) Structure, function and pathophysiology of protease activated receptors. Pharmacology & Therapeutics 130:248–282.

Adelmant G, Gilbert JD, Freytag SO (1998) Human translocation liposarcoma-CCAAT/enhancer binding protein (C/EBP) homologous protein (TLS-CHOP) oncoprotein prevents adipocyte differentiation by directly interfering with C/EBPbeta function. Journal of Biological Chemistry 273:15574–15581.

Agarwal AK, Garg A (2009) A novel heterozygous mutation in peroxisome proliferator-activated receptor-γ gene in a patient with familial partial lipodystrophy. The Journal of Clinical Endocrinology & Metabolism 87:408–408.

Ahdjoudj S, Lasmoles F, Holy X, et al (2002) Transforming growth factor β2 inhibits adipocyte differentiation induced by skeletal unloading in rat bone marrow stroma. Journal of Bone and Mineral Research 17:668–677.

Aherne W, Hull D (1966) Brown adipose tissue and heat production in the newborn infant. The Journal of Pathology 91:223–234.

Ahrens M, Ankennauer T, Schroder D, et al (1993) Expression of human bone morphogenetic proteins-2 or -4 in murine mesenchymal progenitor C3H10T½ cells induces differentiation into distinct mesenchymal cell lineages. DNA and Cell Biology 12:871–880.

Ai M, Holmen SL, Van Hul W, et al (2005) Reduced affinity to and inhibition by DKK1 form a common mechanism by which high bone mass-associated missense mutations in LRP5 affect canonical Wnt signaling. Molecular and Cellular Biology 25:4946–4955.

Ailhaud G (1982) Adipose cell differentiation in culture. Molecular and Cellular Biochemistry 49:17–31.

Akhter MP, Wells DJ, Short SJ, et al (2004) Bone biomechanical properties in LRP5 mutant mice. Bone 35:162–169.

Akiyama H, Chaboissier M-C, Martin JF, et al (2002) The transcription factor Sox9 has essential roles in successive steps of the chondrocyte differentiation pathway and is required for expression of Sox5 and Sox6. Genes & Development 16:2813–2828.

Akiyama H, Furukawa S, Wakisaka S, Maeda T (2009) Elevated expression of CTRP3/cartducin contributes to promotion of osteosarcoma cell proliferation. Oncology Reports 21:1477–1481.

Akiyama H, Furukawa S, Wakisaka S, Maeda T (2007) CTRP3/cartducin promotes proliferation and migration of endothelial cells. Molecular and Cellular Biochemistry 304:243–248.

Akune T, Ogata N, Hoshi K, et al (2002) Insulin receptor substrate-2 maintains predominance of anabolic function over catabolic function of osteoblasts. The Journal of Cell Biology 159:147–156.

Akune T, Ohba S, Kamekura S, et al (2004) PPAR γ insufficiency enhances osteogenesis through osteoblast formation from bone marrow progenitors. Journal of Clinical Investigation 113:846–855.

Al-Ani B, Saifeddine M, Hollenberg MD (1995) Detection of functional receptors for the proteinase-activated-receptor-2-activating polypeptide, SLIGRL-NH 2, in rat vascular and gastric smooth muscle. Canadian Journal of Physiology and Pharmacology 73:1203–1207.

Alarmo E-L, Kallioniemi A (2010) Bone morphogenetic proteins in breast cancer: dual role in tumourigenesis? Endocrine Related Cancer 17:R123–39.

Alberelli MA, De Candia E (2014) Functional role of protease activated receptors in vascular biology. Vascular Pharmacology 62:72–81.

Albers J, Schulze J, Beil FT, et al (2011) Control of bone formation by the serpentine receptor Frizzled-9. The Journal of Cell Biology 192:1057–1072.

Algate K, Haynes DR, Bartold PM, et al (2015) The effects of tumour necrosis factor-α on bone cells involved in periodontal alveolar bone loss; osteoclasts, osteoblasts and osteocytes. Journal of Periodontal Research 51:549–566.

Algate K, Haynes DR, Bartold PM, et al (2016) The effects of tumour necrosis factor-α on bone cells involved in periodontal alveolar bone loss; osteoclasts, osteoblasts and osteocytes. Journal of Periodontal Research 51:549–566.

Algermissen B, Sitzmann J, Nürnberg W, et al (2000) Distribution and potential biologic function of the thrombin receptor PAR-1 on human keratinocytes. Archives of Dermatological Research 292:488–495.

Ali AA, Weinstein RS, Stewart SA, et al (2011) Rosiglitazone causes bone loss in mice by suppressing osteoblast differentiation and bone formation. Endocrinology 146:1226–1235.

Allan EH, Ho PWM, Umezawa A, et al (2003) Differentiation potential of a mouse bone marrow stromal cell line. Journal of Cellular Biochemistry 90:158–169.

Almuraikhy S, Kafienah W, Bashah M, et al (2016) Interleukin-6 induces impairment in human subcutaneous adipogenesis in obesity-associated insulin resistance. Diabetologia 59:2406–2416.

An YH, Martin KL (2003) Handbook of histology methods of bone and cartilage, Humana Press. Totowa, NJ

Anbinder AL, Moraes RM, Lima GMG, et al (2016) Periodontal disease exacerbates systemic ovariectomy-induced bone loss in mice. Bone 83:241–247.

Anderson JE, Lentz DL, Johnson RB (1993) Recovery from disuse osteopenia coincident to restoration of muscle strength in mdx mice. Bone 14:625–634.

Anderson LA, McTernan PG, Barnett AH, Kumar S (2011) The effects of androgens and estrogens on preadipocyte proliferation in human adipose tissue: influence of gender and site. The Journal of Clinical Endocrinology & Metabolism 86:5045–5051.

Angel P, Karin M (1991) The role of Jun, Fos and the AP-1 complex in cell-proliferation and transformation. Biochimica et Biophysica Acta (BBA) - Reviews on Cancer 1072:129–157.

Antonio de Luis D, Sagrado MG, Aller R, et al (2012) Role of G1359A polymorphism of the cannabinoid receptor gene on weight loss and adipocytokines levels after two different hypocaloric diets. The Journal of Nutritional Biochemistry 23:287–291.

Apolinário LM, De Carvalho SC, Santo-Neto H, Marques MJ (2015) Long-Term Therapy With Omega-3 Ameliorates Myonecrosis and Benefits Skeletal Muscle Regeneration in Mdx Mice. Anat Rec (Hoboken) 298:1589–1596.

Arner P (1997) Obesity and the adipocyte. Regional adipocity in man. Journal of Endocrinology 155:191-192.

Arts J, Kuiper GGJM, Janssen JMMF, et al (2011) Differential expression of estrogen receptors α and β mRNA during differentiation of human osteoblast SV-HFO cells. Endocrinology 138:5067–5070.

Asfaha S, Brussee V, Chapman K, et al (2002) Proteinase-activated receptor-1 agonists attenuate nociception in response to noxious stimuli. British Journal of Pharmacology 135:1101–1106.

Aslan H, Ravid Amir O, Clancy BM, et al (2006) Advanced molecular profiling in vivo detects novel function of dickkopf-3 in the regulation of bone formation. Journal of Bone and Mineral Research 21:1935–1945.

Aubert RE, Herrera V, Chen W, et al (2010) Rosiglitazone and pioglitazone increase fracture risk in women and men with type 2 diabetes. Diabetes, Obesity and Metabolism 12:716–721.

Austin KM, Covic L, Kuliopulos A (2013a) Matrix metalloproteases and PAR1 activation. Blood 121:431–439.

Austin KM, Nguyen N, Javid G, et al (2013b) Noncanonical matrix metalloprotease-1-protease-activated receptor-1 signaling triggers vascular smooth muscle cell dedifferentiation and arterial stenosis. Journal of Biological Chemistry 288:23105–23115.

Bakker AD, Klein-Nulend J (2012) Osteoblast Isolation from Murine Calvaria and Long Bones. In: Helfrich M., Ralston S. (eds) Bone Research Protocols. Methods in Molecular Biology (Methods and Protocols). Humana Press, Totowa, NJ, pp 19–29.

Baron R, Kneissel M (2013) WNT signaling in bone homeostasis and disease: from human mutations to treatments. Nature Medicine 19:179–192.

Barroso I, Gurnell M, Crowley VEF, et al (1999) Dominant negative mutations in human PPARgamma associated with severe insulin resistance, diabetes mellitus and hypertension. Nature 402:880–883.

Bastidas-Coral AP, Bakker AD (2016) Cytokines TNF-α, IL-6, IL-17F, and IL-4 Differentially affect osteogenic differentiation of human adipose stem cells. Stem Cells International 2016:1–9.

Battinelli EM, Markens BA, Kulenthirarajan RA, et al (2014) Anticoagulation inhibits tumor cell–mediated release of platelet angiogenic proteins and diminishes platelet angiogenic response. Blood 123:101–112.

Baum R, Gravallese EM (2013) Impact of Inflammation on the Osteoblast in Rheumatic Diseases. Current Osteoporosis Reports 12:9–16.

Beecher KL, Andersen TT, Fenton JW, Festoff BW (1994) Thrombin receptor peptides induce shape change in neonatal murine astrocytes in culture. Journal of Neuroscience Research 37:108–115.

Beenken A, Mohammadi M (2009) The FGF family: biology, pathophysiology and therapy. Nature Reviews Drug Discovery 8:235–253.

Bennett CN, Longo KA, Wright WS, et al (2005) Regulation of osteoblastogenesis and bone mass by Wnt10b. Proceedings of the National Academy of Sciences 102:3324–3329.

Bennett CN, Ouyang H, Ma YL, et al (2007) Wnt10b Increases Postnatal Bone Formation by Enhancing Osteoblast Differentiation. Journal of Bone and Mineral Research 22:1924–1932.

Bennett CN, Ross SE, Longo KA, et al (2002) Regulation of Wnt signaling during adipogenesis. Journal of Biological Chemistry 277:30998–31004.

Bennett JH, Joyner CJ, Triffitt JT, Owen ME (1991) Adipocytic cells cultured from marrow have osteogenic potential. Journal of Cell Science 99 (Pt 1):131–139.

Berberoglu Z, Gursoy A, Bayraktar N, et al (2007) Rosiglitazone decreases serum bone-specific alkaline phosphatase activity in postmenopausal diabetic women. The Journal of Clinical Endocrinology & Metabolism 92:3523–3530.

Berendsen AD, Olsen BR (2013) How vascular endothelial growth factor-a (VEGF) regulates differentiation of mesenchymal stem cells. Journal of Histochemistry & Cytochemistry 62:103–108.

Berendsen AD, Olsen BR (2014) Osteoblast–adipocyte lineage plasticity in tissue development, maintenance and pathology. Cellular and Molecular Life Sciences 71:493–497.

Beresford JN, Bennett JH, Devlin C, et al (1992) Evidence for an inverse relationship between the differentiation of adipocytic and osteogenic cells in rat marrow stromal cell cultures. Journal of Cell Science 102 (Pt 2):341–351.

Berridge MJ (2009) Inositol trisphosphate and calcium signalling mechanisms. Biochimica et Biophysica Acta (BBA) - Molecular Cell Research 1793:933–940.

Bethel M, Chitteti BR, Srour EF, Kacena MA (2013) The changing balance between osteoblastogenesis and adipogenesis in aging and its impact on hematopoiesis. Current Osteoporosis Reports 11:99–106.

Béliveau F, Désilets A, Leduc R (2009) Probing the substrate specificities of matriptase, matriptase-2, hepsin and DESC1 with internally quenched fluorescent peptides. The FEBS Journal 276:2213–2226.

Bi P, Yue F, Karki A, et al (2016) Notch activation drives adipocyte dedifferentiation and tumorigenic transformation in mice. Journal of Experimental Medicine 213:2019–2037.

Bialek P, Kern B, Yang X, et al (2004) A twist code determines the onset of osteoblast differentiation. Developmental Cell 6:423–435.

Bialek P, Parkington J, Li X, et al (2014) A myostatin and activin decoy receptor

enhances bone formation in mice. Bone 60:162–171.

Bilić J, Huang Y-L, Davidson G, et al (2007) Wnt induces lrp6 signalosomes and promotes dishevelled-dependent LRP6 phosphorylation. Science 316:1619–1622.

Bland R (2000) Steroid hormone receptor expression and action in bone. Clinical Science 98:217–240.

Boitano S, Hoffman J, Flynn AN, et al (2015) The novel PAR2 ligand C391 blocks multiple PAR2 signalling pathways in vitro and in vivo. British Journal of Pharmacology 172:4535–4545.

Boland GM, Perkins G, Hall DJ, Tuan RS (2004) Wnt 3a promotes proliferation and suppresses osteogenic differentiation of adult human mesenchymal stem cells. Journal of Cellular Biochemistry 93:1210–1230.

Bonewald LF (2011) The amazing osteocyte. Journal of Bone and Mineral Research 26:229–238.

Boskey AL, PG R (2013) The composition of bone. In: Rosen CJ, Bouillon R, Compston JE (eds), Primer on the metabolic bone diseases and disorders of mineral metabolism. 8 edn. Wiley, pp 49–58.

Bostick, B., Yue, Y., Long, C., Marschalk, N., Fine, D. M., Chen, J., & Duan, D. (2009). Cardiac expression of a mini-dystrophin that normalizes skeletal muscle force only partially restores heart function in aged mdx mice. Molecular Therapy, 17(2), 253–261.

Bouloumié A, Sengenès C, Portolan G, et al (2001) Adipocyte produces matrix metalloproteinases 2 and 9. Diabetes 50:2080–2086.

Bourin P, Bunnell BA, Casteilla L, et al (2013) Stromal cells from the adipose tissue-derived stromal vascular fraction and culture expanded adipose tissue-derived stromal/stem cells: a joint statement of the International Federation for Adipose Therapeutics and Science (IFATS) and the International Society for Cellular Therapy (ISCT). Cytotherapy 15:641–648.

Bouxsein ML, Boyd SK, Christiansen BA, et al (2010) Guidelines for assessment of bone microstructure in rodents using micro–computed tomography. Journal of Bone and Mineral Research 25:1468–1486.

Bowers RR, Kim JW, Otto TC, Lane MD (2006) Stable stem cell commitment to the adipocyte lineage by inhibition of DNA methylation: role of the BMP-4 gene. Proceedings of the National Academy of Sciences 103:13022–13027.

Bowers RR, Lane MD (2007) A Role for bone morphogenetic protein-4 in adipocyte development. Cell Cycle 6:385–389.

Boyce BF (2013a) Advances in the regulation of osteoclasts and osteoclast functions. Journal of Dental Research 92:860–867.

Boyce BF (2013b) Advances in the regulation of osteoclasts and osteoclast functions. Journal of Dental Research 92:860–867.

Boyce BF, Rosenberg E, de Papp AE, Duong LT (2012) The osteoclast, bone remodelling and treatment of metabolic bone disease. European Journal of Clinical Investigation 42:1332–1341.

Böhm SK, Khitin LM, Grady EF, et al (1996a) Mechanisms of desensitization and resensitization of proteinase-activated receptor-2. Journal of Biological Chemistry 271:22003–22016.

Böhm SK, Kong W, Bromme D, et al (1996b) Molecular cloning, expression and potential functions of the human proteinase-activated receptor-2. Biochemical Journal 314 (Pt 3):1009–1016.

Bretschneider E, Kaufmann R, Braun M, et al (2001) Evidence for functionally active protease-activated receptor-4 (PAR-4) in human vascular smooth muscle cells. British Journal of Pharmacology 132:1441–1446.

Buresi MC, Buret AG, Hollenberg MD, MacNaughton WK (2002) Activation of proteinase-activated receptor 1 stimulates epithelial chloride secretion through a unique MAP kinase- and cyclo-oxygenase-dependent pathway. The FASEB Journal 16:1515–1525.

Burger EH, Klein-Nulend J (1999) Mechanotransduction in bone - role of the lacuno-canalicular network. The FASEB Journal 13:S101–S112.

Burns RB, Dobson CB (1981) Standard error of the difference between means. In: Burns RB, Dobson CB (eds), Experimental psychology. Springer, Netherlands, Dordrecht, pp 151–157.

Cai X, Gong P, Huang Y, Lin Y (2011) Notch signalling pathway in tooth development and adult dental cells. Cell Proliferation 44:495–507.

Cakouros D, Raices RM, Gronthos S, Glackin CA (2010) Twist-ing cell fate: mechanistic insights into the role of twist in lineage specification/differentiation and tumorigenesis. Journal of Cellular Biochemistry 110:1288–1298.

Camerer E, Barker A, Duong DN, et al (2010) Local protease signaling contributes to neural tube closure in the mouse embryo. Developmental Cell 18:25–38.

Camerer E, Huang W, Coughlin SR (2000) Tissue factor- and factor X-dependent activation of protease-activated receptor 2 by factor VIIa. Proceedings of the National Academy of Sciences 97:5255–5260.

Camerer E, Kataoka H, Kahn M, et al (2002) Genetic evidence that protease-activated receptors mediate factor Xa signaling in endothelial cells. Journal of Biological Chemistry 277:16081–16087.

Canalis E, Parker K, Zanotti S (2012) Gremlin1 is required for skeletal development and postnatal skeletal homeostasis. Journal of Cellular Physiology 227:269–277.

Cannon B, Nedergaard J (2008) Developmental biology: neither fat nor flesh. Nature 454:947-948.

Cao Z, Umek RM, McKnight SL (1991) Regulated expression of three C/EBP isoforms during adipose conversion of 3T3-L1 cells. Genes & Development 5:1538–1552.

Carlevaro MF, Cermelli S, Cancedda R, Cancedda FD (2000) Vascular endothelial growth factor (VEGF) in cartilage neovascularization and chondrocyte differentiation: auto-paracrine role during endochondral bone formation. Journal of Cell Science 113:59–69.

Carreira AC, Lojudice FH, Halcsik E, et al (2014) Bone morphogenetic proteins facts, challenges, and future perspectives. Journal of Dental Research 93:335–345.

Case N, Rubin J (2010) Beta-catenin--a supporting role in the skeleton. Journal of Cellular Biochemistry 110:545–553.

Catalioto R-M, Gaillard D, Ailhaud G, Négrel R (2009) terminal differentiation of mouse preadipocyte cells: the mitogenic-adipogenic role of growth hormone is mediated by the protein kinase C signalling pathway. Growth Factors 6:255–264.

Cattaruzza F, Amadesi S, Carlsson JF, et al (2014) Serine proteases and protease-activated receptor 2 mediate the proinflammatory and algesic actions of diverse stimulants. British Journal of Pharmacology 171:3814–3826.

Cavanaugh KP, Gurwitz D, Cunningham DD, Bradshaw RA (1990) Reciprocal modulation of astrocyte stellation by thrombin and protease Nexin-1. Journal of Neurochemistry 54:1735–1743.

Chan TF, Couchourel D, Abed É, et al (2011) Elevated Dickkopf-2 levels contribute to the abnormal phenotype of human osteoarthritic osteoblasts. Journal of Bone and Mineral Research 26:1399–1410.

Charbord P, Tavian M, Humeau L, Peault B (1996) Early ontogeny of the human marrow from long bones: an immunohistochemical study of hematopoiesis and its microenvironment. Blood 87:4109–4119.

Chartoumpekis DV, Palliyaguru DL, Wakabayashi N, et al (2015) Notch intracellular domain overexpression in adipocytes confers lipodystrophy in mice. Molecular Metabolism 4:543–550.

Chen D (1998) Differential roles for bone morphogenetic protein (BMP) receptor type IB and IA in differentiation and specification of mesenchymal precursor cells to osteoblast and adipocyte lineages. The Journal of Cell Biology 142:295–305.

Chen G, Deng C, Li Y-P (2012) TGF-β and BMP signaling in osteoblast differentiation and bone formation. International Journal of Biological Sciences 8:272–288.

Chen H, Shoumura S, Emura S, Bunai Y (2008) Regional variations of vertebral trabecular bone microstructure with age and gender. Osteoporosis International 19:1473–1483.

Chen H, Zhou X, Shoumura S, et al (2010) Age- and gender-dependent changes in three-dimensional microstructure of cortical and trabecular bone at the human femoral neck. Osteoporosis International 21:627–636.

Chen J, Ishii M, Wang L, et al (1994a) Thrombin receptor activation. Confirmation of the intramolecular tethered liganding hypothesis and discovery of an alternative intermolecular liganding mode. Journal of Biological Chemistry 269:16041–16045.

Chen Q, Liu W, Sinha KM, et al (2013) Identification and characterization of microRNAs controlled by the osteoblast-specific transcription factor Osterix. PLoS One 8:e58104.

Chen YH, Pouysségur J, Courtneidge SA, Van Obberghen-Schilling E (1994b) Activation of Src family kinase activity by the G protein-coupled thrombin receptor in growth-responsive fibroblasts. Journal of Biological Chemistry 269:27372–27377.

Cheung W-M, Andrade-Gordon P, Derian CK, Damiano BP (2011) Receptor-activating peptides distinguish thrombin receptor (PAR-1) and protease activated receptor 2 (PAR-2) mediated hemodynamic responses in vivo. Canadian Journal of Physiology and Pharmacology 76:16–25.

Chiu L-L, Perng D-W, Yu C-H, et al (2007) Mold allergen, pen C 13, induces IL-8 expression in human airway epithelial cells by activating protease-activated receptor 1 and 2. The Journal of Immunology 178:5237–5244.

Chong ASC, Hashim R, Chow-Yang L, Ali AB (2002) Partial characterization and activities of proteases from the digestive tract of discus fish (Symphysodon aequifasciata). Aquaculture 203:321–333.

Chow J, Tobias JH, Colston KW, Chambers TJ (1992) Estrogen maintains trabecular bone volume in rats not only by suppression of bone resorption but also by stimulation of bone formation. Journal of Clinical Investigation 89:74–78.

Chow JM, Moffatt JD, Cocks TM (2000) Effect of protease-activated receptor (PAR)-1, −2 and −4-activating peptides, thrombin and trypsin in rat isolated airways. British Journal of Pharmacology 131:1584–1591.

Chow JW, Wilson AJ, Chambers TJ, Fox SW (1998) Mechanical loading stimulates bone formation by reactivation of bone lining cells in 13-week-old rats. Journal of Bone and Mineral Research 13:1760–1767.

Chui PC, Guan H-P, Lehrke M, Lazar MA (2005) PPARγ regulates adipocyte cholesterol metabolism via oxidized LDL receptor 1. Journal of Clinical Investigation 115:2244–2256.

Cicala C, Morello S, Santagada V, et al (2001) Pharmacological dissection of vascular effects caused by activation of protease-activated receptors 1 and 2 in anesthetized rats. The FASEB Journal 15:1433–1435.

Civitelli R, Beyer EC, Warlow PM, et al (1993) Connexin43 mediates direct

intercellular communication in human osteoblastic cell networks. Journal of Clinical Investigation 91:1888–1896.

Cladman W, Chidiac P (2002) Characterization and comparison of RGS2 and RGS4 as GTPase-activating proteins for m2 muscarinic receptor-stimulated G(i). Molecular Pharmacology 62:654–659.

Clarke B (2008) Normal bone anatomy and physiology. Clinical Journal of the American Society of Nephrology 3:S131–S139.

Cock TA, Back J, Elefteriou F, et al (2004) Enhanced bone formation in lipodystrophic PPARγhyp/hyp mice relocates haematopoiesis to the spleen. EMBO reports 5:1007–1012.

Cocks TM, Sozzi V, Moffatt JD, Selemidis S (1999) Protease-activated receptors mediate apamin-sensitive relaxation of mouse and guinea pig gastrointestinal smooth muscle. Gastroenterology 116:586–592.

Colvard DS, Eriksen EF, Keeting PE, et al (1989) Identification of androgen receptors in normal human osteoblast-like cells. Proceedings of the National Academy of Sciences 86:854–857.

Compton SJ, Cairns JA, Palmer KJ, et al (2000) A polymorphic protease-activated receptor 2 (PAR2) displaying reduced sensitivity to trypsin and differential responses to PAR agonists. Journal of Biological Chemistry 275:39207–39212.

Corselli M, Chen C-W, Bin Sun, et al (2012) The tunica adventitia of human arteries and veins as a source of mesenchymal stem cells. Stem Cells and Development 21:1299–1308.

Corselli M, Crisan M, Murray IR, et al (2013) Identification of perivascular mesenchymal stromal/stem cells by flow cytometry. Cytometry Part A 83A:714–720.

Corvera CU, Déry O, McConalogue K, et al (1997) Mast cell tryptase regulates rat colonic myocytes through proteinase-activated receptor 2. Journal of Clinical Investigation 100:1383–1393.

Cottrell GS, Amadesi S, Grady EF, Bunnett NW (2004) Trypsin IV, a novel agonist of protease-activated receptors 2 and 4. Journal of Biological Chemistry 279:13532–13539.

Coulton GR, Morgan JE, Partridge TA, Sloper JC (1988) The mdx mouse skeletal muscle myopathy: I. A histological, morphometric and biochemical investigation. Neuropathology and Applied Neurobiology 14:53–70.

Cousin B, Munoz O, André M, et al (1999) A role for preadipocytes as macrophage-like cells. The FASEB Journal 13:305–312.

Covic L, Gresser AL, Kuliopulos A (2000) biphasic kinetics of activation and signaling for PAR1 and PAR4 thrombin receptors in platelets. Biochemistry 39:5458–5467.

Cuffe JE, Bertog M, Velázquez Rocha S, et al (2002) Basolateral PAR-2 receptors mediate KCl secretion and inhibition of Na^+ absorption in the mouse distal colon. The Journal of Physiology 539:209–222.

Cumashi A, Ansuini H, Celli N, De Blasi A (2001) Neutrophil proteases can inactivate human PAR3 and abolish the co-receptor function of PAR3 on murine platelets. Thrombosis and Haemostasis 85:533-538.

Dankbar B, Fennen M, Brunert D, et al (2015) Myostatin is a direct regulator of osteoclast differentiation and its inhibition reduces inflammatory joint destruction in mice. Nature Medicine 21:1085–1090. d

Darlington GJ, Ross SE, MacDougald OA (1998) The role of C/EBP genes in adipocyte differentiation. Journal of Biological Chemistry 273:30057–30060.

Davey RA, Clarke MV, Sastra S, et al (2011) Decreased body weight in young Osterix-Cre transgenic mice results in delayed cortical bone expansion and accrual. Transgenic Research 21:885–893.

de Jonge E, Friederich PW, Vlasuk GP, et al (2003) Activation of coagulation by administration of recombinant factor VIIa elicits interleukin 6 (IL-6) and IL-8 release in healthy human subjects. Clin Diagn Lab Immunol 10:495–497.

Deconinck N, Dan B (2007) Pathophysiology of Duchenne muscular dystrophy: current hypotheses. Pediatric Neurology 36:1–7.

DeFea KA, Zalevsky J, Thoma MS, et al (2000) β-Arrestin–dependent endocytosis of proteinase-activated receptor 2; is required for intracellular targeting of activated Erk1/2. The Journal of Cell Biology 148:1267–1282.

Deldar A, Weiss L, Lewis H (1985) Bone lining cells and hematopoiesis: An electron microscopic study of canine bone marrow. The Anatomical Record 213:187–201.

Dempster DW, Compston JE, Drezner MK, et al (2012) Standardized nomenclature, symbols, and units for bone histomorphometry: A 2012 update of the report of the ASBMR Histomorphometry Nomenclature Committee. Journal of Bone and Mineral Research 28:2–17.

Dequeker J (1971) Periosteal and endosteal surface remodeling in pathologic conditions. Investigative Radiology 6:260–265.

Derian CK, Damiano BP, Addo MF, et al (2003) Blockade of the thrombin receptor protease-activated receptor-1 with a small-molecule antagonist prevents thrombus formation and vascular occlusion in nonhuman primates. Journal of Pharmacology and Experimental Therapeutics 304:855–861.

Derynck R, Zhang Y, Feng X-H (1998) Transcriptional activators of TGF-β responses: Smads. Cell 95:737–740.

Devchand PR, Keller H, Peters JM, Vazquez M (1996) The PPARa-leukotriene B4 pathway to inflammation control. Nature 384:39-43.

Déry O, Thoma MS, Wong H, et al (1999) Trafficking of proteinase-activated receptor-2 and beta-arrestin-1 tagged with green fluorescent protein. beta-Arrestin-dependent endocytosis of a proteinase receptor. Journal of Biological Chemistry 274:18524–18535.

Di Iorgi N, Mittelman SD, Gilsanz V (2008) Differential effect of marrow adiposity and visceral and subcutaneous fat on cardiovascular risk in young, healthy adults. International Journal of Obesity 32:1854–1860.

Diarra D, Stolina M, Polzer K, Zwerina J (2007) Dickkopf-1 is a master regulator of joint remodeling. Nature 13:156–163.

Dodig M, Kronenberg MS, Bedalov A, et al (1996) Identification of a TAAT-containing motif required for high level expression of the COL1A1 promoter in differentiated osteoblasts of transgenic mice. Journal of Biological Chemistry 271:16422–16429.

Dodig M, Tadic T, Kronenberg MS, et al (1999) Ectopic Msx2 overexpression inhibits and Msx2 antisense stimulates calvarial osteoblast differentiation. Developmental Biology 209:298–307.

Dong X-Y, Tang S-Q (2010) Insulin-induced gene: A new regulator in lipid metabolism. Peptides 31:2145–2150.

Dorheim MA, Sullivan M, Dandapani V, et al (1993) Osteoblastic gene expression during adipogenesis in hematopoietic supporting murine bone marrow stromal cells. Journal of Cellular Physiology 154:317–328.

Drake MT, Clarke BL, Lewiecki EM (2015) The Pathophysiology and Treatment of Osteoporosis. Clinical Therapeutics 37:1837–1850.

Dreyer C, Krey G, Keller H, et al (1992) Control of the peroxisomal β-oxidation pathway by a novel family of nuclear hormone receptors. Cell 68:879–887.

Ducy P, Karsenty G (1995) Two distinct osteoblast-specific cis-acting elements control expression of a mouse osteocalcin gene. Molecular and Cellular Biology 15:1858–1869.

Ducy P, Zhang R, Geoffroy V, et al (1997) Osf2/Cbfa1: A transcriptional activator of osteoblast differentiation. Cell 89:747–754.

Dudley AT, Lyons KM, Robertson EJ (1995) A requirement for bone morphogenetic protein-7 during development of the mammalian kidney and eye. Genes & Development 9:2795–2807.

Dulon S, Candé C, Bunnett NW, et al (2003) Proteinase-activated receptor-2 and human

lung epithelial cells. 28:339–346.

Dulon S, Leduc D, Cottrell GS, et al (2005) Pseudomonas aeruginosa elastase disables proteinase-activated receptor 2 in respiratory epithelial cells. 32:411–419.

Duque G, Li W, Adams M, et al (2011) Effects of risedronate on bone marrow adipocytes in postmenopausal women. Osteoporosis International 22:1547–1553.

Eghbali-Fatourechi G, Khosla S, Sanyal A, et al (2003) Role of RANK ligand in mediating increased bone resorption in early postmenopausal women. Journal of Clinical Investigation 111:1221–1230.

Elefteriou F, Yang X (2011) Genetic mouse models for bone studies--strengths and limitations. Bone 49:1242–1254.

Epker BN, Frost HM (1966) Periosteal appositional bone growth from age two to age seventy in man. A tetracycline evaluation. The Anatomical Record 154:573–577.

Epker BN, Frost HM (1965) A histological study of remodeling at the periosteal, haversian canal, cortical endosteal, and trabecular endosteal surfaces in human rib. The Anatomical Record 152:129–135.

Erlanger BF, Kokowsky N, Cohen W (1961) The preparation and properties of two new chromogenic substrates of trypsin. Archives of Biochemistry and Biophysics 95:271–278.

Evans H, de Lahunta A (2013) Miller's anatomy of the dog, 4 edn. Elsevier, St. Louis, Missouri

Everts V, Delaisse JM, Korper W, et al (2002) The bone lining cell: Its role in cleaning howship's lacunae and initiating bone formation. Journal of Bone and Mineral Research 17:77–90.

Fakhry M, Hamade E, Badran B, et al (2013) Molecular mechanisms of mesenchymal stem cell differentiation towards osteoblasts. World Journal of Stem Cells 5:136–148.

Falip C, Alison M, Boutry N, et al (2013) Chronic recurrent multifocal osteomyelitis (CRMO): a longitudinal case series review. Pediatric Radiology 43:355–375.

Fallarini S, Magliulo L, Paoletti T, et al (2010) Expression of functional GPR35 in human iNKT cells. Biochemical and Biophysical Research Communications 398:420–425.

Faurschou M, Borregaard N (2003) Neutrophil granules and secretory vesicles in inflammation. Microbes and Infection 5:1317–1327.

Faust IM, Miller WH (1983) Hyperplastic growth of adipose tissue in obesity. The adipocyte and obesity. Cellular and Molecular Mechanisms 41-51.

Fedorenko A, Lishko PV, Kirichok Y (2012) Mechanism of fatty-acid-dependent UCP1

uncoupling in brown fat mitochondria. Cell 151:400–413.

Ferrell WR, Lockhart JC, Kelso EB, et al (2003) Essential role for proteinase-activated receptor-2 in arthritis. Journal of Clinical Investigation 111:35–41.

Fields RC, Schoenecker JG, Hart JP, et al (2003) Protease-activated receptor-2 signaling triggers dendritic cell development. The American Journal of Pathology 162:1817–1822.

Fleury A, Hoch L, Martinez MC, et al (2016) Hedgehog associated to microparticles inhibits adipocyte differentiation via a non-canonical pathway. Scientific Reports 6:23479.

Florencio-Silva R, Sasso GRDS, Sasso-Cerri E, et al (2015) Biology of bone tissue: structure, function, and factors that influence bone cells. BioMed Research International.

Fontaine C, Cousin W, Plaisant M, et al (2008) Hedgehog signaling alters adipocyte maturation of human mesenchymal stem cells. Stem Cells International 26:1037–1046.

Franceschi RT, Wang D, Krebsbach PH, Rutherford RB (2000) Gene therapy for bone formation: in vitro and in vivo osteogenic activity of an adenovirus expressing BMP7. Journal of Cellular Biochemistry 78:476–486.

Francke U (1999) Williams-Beuren syndrome:genes and mechanisms. Human Molecular Genetics 8:1947–1954.

Franco GCN, Kajiya M, Nakanishi T, et al (2011) Inhibition of matrix metalloproteinase-9 activity by doxycycline ameliorates RANK ligand-induced osteoclast differentiation in vitro and in vivo. Experimental Cell Research 317:1454–1464.

Franz Odendaal TA, Hall BK, Witten PE (2006) Buried alive: How osteoblasts become osteocytes. Developmental Dynamics 235:176–190.

Freytag SO, Geddes TJ (1992) Reciprocal regulation of adipogenesis by Myc and C/EBP alpha. Science 256:379–382.

Fu M, Rao M, Bouras T, et al (2005) Cyclin D1 inhibits peroxisome proliferator-activated receptor gamma-mediated adipogenesis through histone deacetylase recruitment. Journal of Biological Chemistry 280:16934–16941.

Fujino T, Asaba H, Kang M-J, et al (2003) Low-density lipoprotein receptor-related protein 5 (LRP5) is essential for normal cholesterol metabolism and glucose-induced insulin secretion. Proceedings of the National Academy of Sciences 100:229–234.

Fukumura D, Ushiyama A, Duda DG, et al (2003) Paracrine regulation of angiogenesis

and adipocyte differentiation during in vivo adipogenesis. Circulation Research 93:e88–97.

Fukuyo S, Yamaoka K, Sonomoto K, et al (2014) IL-6-accelerated calcification by induction of ROR2 in human adipose tissue-derived mesenchymal stem cells is STAT3 dependent. Rheumatology (Oxford) 53:1282–1290.

Furman MI, Krueger LA, Frelinger AL III, et al (2000a) GPIIb-IIIa antagonist-induced reduction in platelet surface factor V/Va binding and phosphatidylserine expression in whole blood. Thrombosis and Haemostasis 84:492–498.

Furman MI, Nurden P, Berndt MC (2000b) The cleaved peptide of PAR1 results in a redistribution of the platelet surface GPIb-IX-V complex to the surface-connected canalicular system. Thrombosis and Haemostasis 84:897–903.

Gao C, Liu S, Hu HZ, et al (2002) Serine proteases excite myenteric neurons through protease-activated receptors in guinea pig small intestine. Gastroenterology 123:1554–1564.

Gaskinst HR, Kim JW, Wright JT, et al (2009) Regulation of insulin-like growth factor-1 ribonucleic acid expression, polypeptide secretion, and binding protein activity by growth hormone in porcine preadipocyte cultures. Endocrinology 126:622–630.

Gazzerro E, Pereira RC, Jorgetti V, et al (2005) Skeletal overexpression of gremlin impairs bone formation and causes osteopenia. Endocrinology 146:655–665.

Ge L (2003) A β-arrestin-dependent scaffold is associated with prolonged MAPK activation in pseudopodia during Protease-activated Receptor-2-induced chemotaxis. Journal of Biological Chemistry 278:34418–34426.

Ge Q, Maury E, Rycken L, et al (2012) Endocannabinoids regulate adipokine production and the immune balance of omental adipose tissue in human obesity. International Journal of Obesity 37:874–880.

Gearing KL, Göttlicher M, Teboul M, et al (1993) Interaction of the peroxisome-proliferator-activated receptor and retinoid X receptor. Proceedings of the National Academy of Sciences 90:1440–1444.

Geloen A, Collet AJ, Guay G, Bukowiecki LJ (1989a) Insulin stimulates in vivo cell proliferation in white adipose tissue. The American journal of physiology 256:C190–6.

Geloen A, Roy PE, Bukowiecki LJ (1989b) Regression of white adipose tissue in diabetic rats. The American journal of physiology 257:E547–53.

Geoffroy V, Kneissel M, Fournier B, et al (2002) High bone resorption in adult aging transgenic mice overexpressing cbfa1/runx2 in cells of the osteoblastic lineage. Molecular and Cellular Biology 22:6222–6233.

Georgy SR, Pagel CN, Ghasem-Zadeh A, et al (2012) Proteinase-activated receptor-2 is required for normal osteoblast and osteoclast differentiation during skeletal growth

and repair. Bone 50:704–712.

Georgy SR, Pagel CN, Wong DM, et al (2010) Proteinase-activated receptor-2 (PAR2) and mouse osteoblasts: Regulation of cell function and lack of specificity of PAR2-activating peptides. Clinical and Experimental Pharmacology and Physiology 37:328–336.

Gesta S, Tseng Y-H, Kahn CR (2007) Developmental origin of fat: Tracking obesity to its source. Cell 131:242–256.

Gieseler F, Ungefroren H, Settmacher U, et al (2013) Proteinase-activated receptors (PARs) – focus on receptor-receptor-interactions and their physiological and pathophysiological impact. Cell Communication and Signaling 11:86.

Gilbert L, He X, Farmer P, et al (2000) Inhibition of osteoblast differentiation by tumor necrosis factor-α. Endocrinology 141:3956–3964.

Gimble JM, Robinson CE, Wu X, Kelly KA (1996) The function of adipocytes in the bone marrow stroma: an update. Bone 19:421–428.

Giorgetti S, Ballotti R, Kowalski-Chauvel A, et al (1993) The insulin and insulin-like growth factor-I receptor substrate IRS-1 associates with and activates phosphatidylinositol 3-kinase in vitro. Journal of Biological Chemistry 268:7358–7364.

Glatt V, Canalis E, Stadmeyer L, Bouxsein ML (2007) Age-related changes in trabecular architecture differ in female and male C57BL/6J mice. Journal of Bone and Mineral Research 22:1197–1207.

Gordeladze JO, Reseland JE, Duroux-Richard I (2010) From stem cells to bone: phenotype acquisition, stabilization, and tissue engineering in animal models. ILAR Journal 51:42–61.

Goulet RW, Goldstein SA, Ciarelli MJ, et al (1994) The relationship between the structural and orthogonal compressive properties of trabecular bone. Journal of Biomechanics 27:375–389.

Grady RM, Teng H, Nichol MC, et al (1997) Skeletal and cardiac myopathies in mice lacking utrophin and dystrophin: A model for Duchenne muscular dystrophy. Cell 90:729–738.

Gravallese EM, Harada Y, Wang JT, et al (1998) Identification of cell types responsible for bone resorption in rheumatoid arthritis and juvenile rheumatoid arthritis. The American Journal of Pathology 152:943–951.

Gregoire FM, Smas CM, Sul HS (1998) Understanding adipocyte differentiation. Physiological Reviews 78:783-809.

Grey A (2008) Skeletal consequences of thiazolidinedione therapy. Osteoporosis International 19:129–137.

Grey A, Chen Q, Xu X, et al (2003) Parallel phosphatidylinositol-3 kinase and p42/44 mitogen-activated protein kinase signaling pathways subserve the mitogenic and antiapoptotic actions of insulin-like growth factor i in osteoblastic cells. Endocrinology 144:4886–4893.

Guadix JA, Zugaza JL, Gálvez-Martín P (2017) Characteristics, applications and prospects of mesenchymal stem cells in cell therapy. Medicina Clinica 148:408–414.

Guo B, Zhang Z-K, Liang C, et al (2017) Molecular communication from skeletal muscle to bone: a review for muscle-derived myokines regulating bone metabolism. Calcified Tissue International 100:184–192.

Guo L, Li X, Tang Q-Q (2015) Transcriptional regulation of adipocyte differentiation: a central role for CCAAT/enhancer-binding protein (C/EBP) β. Journal of Biological Chemistry 290:755–761.

Gustafson B, Hammarstedt A, Hedjazifar S (2015) BMP4 and BMP antagonists regulate human white and beige adipogenesis. Diabetes 2015:1670-1681.

Hadjidakis DJ, Androulakis II (2006) Bone remodeling. Annals of the New York Academy of Sciences 1092:385–396.

Hall BK, Miyake T (2000) All for one and one for all: Condensations and the initiation of skeletal development. Bioessays 22:138–147.

Hamilton JR, Frauman AG, Cocks TM (2001) Increased expression of protease-activated receptor-2 (PAR2) and PAR4 in human coronary artery by inflammatory stimuli unveils endothelium-dependent relaxations to PAR2 and PAR4 agonists. Circulation Research 89:92–98.

Hamilton JR, Moffatt JD, Tatoulis J, Cocks TM (2002) Enzymatic activation of endothelial protease-activated receptors is dependent on artery diameter in human and porcine isolated coronary arteries. British Journal of Pharmacology 136:492–501.

Hamm HE (1998) The many faces of G protein signaling. Journal of Biological Chemistry 273:669–672.

Han Y, Cho DH, Chung DJ, Lee K-Y (2016) Osterix plays a critical role in BMP4-induced promoter activity of connexin43. Biochemical and Biophysical Research Communications 478:683–688.

Hansen KK, Sherman PM, Cellars L, et al (2005) A major role for proteolytic activity and proteinase-activated receptor-2 in the pathogenesis of infectious colitis. Proceedings of the National Academy of Sciences 102:8363–8368.

Harada S-I, Rodan GA (2003) Control of osteoblast function and regulation of bone mass. Nature 423:349–355.

Hardy R, Cooper MS (2009) Bone loss in inflammatory disorders. Journal of

Endocrinology 201:309–320.

Harris BZ, Venkatasubrahmanyam S, Lim WA (2002) Coordinated folding and association of the LIN-2, -7 (L27) domain; An obligate heterodimerization module involved in assembly of signaling and cell polarity complexes. Journal of Biological Chemistry 277:34902–34908.

Harvey N, Dennison E, Cooper C (2013) The epidemiology of osteoporotic fractures. In: Rosen, R. Bouillon, and J.E. Compston (ed), Primer on the Metabolic Bone Diseases and Disorders of Mineral Metabolism, 8 edn. Wiley, pp 348–356.

Haslett JN, Sanoudou D, Kho AT, et al (2002) Gene expression comparison of biopsies from Duchenne muscular dystrophy (DMD) and normal skeletal muscle. Proceedings of the National Academy of Sciences 99:15000–15005.

Hausman GJ, Thomas GB (1986) Structural and histochemical aspects of perirenal adipose tissue in fetal pigs: Relationships between stromal-vascular characteristics and fat cell concentration and enzyme activity. Journal of Morphology 190:271–283.

Heinonen J, Taipaleenmäki H, Roering P, et al (2011) Snorc is a novel cartilage specific small membrane proteoglycan expressed in differentiating and articular chondrocytes. Osteoarthritis and Cartilage 19:1026–1035.

Heinonen J, Zhang FP, Surmann-Schmitt C, et al (2017) Defects in chondrocyte maturation and secondary ossification in mouse knee joint epiphyses due to Snorc deficiency. Osteoarthritis and Cartilage 25:1132–1142.

Henriksen K, Flores C, Thomsen JS, et al (2011) Dissociation of bone resorption and bone formation in adult mice with a non-functional V-ATPase in osteoclasts leads to increased bone strength. PLoS One 6:e27482.

Hirota Y, Osuga Y, Hirata T, et al (2005) Activation of protease-activated receptor 2 stimulates proliferation and interleukin (IL)-6 and IL-8 secretion of endometriotic stromal cells. Human Reproduction 20:3547–3553.

Hoffman EP, Brown RH Jr., Kunkel LM (1987) Dystrophin: The protein product of the Duchenne muscular dystrophy locus. Cell 51:919–928.

Hofker MH, Van Deursen J (2003) Transgenic mouse: methods and protocols, 2nd edn. Humana Press, Totowa, NJ, pp: 205-232.

Hogenboom S (2003) Cholesterol biosynthesis is not defective in peroxisome biogenesis defective fibroblasts. Molecular Genetics and Metabolism 80:290–295.

Hojo H, Ohba S, He X, et al (2016) Sp7/Osterix is restricted to bone-forming vertebrates where it acts as a Dlx co-factor in osteoblast specification. Developmental Cell 37:238–253.

Holmen SL, Giambernardi TA, Zylstra CR, et al (2004) Decreased BMD and limb deformities in mice carrying mutations in both Lrp5 and Lrp6. Journal of Bone and

Mineral Research 19:2033–2040.

Holzenberger M, Hamard G, Zaoui R, et al (2011) Experimental IGF-I receptor deficiency generates a sexually dimorphic pattern of organ-specific growth deficits in mice, affecting fat tissue in particular. Endocrinology 142:4469–4478.

Holzhausen M, Spolidorio LC, Ellen RP, et al (2006) Protease-activated receptor-2 activation: a major role in the pathogenesis of Porphyromonas gingivalis infection. The American Journal of Pathology 168:1189–1199.

Holzhausen M, Spolidorio LC, Vergnolle N (2005) Proteinase-activated receptor-2 (PAR2) agonist causes periodontitis in rats. Journal of Dental Research 84:154–159.

Hong JH, Hong JY, Park B, et al (2012) Chitinase activates protease-activated receptor-2 in human airway epithelial cells. American Journal of Respiratory Cell and Molecular Biology 39:530–535.

Hoyte DAN (1971) Mechanisms of growth in the cranial vault and base. Journal of Dental Research 50: 1447-1461.

Huesa C, Ortiz AC, Dunning L, et al (2016) Proteinase-activated receptor 2 modulates OA-related pain, cartilage and bone pathology. Annals of the Rheumatic Diseases 75:1989–1997.

Hunziker EB (1994) Mechanism of longitudinal bone growth and its regulation by growth plate chondrocytes. Microscopy Research and Technique 28:505–519.

Hurley MM, Okada Y, Xiao L, et al (2006) Impaired bone anabolic response to parathyroid hormone in $Fgf2^{-/-}$ and $Fgf2^{+/-}$ mice. Biochemical and Biophysical Research Communications 341:989–994.

Hutley L, Shurety W, Newell F, et al (2004) Fibroblast growth factor 1. Diabetes 53:3097–3106.

Ibrahim MM (2010) Subcutaneous and visceral adipose tissue: structural and functional differences. Obesity Reviews 11:11–18.

Ikawa K, Nishioka T, Yu Z, et al (2005) Involvement of neutrophil recruitment and protease-activated receptor 2 activation in the induction of IL-18 in mice. Journal of Leukocyte Biology 78:1118–1126.

Imam SK (2016) White adipose tissue: Beyond fat storage. In: Ahmad S., Imam S. (eds), Obesity. Springer International Publishing, Cham, pp 1–12.

Iñiguez-Ariza NM, Clarke BL (2015) Bone biology, signaling pathways, and therapeutic targets for osteoporosis. Maturitas 82:245–255.

Ishihara H, Connolly AJ, Zeng D, et al (1997) Protease-activated receptor 3 is a second thrombin receptor in humans. Nature 386:502–506.

Ishii M, Merrill AE, Chan Y-S, et al (2003) Msx2 and Twist cooperatively control the development of the neural crest-derived skeletogenic mesenchyme of the murine skull vault. Development 130:6131–6142.

Ito T, Arimitsu N, Takeuchi M, et al (2006) Transcription elongation factor S-II is required for definitive hematopoiesis. Molecular and Cellular Biology 26:3194–3203.

Jackson MT, Moradi B, Zaki S, et al (2014) Depletion of protease-activated receptor 2 but not protease-activated receptor 1 may confer protection against osteoarthritis in mice through extracartilaginous mechanisms. Arthritis & Rheumatology 66:3337–3348.

Jacobson PA (1995) Rapidly forming apatitic mineral in an osteoblastic cell line (UMR 106-01 BSP). Journal of Biological Chemistry 270:9420–9428.

Jaffré F, Friedman AE, Hu Z, et al (2012) β-adrenergic receptor stimulation transactivates protease-activated receptor 1 via matrix metalloproteinase 13 in cardiac cells. Circulation 125:2993–3003.

James AW (2013) Review of Signaling pathways governing MSC osteogenic and adipogenic differentiation. Scientifica 2013:1–17.

James AW, Zara JN, Corselli M, et al (2012) An abundant perivascular source of stem cells for bone tissue engineering. Stem Cells Trans Med 1:673–684.

Jemtland R, Divieti P, Lee K, Segre GV (2003) Hedgehog promotes primary osteoblast differentiation and increases PTHrP mRNA expression and iPTHrP secretion. Bone 32:611–620.

Jenkins AL, Bootman MD, Taylor CW, et al (1993) Characterization of the receptor responsible for thrombin-induced intracellular calcium responses in osteoblast-like cells. Journal of Biological Chemistry 268:21432–21437.

Jenkins AL, Chinni C, De Niese MR, et al (2000) Expression of protease-activated receptor-2 during embryonic development. Developmental Dynamics 218:465–471.

Jilka RL, O'Brien CA, Roberson PK, et al (2014) Dysapoptosis of osteoblasts and osteocytes increases cancellous bone formation but exaggerates cortical porosity with age. Journal of Bone Mineral Research 29:103-117.

Jimi E, Aoki K, Saito H, et al (2004) Selective inhibition of NF-κB blocks osteoclastogenesis and prevents inflammatory bone destruction in vivo. Nature Medicine 10:617–624.

Jin E, Fujiwara M, Pan X, et al (2003) Protease-activated receptor (PAR)-1 and PAR-2 participate in the cell growth of alveolar capillary endothelium in primary lung adenocarcinomas. Cancer 97:703–713.

Jin W, Takagi T, Kanesashi S-N, et al (2006) Schnurri-2 controls BMP-dependent adipogenesis via interaction with Smad proteins. Developmental Cell 10:461–471.

Johnson JJ, Miller DL, Jiang R, et al (2016) Protease-activated Receptor-2 (PAR-2)-mediated Nf-κB activation suppresses inflammation-associated tumor suppressor MicroRNAs in oral squamous cell carcinoma. The Journal of Biological Chemistry 291:6936–6945.

Jonitz-Heincke A, Lochner K, Schulze C, et al (2016) Contribution of human osteoblasts and macrophages to bone matrix degradation and proinflammatory cytokine release after exposure to abrasive endoprosthetic wear particles. Molecular medicine reports 14:1491–1500.

Joshi D, Garg T, Goyal AK, Rath G (2014) Advanced drug delivery approaches against periodontitis. Drug Delivery 23:363–377.

Jowsey J (1977) The bone biopsy. Plenum Medical Book Company, New York.

Kahn ML, Hammes SR, Botka C, Coughlin SR (1998a) Gene and locus structure and chromosomal localization of the protease-activated receptor gene family. Journal of Biological Chemistry 273:23290–23296.

Kahn ML, Nakanishi-Matsui M, Shapiro MJ, et al (1999) Protease-activated receptors 1 and 4 mediate activation of human platelets by thrombin. Journal of Clinical Investigation 103:879–887.

Kahn ML, Zheng Y-W, Huang W, et al (1998b) A dual thrombin receptor system for platelet activation. Nature 394:690–694.

Kahn SE, Zinman B, Lachin JM, et al (2008) Rosiglitazone-associated fractures in type 2 diabetes: An analysis from a diabetes outcome progression trial (ADOPT). Diabetes Care 31:845–851.

Kameda T, Koike C, Saitoh K, et al (1999) Developmental patterning in chondrocytic cultures by morphogenic gradients: BMP induces expression of Indian hedgehog and Noggin. Genes to Cells 4:175–184.

Kaneshiro S, Ebina K, Shi K, et al (2014) IL-6 negatively regulates osteoblast differentiation through the SHP2/MEK2 and SHP2/Akt2 pathways in vitro. Journal of Bone and Mineral Metabolism 32:378–392.

Kanke T (2001) Proteinase-activated receptor-2-mediated activation of stress-activated protein kinases and inhibitory kappa B kinases in NCTC 2544 keratinocytes. Journal of Biological Chemistry 276:31657–31666.

Kanno T, Takahashi T, Tsujisawa T, et al (2007) Mechanical stress-mediated Runx2 activation is dependent on Ras/ERK1/2 MAPK signaling in osteoblasts. Journal of Cellular Biochemistry 101:1266–1277.

Katagiri T, Takahashi N (2002) Regulatory mechanisms of osteoblast and osteoclast differentiation. Oral Diseases 8:147–159.

Katagiri T, Yamaguchi A, Komaki M, et al (1994) Bone morphogenetic protein-2 converts the differentiation pathway of C2C12 myoblasts into the osteoblast

lineage. The Journal of Cell Biology 127:1755–1766.

Kato T, Takai T, Fujimura T, et al (2009) Mite serine protease activates protease-activated receptor-2 and induces cytokine release in human keratinocytes. Allergy 64:1366–1374.

Katoh M, Katoh M, Katoh M (2004) Identification and characterization of ARHGAP24 and ARHGAP25 genes in silico. International Journal of Molecular Medicine 14:333–338.

Kawabata A, Kinoshita M, Nishikawa H, et al (2001a) The protease-activated receptor-2 agonist induces gastric mucus secretion and mucosal cytoprotection. Journal of Clinical Investigation 107:1443–1450.

Kawabata A, Kuroda R, Nagata N, et al (2001b) In vivo evidence that protease-activated receptors 1 and 2 modulate gastrointestinal transit in the mouse. British Journal of Pharmacology 133:1213–1218.

Kawabata A, Nishikawa H, Kuroda R, et al (2000) Proteinase-activated receptor-2 (PAR-2): regulation of salivary and pancreatic exocrine secretion in vivo in rats and mice. British Journal of Pharmacology 129:1808–1814.

Kawai M, Devlin MJ, Rosen CJ (2009) Fat targets for skeletal health. Nature Reviews Rheumatology 5:365–372.

Kawai M, Mushiake S, Bessho K, et al (2007) Wnt/Lrp/β-catenin signaling suppresses adipogenesis by inhibiting mutual activation of PPARγ and C/EBPα. Biochemical and Biophysical Research Communications 363:276–282.

Kawai T, Matsuyama T, Hosokawa Y, et al (2006) B and T lymphocytes are the primary sources of RANKL in the bone resorptive lesion of periodontal disease. The American Journal of Pathology 169:987–998.

Kawano Y, Kypta R (2003) Secreted antagonists of the Wnt signalling pathway. Journal of Cell Science 116:2627–2634.

Kazakia GJ, Speer D, Shanbhag S, et al (2011) Mineral composition is altered by osteoblast expression of an engineered gs-coupled receptor. Calcified Tissue International 89:10–20.

Keiji M, Masahiko S, Takane H, et al (2002) Two major Smad pathways in TGF-b superfamily signaling. Genes to Cells 7: 1191-1204.

Keller H, Dreyer C, Medin J, et al (1993) Fatty acids and retinoids control lipid metabolism through activation of peroxisome proliferator-activated receptor-retinoid X receptor heterodimers. Proceedings of the National Academy of Sciences 90:2160–2164.

Kelso EB, Lockhart JC, Hembrough T, et al (2006) Therapeutic promise of proteinase-activated receptor-2 antagonism in joint inflammation. The Journal of Pharmacology and Experimental Therapeutics 316:1017–1024.

Kennedy OD, Herman BC, Laudier DM, et al (2012) Activation of resorption in fatigue-loaded bone involves both apoptosis and active pro-osteoclastogenic signaling by distinct osteocyte populations. Bone 50:1115–1122.

Khalid AB, Goodyear SR, Ross RA, Aspden RM (2016) Mechanical and material properties of cortical and trabecular bone from cannabinoid receptor-1-null (Cnr1−/−) mice. Medical Engineering & Physics 38:1044–1054.

Kharraz Y, Guerra J, Pessina P, Serrano AL (2014) Understanding the process of fibrosis in Duchenne muscular dystrophy. BioMed Research International 2014.

Kim S, Foster C, Lecchi A, et al (2002) Protease-activated receptors 1 and 4 do not stimulate Gi signaling pathways in the absence of secreted ADP and cause human platelet aggregation independently of Gisignaling. Blood 99:3629–3636.

Kimble RB, Srivastava S, Ross FP, et al (1996) Estrogen deficiency increases the ability of stromal cells to support murine osteoclastogenesis via an interleukin-1and tumor necrosis factor-mediated stimulation of macrophage colony-stimulating factor production. Journal of Biological Chemistry 271:28890–28897.

Kini U, Nandeesh BN (2012) Physiology of bone formation, remodeling, and metabolism. In: Fogelman I, Gnanasegaran G, Van der Wall H (eds), Radionuclide and hybrid bone imaging. Springer, London, pp 29–57.

Kirchmair R, Gander R, Egger M, et al (2004) The neuropeptide secretoneurin acts as a direct angiogenic cytokine in vitro and in vivo. Circulation 109:777–783.

Kirilak Y, Pavlos NJ, Willers CR (2006) Fibrin sealant promotes migration and proliferation of human articular chondrocytes: possible involvement of thrombin and protease-activated receptors. International Journal of Molecular Medicine, 17:551-558.

Kirkland JL, Tchkonia T, Pirtskhalava T, et al (2002) Adipogenesis and aging: does aging make fat go MAD? Experimental Gerontology 37:757–767.

Kishore U, Gaboriaud C, Waters P, et al (2004) C1q and tumor necrosis factor superfamily: modularity and versatility. Trends in immunology 25:551–561.

Kletzien RF, Foellmi LA, Harris PK, et al (1992) Adipocyte fatty acid-binding protein: regulation of gene expression in vivo and in vitro by an insulin-sensitizing agent. Molecular Pharmacology 42:558–562.

Kliewer SA, Forman BM, Blumberg B, et al (1994) Differential expression and activation of a family of murine peroxisome proliferator-activated receptors. Proceedings of the National Academy of Sciences 91:7355–7359.

Kliewer SA, Lenhard JM, Willson TM, et al (1995) A prostaglandin J2 metabolite binds peroxisome proliferator-activated receptor γ and promotes adipocyte differentiation. Cell 83:813–819.

Kliewer SA, Sundseth SS, Jones SA, et al (1997) Fatty acids and eicosanoids regulate

gene expression through direct interactions with peroxisome proliferator-activated receptors alpha and gamma. Proceedings of the National Academy of Sciences 94:4318–4323.

Klinger P, Surmann Schmitt C, Brem M, et al (2011) Chondromodulin 1 stabilizes the chondrocyte phenotype and inhibits endochondral ossification of porcine cartilage repair tissue. Arthritis & Rheumatology 63:2721–2731.

Kobayashi H, Gao Y-H, Ueta C, et al (2000) Multilineage differentiation of Cbfa1-deficient calvarial cells in vitro. Biochemical and Biophysical Research Communications 273:630–636.

Kobayashi T, Kronenberg H (2004) Minireview: Transcriptional regulation in development of bone. Endocrinology 146:1012–1017.

Kobayashi YM, Rader EP, Crawford RW, Campbell, KP (2012) Endpoint measures in the mdx mouse relevant for muscular dystrophy pre-clinical studies. Neuromuscular Disorders 22:34-42.

Koch H, Jadlowiec JA, Campbell DPG (2006) Insulin-like growth factor-I induces early osteoblast gene expression in human mesenchymal stem cells. Stem cells and development 14:621–631.

Kodama H, Nose M, Niida S, Yamasaki A (1991) Essential role of macrophage colony-stimulating factor in the osteoclast differentiation supported by stromal cells. Journal of Experimental Medicine 173:1291–1294.

Koike J, Takagi A, Miwa T, et al (1999) Molecular cloning of frizzled-10, a novel member of the frizzled gene family. Biochemical and Biophysical Research Communications 262:39–43.

Komori T (2017) Roles of Runx2 in skeletal development. In: Groner Y, Ito Y, Liu P, et al. (eds) RUNX Proteins in Development and Cancer. Springer, Singapore, Singapore, pp 83–93.

Komori T, Yagi H, Nomura S, et al (1997) Targeted disruption of Cbfa1 results in a complete lack of bone formation owing to maturational arrest of osteoblasts. Cell 89:755–764.

Kondoh S, Inoue K, Igarashi K, et al (2014) Estrogen receptor α in osteocytes regulates trabecular bone formation in female mice. Bone 60:68–77.

Kong YY, Feige U, Sarosi I, et al (1999) Activated T cells regulate bone loss and joint destruction in adjuvant arthritis through osteoprotegerin ligand. Nature 402:304–309.

Koshikawa N, Nagashima Y, Miyagi Y, et al (1997) Expression of trypsin in vascular endothelial cells. FEBS Letters 409:442–448.

Kronenberg HM (2003) Developmental regulation of the growth plate. Nature 423:332–336.

Kronenberg HM (2007) The role of the perichondrium in fetal bone development. Annals of the New York Academy of Sciences 1116:59–64.

KS L, Hong SH, Bae SC (2002) Both the Smad and p38 MAPK pathways play a crucial role in Runx2 expression following induction by transforming growth factor-beta and bone morphogenetic protein. Oncogene 21:7156–7163.

Kubota R, Numaguchi Y, Ishii M, et al (2010) Ischemia-induced angiogenesis is impaired in aminopeptidase A deficient mice via down-regulation of HIF-1α. Biochemical and Biophysical Research Communications 402:396–401.

Kudo O, Sabokbar A, Pocock A, et al (2003) Interleukin-6 and interleukin-11 support human osteoclast formation by a RANKL-independent mechanism. Bone 32:1–7.

Kuhlwilm M, Davierwala A, Pääbo S (2013) Identification of Putative target genes of the transcription factor Runx2. PLoS One 8:e83218.

Kularathna P, Pagel CN, Hooper JD, Mackie EJ (2013) Adipogenesis occurs at the expense of osteoblast differentiation in primary osteoblasts deficient in protease-activated receptor 2. Bone Abstracts.

Kularathna PK (2015) The Role of proteinase activated receptor-2 in osteoblast behaviour in prostate cancer bone metastasis. Doctoral Dissertation, The University of Melbourne. Melbourne.

Kuliopulos A, Covic L, Stacy K Seeley, et al (1999) Plasmin desensitization of the PAR1 thrombin receptor: Kinetics, Sites of truncation, and implications for thrombolytic therapy. Biochemistry 38:4572–4585.

Kumar A, Ruan M, Clifton K, et al (2012) TGF-β mediates suppression of adipogenesis by estradiol through connective tissue growth factor induction. Endocrinology 153:254–263.

Kunkel LM (1986) Analysis of deletions in DNA from patients with Becker and Duchenne muscular dystrophy. Nature 322:73–77.

Kuwasako K, Kitamura K, Nagata S, et al (2012) Characterization of the single transmembrane domain of human receptor activity-modifying protein 3 in adrenomedullin receptor internalization. Biochemical and Biophysical Research Communications 420:582–587.

Kyrou I, Weickert MO, Gharanei S, et al (2017) Fibroblast growth factors: new insights, new targets in the management of diabetes. Minerva Endocrinologica 42:248–270.

Lai C-F, Cheng S-L (2002) Signal transductions induced by bone morphogenetic protein-2 and transforming growth factor-beta in normal human osteoblastic cells. Journal of Biological Chemistry 277:15514–15522.

Lam DK, Dang D, Zhang J, et al (2012) Novel animal models of acute and chronic cancer pain: a pivotal role for PAR2. Journal of Neuroscience 32:14178–14183.

Lam DK, Schmidt BL (2010) Serine proteases and protease-activated receptor 2-dependent allodynia: A novel cancer pain pathway. Pain 149:263–272.

Lamba J, Lamba V, Strom S, et al (2008) Novel single nucleotide polymorphisms in the promoter and intron 1 of human pregnane X receptor/NR1I2 and their association with CYP3A4 expression. Drug Metabolism and Disposition: the Biological Fate of Chemicals 36:169–181.

Lan RS, Knight DA, Stewart GA, Henry PJ (2001) Role of PGE2 in protease-activated receptor-1, −2 and −4 mediated relaxation in the mouse isolated trachea. British Journal of Pharmacology 132:93–100.

Lang TF (2011) The bone-muscle relationship in men and women. Journal of Osteoporosis 2011.

Larson CM, Henderson RC (2000) Bone mineral density and fractures in boys with duchenne muscular dystrophy. Journal of Pediatric Orthopaedics 20:71.

Lattin JE, Schroder K, Su AI, et al (2008) Expression analysis of G Protein-Coupled Receptors in mouse macrophages. Immunome Research 2008 4:5.

Lazarenko OP, Rzonca SO, Hogue WR, et al (2007) Rosiglitazone induces decreases in bone mass and strength that are reminiscent of aged bone. Endocrinology 148:2669–2680.

LeBlanc J (1954) Subcutaneous Fat and Skin Temperature. Biochemistry and Cell Biology 32:354–358.

Lecka-Czernik B, Lecka-Czernik B, Moerman EJ, et al (2002) Divergent effects of selective peroxisome proliferator-activated receptor-γ2 ligands on adipocyte versus osteoblast differentiation. Endocrinology 143:2376–2384.

Lee H-J, Jo S-B, Romer AI, et al (2015) Overweight in Mice and enhanced adipogenesis in vitro are associated with lack of the hedgehog coreceptor boc. Diabetes 64:2092–2103.

Lee M-H, Kwon T-G, Park H-S, et al (2003) BMP-2-induced Osterix expression is mediated by Dlx5 but is independent of Runx2. Biochemical and Biophysical Research Communications 309:689–694.

Lefkowitz RJ, Shenoy SK (2005) Transduction of receptor signals by ß-Arrestins. Science 308:512–517.

Lehmann JM, Moore LB, Smith-Oliver TA, et al (1995) An antidiabetic thiazolidinedione is a high affinity ligand for peroxisome proliferator-activated receptor gamma (PPAR gamma). Journal of Biological Chemistry 270:12953–12956.

Lerner DJ, Chen M, Tram T, Coughlin SR (1996) Agonist recognition by proteinase-activated receptor 2 and thrombin receptor. Importance of extracellular loop interactions for receptor function. Journal of Biological Chemistry 271:13943–

13947.

Leupin O, Piters E, Halleux C, et al (2011) Bone overgrowth-associated mutations in the LRP4 gene impair sclerostin facilitator function. Journal of Biological Chemistry 286:19489–19500.

Levanon D (1994) AML1, AML2, and AML3, the human members of the runt domain Gene-Family: cDNA structure, expression, and chromosomal localization. Genomics 23:425–432.

Levy JR, Murray E, Manolagas S, Olefsky JM (2009) Demonstration of insulin receptors and modulation of alkaline phosphatase activity by insulin in rat osteoblastic cells. Endocrinology 119:1786–1792.

Lewinska M, Juvan P, Perse M, et al (2014) Hidden disease susceptibility and sexual dimorphism in the heterozygous knockout of Cyp51 from cholesterol synthesis. PLoS One 9:e112787.

Li J, Takaishi K, Cook W, et al (2003) Insig-1 “brakes” lipogenesis in adipocytes and inhibits differentiation of preadipocytes. Proceedings of the National Academy of Sciences 100:9476–9481.

Li J, Yu X, Pan W, Unger RH (2002) Gene expression profile of rat adipose tissue at the onset of high-fat-diet obesity. American Journal of Physiology Endocrinology and Metabolism 282:E1334–41.

Li X, Zhang Y, Kang H, et al (2005) Sclerostin binds to LRP5/6 and antagonizes canonical Wnt signaling. Journal of Biological Chemistry 280:19883–19887.

Li Y-L, Xiao Z-S (2007) Advances in Runx2 regulation and its isoforms. Med Hypotheses 68:169–175.

Lima LG, Monteiro RQ (2013) Activation of blood coagulation in cancer: implications for tumour progression. Bioscience Reports 33:701–710.

Lin C, Duitman J, Daalhuisen J, et al (2014) Targeting protease activated receptor-1 with P1pal-12 limits bleomycin-induced pulmonary fibrosis. Thorax 69:152–160.

Lindner JR, Kahn ML, Coughlin SR, et al (2000a) Delayed onset of inflammation in protease-activated receptor-2-deficient mice. The Journal of Immunology 165:6504–6510.

Lindner JR, Kahn ML, Coughlin SR, et al (2000b) Delayed onset of inflammation in protease-activated receptor-2-deficient mice. The Journal of Immunology 165:6504–6510.

Lintern KB, Guidato S, Rowe A, et al (2009) Characterization of wise protein and its molecular mechanism to interact with both Wnt and BMP signals. Journal of Biological Chemistry 284:23159–23168.

Liu J, Farmer SR (2004) Regulating the Balance between Peroxisome Proliferator-

activated Receptor γ and β-Catenin Signaling during Adipogenesis: A glycogen Synthase Kinase 3β Phosphorylation-defective mutant of β-catenin Inhibits Expression of a Subset of Adipogenic Genes. Journal of Biological Chemistry 279:45020–45027.

Liu S, Liu YP, Yue DM, Liu GJ (2013) Protease-activated receptor 2 in dorsal root ganglion contributes to peripheral sensitization of bone cancer pain. European Journal of Pain 18:326–337.

Liu Y-H, Tang Z, Kundu RK, et al (1999) Msx2 gene dosage influences the number of proliferative osteogenic cells in growth centers of the developing murine skull: A possible mechanism for MSX2-mediated craniosynostosis in humans. Developmental Biology 205:260–274.

Liu Z, Xu J, Colvin JS, Ornitz DM (2002) Coordination of chondrogenesis and osteogenesis by fibroblast growth factor 18. Genes & Development 16:859–869.

Loew, Perrault, Morales, et al (2000) Proteolysis of the exodomain of recombinant protease-activated receptors: Prediction of receptor activation or inactivation by MALDI mass spectrometry. Biochemistry 39: 10812-10822.

Logan M, Martin JF, Nagy A, et al (2002) Expression of Cre recombinase in the developing mouse limb bud driven by a Prxl enhancer. Genesis 33:77–80.

Lourbakos A, Potempa J, Travis J, et al (2001) Arginine-specific protease from Porphyromonas gingivalis activates protease-activated receptors on human oral epithelial cells and induces interleukin-6 secretion. Infection and Immunity 69:5121–5130.

Lundholm K, Rebuffe Scrive M, BJC Rntorp P (1985) Glucocorticoid hormone binding to human adipose tissue. European Journal of Clinical Investigation 15:267–271.

Luo G, Hofmann C, Bronckers AL, et al (1995) BMP-7 is an inducer of nephrogenesis, and is also required for eye development and skeletal patterning. Genes & Development 9:2808–2820.

Luu W, Hart-Smith G, Sharpe LJ, Brown AJ (2015) The terminal enzymes of cholesterol synthesis, DHCR24 and DHCR7, interact physically and functionally. Journal of Lipid Research 56:888–897.

Lynch ME, Main RP, Xu Q, et al (2011) Tibial compression is anabolic in the adult mouse skeleton despite reduced responsiveness with aging. Bone 49:439–446.

Ma J-N, Burstein ES (2013) The protease activated receptor 2 (PAR2) polymorphic variant F240S constitutively activates PAR2 receptors and potentiates responses to small-molecule PAR2 agonists. Journal of Pharmacology and Experimental Therapeutics 347:697–704.

MacDonald BT, Tamai K, He X (2009) Wnt/β-catenin signaling: Components, mechanisms, and diseases. Developmental Cell 17:9–26.

MacDougald OA, Lane MD (1995) Transcriptional regulation of gene expression during adipocyte differentiation. Annual Review of Biochemistry 64:345–373.

Mackie EJ, Ahmed YA, Tatarczuch L, et al (2008a) Endochondral ossification: How cartilage is converted into bone in the developing skeleton. The International Journal of Biochemistry & Cell Biology 40:46–62.

Mackie EJ, Loh LH, Sivagurunathan S, et al (2008b) Protease-activated receptors in the musculoskeletal system. The International Journal of Biochemistry & Cell Biology 40:1169–1184.

Maeda K, Okubo K, Shimomura I, et al (1997) Analysis of an expression profile of genes in the human adipose tissue. Gene 190:227–235.

Maeda T, Wakisaka S (2010) CTRP3/cartducin is induced by transforming growth factor-β1 and promotes vascular smooth muscle cell proliferation. Cell Biology International 34:261–266.

Mak W, Shao X, Dunstan CR, et al (2009) Biphasic glucocorticoid-dependent regulation of Wnt expression and its inhibitors in mature osteoblastic cells. Calcified Tissue International 85:538–545.

Malicet C, Rochman M, Postnikov Y, Bustin M (2011) Distinct properties of human HMGN5 reveal a rapidly evolving but functionally conserved nucleosome binding protein. Molecular and Cellular Biology 31:2742–2755.

Malinauskas T, Aricescu AR, Lu W, et al (2011) Modular mechanism of Wnt signaling inhibition by Wnt inhibitory factor 1. Nature Structural & Molecular Biology 18:886–89.

Manolagas SC (1998) The role of IL-6 type cytokines and their receptors in bonea. Annals of the New York Academy of Sciences 840:194–204.

Matsuo K, Irie N (2008) Osteoclast–osteoblast communication. Archives of Biochemistry and Biophysics 473:201–209.

Matthews E, Brassington R, Kuntzer T, et al (2016) Corticosteroids for the treatment of Duchenne muscular dystrophy. John Wiley & Sons, Ltd, Chichester, UK.

Mazess RB (1982) On aging bone loss. Clinical Orthopaedics and Related Research 165:239–252.

McCabe LR, Banerjee C, Kundu R, et al (1996) Developmental expression and activities of specific fos and jun proteins are functionally related to osteoblast maturation: role of Fra-2 and Jun D during differentiation. Endocrinology 137:4398–4408.

McGown C, Birerdinc A, Younossi ZM (2014) Adipose tissue as an endocrine organ. Clinics in Liver Disease 18:41–58.

McGreevy JW, Hakim CH, McIntosh MA, Duan D (2015) Animal models of Duchenne

muscular dystrophy: from basic mechanisms to gene therapy. Disease Models and Mechanisms 8:195–213.

McGuire JJ (2002) Proteinase-Activated Receptor-2 (PAR2): Vascular effects of a PAR2-derived activating peptide via a receptor different than PAR2. Journal of Pharmacology and Experimental Therapeutics 303:985–992.

McInnes IB, Buckley CD, Isaacs JD (2015) Cytokines in rheumatoid arthritis - shaping the immunological landscape. Nature Reviews Rheumatology 12:63–68.

McInnes IB, Schett G (2017) Pathogenetic insights from the treatment of rheumatoid arthritis. The Lancet 389:2328–2337.

McNamara CA, Sarembock IJ, Gimple LW, et al (1993) Thrombin stimulates proliferation of cultured rat aortic smooth muscle cells by a proteolytically activated receptor. Journal of Clinical Investigation 91:94–98.

Melton LJ, Chrischilles EA, Cooper C, et al (2005) How many women have osteoporosis? Journal of Bone and Mineral Research 20:886–892.

Mendell JR, Goemans N, Lowes LP, et al (2016) Longitudinal effect of eteplirsen versus historical control on ambulation in Duchenne muscular dystrophy. Annals of Neurology 79:257–271.

Mendell JR, Rodino Klapac LR, Sahenk Z, et al (2013) Eteplirsen for the treatment of Duchenne muscular dystrophy. Annals of Neurology 74:637–647.

Menton DN, Simmons DJ, Chang SL, Orr BY (1984) From bone lining cell to osteocyte - an SEM study. The Anatomical Record 209:29–39.

Merriman HL, van Wijnen AJ, Hiebert S, et al (1995) The tissue-specific nuclear matrix protein, NMP-2, is a member of the AML/PEBP2/Runt domain transcription factor family: Interactions with the osteocalcin gene promoter. 34:13125–13132.

Miegueu P, St-Pierre DH, Munkonda MN, et al (2013) Amylin stimulates fatty acid esterification in 3T3-L1 adipocytes. Molecular and Cellular Endocrinology 366:99–107.

Mihara K, Ramachandran R, Renaux B, et al (2013) Neutrophil elastase and proteinase-3 trigger G protein-biased signaling through proteinase-activated receptor-1 (PAR1). Journal of Biological Chemistry 288:32979–32990.

Miki H, Yamauchi T, Suzuki R, et al (2001) Essential role of insulin receptor substrate 1 (IRS-1) and IRS-2 in adipocyte differentiation. Molecular and Cellular Biology 21:2521–2532.

Miki M, Nakamura Y, Takahashi A, Nakaya Y (2003) Effect of human airway trypsin-like protease on intracellular free Ca^{2+} concentration in human bronchial epithelial cells. Journal of Medical Investigation 50:95-107.

Miller SC, de Saint-Georges L, BM B, Jee WS (1989) Bone lining cells: Structure and

function. Scanning Microscopy 3:953–60.

Minaire P, Meunier P, Edouard C, et al (1974) Quantitative histological data on disuse osteoporosis. Calcified Tissue Research 17:57–73.

Minematsu T, Huang L, Ibuki A, et al (2012) Altered expression of matrix metalloproteinases and their tissue inhibitors in matured rat adipocytes in vitro. Biological Research for Nursing 14:242–249.

Minguell JJ, Erices A, Conget P (2001) Mesenchymal stem cells. Experimental Biology and Medicine 226:507–520.

Mishina Y, Starbuck MW, Gentile MA, et al (2004) Bone morphogenetic protein type IA receptor signaling regulates postnatal osteoblast function and bone remodeling. Journal of Biological Chemistry 279:27560–27566. doi: 10.1074/jbc.M404222200

Miura S, Mitsui K, Heishi T, et al (2010) Impairment of VEGF-A-stimulated lamellipodial extensions and motility of vascular endothelial cells by chondromodulin-I, a cartilage-derived angiogenesis inhibitor. Experimental Cell Research 316:775–788.

Miyama K, Yamada G, Yamamoto TS, et al (1999) A BMP-inducible gene, Dlx5, regulates osteoblast differentiation and mesoderm induction. Developmental Biology 208:123–133.

Miyaura C, Toda K, Inada M, et al (2001) Sex- and age-related response to aromatase deficiency in bone. Biochemical and Biophysical Research Communications 280:1062–1068.

Miyazono K, Kamiya Y, Morikawa M (2010) Bone morphogenetic protein receptors and signal transduction. The Journal of Biochemistry 147:35–51.

Mize GJ, Wang W, Takayama TK (2008) Prostate-specific Kallikreins-2 and -4 enhance the proliferation of DU-145 prostate cancer cells through protease-activated receptors-1 and -2. Molecular Cancer Research 6:1043–1051.

Moerman EJ, Teng K, Lipschitz DA, Lecka-Czernik B (2004) Aging activates adipogenic and suppresses osteogenic programs in mesenchymal marrow stroma/stem cells: the role of PPAR-γ2 transcription factor and TGF-β/BMP signaling pathways. Aging Cell 3:379–389.

Mohamed-Ali V, Pinkney JH, Coppack SW (1998) Adipose tissue as an endocrine and paracrine organ. International Journal of Obesity & Related Metabolic Disorders 22.

Moitra J, Mason MM, Olive M, et al (1998) Life without white fat: A transgenic mouse. Genes & Development 12:3168-3181.

Moldes M, Zuo Y, Morrison RF, et al (2003) Peroxisome-proliferator-activated receptor γ suppresses Wnt/β-catenin signalling during adipogenesis. Biochemical Journal 376:607–613.

Molino M, Barnathan ES, Numerof R, et al (1997) Interactions of mast cell tryptase with thrombin receptors and PAR-2. Journal of Biological Chemistry 272:4043–4049.

Monroe DG, McGee-Lawrence ME, Oursler MJ, Westendorf JJ (2012) Update on Wnt signaling in bone cell biology and bone disease. Gene 492:1–18.

Montero A, Okada Y, Tomita M, et al (2000) Disruption of the fibroblast growth factor-2 gene results in decreased bone mass and bone formation. Journal of Clinical Investigation 105:1085–1093.

Montgomery E, Pennington C, Isales CM, Hamrick MW (2005) Muscle-bone interactions in dystrophin-deficient and myostatin-deficient mice. The Anatomical Record Part A, Discoveries in Molecular, Cellular, and Evolutionary Biology 286:814–822.

Monzani E, Bazzotti R, Perego C, La Porta CAM (2009) AQP1 is not only a water channel: It contributes to cell migration through Lin7/Beta-Catenin. PLoS One 4:e6167.

Moreno-Navarrete JM, Fernández-Real JM (2017) Adipocyte differentiation. In: Symonds ME (ed) Adipose Tissue Biology. Springer, Cham, pp 69–90.

Morgenroth VH, Hache LP, Clemens PR (2012) Insights into bone health in Duchenne muscular dystrophy. BoneKEy Reports 1:9.

Mori Y, Hiraki Y, Shukunami C, et al (1997) Stimulation of osteoblast proliferation by the cartilage-derived growth promoting factors chondromodulin-I and -II. FEBS Letters 406:310–314.

Morris AJ, Malbon CC (1999) Physiological regulation of G protein-linked signaling. Physiological Reviews 79:1373–1430.

Mosnier LO, Sinha RK, Burnier L, et al (2012) Biased agonism of protease-activated receptor 1 by activated protein C caused by noncanonical cleavage at Arg46. Blood 120:5237–5246.

Moustakas A (2002) From mono- to oligo-Smads: The heart of the matter in TGF-beta signal transduction. Genes & Development 16:1867–1871.

Muller PY, Janovjak H, Miserez AR, Dobbie Z (2002) Short technical report processing of gene expression data generated by quantitative Real-Time RT-PCR. Biotechniques 32:1372-1379.

Murshed M (2005) Unique coexpression in osteoblasts of broadly expressed genes accounts for the spatial restriction of ECM mineralization to bone. Genes & Development 19:1093–1104.

Muruganandan S, Roman AA, Sinal CJ (2008) Adipocyte differentiation of bone marrow-derived mesenchymal stem cells: Cross talk with the osteoblastogenic program. Cellular and Molecular Life Sciences 66:236–253.

Naganawa T, Xiao L, Coffin JD, et al (2008) Reduced expression and function of bone morphogenetic protein-2 in bones of Fgf2 null mice. Journal of Cellular Biochemistry 103:1975–1988.

Nagy V, Penninger JM (2015) The RANKL-RANK story. Gerontology 61:534–542.

Naka T, Nishimoto N, Kishimoto T (2002) The paradigm of IL-6: from basic science to medicine. Arthritis Research 4 Suppl 3:S233–42.

Nakagaki WR, Bertran CA, Matsumura CY, et al (2011) Mechanical, biochemical and morphometric alterations in the femur of mdx mice. Bone 48:372–379.

Nakanishi-Matsui M, Zheng Y-W, Sulciner DJ, et al (2000) PAR3 is a cofactor for PAR4 activation by thrombin. Nature 404:609–613.

Nakashima K, Zhou X, Kunkel G, et al (2002) The novel zinc finger-containing transcription factor Osterix is required for osteoblast differentiation and bone formation. Cell 108:17–29.

Naveiras O, Nardi V, Wenzel PL, et al (2009) Bone-marrow adipocytes as negative regulators of the haematopoietic microenvironment. Nature 460:259–263.

Nelson CE, Hakim CH, Ousterout DG, et al (2016) In vivo genome editing improves muscle function in a mouse model of Duchenne muscular dystrophy. Science 351:403–407.

Neubauer M, Fischbach C, Bauer-Kreisel P, et al (2004) Basic fibroblast growth factor enhances PPARγ ligand-induced adipogenesis of mesenchymal stem cells. FEBS Letters 577:277–283.

Nieman MT (2008) Protease-activated receptor 4 uses anionic residues to interact with α-thrombin in the absence or presence of protease-activated receptor 1. Biochemistry 47:13279–13286.

Niemand C, Nimmesgern A, Haan S, et al (2003) Activation of STAT3 by IL-6 and IL-10 in primary human macrophages is differentially modulated by suppressor of cytokine signaling 3. The Journal of Immunology 170:3263–3272.

Nijweide PJ, Burger EH, Feyen JH (1986) Cells of bone: proliferation, differentiation, and hormonal regulation. Physiological Reviews 66:855-886.

Nishimura R, Wakabayashi M, Hata K, et al (2012) Osterix regulates calcification and degradation of chondrogenic matrices through matrix metalloproteinase 13 (MMP13) expression in association with transcription factor Runx2 during endochondral ossification. Journal of Biological Chemistry 287:33179–33190.

Nishio Y, Dong Y, Paris M, et al (2006) Runx2-mediated regulation of the zinc finger Osterix/Sp7 gene. Gene 372:62–70.

Nishizuka M, Honda K, Tsuchiya T, et al (2001) RGS2 promotes adipocyte differentiation in the presence of ligand for peroxisome proliferator-activated

receptor gamma. Journal of Biological Chemistry 276:29625–29627.

Novotny SA, Warren GL, Lin AS, et al (2012) Prednisolone treatment and restricted physical activity further compromise bone of mdx mice. Journal of Musculoskeletal & Neuronal Interactions 12:16–23.

Novotny SA, Warren GL, Lin AS, et al (2011) Bone is functionally impaired in dystrophic mice but less so than skeletal muscle. Neuromuscular Disorders 21:183–193.

Nöth U, Osyczka AM, Tuli R, et al (2002) Multilineage mesenchymal differentiation potential of human trabecular bone-derived cells. Journal of Orthopaedic Research 20:1060–1069.

Nusse R, Varmus HE (1982) Many tumors induced by the mouse mammary tumor virus contain a provirus integrated in the same region of the host genome. Cell 31:99–109.

Nusse R, Varmus HE (1992) Wnt genes. Cell 69:1073–1087.

Nystedt S, Emilsson K, Larsson A-K, et al (1995a) Molecular cloning and functional expression of the gene encoding the human proteinase-activated receptor 2. European Journal of Biochemistry 232:84–89.

Nystedt S, Emilsson K, Wahlestedt C, Sundelin J (1994) Molecular cloning of a potential proteinase activated receptor. Proceedings of the National Academy of Sciences 91:9208–9212.

Nystedt S, Larsson AK, Åberg H, Sundelin J (1995b) The mouse proteinase-activated receptor-2 cDNA and gene. Molecular cloning and functional expression. Journal of Biological Chemistry 270:5950–5955.

O'Brien CA, Nakashima T, Takayanagi H (2013) Osteocyte control of osteoclastogenesis. Bone 54:258–263.

O'Brien PJ (2000) Thrombin responses in human endothelial cells: Contributions from receptors other than PAR1 include the transactivation of PAR2 by thrombin-cleaved PAR1. Journal of Biological Chemistry 275:13502–13509.

Ochi M, Yoshioka H, Sawada T, et al (1991) New adipocyte formation in mice during refeeding after long-term deprivation. The American Journal of Physiology 260:R468–74.

Oda R, Suardita K, Fujimoto K, et al (2003) Anti-membrane-bound transferrin-like protein antibodies induce cell-shape change and chondrocyte differentiation in the presence or absence of concanavalin A. Journal of Cell Science 116:2029–2038.

Ogata N, Chikazu D, Kubota N, et al (2000) Insulin receptor substrate-1 in osteoblast is indispensable for maintaining bone turnover. Journal of Clinical Investigation 105:935–943.

Ohazama A, Porntaveetus T, Ota MS, et al (2010) Lrp4: A novel modulator of extracellular signaling in craniofacial organogenesis. American Journal of Medical Genetics Part A 152A:2974–2983.

Ohbayashi N, Shibayama M, Kurotaki Y, et al (2002) FGF18 is required for normal cell proliferation and differentiation during osteogenesis and chondrogenesis. Genes & Development 16:870–879.

Oikonomopoulou K, Hansen KK, Saifeddine M, et al (2006) Proteinase-activated receptors, targets for kallikrein signaling. Journal of Biological Chemistry 281:32095–32112.

Oka S, Ota R, Shima M, et al (2010) GPR35 is a novel lysophosphatidic acid receptor. Biochemical and Biophysical Research Communications 395:232–237.

Olsen BR, Reginato AM, Wang W (2003) Bone development. Annual Review of Cell and Developmental Biology 16:191–220.

Orimo H (2010) The mechanism of mineralization and the role of alkaline phosphatase in health and disease. Journal of Nippon Medical School 77:4–12.

Ortuño MJ, Susperregui ARG, Artigas N, et al (2013) Osterix induces Col1a1 gene expression through binding to Sp1 sites in the bone enhancer and proximal promoter regions. Bone 52:548–556.

Otto F, Thornell AP, Crompton T, et al (1997) Cbfa1, a candidate gene for cleidocranial dysplasia syndrome, is essential for osteoblast differentiation and bone development. Cell 89:765–771.

Owen M (1988) Marrow stromal stem cells. Journal of Cell Science 1988:63–76.

Owen TA, Bortell R, Yocum SA, et al (1990) Coordinate occupancy of AP-1 sites in the vitamin D-responsive and CCAAT box elements by Fos-Jun in the osteocalcin gene: model for phenotype suppression of transcription. Proceedings of the National Academy of Sciences 87:9990–9994.

Ozawa H, Takata K (1995) The granin family. Its role in sorting and secretory granule formation. Cell Structure and Function 20:415–420.

Pagel CN, De Niese MR, Abraham LA, et al (2003) Inhibition of osteoblast apoptosis by thrombin. Bone 33:733–743.

Pagel CN, Song SJ, Loh LH, et al (2009) Thrombin-stimulated growth factor and cytokine expression in osteoblasts is mediated by protease-activated receptor-1 and prostanoids. Bone 44:813–821.

Pairault J, Green H (1979) A study of the adipose conversion of suspended 3T3 cells by using glycerophosphate dehydrogenase as differentiation marker. Proceedings of the National Academy of Sciences 76:5138–5142.

Palumbo C (1986) A three-dimensional ultrastructural study of osteoid-osteocytes in the

tibia of chick embryos. Cell and Tissue Research 246:125–131.

Panigrahy D, Singer S, Shen LQ, et al (2002) PPARgamma ligands inhibit primary tumor growth and metastasis by inhibiting angiogenesis. Journal of Clinical Investigation 110:923–932.

Parfitt AM (1984) Age-related structural changes in trabecular and cortical bone: Cellular mechanisms and biomechanical consequences. Calcified Tissue International 36:S123–S128.

Park KS, Cha Y, Kim CH, et al (2013) Transcription elongation factor Tcea3 regulates the pluripotent differentiation potential of mouse embryonic stem cells via the Lefty1-Nodal-Smad2 pathway. Stem Cells International 31:282–292.

Pellegrinelli V, Carobbio S, Vidal-Puig A (2016) Adipose tissue plasticity: how fat depots respond differently to pathophysiological cues. Diabetologia 59:1075–1088.

Pereira RC, Economides AN, Canalis E (2000) Bone morphogenetic proteins induce gremlin, a protein that limits their activity in osteoblasts. Endocrinology 141:4558–4563.

Pers J-O, Saraux A, Pierre R, Youinou P (2008) Anti–TNF-α immunotherapy is associated with increased gingival inflammation without clinical attachment loss in subjects with rheumatoid arthritis. Journal of Periodontology 79:1645–1651.

Pfaffl MW, Tichopad A, Prgomet C, Neuvians TP (2004) Determination of stable housekeeping genes, differentially regulated target genes and sample integrity: BestKeeper – Excel-based tool using pair-wise correlations. Biotechnology Letters 26:509–515.

Phelps E, Bezouglaia O, Tetradis S, Nervina JM (2005) Parathyroid hormone induces receptor activity modifying protein-3 (RAMP3) expression primarily via 3′,5′-cyclic adenosine monophosphate signaling in osteoblasts. Calcified Tissue International 77:96–103.

Pilgrim C (1971) DNA synthesis and differentiation in developing white adipose tissue. Developmental Biology 26:69–76.

Poirier H, Braissant O, Niot I, et al (1997) 9-cis-Retinoic acid enhances fatty acid-induced expression of the liver fatty acid-binding protein gene. FEBS Letters 412:480–484.

Poissonnet CM, Burdi AR, Bookstein FL (1983) Growth and development of human adipose tissue during early gestation. Early Human Development 8:1–11.

Poli V, Balena R, Fattori E, et al (1994) Interleukin-6 deficient mice are protected from bone loss caused by estrogen depletion. The EMBO Journal 13:1189–1196.

Porter JD, Khanna S, Kaminski HJ, et al (2002) A chronic inflammatory response dominates the skeletal muscle molecular signature in dystrophin-deficient mdx mice. Human Molecular Genetics 11:263–272.

Porter SA, Massaro JM, Hoffmann U, et al (2009) Abdominal subcutaneous adipose tissue: a protective fat depot? Diabetes Care 32:1068–1075.

Post S, Heijink IH, Petersen AH, et al (2014) Protease-activated receptor-2 activation contributes to house dust mite-induced ige responses in mice. PLoS One 9:e91206.

Poulton IJ, McGregor NE, Pompolo S, et al (2012) Contrasting roles of leukemia inhibitory factor in murine bone development and remodeling involve region-specific changes in vascularization. Journal of Bone and Mineral Research 27:586–595.

Prockop DJ (1997) Marrow Stromal Cells as Stem Cells for Nonhematopoietic Tissues. Science 276:71–74.

Qiao Y, Tomonaga S, Suenaga M, et al (2017) Modulation of adipocyte function by the TGF-β family. Cytokine.

Qiu M, Bulfone A, Ghattas I, et al (1997) Role of the Dlx homeobox genes in proximodistal patterning of the branchial arches: mutations of Dlx-1, Dlx-2, and Dlx-1 and -2 alter morphogenesis of proximal skeletal and soft tissue structures derived from the first and second arches. Developmental Biology 185:165–184.

Rabkin SW (2007) Epicardial fat: properties, function and relationship to obesity. Obesity Reviews 8:253–261.

Raisz LG (2005) Pathogenesis of osteoporosis: concepts, conflicts, and prospects. Journal of Clinical Investigation 115:3318–3325.

Rajewsky K, Gu H, Kühn R, et al (1996) Conditional gene targeting. Journal of Clinical Investigation 98:600–603.

Rajkumar K, Modric T, Murphy LJ (1999) Impaired adipogenesis in insulin-like growth factor binding protein-1 transgenic mice. Journal of Endocrinology 162:457–465.

Ramachandran R, Mihara K, Chung H, et al (2011) Neutrophil elastase acts as a biased agonist for proteinase-activated receptor-2 (PAR2). Journal of Biological Chemistry 286:24638–24648.

Ramachandran R, Mihara K, Mathur M, et al (2009) Agonist-biased signaling via proteinase activated receptor-2: differential activation of calcium and mitogen-activated protein kinase pathways. Molecular Pharmacology 76:791–801.

Ramsay AJ, Dong Y, Hunt ML, et al (2008) Kallikrein-related peptidase 4 (KLK4) initiates intracellular signaling via protease-activated receptors (PARs) KLK4 and PAR-2 are co-expressed during prostate cancer progression. Journal of Biological Chemistry 283:12293–12304.

Rashid H, Ma C, Chen H, et al (2014) Sp7 and Runx2 molecular complex synergistically regulate expression of target genes. Connective Tissue Research 55:83–87.

Raucci A, Bellosta P, Grassi R, et al (2008) Osteoblast proliferation or differentiation is regulated by relative strengths of opposing signaling pathways. Journal of Cellular Physiology 215:442–451.

Rayalam S, Baile CA (2016) Adipocyte growth and factors influencing adipocyte life cycle. In: Symonds ME (ed), Adipose Tissue Biology. Springer, New York, NY, pp 199–230.

Rebuffe Scrive M, Krotkiewski M, Elfverson J, Bjorntorp P (2009) Muscle and adipose tissue morphology and metabolism in Cushing's syndrome. The Journal of Clinical Endocrinology & Metabolism 67:1122–1128.

Recker RR, Heaney RP (1993) Peak bone mineral density in young women. Journal of the American Medical Association 270:2926–2926.

Redlich K, Smolen JS (2012) Inflammatory bone loss: pathogenesis and therapeutic intervention. Nature Reviews Drug Discovery 11:234–250.

Reinisch N, Kirchmair R, Kähler CM, et al (2001) Attraction of human monocytes by the neuropeptide secretoneurin. FEBS Letters 334:41–44.

Retting KN, Song B, Yoon BS, Lyons KM (2009) BMP canonical Smad signaling through Smad1 and Smad5 is required for endochondral bone formation. Development 136:1093–1104.

Reznikov N, Shahar R, Weiner S (2014) Bone hierarchical structure in three dimensions. Acta Biomaterialia 10:3815–3826.

Ricciardolo FLM, Steinhoff M, Amadesi S, et al (2000) Presence and bronchomotor activity of protease-activated receptor-2 in guinea pig airways. American Journal of Respiratory and Critical Care Medicine 161:1672–1680.

Ricks TK, Trejo J (2009) Phosphorylation of protease-activated receptor-2 differentially regulates desensitization and internalization. Journal of Biological Chemistry 284:34444–34457.

Rizzoli R, Poser J, Bürgi U (1986) Nuclear thyroid hormone receptors in cultured bone cells. Metabolism 35:71–74.

Robin J, Kharbanda R, Mclean P, et al (2003) Protease-Activated Receptor 2–Mediated Vasodilatation in Humans In Vivo. Circulation 107:954–959.

Robledo RF, Rajan L, Li X, Lufkin T (2002) The Dlx5 and Dlx6 homeobox genes are essential for craniofacial, axial, and appendicular skeletal development. Genes & Development 16:1089–1101.

Robling A (2017) Osteocytes orchestrate mechanical signal transduction in bone via Wnt. The FASEB Journal 31:7.3–7.3.

Robling AG, Castillo AB, Turner CH (2006) Biomechanical and molecular regulation of bone remodeling. Annual Review of Biomedical Engineering 8:455–498.

Rodda SJ (2006) Distinct roles for Hedgehog and canonical Wnt signaling in specification, differentiation and maintenance of osteoblast progenitors. Development 133:3231–3244.

Rodriguez AM, Elabd C, Amri E-Z, et al (2005) The human adipose tissue is a source of multipotent stem cells. Biochimie 87:125–128.

Rodrigues M, Echigoya Y, Fukada S-I, Yokota T (2016) Current translational research and murine models for Duchenne muscular dystrophy. Journal of Neuromuscul Diseases 3:29–48.

Rohatgi R, Milenkovic L, Scott MP (2007) Patched1 regulates hedgehog signaling at the primary cilium. Science 317:372–376.

Ron D, Habener JF (1992) CHOP, a novel developmentally regulated nuclear protein that dimerizes with transcription factors C/EBP and LAP and functions as a dominant-negative inhibitor of gene transcription. Genes & Development 6:439–453.

Roosterman D, Schmidlin F, Bunnett NW (2003) Rab5a and rab11a mediate agonist-induced trafficking of protease-activated receptor 2. American Journal of Physiology - Cell Physiology 284:C1319–C1329.

Rosen CJ, Bouxsein ML (2006) Mechanisms of disease: Is osteoporosis the obesity of bone? Nature Clinical Practice Rheumatology 2:35–43.

Rosen ED, MacDougald OA (2006) Adipocyte differentiation from the inside out. Nature Reviews Molecular Cell Biology 7:885–896.

Rosen ED, Sarraf P, Troy AE, et al (1999) PPARγ is required for the differentiation of adipose tissue in vivo and in vitro. Molecular Cell 4:611–617.

Ross DA, Rao PK, Kadesch T (2004) Dual roles for the Notch target gene Hes-1 in the differentiation of 3T3-L1 preadipocytes. Molecular and Cellular Biology 24:3505–3513.

Ross SE, Hemati N, Longo KA, et al (2000) Inhibition of adipogenesis by Wnt signaling. Science 289:950–953.

Rothmeier AS, Ruf W (2011) Protease-activated receptor 2 signaling in inflammation. Seminars in Immunopathology 34:133–149.

Rowland AF, Larance M, Hughes WE, James DE (2011) Identification of RhoGAP22 as an Akt-dependent regulator of cell motility in response to insulin. Molecular and Cellular Biology 31:4789–4800.

Roy AA, Nunn C, Ming H, et al (2006) Up-regulation of endogenous RGS2 mediates cross-desensitization between Gs and Gq signaling in osteoblasts. Journal of Biological Chemistry 281:32684–32693.

Rozman C, Feliu E, Berga L, et al (1989) Age-related variations of fat tissue fraction in

normal human bone marrow depend both on size and number of adipocytes: a stereological study. Experimental Hematology 17:34–37.

Röhrborn D, Eckel J, Sell H (2014) Shedding of dipeptidyl peptidase 4 is mediated by metalloproteases and up-regulated by hypoxia in human adipocytes and smooth muscle cells. FEBS Letters 588:3870–3877.

Ruat M, Hoch L, Faure H, Rognan D (2014) Targeting of Smoothened for therapeutic gain. Trends in Pharmacological Sciences 35:237–246.

Ruchika S, Waller AP, Agrawal S, et al (2015) Thrombin induces protease activated receptor (PAR)-3/-4 interaction in human podocytes. Blood 126:3488–3488.

Rufo A, De Benedetti F, Teti A (2013) Muscle and bone in muscular dystrophy: Why not? In: Muscular dystrophy: Causes and management. Nova Science Publishers, Inc, pp. 427-437.

Rufo A, Del Fattore A, Capulli M, et al (2011) Mechanisms inducing low bone density in Duchenne muscular dystrophy in mice and humans. Journal of Bone and Mineral Research 26:1891–1903.

Russo A, Soh UJK, Trejo J (2009) Proteases display biased agonism at protease-activated receptors: Location matters! Molecular Interventions 9:87–96.

Rzonca SO, Suva LJ, Gaddy D, et al (2011) Bone is a target for the antidiabetic compound rosiglitazone. Endocrinology 145:401–406.

Saito A, Osuga Y, Yoshino O, et al (2011) TGF-β1 induces proteinase-activated receptor 2 (PAR2) expression in endometriotic stromal cells and stimulates PAR2 activation-induced secretion of IL-6. Human Reproduction 26:1892–1898.

Sakaue H, Konishi M, Ogawa W, et al (2002) Requirement of fibroblast growth factor 10 in development of white adipose tissue. Genes & Development 16:908–912.

Salajegheh A (2016) Monobutyrin. In: Salajegheh A (Ed), Angiogenesis in health, disease and malignancy. Springer, Cham, pp 209–212.

Sambrook PN, Seeman E, Phillips SR, Ebeling PR (2002) Preventing osteoporosis: outcomes of the Australian fracture prevention summit. Medical Journal of Australia 176:S1–S16.

Sandouk T, Reda D, Hofmann C (1993) Antidiabetic agent pioglitazone enhances adipocyte differentiation of 3T3-F442A cells. The American Journal of Physiology 264:C1600–8.

Santulli RJ, Derian CK, Darrow AL, et al (1995) Evidence for the presence of a protease-activated receptor distinct from the thrombin receptor in human keratinocytes. Proceedings of the National Academy of Sciences 92:9151–9155.

Sato F, Miyaoka Y, Miyajima A, Tanaka M (2014) Oncostatin M maintains the hematopoietic microenvironment in the bone marrow by modulating adipogenesis and osteogenesis. PLoS One 9:e116209.

Sánchez-Duffhues G, Hiepen C, Knaus P, Dijke ten P (2015) Bone morphogenetic protein signaling in bone homeostasis. Bone 80:43–59.

Scarborough RM, Naughton MA, Teng W, et al (1992) Tethered ligand agonist peptides. Structural requirements for thrombin receptor activation reveal mechanism of proteolytic unmasking of agonist function. Journal of Biological Chemistry 267:13146–13149.

Scherer PE (2006) Adipose Tissue. Diabetes 55:1537–1545.

Schmid A, Kopp A, Hanses F, et al (2014) C1q/TNF-related protein-3 (CTRP-3) attenuates lipopolysaccharide (LPS)-induced systemic inflammation and adipose tissue Erk-1/-2 phosphorylation in mice in vivo. Biochemical and Biophysical Research Communications 452:8–13.

Schmidlin F, Amadesi S, Vidil R, et al (2012) Expression and function of proteinase-activated receptor 2 in human bronchial smooth muscle. American Journal of Respiratory and Critical Care Medicine 164:1276–1281.

Schneider W, Bortfeld T, Schlegel W (2000) Correlation between CT numbers and tissue parameters needed for Monte Carlo simulations of clinical dose distributions. Physics in Medicine & Biology 45:459–478.

Schoonjans K, Peinado-Onsurbe J, Lefebvre AM, et al (1996) PPARalpha and PPARgamma activators direct a distinct tissue-specific transcriptional response via a PPRE in the lipoprotein lipase gene. The EMBO Journal 15:5336–5348.

Schwartz AV, Sigurdsson S, Hue TF, et al (2013) vertebral bone marrow fat associated with lower trabecular BMD and prevalent vertebral fracture in older adults. The Journal of Clinical Endocrinology & Metabolism 98:2294–2300.

Scott G, Leopardi S, Parker L, et al (2003) The proteinase-activated receptor-2 mediates phagocytosis in a Rho-dependent manner in human keratinocytes. The Journal of Investigative Dermatology 121:529–541.

Seitz I, Hess S, Schulz H, et al (2006) Membrane-type serine protease-1/ Matriptase induces IL-6, IL-8 and MCP-1 in endothelial cells by activation of protease activated receptor-2: Potential implications in atherosclerosis. Circulation 114:II_258–II_258.

Sekyere EO, Dunn LL, Suryo Rahmanto Y, Richardson DR (2006) Role of melanotransferrin in iron metabolism: studies using targeted gene disruption in vivo. Blood 107:2599–2601.

Shalev A, Siegrist-Kaiser CA, Yen PM, et al (1996) The peroxisome proliferator-

activated receptor alpha is a phosphoprotein: Regulation by insulin. Endocrinology 137:4499–4502.

Shapiro SD (1998) Matrix metalloproteinase degradation of extracellular matrix: Biological consequences. Current Opinion in Cell Biology 10:602–608.

Shi C, Iura A, Terajima M, et al (2016) Deletion of BMP receptor type IB decreased bone mass in association with compromised osteoblastic differentiation of bone marrow mesenchymal progenitors. Scientific Reports 6:24256.

Shi J, Luo Q, Chen F, et al (2010) Induction of IL-6 and IL-8 by house dust mite allergen Der p1 in cultured human nasal epithelial cells is associated with PAR/PI3K/NFkappaB signaling. Journal for Oto-Rhino-Laryngology and its Related Specialties 72:256–265.

Shichijo M, Kondo S, Ishimori M, et al (2006) PAR-2 deficient CD4+ T cells exhibit downregulation of IL-4 and upregulation of IFN-γ after antigen challenge in mice. Allergology International 55:271–278.

Shimomura I, Hammer RE, Richardson JA, et al (1998) Insulin resistance and diabetes mellitus in transgenic mice expressing nuclear SREBP-1c in adipose tissue: Model for congenital generalized lipodystrophy. Genes & Development 12:3182–3194.

Shin CS, Lecanda F, Sheikh S, et al (2000) Relative abundance of different cadherins defines differentiation of mesenchymal precursors into osteogenic, myogenic, or adipogenic pathways. Journal of Cellular Biochemistry 78:566–577.

Shin JH, Hakim CH, Zhang K, Duan D (2011) Genotyping mdx, mdx3cv, and mdx4cv mice by primer competition polymerase chain reaction. Muscle and Nerve 43:283–286.

Shirakabe K, Terasawa K, Miyama K, et al (2001) Regulation of the activity of the transcription factor Runx2 by two homeobox proteins, Msx2 and Dlx5. Genes to Cells 6:851–856.

Shiraki T, Aoyama T, Yokoyama C, et al (2014) LOX-1 Plays an important role in ischemia-induced angiogenesis of limbs. PLoS One 9:e114542.

Sicinski P, Geng Y, Ryder-Cook AS, et al (1989) The molecular basis of muscular dystrophy in the mdx mouse: a point mutation. Science 244:1578–1580.

Siddiqui JA, Partridge NC (2016) Physiological Bone Remodeling: Systemic Regulation and Growth Factor Involvement. Physiology 31:233–245.

Sidlauskas K, Sutton E, Biddle M (2014) Osteoporosis in men: Epidemiology and treatment with denosumab. Clinical Interventions in Aging 9:593–601.

Sims NA (2016) Cell-specific paracrine actions of IL-6 family cytokines from bone, marrow and muscle that control bone formation and resorption. The International Journal of Biochemistry & Cell Biology 79:14–23.

Sims NA, Martin TJ (2014) Coupling the activities of bone formation and resorption: a multitude of signals within the basic multicellular unit. BoneKEy Reports 3.

Singh PP, van der Kraan AGJ, Xu J, et al (2012) Membrane-bound receptor activator of NFκB ligand (RANKL) activity displayed by osteoblasts is differentially regulated by osteolytic factors. Biochemical and Biophysical Research Communications 422:48–53.

Sinha KM, Zhou X (2013) Genetic and molecular control of Osterix in skeletal formation. Journal of Cellular Biochemistry 114:975–984.

Smith R, Jenkins A, Lourbakos A, et al (2000) Evidence for the activation of PAR-2 by the sperm protease, acrosin: expression of the receptor on oocytes. FEBS Letters 484:285–290.

Smith R, Ransjö M, Tatarczuch L, et al (2004) Activation of protease-activated receptor-2 leads to inhibition of osteoclast differentiation. Journal of Bone and Mineral Research 19:507–516.

Sobiak B, Graczyk-Jarzynka A, Leśniak W (2015) Comparison of DNA methylation and expression pattern of S100 and other epidermal differentiation complex genes in differentiating keratinocytes. Journal of Cellular Biochemistry 117:1092–1098.

Soh UJ, Dores MR, Chen B, Trejo J (2010) Signal transduction by protease-activated receptors. British Journal of Pharmacology 160:191–203.

Song B, Chi Y, Li X, et al (2015) Inhibition of notch signaling promotes the adipogenic differentiation of mesenchymal stem cells through autophagy activation and PTEN-PI3K/AKT/mTOR pathway. Cellular Physiology and Biochemistry 36:1991–2002.

Song L, Liu M, Ono N, et al (2012) Loss of wnt/β-catenin signaling causes cell fate shift of preosteoblasts from osteoblasts to adipocytes. Journal of Bone and Mineral Research 27:2344–2358.

Song S-J, Pagel CN, Campbell TM, et al (2005a) The role of protease-activated receptor-1 in bone healing. The American Journal of Pathology 166:857–868.

Song SJ, Pagel CN, Pike RN, Mackie EJ (2005b) Studies on the receptors mediating responses of osteoblasts to thrombin. The International Journal of Biochemistry & Cell Biology 37:206–213.

Sottile V, Seuwen K, Kneissel M (2004) Enhanced marrow adipogenesis and bone resorption in estrogen-deprived rats treated with the PPARgamma agonist BRL49653 (Rosiglitazone). Calcified Tissue International 75:329–337.

Spiegelman BM, Farmer SR (1982) Decreases in tubulin and actin gene expression prior to morphological differentiation of 3T3 adipocytes. Cell 29:53–60.

Spinella-Jaegle S, Rawadi G, Kawai S, et al (2001) Sonic hedgehog increases the commitment of pluripotent mesenchymal cells into the osteoblastic lineage and abolishes adipocytic differentiation. Journal of Cell Science 114:2085–2094.

St-Jacques B, Hammerschmidt M, McMahon AP (1999) Indian hedgehog signaling regulates proliferation and differentiation of chondrocytes and is essential for bone formation. Genes & Development 13:2072–2086.

Stalheim L (2005) Multiple independent functions of arrestins in the regulation of protease-activated receptor-2 signaling and trafficking. Molecular Pharmacology 67:78–87.

Stephens AS, Morrison NA (2014) Novel target genes of RUNX2 Transcription Factor and 1,25-Dihydroxyvitamin D3. Journal of Cellular Biochemistry 115:1594–1608.

Steppan CM, Bailey ST, Bhat S, et al (2001) The hormone Resistin links obesity to diabetes. Nature 409:307–312.

Stern SM, Ferguson PJ (2013) Autoinflammatory bone diseases. Rheumatic Disease Clinics of North America 39:735–749.

Striggow F, Riek M, Breder J, et al (2000) The protease thrombin is an endogenous mediator of hippocampal neuroprotection against ischemia at low concentrations but causes degeneration at high concentrations. Proceedings of the National Academy of Sciences 97:2264–2269.

Stumvoll M, Häring H-U (2002) Glitazones: Clinical effects and molecular mechanisms. Annals of Medicine 34:217–224.

Su AI, Wiltshire T, Batalov S, et al (2004) A gene atlas of the mouse and human protein-encoding transcriptomes. Proceedings of the National Academy of Sciences 101:6062–6067.

Sugihara H, Yonemitsu N, Toda S, et al (1988) Unilocular fat cells in three-dimensional collagen gel matrix culture. Journal of Lipid Research 29:691–697.

Suh JM, Gao X, McKay J, et al (2006) Hedgehog signaling plays a conserved role in inhibiting fat formation. Cell Metabolism 3:25–34.

Suidan HS, Bouvier J, Schaerer E, et al (1994) Granzyme A released upon stimulation of cytotoxic T lymphocytes activates the thrombin receptor on neuronal cells and astrocytes. Proceedings of the National Academy of Sciences 91:8112–8116.

Sung TS, Kim HU, Kim JH, et al (2015) Protease-activated receptors modulate excitability of murine colonic smooth muscles by differential effects on interstitial cells. The Journal of Physiology 593:1169–1181.

Suo Z, Wu M, Citron BA, et al (2003) Persistent protease-activated receptor 4 signaling mediates thrombin-induced microglial activation. Journal of Biological Chemistry 278:31177–31183.

Taghavi N (2016) A study of protease-activated receptor-2 in skeletal muscle. Doctoral Dissertation, The University of Melbourne. Melbourne.

Taghavi N, Sanaei R, Samuel CS, et al (2017) Protease-activated receptor-2 triggers mast cell degranulation and exacerbates bone and muscle pathology in dystrophin deficiency. Combined Meeting of Australian and New Zealand Bone and Mineral Society, Japanese Bone and Mineral Society and the International Federation of Musculoskeletal Research Societies, Brisbane, August 2017.

Taipaleenmäki H, Bjerre Hokland L, Chen L, et al (2012) Mechanisms in endocrinology: micro-RNAs: targets for enhancing osteoblast differentiation and bone formation. European Journal of Endocrinology 166:359–371.

Takada I, Mihara M, Suzawa M, et al (2007) A histone lysine methyltransferase activated by non-canonical Wnt signalling suppresses PPAR-γ transactivation. Nature Cell Biology 9:1273–1285.

Takami M, Woo J-T, Nagai K (1999) Osteoblastic cells induce fusion and activation of osteoclasts through a mechanism independent of macrophage-colony-stimulating factor production. Cell and Tissue Research 298:327–334.

Takeda S, Bonnamy JP, Owen MJ, et al (2001) Continuous expression of Cbfa1 in nonhypertrophic chondrocytes uncovers its ability to induce hypertrophic chondrocyte differentiation and partially rescues Cbfa1-deficient mice. Genes & Development 15:467–481.

Takeuchi T, Harris JL, Huang W, et al (2000) Cellular localization of membrane-type serine protease 1 and identification of protease-activated receptor-2 and single-chain urokinase-type plasminogen activator as substrates. Journal of Biological Chemistry 275:26333–26342.

Takigawa M, Nakanishi T, Kubota S, Nishida T (2003) Role of CTGF/HCS24/ecogenin in skeletal growth control. Journal of Cellular Physiology 194:256–266.

Tamai K, Semenov M, Kato Y, et al (2000) LDL-receptor-related proteins in Wnt signal transduction. Nature 407:530–535.

Tan JTM, McLennan SV, Song WW, et al (2008) Connective tissue growth factor inhibits adipocyte differentiation. American Journal of Physiology - Cell Physiology 295:C740–51.

Tan SH, Senarath-Yapa K, Chung MT, et al (2014) Wnts produced by Osterix-expressing osteolineage cells regulate their proliferation and differentiation. Proceedings of the National Academy of Sciences 111:E5262–71.

Tanaka T, Yoshida N, Kishimoto T, Akira S (1997) Defective adipocyte differentiation in mice lacking the C/EBPβ and/or C/EBPδ gene. The EMBO Journal 16:7432–7443.

Tang Q-Q, Lane MD (2012) Adipogenesis: From stem cell to adipocyte. Annual review of biochemistry 81:715–736.

Tang Q-Q, Otto TC, Lane MD (2004) Commitment of C3H10T1/2 pluripotent stem cells to the adipocyte lineage. Proceedings of the National Academy of Sciences

101:9607–9611.

Tang W, Yang F, Li Y, et al (2012) Transcriptional regulation of Vascular Endothelial Growth Factor (VEGF) by osteoblast-specific transcription factor Osterix (Osx) in osteoblasts. Journal of Biological Chemistry 287:1671–1678.

Tao H, Umek RM (1999) Reciprocal regulation of gadd45 by C/EBPalpha and c-Myc. DNA and Cell Biology 18:75–84.

Tao K-M, Tao Y, Chen C-Y, et al (2014) Proteinase-activated receptor 1 contributed to up-regulation of enkephalin in keratinocytes of patients with obstructive jaundice. Anesthesiology 121:127–139.

Taxman DJ, Moore CB, Guthrie EH, Huang MT-H (2010) Short hairpin RNA (shRNA): design, delivery, and assessment of gene knockdown. In: Bone research protocols. Humana Press, Totowa, NJ, pp 139–156.

Teplyuk NM, Zhang Y, Lou Y, et al (2009) The osteogenic transcription factor Runx2 controls genes involved in sterol/steroid metabolism, including Cyp11a1 in osteoblasts. Molecular Endocrinology 23:849–861.

Thomas T, Gori F, Spelsberg TC, et al (2011) Response of bipotential human marrow stromal cells to insulin-like growth factors: Effect on binding protein production, proliferation, and commitment to osteoblasts and adipocytes. Endocrinology 140:5036–5044.

Thompson EM, Matsiko A, Farrell E, et al (2015) Recapitulating endochondral ossification: a promising route to in vivo bone regeneration. Journal of Tissue Engineering and Regenerative Medicine 9:889–902.

Tillu DV, Hassler SN, Burgos-Vega CC, et al (2015) Protease activated receptor 2 (PAR2) activation is sufficient to induce the transition to a chronic pain state. Pain 156:859–867.

Titorencu I, Pruna V, Jinga VV, Simionescu M (2014) Osteoblast ontogeny and implications for bone pathology: an overview. Cell and Tissue Research 355:23–33.

Tondreau T, Meuleman N, Stamatopoulos B, et al (2009) In vitro study of matrix metalloproteinase/tissue inhibitor of metalloproteinase production by mesenchymal stromal cells in response to inflammatory cytokines: the role of their migration in injured tissues. Cytotherapy 11:559–569.

Tonna S, Sims NA (2014) Talking among ourselves: Paracrine control of bone formation within the osteoblast lineage. Calcified tissue international 94:35-45.

Tontonoz P, Hu E, Graves RA, et al (1994a) mPPAR gamma 2: tissue-specific regulator of an adipocyte enhancer. Genes & Development 8:1224–1234.

Tontonoz P, Hu E, Spiegelman BM (1994b) Stimulation of adipogenesis in fibroblasts by PPARγ2, a lipid-activated transcription factor. Cell 79:1147–1156.

Toriwaki J, Yonekura T (2002) Euler number and connectivity indexes of a three dimensional digital picture. Forma 17:183–209.

Tou L, Quibria N, Alexander JM (2003) Transcriptional regulation of the human Runx2/Cbfa1 gene promoter by bone morphogenetic protein-7. Molecular and Cellular Endocrinology 205:121–129.

Towler DA, Rutledge SJ, Rodan GA (1994) Msx-2/Hox 8.1: a transcriptional regulator of the rat osteocalcin promoter. Molecular Endocrinology 8:1484–1493.

Toyoda N, Gabazza E, Inoue H, et al (2003) Expression and cytoprotective effect of protease-activated receptor-1 in gastric epithelial cells. Scandinavian Journal of Gastroenterology 38:253–259.

Trayhurn P, Beattie JH (2001) Physiological role of adipose tissue: white adipose tissue as an endocrine and secretory organ. Proceedings of the Nutrition Society 60:329–339.

Truett GE, Heeger P, Mynatt RL, et al (2000) Preparation of PCR-quality mouse genomic DNA with hot sodium hydroxide and tris (HotSHOT). BioTechniques 29:52–54.

Tsopanoglou NE, Maragoudakis ME (1999) On the mechanism of thrombin-induced angiogenesis. Potentiation of vascular endothelial growth factor activity on endothelial cells by up-regulation of its receptors. Journal of Biological Chemistry 274:23969–23976.

Tsutsui H, Kinouchi T, Wakano Y, Ohnishi Y (1987) Purification and characterization of a protease from Bacteroides gingivalis 381. Infection and Immunity 55:420–427.

Ubl JJ, Reiser G (1996) Activity of protein kinase C is necessary for sustained thrombin-induced [Ca2+]i oscillations in rat glioma cells. Pfluegers Arch 433:312–320.

Ubl JJ, Reiser G (1997) Characteristics of thrombin-induced calcium signals in rat astrocytes. Glia 21:361–369.

Ueta C, Iwamoto M, Kanatani N, et al (2001) Skeletal malformations caused by overexpression of Cbfa1 or its dominant negative form in chondrocytes. The Journal of Cell Biology 153:87–100.

Ullah M, Stich S, Notter M, et al (2013) Transdifferentiation of mesenchymal stem cells-derived adipogenic-differentiated cells into osteogenic- or chondrogenic-differentiated cells proceeds via dedifferentiation and have a correlation with cell cycle arresting and driving genes. Differentiation 85:78–90.

Ulsamer A, Ortuño MJ, Ruiz S, et al (2008) BMP-2 induces Osterix expression through up-regulation of Dlx5 and its phosphorylation by p38. Journal of Biological Chemistry 283:3816–3826.

Uphoff CC, Drexler HG (2011) Detecting mycoplasma contamination in cell cultures

by polymerase chain reaction. Cancer Cell Culture: Methods and Protocols (2011): 93-103.

Urban JD, Clarke WP, Zastrow von M, et al (2007) Functional selectivity and classical concepts of quantitative pharmacology. The Journal of Pharmacology and Experimental Therapeutics 320:1–13.

Urist MR (1965) Bone: Formation by autoinduction. Science 150:893–899.

Varjosalo M, Taipale J (2008) Hedgehog: functions and mechanisms. Genes & Development 22:2454-2472.

Vaughan PJ, Pike CJ, Cotman CW, Cunningham DD (1995) Thrombin receptor activation protects neurons and astrocytes from cell death produced by environmental insults. The Journal of Neuroscience 15:5389–5401.

Venter JC, Adams MD, Myers EW, et al (2001) The Sequence of the Human Genome. Science 291:1304–1351.

Vergnolle N (1999) Proteinase-activated receptor-2-activating peptides induce leukocyte rolling, adhesion, and extravasation in vivo. The Journal of Immunology 163:5064–5069.

Vergnolle N, Bunnett NW, Sharkey KA, et al (2001a) Proteinase-activated receptor-2 and hyperalgesia: A novel pain pathway. Nature Medicine 7:821–826.

Vergnolle N, Hollenberg MD, Sharkey KA, Wallace JL (1999a) Characterization of the inflammatory response to proteinase-activated receptor-2 (PAR2)-activating peptides in the rat paw. British Journal of Pharmacology 127:1083–1090.

Vergnolle N, Hollenberg MD, Wallace JL (1999b) Pro- and anti-inflammatory actions of thrombin: a distinct role for proteinase-activated receptor-1 (PAR1). British Journal of Pharmacology 126:1262–1268.

Vergnolle N, Wallace JL, Bunnett NW (2001b) Protease-activated receptors in inflammation, neuronal signaling and pain. Trends in Pharmacological Sciences 22:146–152.

Vu T-KH, Hung DT, Wheaton VI, Coughlin SR (1991) Molecular cloning of a functional thrombin receptor reveals a novel proteolytic mechanism of receptor activation. Cell 64:1057–1068.

Wada T, Nakashima T, Hiroshi N, Penninger JM (2006) RANKL–RANK signaling in osteoclastogenesis and bone disease. Trends in Molecular Medicine 12:17–25.

Walker EC, McGregor NE, Poulton IJ, et al (2008) Cardiotrophin-1 is an osteoclast-derived stimulus of bone formation required for normal bone remodeling. Journal of Bone and Mineral Research 23:2025–2032.

Walker JKL, DeFea KA (2014) Role for β-arrestin in mediating paradoxical β2AR and PAR2 signaling in asthma. Current Opinion in Pharmacology 16:142–147.

Wang C, Pattabiraman N, Zhou JN, et al (2003) Cyclin D1 repression of peroxisome proliferator-activated receptor gamma expression and transactivation. Molecular and Cellular Biology 23:6159–6173.

Wang C, Tian L, Zhang K, et al (2016a) Interleukin-6 gene knockout antagonizes high-fat-induced trabecular bone loss. Journal of Molecular Endocrinology 57:161–170.

Wang C-WJ, McCauley LK (2016) Osteoporosis and periodontitis. Current Osteoporosis Reports 14:284–291.

Wang D, Zhou Y, Lei W, et al (2010) Signal transducer and activator of transcription 3 (STAT3) regulates adipocyte differentiation via peroxisome-proliferator-activated receptor gamma (PPARgamma). Biology of the Cell 102:1–12.

Wang EA, Israel DI, Kelly S, Luxenberg DP (2009) Bone morphogenetic protein-2 causes commitment and differentiation in C3Hl0T1/2 and 3T3 cells. Growth Factors 9:57–71.

Wang H, Ubl JJ, Reiser G (2002) Four subtypes of protease-activated receptors, co-expressed in rat astrocytes, evoke different physiological signaling. Glia 37:53–63.

Wang L, Ciani C, Doty SB, Fritton SP (2004) Delineating bone's interstitial fluid pathway in vivo. Bone 34:499–509.

Wang X, Goh CH, Li B (2007) p38 mitogen-activated protein kinase regulates osteoblast differentiation through Osterix. Endocrinology 148:1629–1637.

Wang Y, Chang H, Rattner A, Nathans J (2016b) Frizzled receptors in development and disease. In: Wassarman PM (ed), Essays on developmental biology, part B. Elsevier, pp 113–139.

Wei LL, Leach MW, Miner RS, Demers LM (1993) Evidence for progesterone receptors in human osteoblast-like cells. Biochemical and Biophysical Research Communications 195:525–532.

Weise M, De-Levi S, Barnes KM, et al (2001) Effects of estrogen on growth plate senescence and epiphyseal fusion. Proceedings of the National Academy of Sciences 98:6871–6876.

Westendorf JJ, Kahler RA, Schroeder TM (2004) Wnt signaling in osteoblasts and bone diseases. Gene 341:19–39.

Wilkison WO, Choy L, Spiegelman BM (1991) Biosynthetic regulation of monobutyrin, an adipocyte-secreted lipid with angiogenic activity. Journal of Biological Chemistry 266:16886–16891.

William Lau KH, Baylink DJ, Zhou XD, et al (2013) Osteocyte-derived insulin-like growth factor I is essential for determining bone mechanosensitivity. AJP: Endocrinology and Metabolism 305:E271–E281.

Wilson S, Greer B, Hooper J, et al (2005) The membrane-anchored serine protease,

TMPRSS2, activates PAR-2 in prostate cancer cells. Biochemical Journal 388:967–972.

Windahl SH, Börjesson AE, Farman HH, et al (2013) Estrogen receptor-α in osteocytes is important for trabecular bone formation in male mice. Proceedings of the National Academy of Sciences 110:2294–2299.

Winkler DG, Sutherland MK, Geoghegan JC, et al (2003) Osteocyte control of bone formation via sclerostin, a novel BMP antagonist. The EMBO Journal 22:6267–6276.

Wong DM, Tam V, Lam R, et al (2010) Protease-activated receptor 2 has pivotal roles in cellular mechanisms involved in experimental periodontitis. Infection and Immunity 78:629–638.

Wozney JM, Rosen V (1998) Bone morphogenetic protein and bone morphogenetic protein gene family in bone formation and repair. Clinical Orthopaedics and Related Research 346:26-37.

Wozniak SE, Gee LL, Wachtel MS, Frezza EE (2009) Adipose tissue: The new endocrine organ? A review article. Digestive Diseases and Sciences 54:1847–1856.

Wölfing B, Buechler C, Weigert J, et al (2008) Effects of the new C1q/TNF-related protein (CTRP-3) "cartonectin" on the adipocytic secretion of adipokines. Obesity 16:1481–1486.

Wronski TJ, Morey-Holton E, Jee WS (1981) Skeletal alterations in rats during space flight. Advances in Space Research 1:135–140.

Wu Y-F, Matsuo N, Sumiyoshi H, Yoshioka H (2010) Sp7/Osterix is involved in the up-regulation of the mouse pro-α1(V) collagen gene (Col5a1) in osteoblastic cells. Matrix Biology 29:701–706.

Wu Z, Rosen ED, Brun R, et al (1999) Cross-regulation of C/EBPα and PPARγ controls the transcriptional pathway of adipogenesis and insulin sensitivity. Molecular Cell 3:151–158.

Wu Z, Xie Y, Bucher NL, Farmer SR (1995) Conditional ectopic expression of C/EBP beta in NIH-3T3 cells induces PPAR gamma and stimulates adipogenesis. Genes & Development 9:2350–2363.

Xiao G, Di Jiang, Thomas P, et al (2000) MAPK pathways activate and phosphorylate the osteoblast-specific transcription factor, Cbfa1. Journal of Biological Chemistry 275:4453–4459.

Xiao G, Jiang D, Ge C, et al (2005) Cooperative interactions between activating transcription factor 4 and Runx2/Cbfa1 stimulate osteoblast-specific osteocalcin gene expression. Journal of Biological Chemistry 280:30689–30696.

Xiao L, Sobue T, Esliger A, et al (2010) Disruption of the Fgf2 gene activates the adipogenic and suppresses the osteogenic program in mesenchymal marrow stromal

stem cells. Bone 47:360–370.

Xiao ZS, Hjelmeland AB, Quarles LD (2004) Selective deficiency of the “bone-related” Runx2-II unexpectedly preserves osteoblast-mediated skeletogenesis. Journal of Biological Chemistry 279:20307-20313.

Xie L, Ortega MT, Mora S, Chapes SK (2010) Interactive changes between macrophages and adipocytes. Clinical and Vaccine Immunology 17:651–659.

Yang X, Matsuda K, Bialek P, et al (2004) ATF4 is a substrate of RSK2 and an essential regulator of osteoblast biology. Cell 117:387–398.

Yasuda H, Shima N, Nakagawa N, et al (1998) Osteoclast differentiation factor is a ligand for osteoprotegerin/osteoclastogenesis-inhibitory factor and is identical to TRANCE/RANKL. Proceedings of the National Academy of Sciences 95:3597–3602.

Yaturu S, Bryant B, Jain SK (2007) Thiazolidinedione treatment decreases bone mineral density in type 2 diabetic men. Diabetes Care 30:1574–1576.

Yau M-K, Lim J, Liu L, Fairlie DP (2016a) Protease activated receptor 2 (PAR2) modulators: a patent review (2010–2015). Expert Opinion on Therapeutic Patents 26:471–483.

Yau M-K, Liu L, Suen JY, et al (2016b) PAR2 modulators derived from GB88. ACS Medicinal Chemistry Letters 7:1179–1184.

Yeh WC, Cao Z, Classon M, McKnight SL (1995) Cascade regulation of terminal adipocyte differentiation by three members of the C/EBP family of leucine zipper proteins. Genes & Development 9:168–181.

Yiu EM, Kornberg AJ (2015) Duchenne muscular dystrophy. Journal of Paediatrics and Child Health 51:759–764.

Yoshitake F, Itoh S, Narita H, et al (2008) Interleukin-6 directly inhibits osteoclast differentiation by suppressing receptor activator of NF-kappaB signaling pathways. Journal of Biological Chemistry 283:11535–11540.

Young MF (2003) Bone matrix proteins: their function, regulation, and relationship to osteoporosis. Osteoporosis International 14:35–42.

Yun-Feng W, Matsuo N, Sumiyoshi H, Yoshioka H (2010) Sp7/Osterix up-regulates the mouse pro-α3(V) collagen gene (Col5a3) during the osteoblast differentiation. Biochemical and Biophysical Research Communications 394:503–508.

Zanello LP, Norman AW (2004) Rapid modulation of osteoblast ion channel responses by 1 ,25(OH)2-vitamin D3 requires the presence of a functional vitamin D nuclear receptor. Proceedings of the National Academy of Sciences 101:1589–1594.

Zania P, Gourni D, Aplin AC, et al (2009) Parstatin, the cleaved peptide on proteinase-activated receptor 1 activation, is a potent inhibitor of angiogenesis. The Journal of

Pharmacology and Experimental Therapeutics 328:378–389.

Zeng X, Tamai K, Doble B, et al (2005) A dual-kinase mechanism for Wnt co-receptor phosphorylation and activation. Nature 438:873–877.

Zhang F, Wang C, Wang H, et al (2013) Ox-LDL promotes migration and adhesion of bone marrow-derived mesenchymal stem cells via regulation of MCP-1 expression. Mediators of Inflammation 2013.

Zhang K, Guo W, Yang Y, Wu J (2011) JAK2/STAT3 pathway is involved in the early stage of adipogenesis through regulating C/EBPβ transcription. Journal of Cellular Biochemistry 112:488–497.

Zhang M, Xuan S, Bouxsein ML, et al (2002) Osteoblast-specific knockout of the insulin-like growth factor (IGF) receptor gene reveals an essential role of IGF signaling in bone matrix mineralization. Journal of Biological Chemistry 277:44005-44012.

Zhang W, Ou G, Hamrick M, et al (2008) Age-related changes in the osteogenic differentiation potential of mouse bone marrow stromal cells. Journal of Bone and Mineral Research 23:1118–1128.

Zhang Y, Proenca R, Maffei M, et al (1994) Positional cloning of the mouse obese gene and its human homologue. Nature 372:425-432.

Zhao G, Monier-Faugere M-C, Langub MC, et al (2011) Targeted overexpression of insulin-like growth factor i to osteoblasts of transgenic mice: Increased trabecular bone volume without increased osteoblast proliferation. Endocrinology 141:2674–2682.

Zhao P, Lieu T, Barlow N, et al (2015) Neutrophil elastase activates protease-activated receptor-2 (PAR2) and transient receptor potential vanilloid 4 (TRPV4) to cause inflammation and pain. The Journal of Biological Chemistry 290:13875–13887.

Zhao P, Metcalf M, Bunnett NW (2014) Biased signaling of protease-activated receptors. Frontiers in Endocrinology 5:943.

Zhou X, Zhang Z, Feng JQ, et al (2010) Multiple functions of Osterix are required for bone growth and homeostasis in postnatal mice. Proceedings of the National Academy of Sciences 107:12919-12924.

Zhu F, Friedman MS, Luo W, et al (2012) The transcription factor osterix (SP7) regulates BMP6-induced human osteoblast differentiation. Journal of Cellular Physiology 227:2677–2685.

Zhu Y, Alvares K, Huang Q, et al (1993) Cloning of a new member of the peroxisome proliferator-activated receptor gene family from mouse liver. Journal of Biological Chemistry 268:26817–26820.

Zielins ER, Paik K, Ransom RC, et al (2016) Enrichment of adipose-derived stromal cells for bmpr1a facilitates enhanced adipogenesis. Tissue Engineering Part A

22:214–221.

Zimmermann R, Strauss JG, Haemmerle G, et al (2004) Fat mobilization in adipose tissue is promoted by adipose triglyceride lipase. Science 306:1383–1386.

Zinman B, Haffner SM, Herman WH, et al (2010) Effect of rosiglitazone, metformin, and glyburide on bone biomarkers in patients with type 2 diabetes. The Journal of Clinical Endocrinology & Metabolism 95:134–142.

Ziros PG, Gil A-PR, Georgakopoulos T, et al (2002) The bone-specific transcriptional regulator Cbfa1 is a target of mechanical signals in osteoblastic cells. Journal of Biological Chemistry 277:23934–23941.

Zoudilova M, Kumar P, Ge L, et al (2007) β-Arrestin-dependent regulation of the cofilin pathway downstream of protease-activated receptor-2. Journal of Biological Chemistry 282:20634–20646.

Zoudilova M, Min J, Richards HL, et al (2010) Arrestins scaffold cofilin with chronophin to direct localized actin filament severing and membrane protrusions downstream of protease-activated receptor-2. Journal of Biological Chemistry 285:14318–14329.

Zuk PA, Zhu M, Ashjian P, et al (2002) Human adipose tissue is a source of multipotent stem cells. Molecular Biology of the Cell 13:4279–4295.

APPENDIX A: COMPLEMENTARY DATA - MICRO CT OF GLOBAL PAR_2 NULL AND WILDTYPE MICE

Table A.1 Micro CT of proximal tibiae in PAR_2 null & WT mice - Males.

Endpoint		20 WEEKS			32 WEEKS	
Genotype	WT	KO	*P*-value*	WT	KO	*P*-value*
TV (mm^3)	2.407±0.045	2.431±0.097	0.580	2.138±0.082	2.226±0.152	0.726
BV (mm^3)	0.413±0.032	0.032±0.046	0.111	0.254±0.038	0.183±0.048	0.155
BV/TV (%)	17.112±1.114	13.342±1.617	0.028	11.784±1.498	7.932±1.816	0.076
Conn.D ($1/mm^3$)	257.002±32.388	256.604±50.843	0.500	299.316±107.521	467.156±144.986	0.845
Tb.N (1/mm)	5.357±0.224	4.688±0.311	0.076	4.309±0.177	3.264±0.260	0.008
Tb.Th (mm)	0.050±0.001	0.047±0.003	0.274	0.051±0.003	0.044±0.004	0.076
Tb.Sp (mm)	0.204±0.008	0.236±0.016	0.048	0.257±0.010	0.338±0.023	0.008
DA	2.036±0.038	1.876±0.044	0.016	1.752±0.048	1.667±0.035	0.111
SMI [t]	1.623±0.063	1.924±0.171	0.151	2.211±0.109	2.277±0.155	1.000
BMD (mg HA/cm^3)	145.854±11.192	109.644±17.889	0.111	99.188±17.198	75.029±20.044	0.211
TMD (mg HA/cm^3)	781.757±11.976	741.768±10.652	0.028	717.572±14.795	622.919±12.109	0.004

* Using Mann-Whitney U test.
[t] All values except SMI were analysed using one-tailed comparisons.

Table A.2 Micro CT of proximal tibiae in PAR_2 null & WT mice - Females.

Endpoint		20 WEEKS			32 WEEKS	
Genotype	WT	KO	*P*-value*	WT	KO	*P*-value*
TV (mm^3)	1.722±0.049	1.598±0.090	0.211	1.839±0.116	1.557±0.108	0.095
BV (mm^3)	0.090±0.01	0.068±0.01	0.111	0.051±0.011	0.047±0.011	0.500
BV/TV (%)	5.210±0.506	4.234±0.429	0.076	2.790±0.676	2.920±0.515	0.722
Conn.D ($1/mm^3$)	50.922±11.707	80.469±29.795	0.580	17.179±8.100	85.295±46.147	0.969
Tb.N (1/mm)	2.672±0.119	2.66±0.109	0.500	1.871±0.138	2.151±0.159	0.857
Tb.Th (mm)	0.051±0.002	0.047±0.002	0.076	0.053±0.002	0.050±0.003	0.278
Tb.Sp (mm)	0.393±0.016	0.393±0.015	0.500	0.566±0.043	0.490±0.039	0.857
DA	1.810±0.044	1.686±0.069	0.155	1.891±0.075	1.592±0.079	0.032
SMI [t]	2.911±0.220	3.012±0.135	0.421	2.798±0.221	2.734±0.276	1.000
BMD (mg HA/cm^3)	21.466±5.434	13.945±5.774	0.790	-12.764±8.612	-1.657±4.516	0.857
TMD (mg HA/cm^3)	802.834±13.690	768.293±25.013	0.845	810.263±21.675	715.880±17.512	0.032

* Using Mann-Whitney U test.
[t] All values except SMI were analysed using one-tailed comparisons

Table A.3 Micro CT of L5 vertebrae in PAR_2 null & WT mice - Males.

Endpoint	20 WEEKS			32 WEEKS		
Genotype	WT	KO	*P*-value*	WT	KO	*P*-value*
TV (mm^3)	2.372±0.05	2.316±0.072	0.500	2.469±0.055	2.533±0.078	0.655
BV (mm^3)	0.66±0.015	0.561±0.018	0.004	0.57±0.051	0.509±0.053	0.155
BV/TV (%)	0.278±0.005	0.243±0.012	0.016	0.231±0.019	0.203±0.024	0.790
Conn.D ($1/mm^3$)	372.222±29.878	478.973±52.148	0.925	648.48±229.44	1653.501±233.631	0.972
Tb.N (1/mm)	6.234±0.142	6.195±0.301	0.421	5.925±0.356	6.592±0.48	0.889
Tb.Th (mm)	0.055±0.001	0.051±0.003	0.211	0.053±0.003	0.046±0.003	0.076
Tb.Sp (mm)	0.182±0.003	0.186±0.008	0.500	0.2±0.006	0.183±0.01	0.845
DA	1.835±0.018	1.699±0.018	0.004	1.606±0.041	1.467±0.023	0.016
SMI [t]	0.411±0.041	0.802±0.118	0.016	0.956±0.076	1.543±0.126	0.008
BMD (mg HA/cm^3)	243.223±5.556	213.047±12.666	0.048	203.875±20.2	206.792±21.608	0.421
TMD (mg HA/cm^3)	793.699±7.002	745.712±10.187	0.008	715.096±19.718	620.956±8.464	0.004

[*] Using Mann-Whitney U test.
[t] All values except SMI were analysed using one-tailed comparisons.

Table A.4 Micro CT of L5 vertebrae in PAR_2 null & WT mice - Females.

Endpoint	20 WEEKS			32 WEEKS		
Genotype	WT	KO	*P*-value*	WT	KO	*P*-value*
TV (mm^3)	2.32±0.021	2.134±0.134	0.274	2.534±0.116	2.104±0.051	0.008
BV (mm^3)	0.442±0.031	0.428±0.027	0.421	0.412±0.055	0.346±0.031	0.095
BV/TV (%)	0.191±0.013	0.201±0.005	0.500	0.161±0.016	0.165±0.015	0.635
Conn.D ($1/mm^3$)	266.558±53.883	344.248±48.131	0.845	219.277±40.6	420.276±82.142	0.969
Tb.N (1/mm)	4.471±0.243	4.711±0.163	0.655	3.737±0.242	3.992±0.256	0.717
Tb.Th (mm)	0.051±0.001	0.051±0.001	0.580	0.051±0.002	0.056±0.001	0.905
Tb.Sp (mm)	0.255±0.012	0.246±0.006	0.500	0.303±0.018	0.298±0.015	0.500
DA	1.625±0.027	1.564±0.041	0.155	1.556±0.015	1.517±0.024	0.143
SMI	0.869±0.111	0.85±0.096	1.000	0.986±0.134	1.297±0.125	0.111
BMD (mg HA/cm^3)	154.109±13.756	166.583±4.724	0.655	123.75±16.654	138.512±16.322	0.635
TMD (mg HA/cm^3)	756.699±17.996	739.695±20.286	0.345	758.534±18.272	693.432±12.709	0.032

[*] Using Mann-Whitney U test.
[t] All values except SMI were analysed using one-tailed comparisons

Table A.5 Micro CT of midshaft tibial cortex in PAR_2 null & WT mice - Males.

Endpoint		**20 WEEKS**			**32 WEEKS**	
Genotype	WT	KO	*P*-value*	WT	KO	*P*-value*
Tt.Ar (mm^2)†	1.264±0.017	1.224±0.024	0.274	1.279±0.047	1.343±0.024	0.7895
Ct.Ar (mm^2)†	0.761±0.011	0.706±0.013	0.274	0.696±0.032	0.681±0.013	0.2105
Ma.Ar (mm^2)	0.504±0.015	0.518±0.026	0.421	0.583±0.018	0.661±0.026	0.032
Ct.Ar/Tt.Ar (%)†	60.183±0.825	57.549±1.251	0.0755	54.335±0.697	50.808±1.251	0.008
Ct.Th (mm)†	0.231±0.004	0.218±0.005	0.274	0.204±0.007	0.19±0.005	0.0755
Ma.Dm (mm)	0.624±0.007	0.655±0.021	0.016	0.647±0.009	0.689±0.021	0.095
/max (mm^4)†	0.149±0.005	0.136±0.004	0.274	0.15±0.012	0.148±0.004	0.155
/min (mm^4)†	0.086±0.002	0.081±0.003	0.111	0.083±0.006	0.09±0.003	0.655
***J* (mm^4)†**	0.2350.006	0.217±0.006	0.345	0.233±0.017	0.238±0.006	0.726
Ct.Po (1)	0.008±0.001	0.004±0.001	0.008	0.005±0.002	0.007±0.001	0.31
Po.N	102.4±6.369	121±17.769	0.421	173.2±45.906	264.2±17.769	0.151
Po.V (mm^3)	0.011±0.001	0.005±0.001	0.008	0.007±0.002	0.009±0.001	0.548
AvgPo.V (mm^3)	1.1E-04±1.2E-05	4.7e-05±3.6E-06	0.016	3.9E-05±1.2E-05	3.51E-05±3.6E-06	1
Po.Dn	75.11±5.017	95.49±14.796	0.151	134.889±32.189	214.742±14.796	0.095
TMD ($mgHA/mm^3$)†	1195.426±5.519	1200.25±4.869	0.726	1212.265±6.934	1188.987±4.869	0.028

* Using Mann-Whitney U test.
† one-tailed comparisons.

Table A.6 Micro CT of midshaft tibial cortex in PAR_2 null & WT mice - Females.

Endpoint		**20 WEEKS**			**32 WEEKS**	
Genotype	WT	KO	*P*-value*	WT	KO	*P*-value*
Tt.Ar (mm^2)†	0.947±0.015	0.963±0.05	0.5795	0.997±0.018	0.963±0.018	0.278
Ct.Ar (mm^2)†	0.53±0.009	0.544±0.025	0.655	0.533±0.012	0.526±0.016	0.5
Ma.Ar (mm^2)	0.418±0.01	0.419±0.027	1	0.464±0.012	0.436±0.021	0.286
Ct.Ar/Tt.Ar (%)†	55.929±0.63	56.607±0.883	0.655	53.457±0.781	54.701±1.686	0.722
Ct.Th (mm)†	0.182±0.003	0.185±0.004	0.726	0.177±0.004	0.181±0.007	0.5475
Ma.Dm (mm)	0.575±0.017	0.569±0.018	0.548	0.604±0.02	0.562±0.033	0.413
/max (mm^4)†	0.069±0.002	0.074±0.007	0.726	0.076±0.003	0.072±0.001	0.2065
/min (mm^4)†	0.053±0.002	0.054±0.005	0.5	0.057±0.002	0.053±0.003	0.2065
***J* (mm^4)†**	0.122±0.004	0.129±0.013	0.655	0.133±0.005	0.125±0.004	0.095
Ct.Po (1)	0.006±0.001	0.008±0.001	0.548	0.005±0.001	0.006±0.001	0.286
Po.N	91.2±18.893	87.4±0.001	0.548	86±17.358	160±47.859	0.111
Po.V (mm^3)	0.006±0.001	0.007±0.001	0.31	0.004±0.001	0.006±0.001	0.19
AvgPo.V (mm^3)	7.3E-05±1.5E-05	1.1E-04±3.5E-05	0.421	5.9E-05±1.5E-05	4.3E-05±6.8E-06	0.556
Po.Dn	98.602±21.399	90.636±20.828	0.069	90.287±16.73	169.49±46.425	0.111
TMD (mgHA/mm^3)†	1199.883±8.178	1208.725±4.008	0.5795	1219.75±2.561	1210.151±3.645	0.0315

* Using Mann-Whitney U test.
† one-tailed comparisons.

APPENDIX B: COMPLEMENTARY DATA - MICRO CT OF MDX-PAR$_2$ NULL AND MDX-WILDTYPE MICE

Table B.1 Micro CT indices of proximal tibiae in mdx-PAR$_2$ null & WT mice - Males.

Age	**20 WEEKS** [a]			**32 WEEKS**		
Genotype	WT	KO	*P*-value*	WT	KO	*P*-value*
TV (mm^3)	1.851±0.196	2.376±0.161	0.505	2.123±0.306	2.47±0.077	0.245
BV (mm^3)	0.146±0.02	0.335±0.046	0.001	0.162±0.035	0.192±0.035	0.331
BV/TV (%)	7.85±0.733	14.106±1.321	0.002	8.085±1.168	7.693±1.333	0.500
Conn.D (1/mm^3)	740.02±64.56	1386.599±139.172	0.000	152.025±70.264	117.086±46.617	0.574
Tb.N (1/mm)	3.581±0.102	4.393±0.212	0.011	3.241±0.3	3.405±0.267	0.426
Tb.Th (mm)	0.043±0.001	0.053±0.003	0.007	0.038±0.005	0.043±0.003	0.426
Tb.Sp (mm)	0.302±0.008	0.259±0.013	0.011	0.346±0.056	0.306±0.035	0.377
DA	1.528±0.022	1.64±0.046	0.025	6.015±4.159	1.838±0.077	0.275
SMI [t]	2.813±0.078	2.589±0.067	0.963	2.115±0.307	2.586±0.254	0.207
BMD (mg HA/cm^3)	91.01±8.257	138.569±12.115	0.007	65.882±9.019	56.83±5.952	0.331
TMD (mg HA/cm^3)	622.09±5.201	646.286±7.548	0.025	771.624±50.419	799.079±50.773	0.500

[a] Data courtesy of Dr. Neda Taghavi *et al*.
[*] Using Mann-Whitney U test.
[t] All values except SMI were analysed using one-tailed comparisons.

Table B.2 Micro CT indices of proximal tibiae in mdx-PAR$_2$ null & WT mice -Females.

Age	**20 WEEKS** [a]			**32 WEEKS**		
Genotype	WT	KO	*P*-value*	WT	KO	*P*-value*
TV (mm^3)	1.649±0.094	1.765±0.15	0.360	1.876±0.106	1.924±0.097	0.268
BV (mm^3)	0.102±0.01	0.167±0.017	0.001	0.048±0.008	0.075±0.008	0.017
BV/TV (%)	6.226±0.57	9.288±0.381	0.000	2.501±0.344	3.896±0.377	0.017
Conn.D (1/mm^3)	323.53±35.03	499.324±26.797	0.001	205.801±64.055	178.481±60.601	0.638
Tb.N (1/mm)	2.876±0.107	3.333±0.064	0.002	1.596±0.154	2.03±0.128	0.028
Tb.Th (mm)	0.05±0.002	0.054±0.001	0.078	0.044±0.002	0.045±0.002	0.268
Tb.Sp (mm)	0.374±0.012	0.326±0.006	0.004	0.68±0.065	0.526±0.037	0.028
DA	1.636±0.044	1.642±0.047	0.371	1.578±0.087	1.787±0.108	0.479
SMI [t]	2.887±0.073	2.573±0.062	0.800	2.915±0.155	2.785±0.094	0.857
BMD (mg HA/cm^3)	67.645±9.253	84.054±6.134	0.091	15.795±8.919	27.107±5.965	0.187
TMD (mg HA/cm^3)	705.007±8.683	728.153±4.716	0.026	689.656±50.922	759.025±43.939	0.268

[a] Data courtesy of Dr. Neda Taghavi *et al*.
[*] Using Mann-Whitney U test.
[t] All values except SMI were analysed using one-tailed comparisons.

Table B.3 Micro CT of midshaft tibial cortex in mdx-PAR_2 null & WT mice - Males.

Endpoint		**20 WEEKS**			**32 WEEKS**	
Genotype	WT	KO	*P*-value*	WT	KO	*P*-value*
Tt.Ar (mm^2)†	1.268±0.016	1.24±0.041	0.345	1.305±0.024	1.299±0.045	0.755
Ct.Ar (mm^2)†	0.76±0.02	0.751±0.032	1.000	0.729±0.013	0.731±0.024	1.000
Ma.Ar (mm^2)	0.508±0.014	0.489±0.01	0.345	0.577±0.013	0.568±0.023	0.345
Ct.Ar/Tt.Ar (%)†	59.942±1.131	60.501±0.567	0.500	55.833±0.473	56.28±0.567	0.331
Ct.Th (mm)†	0.234±0.007	0.232±0.007	0.669	0.217±0.003	0.217±0.004	0.500
Ma.Dm (mm)	0.644±0.009	0.619±0.017	0.282	0.666±0.02	0.684±0.015	0.950
/max (mm^4)†	0.151±0.005	0.157±0.01	0.500	0.155±0.004	0.159±0.009	0.50
/min (mm^4)†	0.086±0.003	0.079±0.006	0.827	0.086±0.004	0.087±0.008	0.286
***J* (mm^4)†**	0.237±0.007	0.236±0.016	0.754	0.24±0.007	0.246±0.017	0.500
Ct.Po (1)	0.004±0.001	0.003±0.001	0.662	0.005±0.002	0.002±0.001	0.852
Po.N	44.5±1.861	49.5±4.667	0.228	149.375±78.676	22.667±4.349	0.029
Po.V (mm^3)	0.005±0.001	0.004±0.001	0.662	0.007±0.003	0.003±0.001	0.852
AvgPo.V (mm^3)	12.2E-05±3.6E-05	7.8E-05±1.7E-05	0.755	8.01E-05±3.2E-05	15E-05±4E-05	0.282
Po.Dn	31.738±1.139	35.699±2.443	0.108	107.738±56.19	16.588±2.871	0.043
TMD ($mgHA/mm^3$)†	1239.636±4.213	1236.26±1.589	0.574	1222.529±29.479	1264.664±5.007	0.377

* Using Mann-Whitney U test.
† one-tailed comparisons.

Table B.4 Micro CT of midshaft tibial cortex in mdx-PAR$_2$ null & WT mice - Females.

Endpoint	**20 WEEKS**			**32 WEEKS**		
Genotype	WT	KO	*P*-value*	WT	KO	*P*-value*
Tt.Ar (mm^2)†	1.012±0.022	1.042±0.026	0.345	1.124±0.032	1.162±0.019	0.246
Ct.Ar (mm^2)†	0.617±0.009	0.617±0.011	0.491	0.654±0.017	0.675±0.013	0.179
Ma.Ar (mm^2)	0.395±0.019	0.425±0.016	0.345	0.47±0.018	0.487±0.013	0.596
Ct.Ar/Tt.Ar (%)†	61.097±1.097±	59.261±0.647	0.859	58.229±0.689	58.095±0.766	0.57
Ct.Th (mm)†	0.214±0.004	0.210±0.002	0.574	0.207±0.003	0.21±0.003	0.239
Ma.Dm (mm)	0.573±0.013	0.593±0.012	0.181	0.536±0.024	0.581±0.019	0.246
/max (mm^4)†	0.094±0.004	0.101±0.003	0.114	0.114±0.006	0.127±0.004	0.042
/min (mm^4)†	0.059±0.002	0.059±0.004	0.5	0.067±0.004	0.072±0.003	0.089
***J* (mm^4)†**	0.153±0.006	0.16±0.007	0.245	0.181±0.010	0.199±0.006	0.063
Ct.Po (1)	0.004±0.001	0.004±0.001	0.573	0.012±0.003	0.008±0.002	0.179
Po.N	47.75±3.529	45±2.955	0.755	309.571±82.365	168.727±55.222	0.479
Po.V (mm^3)	0.004±0.001	0.004±0.001	0.662	0.015±0.003	0.01±0.003	0.246
AvgPo.V (mm^3)	8.2E-05±1.6E-05	1E-04±2.4E-05	0.755	8.7E-05±4.4E-05	9.5E-05±2.3E-05	0.596
Po.Dn	42.62±2.641	41.074±2.042	0.755	252.566±67.288	130.121±41.992	0.285
TMD (mgHA/mm^3)†	1244.38±4.335	1236.899±2.851	0.929	1130.496±38.824	1194.498±30.402	0.268

* Using Mann-Whitney U test.
† one-tailed comparisons.

APPENDIX C: LIST OF GENES OF INTEREST EXAMINED *IN VITRO*

Table C.1 Selected genes of interest.

A number of genes (27) were selected from an RNA-seq data set generated in a study on PAR_2 KO and WT osteoblasts (Kularathna 2015). The genes were evaluated in 3 categories as described in section 5.1.

Gene	Full Name	Cat.	Function	Reference
Arhgap22	Rho GTPase activating protein 22	1	regulation of cell motility; angiogenesis	(Katoh et al. 2004; Rowland et al. 2011)
Bmp7	bone morphogenetic protein-7	1	TGFβ signalling; osteoblast differentiation; adipocyte differentiation	(Franceschi et al. 2000; Tou et al. 2003; Qiao et al. 2017)
C1qtnf3	C1q and TNF related 3	1	Anti-inflammatory adipokine; stimulates adipokine secretion	(Wölfing et al. 2008; Schmid et al. 2014)
Cnr1	cannabinoid receptor 1	2	*Cnr1* null mice have lower Ct.Ar/Tt.Ar; adipokine production	(Antonio de Luis et al. 2012; Ge et al. 2012; Khalid et al. 2016)
Crct1	cysteine rich C-terminal 1	1	epidermal differentiation	(Sobiak et al. 2015)
Ctgf	connective tissue growth factor	3	Chondrocyte proliferation and differentiation; osteoblast differentiation; suppression of adipogenesis;	(Takigawa et al. 2003; Tan et al. 2008; Kumar et al. 2012)
Cyp59	cytochrome P450, family 51	1	steroid biosynthesis; adipocyte function; osteoblast function	(Teplyuk et al. 2009; Lewinska et al. 2014)
Dhcr7	7-dehydrocholesterol reductase	1	steroid biosynthesis; osteoblast function	(Teplyuk et al. 2009; Luu et al. 2015)
Dhcr24	24-dehydrocholesterol reductase	1	steroid biosynthesis; adipocyte differentiation and de-differentiation; osteoblast function	(Ullah et al. 2013; Luu et al. 2015)

Enpep	glutamyl aminopeptidase	2	Inhibition of angiogenesis	(Kubota et al. 2010)
Gpr35	G protein-coupled receptor 35	3	Lysophosphatidic acid receptor; inhibits IL-4 in iNKT cells	(Oka et al. 2010; Fallarini et al. 2010)
Grem1	gremlin 1	1	BMP antagonist; adipocyte differentiation; osteoblast differentiation	(Gazzerro et al. 2005; Canalis et al. 2012; Gustafson et al. 2015)
Hmgn5	high mobility group nucleosome binding domain 5	2	nucleosomal binding and transcriptional activating protein	(Malicet et al. 2011)
Il6	interleukin 6	2	Proinflammatory cytokine; secreted by adipocytes; inhibits adipogenesis; In osteoblasts: inhibits both *Runx2*, and *Pparg*	(Imam 2016; Wang et al. 2016a; Almuraikhy et al. 2016)
Insig1	insulin induced gene 1	1	Glucose homeostasis; steroid biosynthesis; lipidogenesis; adipocyte differentiation	(Li et al. 2003; Dong and Tang 2010)
Lect1	leukocyte cell derived chemotaxin 1; chondromodulin-1	3	Chondrocyte differentiation; inhibition of angiogenesis; osteoblast proliferation	(Mori et al. 1997; Miura et al. 2010; Klinger et al. 2011)
Lin7a	lin-7 homolog A, crumbs cell polarity complex component	2	asymmetric distribution of channels and receptors on the cell membrane; may interact with β-catenin	(Harris et al. 2002; Monzani et al. 2009)
Meltf	melanotransferrin	1	Iron metabolism; plasminogen activation; eosinophil differentiation; cell shape changes; chondrocyte differentiation	(Oda et al. 2003; Sekyere et al. 2006)
Mmp8	matrix metallopeptidase 8	3	degradation of type I, II and III collagens; adipocyte and osteoblast function;	(Shapiro 1998; Minematsu et al. 2012; Jonitz-Heincke et al. 2016)

Mmp9	matrix metallopeptidase 9	1	degrades collagens IV, V and XI, and elastin; shedding of adipokine DPP4 from adipocytes; adipocyte differentiation	(Shapiro 1998; Bouloumié et al. 2001; Franco et al. 2011; Röhrborn et al. 2014)
Mvd	mevalonate diphosphate decarboxylase	1	Steroid biosynthesis	(Hogenboom 2003)
Olr1	oxidized low density lipoprotein receptor 1	1	Angiogenesis; migration and adhesion of MSCs; cholesterol metabolism; adipocyte function	(Chui et al. 2005; Zhang et al. 2013; Shiraki et al. 2014)
Ramp3	receptor activity modifying protein 3	2	Adrenomedullin response; amylin response in adipose tissue; PTH-induced primary response gene in osteoblastic cells	(Phelps et al. 2005; Kuwasako et al. 2012; Miegueu et al. 2013)
Rgs2	regulator of G-protein signaling 2	2	GTPase activating protein; promotes adipogenic differentiation; G_s and G_q signalling in osteoblasts	(Nishizuka et al. 2001; Cladman and Chidiac 2002; Roy et al. 2006)
Scg2	secretogranin 2	2	Packaging of hormones and neuropeptides into secretory vesicles; chemotaxis; angiogenesis;	(Ozawa and Takata 1995; Reinisch et al. 2001; Kirchmair et al. 2004)
Snorc	Small NOvel Rich in Cartilage	3	Cartilage specific membranous protein; may be involved in BMP-2 signalling	(Heinonen et al. 2011)
Tcea3	transcription elongation factor A3	3	Regulation of ESC proliferation and differentiation; haematopoiesis	(Ito et al. 2006; Park et al. 2013)

Cat. - Category number

APPENDIX D: COMPLEMENTARY DATA - MICRO CT AND ADIPOCYTE HISTOMORPHOMETRY OF *F2RL1*$^{WT/WT}$ AND *F2RL1*$^{FL/FL}$ MICE

Table D.1 Metaphyseal cortical indices determined by micro CT - *F2rl1*$^{wt/wt}$ and *F2rl1*$^{fl/fl}$ mice.

The difference in micro CT indices between the *F2rl1*$^{wt/wt}$ and *F2rl1*$^{fl/fl}$ mice (Mean diff) is presented as a percentage relative to the control *F2rl1*$^{wt/wt}$. N = 7-8; significant differences are highlighted.

	Male						Female					
	7 wk			13 wk			7 wk			13 wk		
	Mean diff (%)	SE $_{diff}$ (%)	*p*-value[1]	Mean diff (%)	SE $_{diff}$ (%)	*p*-value	Mean diff (%)	SE $_{diff}$ (%)	*p*-value	Mean diff (%)	SE $_{diff}$ (%)	*p*-value
Tt.Ar	-7.85	4.3	0.121	-0.56	5.53	0.878	-0.3	3.17	0.867	-2.73	3.68	0.536
Ct.Ar	-22.96	16.55	0.094	2.82	6.86	0.798	-1.52	7.14	1.000	-1.39	4.53	0.867
Ma.Ar	-1.4	9.38	1.000	-2.49	8.59	1.000	0.33	6.22	1.000	-3.69	6.74	0.867
Ct.Ar/Tt.Ar	-17.61	17.6	0.232	4.68	7.97	1.000	-1.11	8.5	1.000	1.1	5.23	0.694
Ct.Th	-18.93	10.36	0.094	0.56	5.39	1.000	5.68	5.83	0.463	-0.11	3.4	0.536
Ma.Dm	4.4	4.6	0.232	-5.98	2.79	0.049	-0.36	3.68	0.867	-1.23	2.48	0.867
/max	-35.44	20.49	0.072	9.29	12.62	0.574	-12.26	8.67	0.189	2.72	8.98	0.694
/min	-27.32	23.95	0.152	5.14	12.06	0.721	-12.71	10.88	0.536	-2.37	8.56	1.000
J	-32.01	21.83	0.094	7.53	12.14	0.505	-12.46	9.59	0.281	0.49	7.85	0.867
Ct.Po	16.95	46.51	0.536	-56.71	43.35	0.083	49.22	22.84	0.040	-46.47	51.43	0.867
Po.N	7.74	44.47	0.152	-59.36	51.54	0.083	66.93	24.8	0.006	-62.94	61.04	1.000
Po.V	-27.48	24.07	0.281	-54.57	41.23	0.161	33.53	14.01	0.014	-39.44	48.51	1000
Avg.Po.V	-21.5	17.3	0.152	33.25	24.96	0.328	-12.97	11.14	0.463	10.88	33.19	0.152
Po.Dn	39.54	62.57	0.189	-59.16	51.84	0.065	77.52	42.32	0.021	-64.98	61.84	0.867
TMD	0.7	6.95	0.694	-1.05	5.15	0.878	8.1	4.58	0.152	0.01	2.83	0.955

Two tailed Mann-Whitney U test.

Table D.2 Time related change in metaphyseal cortical bone assessed by micro CT - *F2rl1*$^{wt/wt}$ and *F2rl1*$^{fl/fl}$ mice.

Regression coefficients of time related changes in bone structural and material indices of *F2rl1*$^{wt/wt}$ and *F2rl1*$^{fl/fl}$ mice are presented. Significant differences between the genotypes are highlighted.

	M			F		
Index	**B_{wt}[1]**	**B_{fl}[2]**	**p-value**	**B_{wt}**	**B_{fl}**	**p-value**
Tt.Ar	-0.032	0.000	0.251	-0.062***	-0.069***	0.638
Ct.Ar	0.016	0.050**	0.122	0.003	0.003	0.991
Ma.Ar	-0.048	-0.050*	0.949	-0.065***	-0.073***	0.691
Ct.Ar/Tt.Ar	1.008	2.177**	0.208	1.340**	1.480**	0.814
Ct.Th	0.002	0.007***	0.075	0.002	0.001	0.392
Ma.Dm	-0.006	-0.019***	0.044	-0.016**	-0.017***	0.857
/max	0.006	0.029**	0.052	-0.004	0.002	0.204
/min	0.005	0.017*	0.196	-0.004	-0.00039	0.419
J	0.011	0.045**	0.094	-0.008	0.002	0.273
Ct.Po	0.009	-0.021	0.206	-0.007	-0.026***	0.060
Po.N	262.065	-42.333	0.251	5.429	-184.45***	0.063
Po.V	$1.9x10^{-4}$	$1.2x10^{-5}$	0.370	$-6.3x10^{-5}$	$-1.9x10^{-4}$***	0.099
Avg.Po.V	$6.8x10^{-9}$	$1.3x10^{-7}$*	0.067	$-1.1x10^{-8}$	$4.4x10^{-8}$	0.467
Po.Dn	155.802	-188.908	0.187	0.842	-209.372**	0.069
TMD	11.100	8.058	0.826	25.696***	13.186	0.153

[1] Regression coefficient (slope) of changes over time in *F2rl1*$^{wt/wt}$ mice; a negative value depicts negative changes.

[2] Regression coefficient (slope) of changes over time in the *F2rl1*$^{fl/fl}$ mice.

* $p < 0.05$, ** $p < 0.01$, *** $p < 0.001$ when values were regressed over time in each sex-genotype category indicating significant changes from 7 to 13 weeks.

[3] Regression coefficients were compared using a second multiple linear regression analysis.

Table D.3 Diaphyseal cortical indices determined by micro CT - *F2rl1*$^{wt/wt}$ and *F2rl1*$^{fl/fl}$ mice.

The difference in micro CT indices between the *F2rl1*$^{wt/wt}$ and *F2rl1*$^{fl/fl}$ mice (Mean diff) is presented as a percentage relative to the control *F2rl1*$^{wt/wt}$. N = 7-8; significant differences are highlighted.

	Male						Female					
	7 wk			13 wk			7 wk			13 wk		
	Mean diff (%)	SE $_{diff}$ (%)	*p*-value[1]	Mean diff (%)	SE $_{diff}$ (%)	*p*-value	Mean diff (%)	SE $_{diff}$ (%)	*p*-value	Mean diff (%)	SE $_{diff}$ (%)	*p*-value
Tt.Ar	-6.37	3.58	0.072	6.49	4.63	0.105	4.63	3.03	0.121	-1.02	2.77	0.694
Ct.Ar	-12.67	7.11	0.072	0.11	6.43	0.798	-0.86	5.11	0.694	-2.14	2.68	0.336
Ma.Ar	1.34	3.23	0.779	16.23	4.46	0.003	10.58	4.4	0.029	0.45	3.89	1.000
Ct.Ar/Tt.Ar	-6.77	4.27	0.121	-6.19	2.83	0.065	-4.95	3.54	0.094	-1.09	1.49	0.613
Ct.Th	-11.08	6.74	0.121	-3.45	4.33	0.574	-2.44	3.08	0.463	-1.43	2.04	0.536
Ma.Dm	-1.09	1.81	0.867	4.51	2.21	0.028	6.02	1.7	0.002	0.38	2.18	0.867
/max	-17.58	9.5	0.072	8.7	12.31	0.574	2.47	7.48	0.867	-6.34	5.32	0.232
/min	-12	8.46	0.281	11.68	10.14	0.328	6.37	7.55	0.336	0.71	5.93	1.000
J	-15.31	8.9	0.054	9.87	11.36	0.505	4.11	7.36	0.536	-3.36	5.35	0.463
Ct.Po	34.82	161.93	0.336	9764.2	5282.02	0.003	290.14	301.39	0.613	-45.83	103.6	0.536
Po.N	-57.84	87.1	0.281	3928.57	2040.44	0.007	229.69	252.18	0.281	-67.35	68.38	0.463
Po.V	-22.31	113.21	0.336	8961.15	4922.9	0.005	336.95	331.3	0.613	-49.23	101.75	0.536
Avg.Po.V	-29.73	55.45	0.463	204.83	107.21	0.010	-83.14	96.67	1.000	-31.28	106.94	0.536
Po.Dn	-27.29	105.76	0.536	4233.43	2176.81	0.015	186.32	226.33	0.281	-65.42	69.84	0.463
TMD	1.75	3.44	0.613	4.69	4.94	0.645	0.17	3.1	0.867	-3.41	1.84	0.189

Two tailed Mann-Whitney U test.

Table D.4 Time related change in diaphyseal cortical bone assessed by micro CT - *F2rl1*$^{wt/wt}$ and *F2rl1*$^{fl/fl}$ mice.

Regression coefficients of time related changes in bone structural and material indices of *F2rl1*$^{wt/wt}$ and *F2rl1*$^{fl/fl}$ mice are presented. Significant differences between the genotypes are highlighted.

	M			F		
Index	**B_{wt}[1]**	**B_{fl}[2]**	**p-value**	**B_{wt}**	**B_{fl}**	**p-value**
Tt.Ar	0.020**	0.042***	0.030	0.009*	0.001	0.153
Ct.Ar	0.021**	0.032***	0.211	0.011**	0.010**	0.768
Ma.Ar	-4.4x10^{-4}	0.010**	0.008	-0.003	-0.009*	0.078
Ct.Ar/Tt.Ar	0.913**	0.909*	0.994	0.836**	1.160**	0.317
Ct.Th	0.006***	0.008***	0.373	0.004***	0.004***	0.818
Ma.Dm	-0.002	0.004*	0.047	-0.002	-0.007**	0.035
/max	0.005**	0.008***	0.125	0.002*	0.001*	0.078
/min	0.003**	0.005***	0.080	0.001**	0.001*	0.570
J	0.007**	0.013***	0.103	0.003*	0.002*	0.369
Ct.Po	-0.001	0.006	0.093	-0.001	-0.006	0.339
Po.N	-3.866	27.438	0.044	-3.854	-13.140	0.357
Po.V	-7.0 x10^{-6}	7.1 x10^{-5}	0.071	-8.0x10^{-6}	-3.6x10^{-5}	0.313
Avg.Po.V	-2.5x10^{-8}	3.4x10^{-7}	0.056	-9.3x10^{-7}	-9.9x10^{-8}	0.351
Po.Dn	-3.833	24.632	0.056	-7.510	-21.944	0.402
TMD	12.848	19.477	0.595	7.744	-0.215	0.294

[1] Regression coefficient (slope) of changes over time in *F2rl1*$^{wt/wt}$; a negative value depicts negative changes.

[2] Regression coefficient (slope) of changes over time in *F2rl1*$^{fl/fl}$ group.

* $p < 0.05$, ** $p < 0.01$, *** $p < 0.001$ when values were regressed over time in each sex-genotype category indicating significant changes from 7 to 13 weeks.

[3] Regression coefficients were compared using a second multiple linear regression analysis.

Table D.5 Micro CT of tibial metaphysis in *F2rl1*$^{wt/wt}$ and *F2rl1*$^{fl/fl}$ mice - Males.

Endpoint		7 WEEKS			13 WEEKS	
Genotype	WT	KO	*P*-value*	WT	KO	*P*-value*
TV (mm3)	1.91+0.106	1.901+0.075	0.536	1.731+0.051	1.76+0.083	0.798
BV (mm3)	0.183+0.022	0.145+0.016	0.281	0.177+0.014	0.232+0.021	0.021
BV/TV (%)	9.784+1.29	7.58+0.716	0.232	10.134+0.688	13.085+1.034	0.049
Conn.D (1/mm3)	602.247+95.437	423.964+42.205	0.189	475.647+60.886	581.062+64.894	0.279
Tb.N (1/mm)	2.57+0.282	2.278+0.209	0.613	2.505+0.165	3.298+0.224	0.015
Tb.Th (mm)	0.038+0.002	0.033+0.001	0.072	0.041+0.002	0.04+0.001	0.721
Tb.Sp (mm)	0.196+0.012	0.202+0.015	0.867	0.187+0.005	0.164+0.006	0.021
DA	1.375+0.073	1.648+0.069	0.021	1.451+0.088	1.431+0.07	0.959
SMI	2.637+0.069	2.452+0.056	0.054	2.526+0.073	2.42+0.079	0.382
BMD (mg HA/cm3)	90.615+7.904	71.033+11.266	0.152	102.272+9.834	125.426+12.083	0.161
TMD (mg HA/cm3)	749.164+29.073	719.574+34.294	0.694	779.755+32.691	757.897+25.368	0.798

* Using two-tailed Mann-Whitney U test.

Table D.6 Micro CT of tibial metaphysis in *F2rl1*$^{wt/wt}$ and *F2rl1*$^{fl/fl}$ mice - Females.

Endpoint	7 WEEKS			13 WEEKS		
Genotype	WT	KO	*P*-value*	WT	KO	*P*-value*
TV (mm3)	1.521+0.054	1.524+0.07	0.955	1.169+0.051	1.129+0.04	0.463
BV (mm3)	0.088+0.005	0.098+0.006	0.232	0.052+0.009	0.058+0.003	0.189
BV/TV (%)	5.815+0.287	6.466+0.416	0.189	4.316+0.647	5.142+0.206	0.121
Conn.D (1/mm3)	340.901+34.68	386.289+33.768	0.463	239.348+29.162	273.816+28.027	0.336
Tb.N (1/mm)	1.746+0.086	1.929+0.115	0.189	1.213+0.157	1.475+0.062	0.121
Tb.Th (mm)	0.033+0	0.034+0.001	0.779	0.035+0.001	0.035+0.001	1
Tb.Sp (mm)	0.255+0.009	0.233+0.009	0.152	0.269+0.012	0.242+0.005	0.121
DA	1.377+0.04	1.543+0.077	0.336	1.404+0.063	1.335+0.033	0.694
SMI	2.563+0.02	2.477+0.045	0.232	2.656+0.022	2.604+0.025	0.152
BMD (mg HA/cm3)	32.323+2.541	53.202+4.557	0.006	31.764+7.498	38.508+3.39	0.397
TMD (mg HA/cm3)	642.215+14.206	702.795+32.107	0.189	710.993+27.924	708.299+19.463	0.649

* Using two-tailed Mann-Whitney U test.

Table D.7 Micro CT of metaphyseal cortex in *F2rl1*$^{wt/wt}$ and *F2rl1*$^{fl/fl}$ mice - Males.

Endpoint		**7 WEEKS**			**13 WEEKS**	
Genotype	WT	KO	*P*-value*	WT	KO	*P*-value*
Tt.Ar (mm^2)	2.603+0.083	2.398+0.063	0.121	2.409+0.088	2.396+0.089	0.878
Ct.Ar (mm^2)	0.779+0.097	0.6+0.069	0.094	0.874+0.043	0.899+0.036	0.798
Ma.Ar (mm^2)	1.824+0.141	1.799+0.073	1.000	1.535+0.073	1.497+0.1	1.000
Ct.Ar/Tt.Ar (%)	30.183+4.067	24.867+2.792	0.232	36.232+1.185	37.928+2.426	1.000
Ct.Th (mm)	0.169+0.014	0.137+0.008	0.094	0.18+0.007	0.181+0.006	1.000
Ma.Dm (mm)	0.774+0.028	0.808+0.018	0.232	0.736+0.011	0.692+0.016	0.049
/max (mm^4)	0.299+0.048	0.193+0.031	0.072	0.334+0.029	0.365+0.027	0.574
/min (mm^4)	0.218+0.038	0.159+0.03	0.152	0.247+0.02	0.259+0.02	0.721
***J* (mm^4)**	0.517+0.085	0.352+0.061	0.094	0.581+0.048	0.624+0.046	0.505
Ct.Po (1)	0.206+0.051	0.241+0.074	0.536	0.262+0.092	0.113+0.054	0.083
Po.N	1330.857+216.10	1433.875+508.79	0.152	2903.25+1201.093	1179.875+718.67	0.083
Po.V (mm^3)	0.002+0.0002	0.001+0.0003	0.281	0.003+0.001	0.001+0.0005	0.161
AvgPo.V (mm^3)	1.3E-06+1.70E-07	1.1E-06+1.2E-07	0.152	1.34E-06+1.87E-07	1.79E-06+2.5E-07	0.328
Po.Dn	1530.31+500.16	2135.32+739.5	0.189	2453.119+988.328	1001.88+661.93	0.065
TMD (mgHA/mm^3)	1000.182+47.386	1007.199+43.992	0.867	1066.782+42.789	1055.549+28.463	0.878

* Using two-tailed Mann-Whitney U test.

Table D.8 Micro CT of metaphyseal cortex in *F2rl1*$^{wt/wt}$ and *F2rl1*$^{fl/fl}$ mice - Females.

Endpoint		**7 WEEKS**			**13 WEEKS**	
Genotype	WT	KO	*P*-value*	WT	KO	*P*-value*
Tt.Ar (mm^2)	2.207+0.051	2.2+0.04	0.867	1.834+0.051	1.784+0.037	0.536
Ct.Ar (mm^2)	0.75+0.027	0.738+0.042	1.000	0.769+0.029	0.759+0.014	0.867
Ma.Ar (mm^2)	1.457+0.057	1.462+0.062	1.000	1.064+0.056	1.025+0.036	0.867
Ct.Ar/Tt.Ar (%)	34.03+1.517	33.653+2.231	1.000	42.071+1.845	42.532+0.899	0.694
Ct.Th (mm)	0.159+0.005	0.168+0.007	0.463	0.173+0.005	0.173+0.002	0.536
Ma.Dm (mm)	0.747+0.021	0.744+0.015	0.867	0.651+0.008	0.643+0.013	0.867
/max (mm^4)	0.251+0.01	0.221+0.017	0.189	0.228+0.013	0.234+0.014	0.694
/min (mm^4)	0.202+0.008	0.176+0.019	0.536	0.178+0.012	0.174+0.008	1.000
***J* (mm^4)**	0.453+0.018	0.397+0.036	0.281	0.406+0.024	0.408+0.017	0.867
Ct.Po (1)	0.138+0.015	0.206+0.026	0.040	0.094+0.043	0.05+0.014	0.867
Po.N	861.429+61.724	1438+189.864	0.006	894+504.174	331.286+78.742	1.000
Po.V (mm^3)	0.001+0.0001	0.002+0.0001	0.014	0.001+0.0004	0.001+0.0002	1.000
AvgPo.V (mm^3)	1.4E-06+8.3E-08	1.2E-06+1.2E-07	0.463	1.4E-06+3.1E-07	1.5E-06+2.8E-07	0.152
Po.Dn	882.811+73.565	1567.17+341.499	0.021	887.865+508.532	310.937+71.191	0.867
TMD (mgHA/mm^3)	928.084+13.895	1003.215+37.246	0.152	1082.261+21.188	1082.329+19.021	0.955

* Using two-tailed Mann-Whitney U test.

Table D.9 Micro CT of midshaft cortex in *F2rl1*$^{wt/wt}$ and *F2rl1*$^{fl/fl}$ mice - Males.

Endpoint		**7 WEEKS**			**13 WEEKS**	
Genotype	WT	KO	*P*-value*	WT	KO	*P*-value*
Tt.Ar (mm^2)	0.949+0.025	0.888+0.019	0.072	1.07+0.028	1.14+0.037	0.105
Ct.Ar (mm^2)	0.522+0.026	0.456+0.022	0.072	0.647+0.022	0.647+0.032	0.798
Ma.Ar (mm^2)	0.426+0.009	0.432+0.009	0.779	0.424+0.011	0.493+0.014	0.003
Ct.Ar/Tt.Ar (%)	54.812+1.491	51.1+1.586	0.121	60.29+0.904	56.556+1.316	0.065
Ct.Th (mm)	0.2+0.01	0.178+0.007	0.121	0.236+0.006	0.228+0.007	0.574
Ma.Dm (mm)	0.608+0.007	0.601+0.007	0.867	0.596+0.01	0.623+0.007	0.028
/max (mm^4)	0.069+0.005	0.057+0.004	0.072	0.098+0.006	0.107+0.009	0.574
/min (mm^4)	0.047+0.003	0.042+0.003	0.281	0.063+0.003	0.071+0.005	0.328
***J* (mm^4)**	0.117+0.007	0.099+0.006	0.054	0.162+0.01	0.178+0.014	0.505
Ct.Po (1)	0.005+0.003	0.007+0.006	0.336	0+0	0.043+0.022	0.003
Po.N	27.571+19.192	11.625+11.34	0.281	4.375+1.335	176.25+83.493	0.007
Po.V (mm^3)	4.99E-05+3.6E-05	3.9E-05+3.8E-05	0.336	5.1E-06+1.9E-06	0.0005+0.0002	0.005
AvgPo.V (mm^3)	1.1E-06+3.16E-07	7.5E-07+4.5E-07	0.463	9.1E-07+1.7E-07	2.8E-06+9.02E-07	0.010
Po.Dn	26.861+18.249	19.53+19.137	0.536	3.861+1.181	167.321+78.613	0.015
TMD (mgHA/mm^3)	1231.475+21.711	1253.074+33.003	0.613	1308.561+30.437	1369.937+52.213	0.645

* Using two-tailed Mann-Whitney U test.

Table D.10 Micro CT of midshaft cortex in *F2rl1*$^{wt/wt}$ and *F2rl1*$^{fl/fl}$ mice - Females.

Endpoint		**7 WEEKS**			**13 WEEKS**	
Genotype	WT	KO	*P*-value*	WT	KO	*P*-value*
Tt.Ar (mm^2)	0.788+0.019	0.825+0.012	0.121	0.84+0.015	0.832+0.016	0.694
Ct.Ar (mm^2)	0.41+0.016	0.406+0.01	0.694	0.478+0.009	0.468+0.008	0.336
Ma.Ar (mm^2)	0.378+0.006	0.418+0.014	0.029	0.363+0.008	0.364+0.01	1.000
Ct.Ar/Tt.Ar (%)	51.794+1.072	49.229+1.332	0.094	56.807+0.457	56.187+0.641	0.613
Ct.Th (mm)	0.17+0.004	0.166+0.003	0.463	0.193+0.002	0.19+0.003	0.536
Ma.Dm (mm)	0.561+0.006	0.594+0.006	0.002	0.551+0.007	0.553+0.009	0.867
/max (mm^4)	0.045+0.003	0.046+0.001	0.867	0.055+0.002	0.051+0.002	0.232
/min (mm^4)	0.033+0.002	0.035+0.001	0.336	0.04+0.001	0.04+0.002	1.000
***J* (mm^4)**	0.078+0.005	0.081+0.003	0.536	0.095+0.003	0.092+0.003	0.463
Ct.Po (1)	0.009+0.008	0.036+0.025	0.613	0+0	0+0	0.536
Po.N	24+23.501	79.125+51.394	0.281	0.875+0.479	0.286+0.286	0.463
Po.V (mm^3)	4.9E-05+4.3E-05	0.0002+0.0001	0.613	1.8E-06+1.4E-06	9.2E-07+9.2E-07	0.536
AvgPo.V (mm^3)	6.3E-06+5.6E-06	1.1E-06+3.8E-07	1.000	6.7E-07+4.8E-07	4.6E-07+4.6E-07	0.536
Po.Dn	46.113+45.399	132.031+86.183	0.281	1.053+0.581	0.364+0.364	0.463
TMD ($mgHA/mm^3$)	1289.617+26.51	1291.843+26.161	0.867	1336.08+21.501	1290.554+7.922	0.189

* Using two-tailed Mann-Whitney U test.

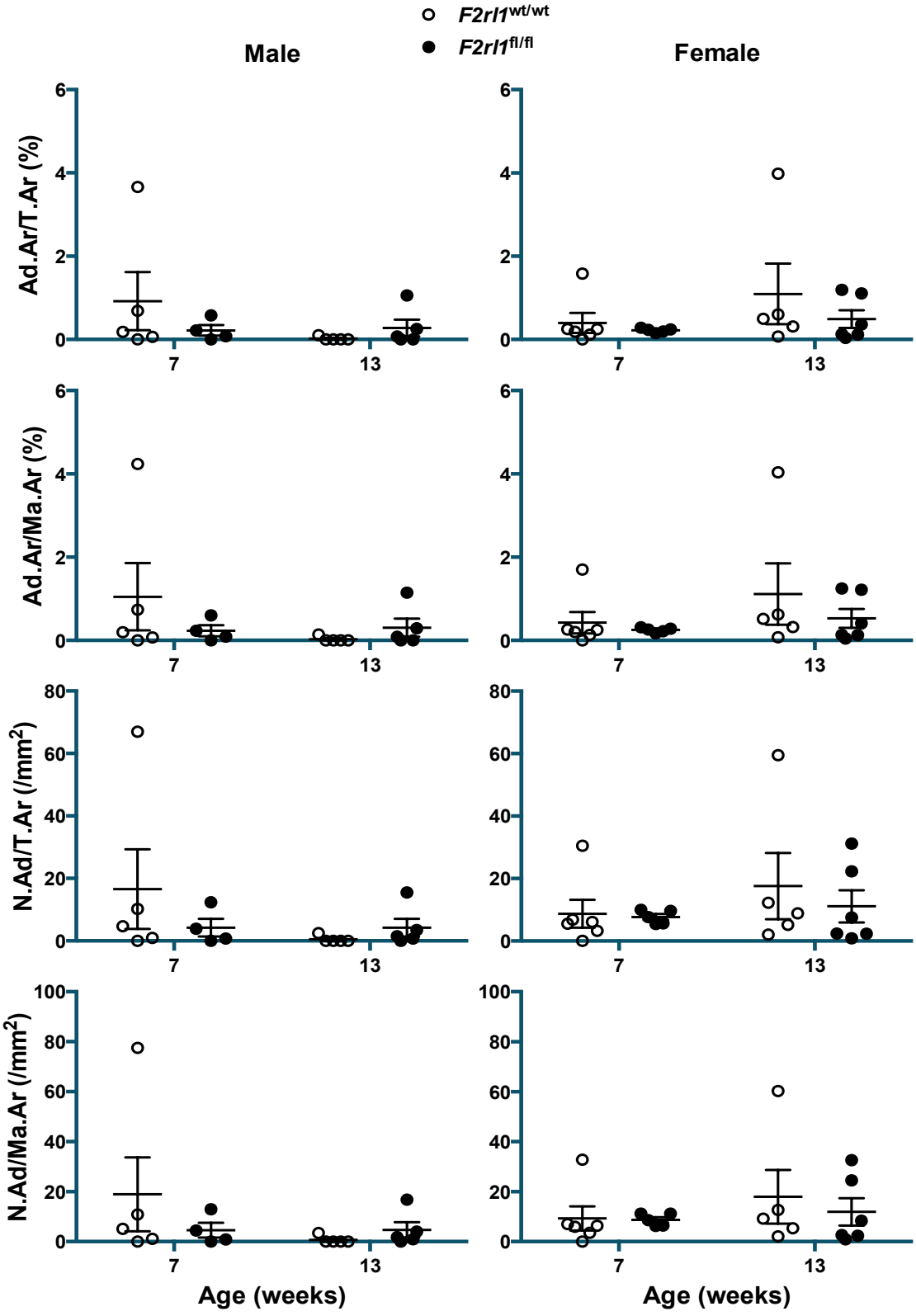


Figure D.1 Histomorphometric evaluation of marrow adiposity - *F2rl1*$^{wt/wt}$ and *F2rl1*$^{fl/fl}$ mice.

Ad.Ar, adipocyte area; **N.Ad**, number of adipocytes; N = 4-6; Mann-Whitney U test did not show any differences between the groups nor did analysis of regression coefficients of change over time ($p > 0.05$).

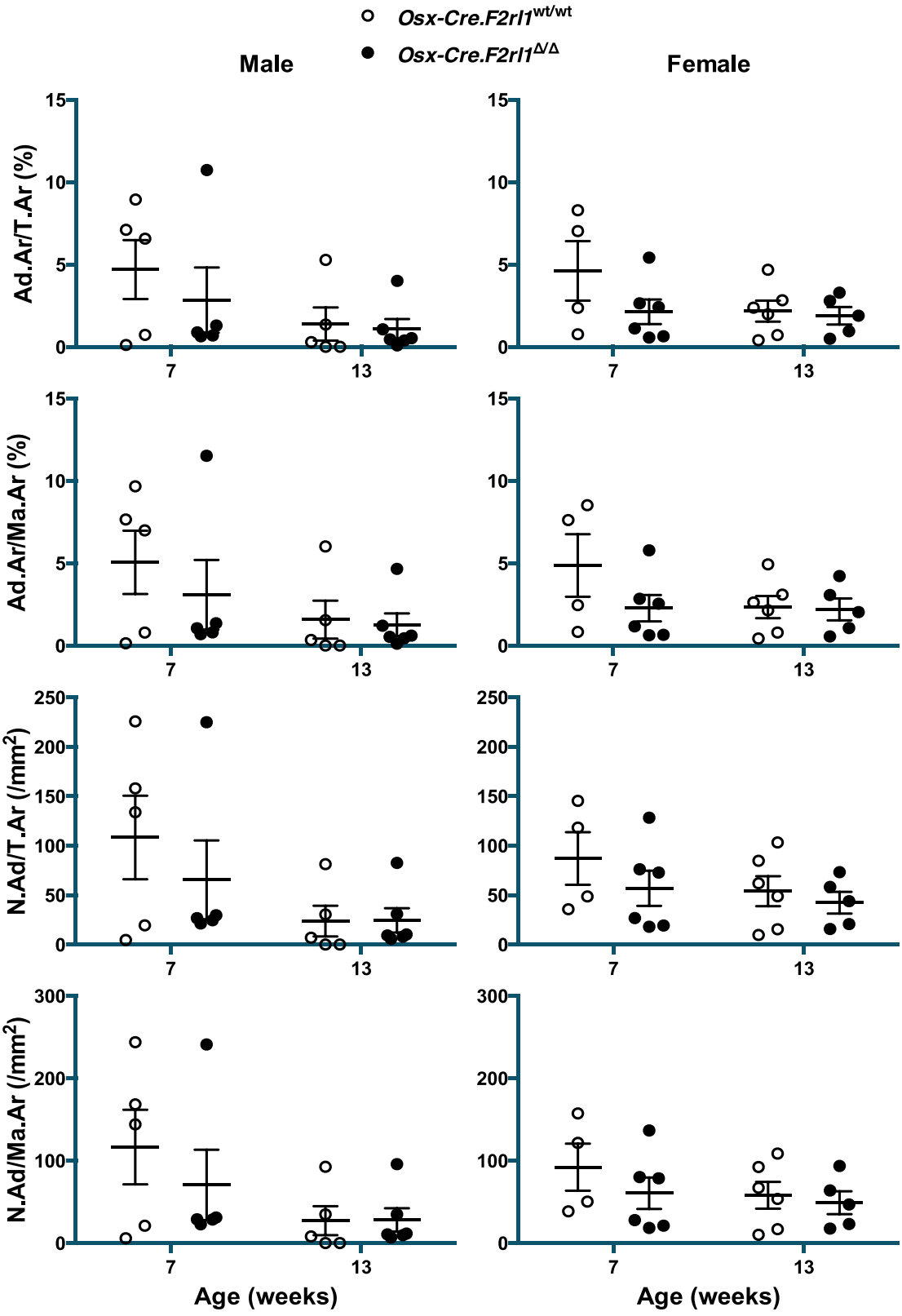


Figure D.2 Histomorphometric evaluation of marrow adiposity - *Osx-Cre* mice.

Ad.Ar, adipocyte area; **N.Ad**, number of adipocytes; N = 4-6; Mann-Whitney U test did not show any differences between the groups nor did analysis of regression coefficients of change over time ($p > 0.05$).

APPENDIX E: COMPLEMENTARY DATA - MICRO CT OF *OSX-CRE* MICE

Table E.1 Micro CT of tibial metaphysis in *Osx-Cre* mice - Males.

Endpoint		**7 WEEKS**			**13 WEEKS**	
Genotype	WT	KO	*P*-value*	WT	KO	*P*-value*
TV (mm^3)	1.526+0.085	1.527+0.106	0.815	1.605+0.068	1.503+0.081	0.331
BV (mm^3)	0.12+0.017	0.111+0.023	0.423	0.196+0.019	0.19+0.013	0.766
BV/TV (%)	7.666+0.755	7.066+0.993	0.277	12+0.817	12.608+0.369	0.882
Conn.D ($1/mm^3$)	453.488+42.353	412.848+85.547	0.321	573.344+58.047	567.758+49.33	0.824
Tb.N (1/mm)	2.304+0.193	2.111+0.26	0.321	2.997+0.198	3.269+0.091	0.552
Tb.Th (mm)	0.033+0.001	0.033+0.001	1.000	0.04+0.001	0.039+0.001	0.261
Tb.Sp (mm)	0.221+0.012	0.205+0.011	0.321	0.182+0.01	0.162+0.003	0.331
DA	1.436+0.038	1.588+0.088	0.093	1.364+0.046	1.505+0.059	0.095
SMI	2.54+0.02	2.578+0.044	0.743	2.497+0.05	2.337+0.057	0.067
BMD (mg HA/cm^3)	49.604+9.68	46.066+7.762	0.815	110.966+9.547	120.389+6.402	0.882
TMD (mg HA/cm^3)	642.235+16.175	658.223+20.729	0.606	758.462+20.276	748.788+18.821	0.766

* Using two-tailed Mann-Whitney U test.

Table E.2 Micro CT of tibial metaphysis in *Osx-Cre* mice - Females.

Endpoint		**7 WEEKS**			**13 WEEKS**	
Genotype	WT	KO	*P*-value*	WT	KO	*P*-value*
TV (mm^3)	1.335+0.104	1.506+0.094	0.130	1.268+0.056	1.247+0.041	0.771
BV (mm^3)	0.081+0.017	0.095+0.013	0.505	0.067+0.004	0.097+0.006	4.30E-04
BV/TV (%)	5.705+0.706	6.184+0.63	0.574	5.252+0.205	7.814+0.416	3.71E-05
Conn.D ($1/mm^3$)	345.077+42.957	384.591+41.918	0.505	297.449+20.714	433.7+31.596	0.002
Tb.N (1/mm)	1.729+0.176	1.891+0.17	0.505	1.497+0.064	2.168+0.092	2.16E-05
Tb.Th (mm)	0.033+0.001	0.032+0.001	0.442	0.035+0.001	0.036+0.001	0.456
Tb.Sp (mm)	0.257+0.013	0.227+0.014	0.130	0.256+0.007	0.208+0.007	1.39E-04
DA	1.452+0.04	1.625+0.083	0.130	1.423+0.046	1.37+0.046	0.582
SMI	2.58+0.04	2.538+0.04	0.505	2.594+0.026	21.235+18.678	0.582
BMD (mg HA/cm^3)	24.207+10.328	39.749+10.276	0.161	34.136+4.308	55.658+5.271	0.007
TMD (mg HA/cm^3)	618.117+22.771	649.067+30.229	0.382	695.507+25.117	694.128+15.104	0.771

* Using two-tailed Mann-Whitney U test.

Table E.3 Micro CT of metaphyseal cortex in *Osx-Cre* mice - Males.

Endpoint	7 WEEKS			13 WEEKS		
Genotype	WT	KO	*P*-value*	WT	KO	*P*-value*
Tt.Ar (mm^2)	2.16+0.096	2.036+0.166	0.423	2.256+0.069	2.051+0.072	0.067
Ct.Ar (mm^2)	0.64+0.041	0.504+0.065	0.074	0.76+0.042	0.638+0.035	0.056
Ma.Ar (mm^2)	1.521+0.111	1.532+0.164	0.743	1.496+0.086	1.412+0.078	0.503
Ct.Ar/Tt.Ar (%)	30.897+3.357	25.636+3.59	0.200	34.704+3.316	31.403+2.139	0.503
Ct.Th (mm)	0.143+0.006	0.129+0.008	0.114	0.164+0.007	0.151+0.005	0.370
Ma.Dm (mm)	0.741+0.013	0.744+0.033	0.423	0.678+0.01	0.687+0.017	0.456
/max (mm^4)	0.21+0.02	0.157+0.036	0.074	0.286+0.026	0.211+0.022	0.067
/min (mm^4)	0.172+0.019	0.119+0.028	0.059	0.205+0.013	0.157+0.012	0.025
***J* (mm^4)**	0.382+0.038	0.276+0.064	0.074	0.491+0.039	0.368+0.033	0.038
Ct.Po (1)	0.12+0.013	0.136+0.015	0.481	0.117+0.04	0.107+0.019	0.503
Po.N	643.444+91.907	659.5+103.408	0.815	852+374.915	673.889+143.162	0.603
Po.V (mm^3)	0.001+0.0001	0.001+0.0001	0.277	0.001+0.0003	0.001+0.0002	0.941
AvgPo.V (mm^3)	1.41E-06+1.7E-07	1.1E-06+9.4E-08	0.114	1.5E-06+1.2E-07	1.3E-06+1.2E-07	0.331
Po.Dn	797.44+83.72	1136.47+176.15	0.114	901.66+423.49	767.59+140.43	0.261
TMD ($mgHA/mm^3$)	898.99+21.765	899.887+30.658	0.743	1028.747+24.61	1021.017+23.031	0.882

* Using two-tailed Mann-Whitney U test.

Table E.4 Micro CT of metaphyseal cortex in *Osx-Cre* mice - Females.

Endpoint	7 WEEKS			13 WEEKS		
Genotype	WT	KO	*P*-value*	WT	KO	*P*-value*
Tt.Ar (mm^2)	1.994+0.102	2.135+0.087	0.279	1.969+0.072	1.908+0.047	0.539
Ct.Ar (mm^2)	0.622+0.042	0.571+0.054	0.505	0.751+0.028	0.688+0.028	0.159
Ma.Ar (mm^2)	1.372+0.11	1.564+0.112	0.161	1.218+0.077	1.22+0.045	0.628
Ct.Ar/Tt.Ar (%)	32.113+3.416	27.531+3.366	0.442	39.172+2.935	36.109+1.464	1.000
Ct.Th (mm)	0.144+0.005	0.14+0.008	0.721	0.168+0.005	0.158+0.005	0.228
Ma.Dm (mm)	0.738+0.012	0.767+0.012	0.161	0.69+0.015	0.662+0.014	0.203
/max (mm^4)	0.185+0.022	0.167+0.024	0.645	0.231+0.015	0.206+0.013	0.203
/min (mm^4)	0.151+0.017	0.132+0.022	0.798	0.182+0.012	0.168+0.01	0.203
***J* (mm^4)**	0.336+0.039	0.299+0.046	0.798	0.413+0.026	0.374+0.022	0.228
Ct.Po (1)	0.134+0.013	0.189+0.052	0.382	0.122+0.031	0.08+0.015	0.771
Po.N	761.125+105.618	996.875+255.492	0.645	847.583+246.724	460.6+77.136	0.346
Po.V (mm^3)	0.001+0.0002	0.001+0.0002	0.798	0.001+0.0002	0.001+0.0001	0.228
AvgPo.V (mm^3)	1.2E-06+5.4E-08	1.1E-06+9.8E-08	0.645	1.5E-06+1.3E-07	1.6E-06+2.1E-07	0.923
Po.Dn	977.642+76.246	1494.473+460.471	0.234	911.011+311.279	518.043+97.29	0.628
TMD ($mgHA/mm^3$)	873.157+26.886	900.999+41.003	0.959	1024.642+33.018	1000.804+14.176	0.582

* Using two-tailed Mann-Whitney U test

Table E.5 Micro CT of midshaft cortex in *Osx-Cre* mice - Males.

Endpoint		7 WEEKS			13 WEEKS	
Genotype	WT	KO	*P*-value*	WT	KO	*P*-value*
Tt.Ar (mm^2)	0.703+0.047	0.62+0.046	0.114	0.948+0.058	0.805+0.049	0.152
Ct.Ar (mm^2)	0.374+0.035	0.317+0.035	0.167	0.559+0.043	0.467+0.031	0.152
Ma.Ar (mm^2)	0.328+0.014	0.304+0.018	0.321	0.388+0.082	0.338+0.02	0.766
Ct.Ar/Tt.Ar (%)	52.615+1.25	50.326+2.64	0.963	58.603+1.591	57.886+0.705	1.000
Ct.Th (mm)	0.163+0.01	0.15+0.01	0.423	0.22+0.013	0.195+0.007	0.152
Ma.Dm (mm)	0.535+0.01	0.511+0.013	0.200	0.559+0.015	0.529+0.017	0.201
/max (mm^4)	0.037+0.007	0.027+0.005	0.114	0.076+0.01	0.05+0.007	0.175
/min (mm^4)	0.028+0.004	0.022+0.004	0.139	0.051+0.006	0.039+0.005	0.067
***J* (mm^4)**	0.065+0.011	0.049+0.009	0.114	0.127+0.016	0.089+0.012	0.152
Ct.Po (1)	0.0001+0.0001	0.01+0.01	0.481	0.024+0.016	0.002+0.001	0.331
Po.N	1.222+0.909	18.875+17.748	0.606	90.182+50.133	10.667+7.984	0.503
Po.V (mm^3)	1.3E-06+1.1E-06	2.6E-05+2.4E-05	0.481	0.0002+0.0001	1.2E-05+9.7E-06	0.331
AvgPo.V (mm^3)	2.1E-07+1.5E-07	6.5E-07+3.2E-07	0.423	1.5E-06+3.1E-07	6.6E-07+1.7E-07	0.038
Po.Dn	1.49+0.999	76.25+74.237	0.541	87.716+54.701	14.039+10.28	0.503
TMD ($mgHA/mm^3$)	1242.363+51.481	1256.16+29.726	0.743	1354.58+26.02	1309.063+28.349	0.261

* Using two-tailed Mann-Whitney U test.

Table E.6 Micro CT of midshaft cortex in *Osx-Cre* mice - Females.

Endpoint		7 WEEKS			13 WEEKS	
Genotype	WT	KO	*P*-value*	WT	KO	*P*-value*
Tt.Ar (mm^2)	0.649+0.051	0.641+0.038	0.959	0.768+0.03	0.71+0.018	0.050
Ct.Ar (mm^2)	0.314+0.024	0.319+0.025	0.878	0.428+0.02	0.398+0.015	0.180
Ma.Ar (mm^2)	0.335+0.031	0.321+0.019	0.798	0.34+0.013	0.312+0.01	0.030
Ct.Ar/Tt.Ar (%)	48.443+1.629	49.581+1.767	0.382	55.575+0.838	55.891+1.231	0.582
Ct.Th (mm)	0.144+0.005	0.147+0.006	0.574	0.182+0.005	0.176+0.004	0.456
Ma.Dm (mm)	0.535+0.021	0.527+0.015	1.000	0.528+0.014	0.506+0.008	0.059
/max (mm^4)	0.029+0.005	0.028+0.004	0.878	0.044+0.004	0.036+0.002	0.093
/min (mm^4)	0.022+0.003	0.022+0.003	1.000	0.034+0.003	0.029+0.002	0.140
***J* (mm^4)**	0.051+0.008	0.05+0.007	1.000	0.079+0.006	0.066+0.004	0.123
Ct.Po (1)	0.028+0.02	0.013+0.013	1.000	0.002+0.001	0.003+0.002	0.539
Po.N	71+54.3	20.375+19.948	1.000	5.917+4.206	11.6+10.06	0.722
Po.V (mm^3)	0.0001+0.0001	4.6E-05+4.5E-05	1.000	9.1E-06+5.4E-06	1.4E-05+1.2E-05	0.539
AvgPo.V (mm^3)	5.7E-07+3.2E-07	4.5E-07+2.8E-07	0.959	1.5E-06+4.4E-07	8.01E-07+2.6E-07	0.346
Po.Dn	137.858+94.253	58.797+58.076	1.000	10.098+7.327	23.195+20.873	0.722
TMD ($mgHA/mm^3$)	1288.26+18.66	1242.184+44.123	0.328	1305.21+36.502	1404.982+31.728	0.093

* Using two-tailed Mann-Whitney U test.

APPENDIX F: LIST OF PUBLICATIONS AND PRESENTATIONS ARISING FROM THIS THESIS

R. Sanaei, P.K. Kularathna, C.N. Pagel, E.J. Mackie. Protease-activated Receptor-2 (PAR_2) Promotes Osteoblastic Differentiation at the Expense of Adipogenesis. Presented at the European Calcified Tissue Society Congress, Salzburg, May 2017.

R. Sanaei, C.N. Pagel, E.J. Mackie. Protease-activated Receptor-2 Gene Ablation and the Bone Phenotype During Ageing: A Micro-CT Study. Presented at the Australian and New Zealand Bone and Mineral Society Annual Scientific Meeting, Hobart, November 2015.

R. Sanaei, C.N. Pagel, E.J. Mackie. The Role of Protease-activated Receptor-2 in Regulation of the Bone-Fat Switch. Presented at the Faculty of Veterinary and Agricultural Sciences Research Symposium, Melbourne, December 2016.

R. Sanaei, C.N. Pagel, E.J. Mackie. Protease-activated Receptor-2 Gene Ablation and the Bone Phenotype During Ageing: A Micro-CT Study. Presented at the Faculty of Veterinary and Agricultural Sciences Postgraduate Symposium, Melbourne, December 2015.

R. Sanaei, C.N. Pagel, E.J. Mackie. Protease-activated Receptor-2 in Bone Morphogenesis and Pathology. Presented at the Faculty of Veterinary and Agricultural Sciences Postgraduate Symposium, Melbourne, December 2014.

Protease-Activated Receptor-2 Promotes Osteogenesis at the Expense of Adipogenesis During the Early Differentiation of Mesenchymal Stem Cells. In preparation.